FLOW AND HEAT TRANSFER IN SMALL CHANNELS

A

THESIS SUBMITTED

TO THE

UNIVERSITY OF MUMBAI

FOR THE

Ph. D. (TECH.) DEGREE

IN

CHEMICAL ENGINEERING

SUBMITTED BY

KARALE CHAITANYA MALLIKARJUN

UNDER THE GUIDANCE OF

PROFESSOR SUNIL S. BHAGWAT

CO-GUIDE

Dr. VIVEK V. RANADE

INSTITUTE OF CHEMICAL TECHNOLOGY,

MATUNGA, MUMBAI-400 019.

JUNE 2010

Acknowledgements

In expressing my intangible gratitude to two iconic research supervisors Prof. Sunil S. Bhagwat (SSB) of Institute of Chemical Technology (ICT) and Dr. Vivek V. Ranade (VVR) of National Chemical Laboratory (NCL), I would like to begin with the *Gurustotram*

गुरु ब्रह्मा गुरु विष्णु गुरु देवो महेश्वरः

गुरु साक्षात् परम ब्रह्मा तस्मै श्री गुरवे नमः

Prof. Sunil. S. Bhagwat is a perfect example of researcher, whose motivation, guidance, inspiration, advice and encouragement have lead me to bring my dream to reality. It is my great pleasure to acknowledge him for the freedom that he has given to me to pursue the research independently and for his constant encouragement with critical appraisal on my work. His guidance and association have been very friendly rather than like a formal student-guide relationship and this would evolve with the time even in my future carrier also.

Dr. Vivek V. Ranade, self-made scientist, has not only introduced me to my research problem, but also taught too many other exciting areas and subjects, sometimes more than science. His knowledge is like an ever-expanding encyclopedia, which has all possible answers to help me out of any problem. In this respect, I must mention that he is also a very good teacher and a wonderful research guide, which is often quite rare. I am very much privileged to work under his esteemed guidance. Without his knowledge, perceptiveness and approach to crack problems, I would never have finished my work in time.

I thank the governing body of ICT, the chemical engineering department, NCL and the CSIR for selecting me for the CSIR–GATE-JRF-SRF fellowship, which rather paved way for my golden research career with Dr. Ranade and Prof. Bhagwat. I am also greatly indebted to all my professors at ICT, for I was fortunate to be taught by them.

In every kind of work, especially in research, one recognizes the contribution from others, as guidance, help or as good company. I have benefited at least as much from

my interactions with my group mates on other projects (especially they bared me lot due to unstoppable questionnaires). Most importantly I like to mention my iFMg lab family - Ajay, Akshay, Apparao, CG, Gupta sir, Ganesh, Latif, Madhavi mam, Mohan, Mukesh, Munshiji, Nayana mam, Prashant, Rayaprolu, Ranjeet sir, Ravi, Sanjesh, Vikranth sir, Yogesh etc., for their support, guidance and assistance rendered in all situations through these 3+ years.

I like to thank my SSB lab family- Amol, Kedar, Bhupesh, Ramesh, Shadab, Rajendra, Salil, GG, Shantbaba, Jitendra, Nipun bhai, Ramesh, Sats, Jyoti mam, Nilesh M., Manish, Rajesh, Amar, Balu, Anant, Sarish, Anik, Sharad, Bhushan, Goraksh, Abhijeet, Nilesh G., Sachin, Meenakshi, Kamalakar, JT, Swapnil.

I also take this chance to mention the support received from my friends- Ashok, Amol, Gampu, Harish, Madhusudan, Sagar, Saurabh, Subodh, Rockey, Vinit, Vijay, Umesh, Satyaprasad, Kedar, Yogesh, Mok, Nitin data, Nimish, Ajit. Thanks to my school mates Bandhu (Sandeep) and Prachi for being with me for such a long time.

I also like to thank all my TLEP group members - Ambarish, Amrita, Abhaji, Balaji, Deepti, Mahesh, Manasi, Namitha mam, Nagesh, Piyush (Joshi buwa), Prasad, Sunil dada, Sudhir (CEO), Rajashri, Reetikaji, Umesh, for the great time spent together.

Outcome of PhD research also needs good support from the technical and administrative support system. I am fortunate to have good support staff from NCL. Specifically, I thank Borkar sir for helping me in setting up the heater arrangement to the experimental setup at NCL. I also like to thank Mr. Jadhav from DM solutions, Mr. Deshpande from Acrypol, Avijit sir and Bhaskar from Applied Thermal Pvt Ltd, Prashant and Dr. Parishwad and from COEP who helped me a lot in developing experimental facility. I also like to thank Dr. Amol Kulkarni for providing me Microreactor lab facility for conducting experimental work. I thank to the administrative staff of ICT, Mr. Sonalkar sir, Mr. Mohite sir and Mrs. Chavhan mam on helping me for completion of every official documentation formalities even approaching them at eleventh hour.

Above all, I really don’t feel the necessity to mention the sacrifices of my parents, sister and nephew - Vedant; after all, they are part of me and in me. It is that intimate relationship with my parents that has made me to sustain till date. I bow to all, for their great sacrifices and love they showered on me. It is the strength of my family that backed me through my research in all its difficult times and I am blessed to have them for me.

There are so many people, whose support, encouragement and inspiration are very much obligatory to accomplish major achievements in life, especially, if it involves elements of fulfilling one’s cherish dreams. Special thanks to *Appi*. For me, this thesis is such an important destiny and I am indeed indebted to lot of people for their well wishes and blessings for completing this journey. A sense of appreciation automatically comes into mind at this stage to show my sincere gratitude to all of them, who played a pivotal role and without whom this thesis would not have been possible.

Last but not the least I would also like to say thanks to the computational facility of iFMg because of which it was possible to complete the simulations in time. My workstations (Lagrange and SVP) are also a part of my thesis; those were functioning efficiently without interruption since the first day. My dell Laptop too deserves thanks as the complete thesis typing was done on it.

At the end of this journey at this point I really feel the true meaning of *Geetasaar* as

Whatever happened was good. Whatever is happening is good. Whatever will happen will also be good. Change is the law of the Universe.

-Chaitanya

Contents

List of Figures

List of Tables

CHAPTER 1

INTRODUCTION

The chapter briefly discusses salient features and applications of micro-reactors comprising small channels. Subsequently, the motivation for taking up the research work is presented. The objectives identified for the work are then listed. Thesis organization based on the adopted methodology is presented at the end of the chapter.

1.1 Introduction

Wide variety of conventional chemical reactors are used in practice. The sizes of these conventional reactors vary from few centimeters (laboratory reactors) to several meters (manufacturing scale). Overall performance of chemical reactors is governed by complex interactions of chemical reactions and transport processes like mixing, heat transfer and mass transfer. In recent years, emphasis is being given to process intensification by eliminating (or at least reducing) limitations imposed by transport processes. Micro-reactors comprising small channels (ranging from few microns to millimeter) have been shown to offer unprecedented opportunities for process intensification [see for example reviews by Ehrfeld *et al.* (2000), Gavriilidis *et al.* (2002) and Hessel *et al.* (2006)]. Smaller characteristic length scales of these reactors result in significant increase in heat and mass transfer rates by providing higher surface area to volume ratio (>10000 m^2/m^3). These reactors also offer easier scale-up (numbering up).

However these small reactors have few limitations such as due to smaller passage the resulting pressure drop can be significantly high. This demands powerful pump systems to deliver the reactants mixture. Fouling issues are difficult to handle and replacement of the reactor will be the only available choice in case reactor gets fouled. Another issue consists of difficulty in handling of solids as possibility of channel blockage is quite high. In case of parallel channels achieving equal flow distribution of the reactant material is also a challenging task. Even with these limitations these small reactors are looked upon as one of the potential candidates for process intensification for several industrially important processes. Microreactors because of their miniaturized and compact structure have better control on delivery of material and energy at right location and at right time. These reactors are seen as the future of chemical process engineering for specialty and fine chemicals. Some applications of these are described in Section 1.1.1.

It is therefore essential to critically understand various transport processes occurring in small channels in order to realize true potential of micro-reactors. This research work was undertaken with this background.

1.1.1 Applications of small reactor systems

Various applications ranging from micro reactors (see for example, Ehrfeld et al. 2000, Gokhale *et al.* 2005) to electronics cooling (see for example, Kandlikar, 2006) are fueling this interest. Possibility of integrating such small (micro) channels directly into the heat-generating devices (micro-processors or reactors) makes them particularly attractive, since thermal contact resistances may be avoided.

Microreactors have been used for carrying out safely high temperature oxidation processes in the explosive regime by Janicke *et al.* (2000). A microreactor with cross-flow heat exchange and Pt-Al_2O_3 catalyst was used to perform catalytic oxidation of hydrogen. The reaction channels were coated with Al_2O_3 and impregnated with Pt as a catalyst. Explosive reaction mixtures with concentration of hydrogen and oxygen up to 50% by volume were operated safely and complete conversion of hydrogen to water was obtained without explosion.

Nitration reactions can often show extremely exothermic behaviour, and this, combined with the decomposition or explosion potential of many nitro compounds, places them amongst the most hazardous industrial processes. In this context, continuous processes are attractive for safety reasons because of the much smaller reaction volumes used. A controlled autocatalytic nitration of phenol in a microreactor was carried out by Ducry and Roberge (2005). A glass microreactor with a 10 x 0.5 mm channel width and 2.0 mL internal volume was used for the nitration experiments. The comparison of the results between the batch reactor and the microreactor is shown in Figure 1.1.

The results showed that higher yields of nitro phenols were obtained when the nitration of phenol was performed in a microreactor. Enhanced heat exchange, good mixing properties, and very rapid radical propagation in a confined volume account for those result. In addition to the small reacting volumes present at any given time, continuous phenol nitration in a microreactor allowed for better control of the exothermic reactions. Thus, the resulting improved yields and enhanced process safety make micro- reactor technology attractive to operate autocatalytic reactions such as nitration on an industrial scale.

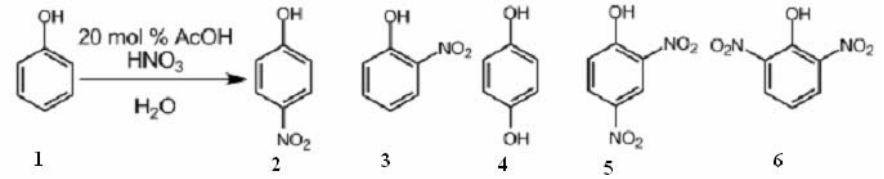

	T (°C)	HNO_3 (equiv)	2+3 (%)	4+5+6 (%)	polymers (%)
Batch	25	1.5	54%	1.1%	32.3%
MR	45	1.5	73%	2.0%	13.2%

Figure 1.1: Comparison between nitration of phenol in batch and microreactor (Ducry and Roberge 2005)

Rebrove *et al.* (2001) studied ammonia oxidation on a Pt catalyst in different types of microchannel architectures which were designed based on their experimental work especially due to strong exothermic nature of the reaction. The authors found that, the heat distribution between the catalytic surface and the gas phase along the microchannel was important to obtain a high selectivity to one of the reaction products (N_2, N_2O, NO), as this was strongly dependent on the reactor temperature. The reactor used was a combined microreactor/heat-exchanger. The schematic of the rector is shown in Figure 1.2. A cross flow microreactor/heat-exchanger could provide almost isothermal conditions (showed in Figure 1.2 – result of the numerical simulations carried by the authors) improving overall selectivity. The aluminium-based microreactor/heat-exchanger showed temperature differences less than 6°C along the axial coordinate, and negligible temperature differences between microchannels along the transverse coordinate (4°C), for reaction conditions corresponding to an adiabatic temperature rise of about 1400°C. Therefore such systems could afford new opportunities for improvement of existing gas/solid catalytic processes with strongly exothermic reactions.

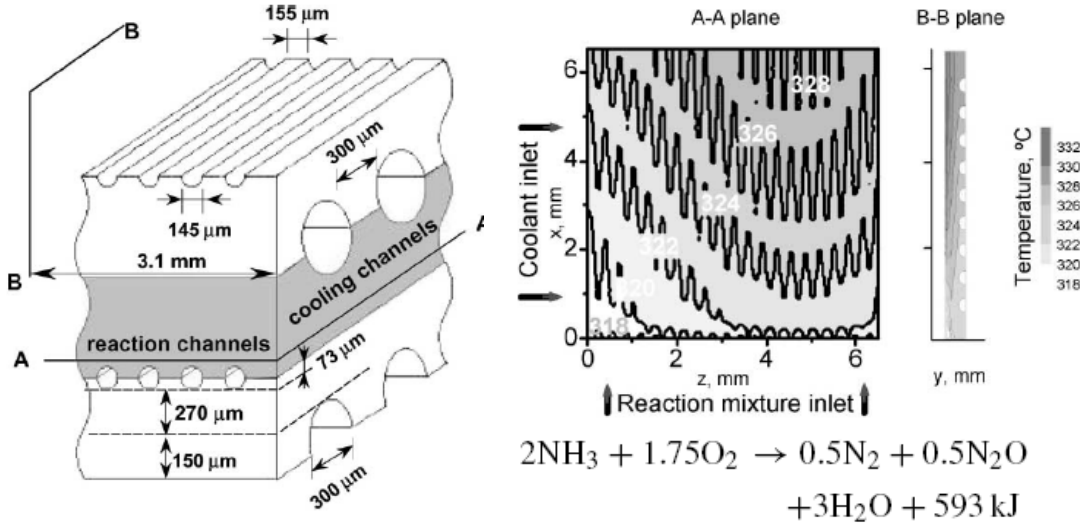

Figure 1.2 Cross-sectional temperature profiles at the planes positioned inside the alumina layer predicted by numerical simulations (Rebrove *et al.* 2001)

Clariant GmbH headed (Wehle et al. 2000) for increasing selectivity for the monochlorination of acetic acid to give chloro-acetic acid. This product is amenable to further chlorination to give dichloro-acetic acid under the reaction conditions. The removal of this impurity demands a laborious and costly separation, either by crystallization or hydrogen reduction with a Pd catalyst.

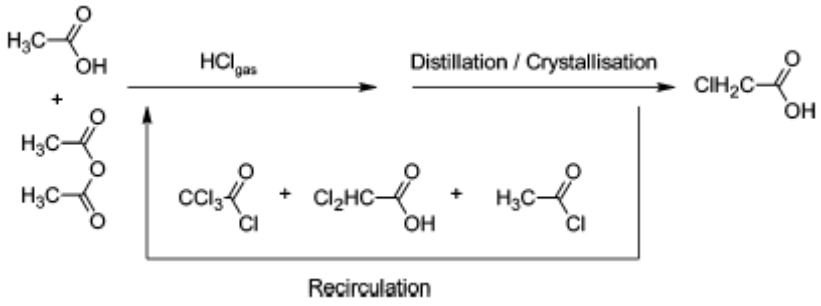

Figure 1.3: Reaction scheme for monochlorination of acetic acid (Wehle *et al.* 2000)

The authors have obtained a yield of 90% with a falling film microreactor which is above that of large-scale bubble-column processing. Selectivity was much better, as less than 0.05% dichloro-acetic acid was formed, while conventional processing typically gives 3.5%.

Along with the applications to reactions, a microchannel heat sink consisting of parallel micro-flow passages was demonstrated to have very small thermal resistance. This technology has been used in micro-electronics and other major application areas,

such as fuel cell systems and advanced heat sink designs. Figure 1.4 shows the schematic of the cooling systems. These practical advantages of micro-channel heat sinks have stimulated researches in experimental, theoretical and also numerical field (Mishan *et al.* 2007).

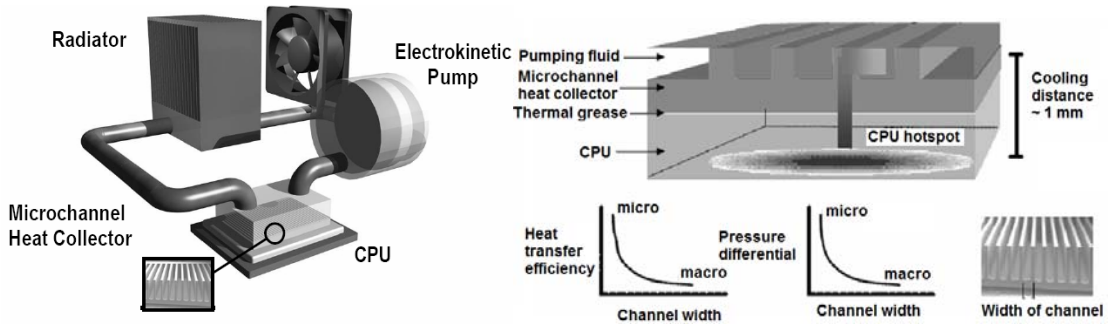

Figure 1.4: Schematic of the Cooligy closed-loop active micro-structure cooling system from Emerson network power (www.Cooligy.com)

1.2 Motivation

Several studies on flow and heat transfer in microchannels were carried out to understand and to quantify extent of disagreement between the conventional correlations obtained from larger channels and the experimental data obtained with micro-channels. An excellent summary of such studies can be found in Morini (2004). Various issues such as conjugate heat transfer, entrance effects, wall roughness, viscous heating and axial conduction may become important for understanding and interpreting flow and heat transfer in small channels compared to conventional size channels. A systematic and quantitative analysis of the extent of contribution from these various issues is however lacking in literature and this formed one of the prime motivation of the present work. In the present work, attempt is made to quantify these issues experimentally as well as computationally.

Recently, there has been a growing interest to develop passive microscale devices that can manipulate and transport relatively small volumes of fluids effectively. The literature (Liu *et al.* 2000) contains a number of devices designed to enhance mixing on the microscale. These devices fall into one of two categories: 1) active mixers that exert some form of active control over the flow field through such means as moving parts or varying pressure gradients or 2) passive mixers that utilize no energy input

except the mechanism (pressure head or pump) used to drive the fluid flow at a constant rate. While active mixers can produce excellent mixing, they are often difficult to fabricate, operate, clean, and integrate into microfluidic systems. However passive mixing is relatively simple to implement. As the fluid flows through a serpentine channel, the secondary flow developments causes fluid mixing which actually results in enhanced transport coefficient with increased pressure drop. One of the examples of such passive mixer is serpentine channel configurations. The serpentine channel consists of a bend section with repeating units. Figure 1.5 shows simple schematic of the serpentine channel. Based on the variations of the dimensions there are various configurations possible. Few limiting cases of this geometry will be sinusoidal channel, saw tooth configuration, etc.

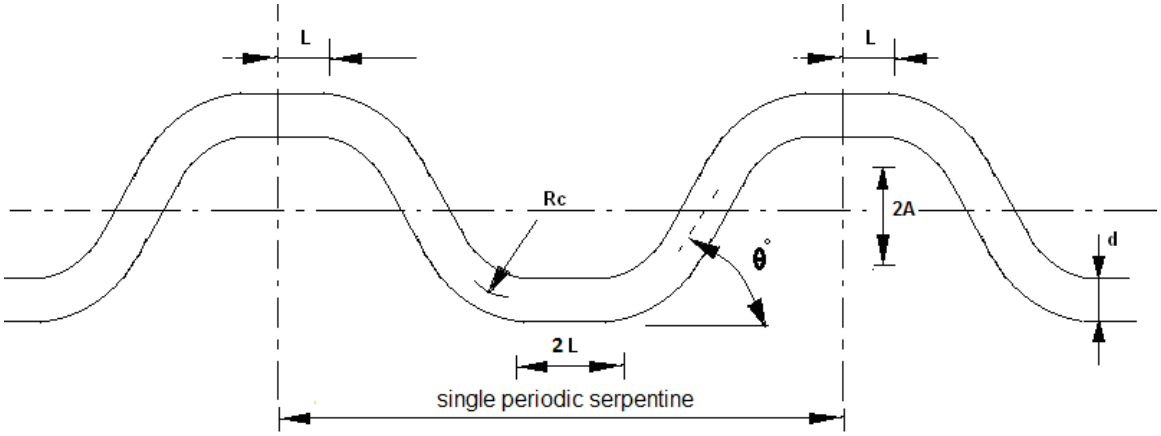

Figure 1.5: Schematic of Serpentine Channel

The necessity or the reason for looking to this area is, resulting limiting values of the transport coefficients which occur in the straight channels. In case of laminar flow, the boundary layer starts developing as the fluid transverse in the flow direction. Therefore in the developed region the heat transfer coefficient is less (compared to entrance region) and becomes constant or independent of Re and Pr along the length of the channel. In such cases it becomes necessary to break or disrupt the boundary layer to overcome the limiting values of heat transfer coefficients. Alternative way to achieve the intense mixing and better transport coefficients is use of passive mixing devices like serpentine channel. However as shown in Figure 1 there are many independent parameters (geometrical and operating parameters) those governs the performance of serpentine channel. The knowledge of proper design methodology for choice of serpentine channel with due considerations to required pumping power is

lacking in literature. In addition to this the experimental investigation of the effect of various geometrical parameters on mixing/heat transfer is difficult as numbers of configurations are possible. In such cases CFD can make a significant contribution, removing the need of experimental investigations to study the effect of various parameters on the heat transfer performance of the serpentine channel. Considering these points, the present work is taken up to understand the effect of various geometrical parameters of serpentine channel on heat transfer enhancement using CFD.

In any continuous flow processes, the residence time characteristics of the reactor is of significant importance. This gives information about the intensity of the dispersion present in the reactor. Despite smaller mixing lengths in microreactors, the laminar profile in straight channels results in large axial dispersion. Serpentine channel helps to overcome this issue due to secondary flow created at bends. The secondary flow structure offers radial mixing that helps to overcome the radial concentration gradient present in the straight channel. However the proper knowledge of the residence time distribution in different serpentine configurations is limited in literature. Therefore in the present work the effect of various geometrical parameters of the serpentine channel on the residence time distribution is investigated using CFD.

Besides achieving so many benefits with these small reactors, these systems also demanded the supporting utilities to perform the operations. These include the pumps to deliver the fluid through these small channels due to higher pressure drop. The use of reciprocating or peristaltic pump naturally was the first choice among the users. However the nature the mechanism of the pumps makes the fluid flow discontinues. Therefore laminar, fully developed, pulsating pipe flows form one of the fundamental classes of flows with periodic time variations in the velocity and pressure properties which have attracted substantial attention in fluid mechanics over the years. Numerous analytical, numerical and few experimental studies that deal with flows of this kind are available. It has also been argued that such flows are of practical importance in various fields, such as biology (simulation of human breathing, flow through arteries, etc.), the automotive industry (simulation of exhaust from I.C. engines) and increasing efforts invested into the studies of fluid mechanics details of laminar, fully developed, pulsating pipe flows are justified in this manner. These

systems also find application in microreactor technology. To withstand the higher pressure drop resulted due to small channels almost in all microreactor operations pulsating/peristaltic pumps are used to deliver the reactants. Therefore because of the pulsating action the flow will be no longer continuous though the time average flow will be same or constant. Therefore one of the key issues concerning pulsating convection heat transfer in tubes is whether a superposed flow pulsation enhances heat transfer in the original steady flow? The answer to this question in the previous studies can be classified into four different opinions: (1) flow pulsation enhances heat transfer (2) it deteriorates heat transfer; (3) it has no effect on heat transfer; and (4) it either enhances or deteriorates heat transfer, depending on flow parameters. There is no satisfactory answer to this question in the literature. Therefore it is necessary to investigate the effect of pulsating flow on fluid friction and heat transfer and is investigated numerically in the present work.

In a convectional chemical engineering practices, reactions involving gas liquid systems are very common. Mechanically agitated contactors, bubble columns, packed columns are the few contactors used for this purpose. However the choice of these contactors depends on several factors such as operating regimes, rate controlling step, production output, heat and mass transfer requirements, interfacial area etc. The characteristic length of these contactors varies from few centimeters to several meters. The interfacial area obtained in these contactors is of the order of 100-300 m^3/m^3 and the volumetric mass transfer coefficient obtained is of the order of $0.2s^{-1}$(Doraiswamy and Sharma 1984). In such cases the performance of several fast reactions such as sulphonations, fluorinations, chlorination is therefore primarily governed by the heat and mass transfer coefficient offered by such contactors.

In recent years, small channel reactors or micro and minireactors are increasing being evaluated for carrying out gas-liquid reactions (see for example Wehle *et al.* 2000, De Mas *et al.* 2003). These small reactors offer an invaluable tool for process development and chemical synthesis. However while handling gas-liquid systems at smaller a scale; a good understanding of the complex multiphase flow characteristics is necessary. Several studies have been conducted to characterize gas-liquid flows in capillaries (Liu *et al.* 2005) however the heat transfer characteristics are not yet well understood (Hestroni *et al.* 2009) compared to the information available in a

conventional two phase system (Ghajar 2004). Therefore in the present work attempt is made to quantify the two phase pressure drop and heat transfer coefficient in a single mini channel experimentally to understand the relationship between the same.

1.2.1 Objectives of present work

The objectives of the present work are to

1. Understand role of developing flow profiles and conjugate heat transport in parallel minichannels
2. Quantify heat transport and mixing in serpentine channels and explore opportunities for manipulating geometrical parameters to enhance heat transfer and controlling residence time distribution (RTD)
3. Understand influence of pulsating flow (amplitude and frequency) on pressure drop and heat transfer in case of laminar pulsating flow
4. Quantify influence of gas flow on two phase pressure drop and heat transfer in a single minichannel.

Overall methodology followed and thesis organization is given in the following section.

1.2.2 Methodology

In conjunction with the aforementioned objectives, the present research work is focused on developing models, methodology and quantitative understanding of flow, mixing and heat transfer in small channels. The size of the channels under the study ranges from few micrometers (700 μm) to millimeters (2 mm). Single phase as well as two phase flow and heat transfer in small channels was studied. The study involved experimental as well as numerical investigations. The overall work is divided into two broad categories. A) Single phase studies in small channels and B) Two phase studies in small channels. The single phase studies are further divided into four categories. These include a) Flow and heat transfer in parallel channels b) Flow and heat transfer in serpentine channels c) Residence time distribution in serpentine channels and d) Flow and heat transfer in laminar pulsating convection. In case of two phase studies the work consists of experimental and numerical investigation of heat transfer in gas-liquid flow in a single minichannel. The methodology adopted is discussed in a sequential manner as following.

Part 1: Flow and heat transfer in parallel minichannels

In this part, flow and heat transfer experiments were carried out with a micro-channel plate comprising of 20 parallel channels. Pressure drop and heat transfer coefficients were experimentally measured. Flow and heat transfer in the experimental set-up were simulated using CFD models to provide useful and quantitative information on developing flow regions, axial heat conduction, conjugate heat transfer, effect of the design inlet and outlet manifolds. The methodology and the results presented here will be useful for further work on flow and heat transfer in micro-channels

Part 2: Flow and heat transfer in serpentine channel

The design guidelines of serpentine channel are limited due to many degrees of freedom available in geometrical parameters. Studying effect of these parameters experimentally will be a difficult task as number of geometries needs to be fabricated. For this purpose CFD technique is utilized. The geometry consists of periodic square channel of 2 mm x 2 mm with 100 mm in total length. The other geometrical parameters are changed (amplitude A, straight length before bend L etc.) in such a way that the total length of the channel remains 100 mm. The simulation parameters are laminar, incompressible flow, Reynolds number of 200 with constant wall temperature of 373K at the wall. The performance of various geometrical parameters was compared on the basis of different criteria's which are normalized with the performance of the straight channel having same length. From the results, a performance design map was generated. The CFD methodology was also validated with the experimental analysis conducted in the present work.

Part 3: Residence time distribution in serpentine channel

The knowledge of residence time distribution (RTD) is of great help in identifying the extent of non-ideal flow behavior of reactors. Accurate knowledge of the extent of axial mixing which ultimately affects the performance of reactors in terms of conversion and yield is thus essential for the modeling and design of reactors. The methodology for residence time distribution is much similar as discussed Part 2. Only difference is instead of energy equation, concentration or species transport equation is solved with momentum and continuity. All geometries were same as those used to study the heat transfer in serpentine channel in Part 2. First the flow field was solved

completely. Then the flow field was freezed and the species equation was solved with pulse injection at the inlet. The concentration of the tracer was monitored at the outlet. This gives exit age distribution of the tracer. The performance of different serpentine configurations was compared by using variance as a parameter calculated from the E-curve. The CFD methodology was also validated by carrying out simulations for standard geometry of pipe flow and comparing the results with literature data.

Part 4: Pressure drop and heat transfer in laminar pulsating flow

From a review of current literature, it is found that there is a need for systematic assessment of the impact of flow pulsation in heat transfer from circular ducts at constant wall temperature. Therefore the present study is an attempt to investigate the heat transfer in a circular isothermal duct with imposed flow pulsation at the inlet. At inlet the velocity profile consisted of a fixed part and a pulsating component that varies sinusoidally in time. It should be noted that the sinusoidal variation on velocity was simplest approximation to the real life systems involving the pulsations. The flow was both thermally as well as hydrodynamically developing while the tube wall was kept at a uniform temperature. The solution of two dimensional Navier–Stokes equations was performed. The present study focuses within the frequency range of 1–100 Hz and dimensionless amplitude between 0 and 1 at a mean Reynolds number of 200.

Part 5: Two phase flow and heat transfer in small channel

The non boiling heat transfer in conventional channel shows that the presence of gas increases two phase heat transfer coefficient than that of a single phase alone (Ghajar 2000). However in case of microchannel systems different trends were observed. Therefore in the present work the two phase heat transfer phenomenon was investigated experimentally as well as numerically. The experimental facility consists of a copper plate of size 12 mm x 8 mm x 200 mm (W x D x L_T). On this plate single square channel of 1mm x1 mm x 200 mm was made using machining technique. The surface was closed using acrylic plate. At the bottom strip was placed so that the heat transfer will be from the channel wall to the gas liquid slug flow flowing through the channel. The temperatures of the liquid and the wall were measured using thermocouples. The effect of different flow rates of gas on pressure drop and liquid phase heat transfer coefficient was studied.

1.2.3 Thesis organization

The thesis is organized into five chapters and appendix section as mentioned below.

Chapter 1 discusses on the background for taking up this research work and the motivation behind the work. The objectives and methodology are discussed therein.

Chapter 2 is on single phase flow and heat transfer in parallel minichannels. The experimental results are compared with the CFD simulations carried out in the same work.

Chapter 3 is on investigating the effect of geometrical parameters of serpentine channel on the performance in terms of heat transfer enhancement.

Chapter 4 is on investigating the effect of geometrical parameters of serpentine channel on the performance in terms residence time distribution.

Chapter 5 is on numerical investigation of pulsating frequency and amplitude on pressure drop and heat transfer at constant wall temperature.

Chapter 6 is on experimental analysis of two phase flow and heat transfer in a single minichannel.

CHAPTER 2

FLOW AND HEAT TRANSFER IN PARALLEL CHANNELS

Flow and heat transfer in microchannels is of significant interest to various applications ranging from electronics cooling to micro-reactors. Various issues such as conjugate heat transfer, entrance effects, wall roughness, viscous heating and axial conduction may become important for understanding and interpreting flow and heat transfer in micro-channels. In the present work, attempt is made to quantify these issues experimentally as well as computationally. Flow and heat transfer experiments were carried out with a micro-channel plate comprising of 20 parallel channels. Pressure drop and heat transfer coefficients were experimentally measured. Flow and heat transfer in the experimental set-up were simulated using CFD models to provide useful and quantitative information on developing flow regions, axial heat conduction, conjugate heat transfer, effect of the design inlet and outlet manifolds. The methodology and the results presented here will be useful for further work on flow and heat transfer in micro-channels.

2.1. Background

In recent years there is a growing interest in flow, heat transfer and reactions in small channels. Various applications ranging from micro reactors (see for example, Ehrfeld et al. 2000, Gokhale *et. al.*2005) to electronics cooling (see for example, Kandlikar, 2006) are fueling this interest. Possibility of integrating such small (micro) channels directly into the heat-generating devices (micro-processors or reactors) makes them particularly attractive, since thermal contact resistances may be avoided. Various issues such as conjugate heat transfer, entrance effects, wall roughness, viscous heating and axial conduction may become important for understanding and interpreting flow and heat transfer in micro-channels. Available information on flow and heat transfer in micro-channels is briefly reviewed here. In light of this review, attempt is made to quantify these issues experimentally as well as computationally in the present work. Experimental set-up and procedure, computational model and obtained results are discussed in the following sections.

A typical microchannel heat sink consists of parallel micro-flow passages. It was demonstrated to have very small thermal resistance. These practical advantages of micro-channel heat sinks have stimulated further experimental, theoretical and computational studies of flow and heat transfer in small channels (Mishan *et. al.*2007). Some of the published work is briefly reviewed here.

Wang and Peng (1993) investigated heat transfer in microchannels having width of 0.2 mm and depth of 0.7 mm using water and methanol as a working fluid. There was a significant deviation between the theory and experiments. It was also observed that the range of transition zone and heat transfer characteristics of both transition and laminar flow are highly affected by liquid temperature, velocity and microchannel size.

Adams *et. al.*(1998) experimentally investigated the single phase forced convection in circular microchannels of 0.76 and 1.09 mm diameter over the Reynolds number range of 2600 to 23000. The experimentally obtained values of Nusselt number were higher than those predicted by the Gnielinski correlation.

Gad-el-Hak (1999) argued that traditional treatments of transport phenomena may not be appropriate for certain situations involving microdevices. The simplistic dimensional analysis approach does miss important physics and was therefore misleading. Liquids such as water should be treated as continuous media with the results obtained from classical theory being applicable in channels larger than 1 μm. However, there remain a number of unresolved issues that require further study.

Harms *et. al.*(1999) studied the developing convective single phase forced convection in single as well as multiple channels having hydraulic diameters of 1.923 mm and 0.404 mm respectively. For the single channel design, the experimentally obtained value of Nusselt number was higher than predicted value at all flow rates. The results for the multiple channel design agree reasonably well with the theory at high flow rates. However, it shows significant deviation with the theory at low flow rates. This deviation was attributed to flow bypass in the manifold.

Kawano *et. al.*(2001) studied microchannel heat transfer in a silicon channel of 0.057 mm x 0.18 mm formed by etching technique. The experimentally obtained values of thermal resistance differ substantially with the calculated values when the Reynolds number was low. As per the authors the deviation was due to the difficulty in estimating all the experimental errors in this range since the flow rate was too low to conduct experiments precisely and there was a major gap between the properties used in the calculation such as viscosity, etc. and the actual properties, since the increase in the temperature of the coolant inside the channel was extremely large.

Warrier *et al.* (2002) conducted experiments of forced convection in small rectangular channels using FC-84 as test fluid. The test section consisted of five parallel aluminum based channels, with hydraulic diameter of Dh, 0.75 mm and length to diameter ratio of 409.8. Experimental results of the variation of local Nu as a function of the axial distance were compared to numerical data presented by Kays and Crawford (1993) and agree quite well, especially near the fully developed region. In addition, the authors measured

the Fanning friction factors and found them about 8–14% higher than the analytically predicted values.

The influence of size effects and scaling on hydrodynamic flow and heat transfer in 2-D micro-channels was investigated by Gao *et al.* (2002). Their test section consisted of a single bronze micro-channel with hydraulic diameter ranging from 200 μm to 2 mm, the ratio of the length to hydraulic diameter was $40 < L/Dh < 400$, and the aspect ratio (depth to width ratio) was $0:004 < H/W < 0:04$. The local Poiseuille number expressed as a function of dimensionless length was compared with the theoretical solution for laminar flow regime and the results demonstrated good agreement. However, for the lowest aspect ratio ($H/W = 0.004$) the values of Nu_x showed departure from the theoretical heat transfer trend and found to be smaller (reduction of 60%) than the conventional value for large scale channels as reported by Shah and London (1978). Attempts to explain these findings with the help of roughness and electro kinetics effects were not met with success.

Lelea *et al.* (2004) experimentally researched the laminar heat transfer and fluid flow in micro tubes having diameters of 0.1, 0.3 and 0.5 mm. The cooling liquid used in these experiments was distilled water. Special care was taken for reducing the heat loss in order to keep experimental uncertainty within an allowable level for the thermal results. There was a good agreement between the theory and the experiments.

Zang *et. al.* (2005) experimentally investigated heat transfer in 21 microchannels of width 0.21 mm and height 2 mm with 10 x 10 mm and 12 x 12 mm chip. An analytical technique based on conventional fluid flow and heat transfer theory was used to perform thermal analysis and to provide design guidelines. The predicted results were compared with experiments and good agreement was achieved in both chip cases for thermal resistances (≤6%) and the pressure drop (≤15%). In addition, the respective thermal resistance elements were examined and the interface resistance was identified to be a key element, accounting for over 50% of the overall thermal resistance at larger flow rates.

In order to explore the validity of classical correlations based on large size channels for predicting the thermal behavior in single-phase flow, Lee *et al.* (2005) studied deionized water flow through parallel array of copper microchannels. The channel width ranged from 0.194 mm to 0.534 mm with channel depth being nominally five times the width in each case and Reynolds number range of 300 – 3500. Numerical predictions obtained based on a classical, continuum approach were found to be in good agreement with the experimental data. The authors noted that the entrance and boundary conditions imposed in the experiment need to be carefully matched in the predictive approaches.

Mishan *et. al.*(2007) studied the effect of developing flow and thermal regime on momentum and heat transfer in microchannels of 0.320 mm wide and 0.750 mm deep. The experimental results have been compared with theoretical predictions from literature and results obtained by numerical modeling of their experiments. The experimental results of pressure drop and heat transfer confirm that the conventional theory is applicable for describing experiments with micro-channels provided the entrance effects are included.

Several studies on flow and heat transfer in microchannels were carried out to understand and to quantify extent of disagreement between the conventional correlations obtained from larger channels and the experimental data obtained with micro-channels. An excellent summary of such studies can be found in Morini (2004). While considering the heat transfer and fluid flow in microchannels, it is essential to include effects such as axial conduction, conjugate heat transfer, entrance effects, temperature and pressure dependent properties, wall roughness, viscous heating etc. With this background, in this work flow and heat transfer in minichannels were investigated experimentally as well as numerically. The experimental setup was designed to measure pressure drop and heat transfer across the channels. Developing flow and heat transfer occurring in this experimental set-up was simulated using Computational Fluid Dynamics (CFD). The experimental set-up, details of numerical simulations and obtained results are discussed in the following. Key conclusions based on this work are outlined at the end.

2.2 Experimental setup and procedure

2.2.1 Test piece

The experimental test piece consisted of a copper block having dimensions of 34 mm x 30 mm x 5 mm. On this block, 20 rectangular channels were machined on one side using wire EDM technique. The micro-channels were of 700 μm wide and 2100 μm deep with an accuracy of ±10 μm. The rest of the experimental test geometry was fabricated in thick acrylic sheet having overall dimensions of 150 mm x 60 mm x 20 mm. Figure 2.1 shows the schematic of the test piece along with the mini-channel plate. The inlet and outlet manifold designs were taken from the work of Mishan et al. (2006). In this acrylic sheet two manifolds were fabricated which are of dimensions 36 mm x 30 mm x 11 mm at ends. The inlet manifold and outlet manifold were provided with small holes of 5 mm diameter which serve as inlet and outlet to fluid stream respectively. Next to inlet manifold there is a convergent section with the depth of 2.5 mm and length of 10 mm. The micro channel test piece was press fitted in the middle section as shown in Figure 2.1. The top of the geometry was closed by 8 mm thick acrylic plate which was provided with 1 mm holes for arrangement of needles to measure pressure as well temperature. The fluid enters from the inlet hole into the inlet manifold where the fluid velocity was reduced because of the expansion in the flow area. The fluid then enters mini-channels through the convergent section followed by the straight section of 5 mm length. This arrangement was made to ensure uniform distribution of fluid through all channels. After passing through the channels the fluid then travels through the straight section followed by divergent section into exit manifold. For heat transfer studies, the microchannel plate was heated using A.C. cartridge heater of size 20 mm x 20 mm with power/heat input controlled by the dimmerstat. The power supplied to cartridge heater was measured by Digital Wattmeter (Conzerve).

2.2.2 Measurement apparatus and procedures

The fluid was pumped using the pump facility provided on the standard Julabo bath. Control valve was used to adjust the flow. The flow rates used in this study were in the range of 100 ml/min to 4000 ml/min that was measured by collecting the volume of liquid in a specific time. Figure 2.1 shows the schematic of the experimental setup.

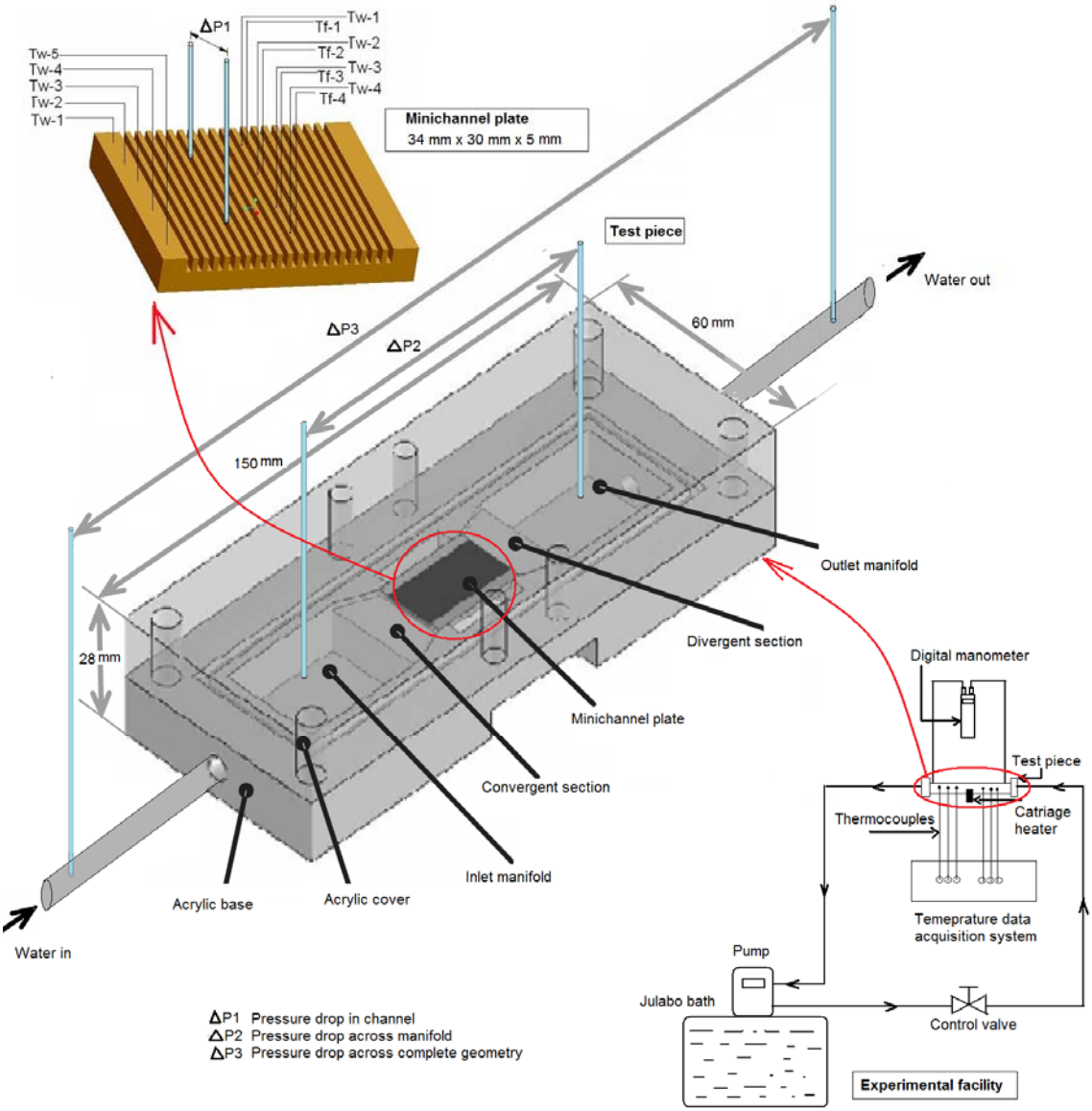

Figure 2.1: Schematic of the experimental facility and test piece

For Pressure drop measurements two holes of diameter 1 mm were drilled on the top polycarbonate cover exactly on the top of the middle channel with 20 mm distance between them. Through these holes two SS tubes/needles having internal diameter of 0.8 mm were inserted so that the tube will be inline with the top surface of the channel. These two tubes were connected to the digital manometer having sensitivity of 7 Pa and accuracy of $\pm$ 0.3% of full scale at 25^{o}C. When fluid moves through the channel the

frictional pressure drop over the 20 mm length was directly measured by the digital manometer. Similar arrangement was made on the 1st and 15th channels. The magnified region of mini-channel plate shown in Figure 2.1 illustrates the pressure drop measurement in 15th channel. These other channel pressure drops will give information about the flow distribution. Along with the channel pressure drop, the total pressure drop across two manifolds was also measured. For this two holes of 1 mm were drilled on the acrylic plate and the pressure drop was measured by digital manometer. In addition to this, pressure drop across whole geometry was also measured to understand the contribution of the different pressure losses at entrance and exit regions. The test piece shown in Figure 2.1 illustrates the pressure measurement schemes across manifold and complete geometry. For heat transfer studies the temperatures were recorded using the data acquisition at scanning rate of 1 s within accuracy of ± 0.5 ^{o}C. Five thermocouples (Omega, J Type, Accuracy: ±0.5 ^{o}C) of size 0.076 mm were placed on the 20th channel wall/fin to measure the wall temperature along the length of the channel. Two thermocouples were placed in two manifolds to measure the inlet and outlet temperature of the water. In some experiments, the water temperature in the middle channel was measured by using four thermocouples placed in channel at equal distance in the direction of flow and four thermocouples were placed on the channel wall to measure the wall temperature. The magnified region of the mini-channel plate shown in Figure 2.1 illustrates the thermocouple locations to measure the temperature of channel wall and fluid. For testing procedure, the Julabo pump was turned on at flow rates from 100 ml/min to 2000 ml/min. The electrical power to the heater was adjusted to a desired level by a variable voltage of the dimmerstat. After allowing the system to establish steady state, flow rate, electrical power and temperatures were measured.

2.2.3 Data reduction

The collected pressure drop data was used to calculate effective friction factor using the following equation:

$$\Delta P = \frac{2 f L_T \rho V^2}{D_h} \quad \text{..... (2.1)}$$

The Poiseuille number (fRe) was then calculated from friction factor (f) and Reynolds number (Re) as:

$$f\,\mathrm{Re} = \frac{\Delta P\, D_h}{2\, L_T\, \rho V^2}\,\mathrm{Re} \quad \ldots\ldots \quad (2.2)$$

The total power given to the cartridge heater was getting distributed in two parts. A) Heat supplied to water (Q1) B) Heat loss to the environment (Q2). The heat taken by the water was calculated as:

$$\mathrm{Q1} = \dot{\mathrm{m}}\,\mathrm{Cp}\,(\mathrm{T_{f,out}} - \mathrm{T_{f,in}}) \quad \ldots\ldots \quad (2.3)$$

The heat loss to the environment (part B) was calculated using the difference between the heat supplied to the cartridge heater and heat taken by water. The overall heat loss to the environment was found to be less than 5%. More than 100 temperature data points were used in calculations for every flow rate.

The bulk water temperature in the channel was measured in only few experiments (Re 148, 208 and 445) as there was a problem of positioning the thermocouple in the channel due to leakage. Therefore in rest of the experiments the bulk water temperature along the length was therefore calculated using the following equation:

$$T_{f,L1} = q1 \times A_{L1} - \dot{m}\,Cp + T_{f,in} \quad \ldots\ldots \quad (2.4)$$

Where,

$$\mathrm{q1} = \frac{\mathrm{Q1}}{(\mathrm{W} \times \mathrm{L} + 2 \times \mathrm{H} \times \mathrm{L}) \times 20} \quad \ldots\ldots \quad (2.5)$$

In the above equation it was assumed that the heat flux is uniform over the length of the channel. Since the thermal conductivity of copper is very high, we assumed that at a given cross-section the side-wall temperature of the micro-channel did not differ significantly from the channel bottom temperature. The local heat transfer coefficient was calculated as:

$$q1 = \frac{Q1}{(W \times L + 2 \times H \times L) \times 20} = h_{L1} \times (T_{w1} - T_{f,L1}) \quad \text{(2.6)}$$

The local Nusselt number was calculated as:

$$Nu_{L1} = \frac{h_{L1} Dh}{k} \quad \text{(2.7)}$$

Similarly the local Nusselt number at various axial locations was calculated.

The local Nusselt number was then integrated over the length to get the average values as:

$$Nu_{avg} = \frac{1}{L} \int Nu_{local} dL \quad \text{(2.8)}$$

2.3. Numerical analysis

The flow and heat transfer in micro-channels used in the experimental work were simulated using commercial CFD code, Fluent 6.3.36. Key aspects are discussed in the following.

2.3.1 Numerical analysis of inlet manifold

Flow distribution is an important issue in multichannel geometry. It is necessary to find out the whether arrangement of the manifold was good enough to ensure equal distribution of the fluid among all channels. For this purpose we first investigated the three dimensional manifold part using CFD. Only inlet manifold was considered in the simulations to understand the flow distribution among the channels. Figure 2.2 shows the schematic of the complete flow domain along with the inlet manifold domain and single channel domain for simplified analysis. The complete domain was meshed using hexahedral map scheme with total cells of 998400. The geometry consists of manifold with inlet of 5 mm and the entrance faces of the 20 minichannels i.e. exit of manifold. Only half geometry was simulated using the symmetry boundary condition to save the

computational time. The velocity inlet with flat profile and pressure outlet boundary conditions were used for inlet and outlet respectively. Laminar, incompressible flow with constant physical properties was simulated. The flow field was solved using the second order upwind scheme. No slip boundary condition was used at all the walls. Simulations were carried out for a flow rate range of 250 ml/min to 1680 ml/min which corresponds to channel Re of 148 to 1000 respectively. The outlet flow rate from all the channels was monitored to understand the flow distribution among the channels.

2.3.2 Numerical analysis of flow and heat transfer in single minichannel

The numerical analysis of flow and heat transfer in a single channel was divided in two parts. In the first part the CFD methodology was developed to understand the effect of different wall thermal boundary conditions. In the later part the developed CFD methodology was applied to investigate the flow and heat transfer in single channel in the present experimental geometry to predict the present experimental data.

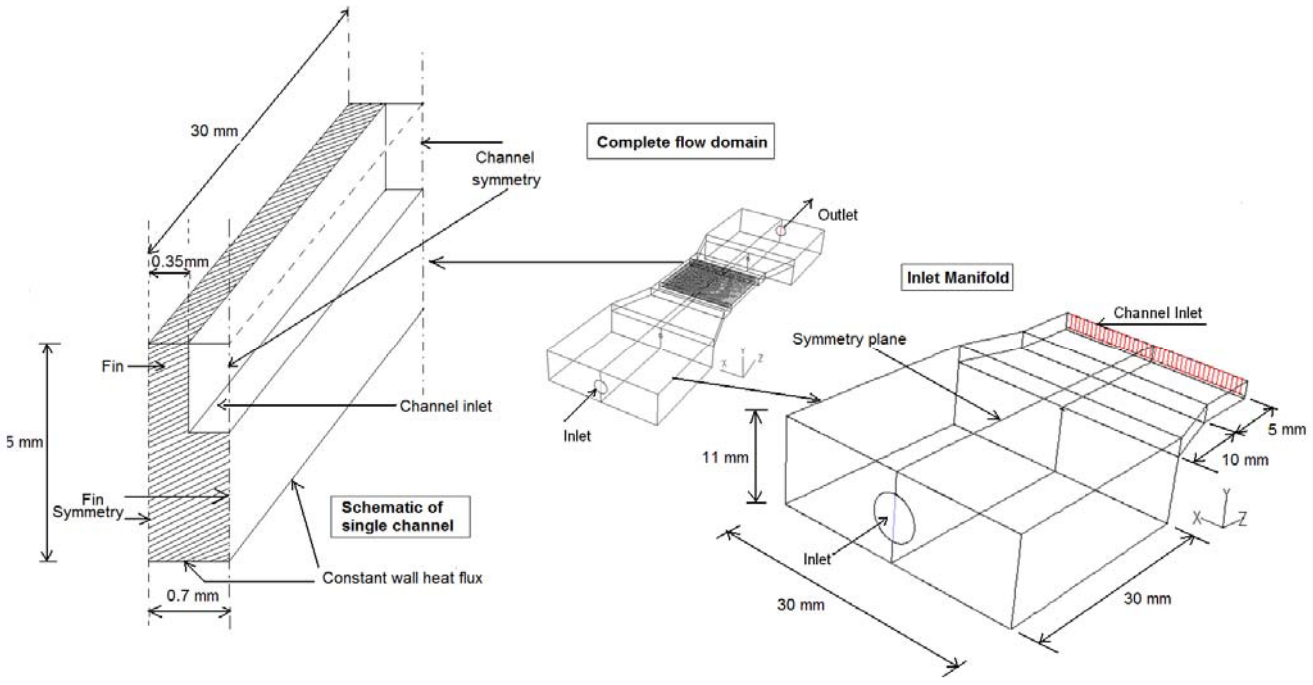

Figure 2.2: Schematic of the flow domain and single channel

2.3.2.1 Numerical analysis to understand the effect of wall thermal boundary conditions

Simulation of a complete multichannel geometry used in the experiment is a computationally expensive task. In order to understand effect or the extent of contribution of different wall thermal boundary conditions, a simplified analysis using a single channel was carried out. The analysis was useful to identify which boundary conditions resemble heat transport taking place in experimental small channels.

In this part the effect of wall boundary conditions on the local as well as average heat transfer coefficient was investigated. For this purpose the experimental data of the Lee *et. al.*(2005) was used. The author studied the heat transfer in 5 different test pieces. In the present work the dimensions of the channel was 0.534 mm x 2.91 mm x 25.4 mm (aspect ratio of 5.45), same as one of the test piece used by the authors. The analysis was conducted on a single channel rather that a complete test piece of 10 channels. The single channel was studied with five different wall boundary conditions. These involves a) a single channel with all four wall supplying heat to the fluid b) a single channel with top wall as adiabatic and 3 wall are supplying heat to the fluid c) thin wall model (a module available in fluent for accounting the thermal resistance of the wall in normal direction) d) a complete 3d conjugate heat transfer analysis.

For grid sensitivity analysis, simulations were carried out by using three different grid sizes for the first case where all four walls were supplying heat to the fluid. The entire solution domain was meshed using hexahedral elements. In the first mesh the symmetric channel width was meshed with 15 elements and height was meshed with 30 elements while the length was meshed with 80 elements having double successive ratio of 1.04. In the second case, the symmetric channel width was meshed with 20 elements and height was meshed with 50 elements while the length was meshed with 100 elements having double successive ratio of 1.08. In the third case the symmetric channel width was meshed with 20 elements with successive ratio of 1.1 and height was meshed with 50 elements with double successive ratio of 1.05 while the length was meshed with 100 elements having double successive ratio of 1.08.

Velocity inlet and pressure outlet boundary condition were used at channel inlet and outlet respectively. The simulations were carried out for thermally developing flow. For thermally developing flow, at inlet, developed velocity profile was given. The material properties of copper were specified for solid regions. The Flow and energy equations were discritized using the second order upwind scheme. The simulations were carried out for adequate iterations to ensure acceptable convergence. The Re range used in the simulations ranges from 400 to 1200. A constant wall heat flux of 45 W/cm^2 at walls was used same as the one obtained by Lee *et. al.*(2005) in their experiments.

The local heat flux and local temperature distributions were obtained from the numerical simulations. With these quantities, the local convective heat transfer coefficient, h(z), can be evaluated using the following equation:

$$h(z)=\frac{1}{A(z)}\sum_{x,y}\frac{q''_{(x,y,z)}}{\left[T_{w(x,y,z)}-T_{m(z)}\right]}dA_{(x,y,z)} \quad \text{..... (2.9)}$$

where A(z) and $q''_{(x,y,z)}$ are the total local heat transfer area and total local heat flux, respectively, as defined below:

$$A(z)=\sum_{x,y} dA_{(x,y,z)} \quad \text{..... (2.10)}$$

$$q''_{(x,y,z)}=\frac{Q_{(x,y,z)}}{A_{(x,y,z)}} \quad \text{..... (2.11)}$$

In Equation (2.9), $Tw_{(x,y,z)}$ is the local wall temperature and $T_{m(z)}$ is local fluid bulk-mean temperature given by:

$$T_{m(z)}=\frac{\sum_{x,y}\rho\, u_{(x,y,z)} Cp\, T_{f(x,y,z)}\, dA_{(x,y,z)}}{\sum_{x,y}\rho\, u_{(x,y,z)} Cp\; dA_{(x,y,z)}} \quad \text{..... (2.12)}$$

The local Nusselt number, $N_u(z)$, was then be calculated using the following equation:

$$N_u(z)=\frac{h(z)\, D_h}{k} \quad \text{..... (2.13)}$$

The average Nusselt number $N_{u\,avg(z)}$ can similarly be computed as:

$$N_{u\,avg(z)} = \frac{D_h}{k} \times \frac{1}{\sum_{x,y,z} dA_{(x,y,z)}} \times \sum_{x,y,z} \frac{q''_{(x,y,z)}}{\left[T_{w(x,y,z)} - T_{m(z)}\right]} dA_{(x,y,z)} \quad \text{..... (2.14)}$$

Figure 2.3 (a) shows the effect of a different grid sizes on the local heat transfer coefficient when all four walls are supplying heat to the fluid for Re of 490. It can be seen that all three grid sizes were found to give the similar results with less than 5% deviation in the value of average Nusselt number.

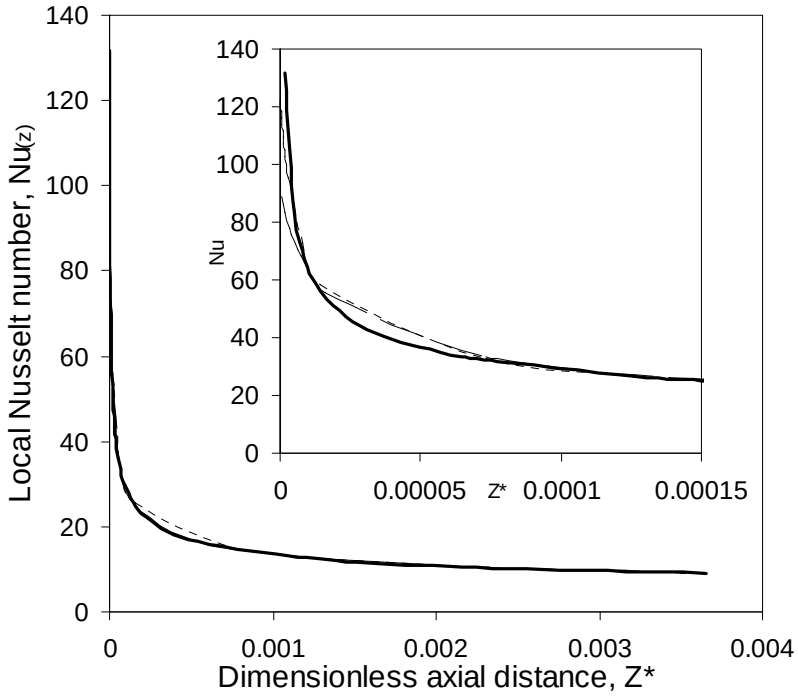

Figure 2.3 (a): Effect of various grid size local Nusselt number
(.....) 15 x 60 x 80 (SR 1.04); (____) 20 x 100 x 100 (SR 1.08); (____) 20 (SR 1.1) x 100 (SR 1.05) x 100 (SR 1.08); (Re- 490, Q- 40W)

Table 2.1 illustrates the summary of the simulation parameters used to study the effect of wall thermal boundary conditions. The rest of the simulation methodology for discritization and analysis was same as discussed in the previous paragraphs.

Figure 2.3 (b) shows the effect of different wall thermal boundary conditions on the average Nusselt number for different Re. For comparison the experimental data of Lee *et.*

al.(2005) is also shown in the Figure 2.3 (b). It can be seen that the predictions of the case 1 and case 2 i.e. neglecting the conduction in the solid wall of channel are in qualitative agreement with (10-13% deviation) the experimental data. Accounting for wall thermal resistance in one direction (1D) i.e. Case 3 resulted in some reduction in deviation from the experimental data. Complete 3d conjugate analysis (Case 4) however leads to good agreement with the experimental data (within less than ±3%). When highly conducting material like aluminium is used for the test piece in the experiments, it is therefore more accurate to carry out detailed conjugate heat transfer analysis than using constant wall heat flux boundary condition at the channel walls. More discussion on this can be found in Shah and London (1878). All the further simulations were carried out with conjugate analysis.

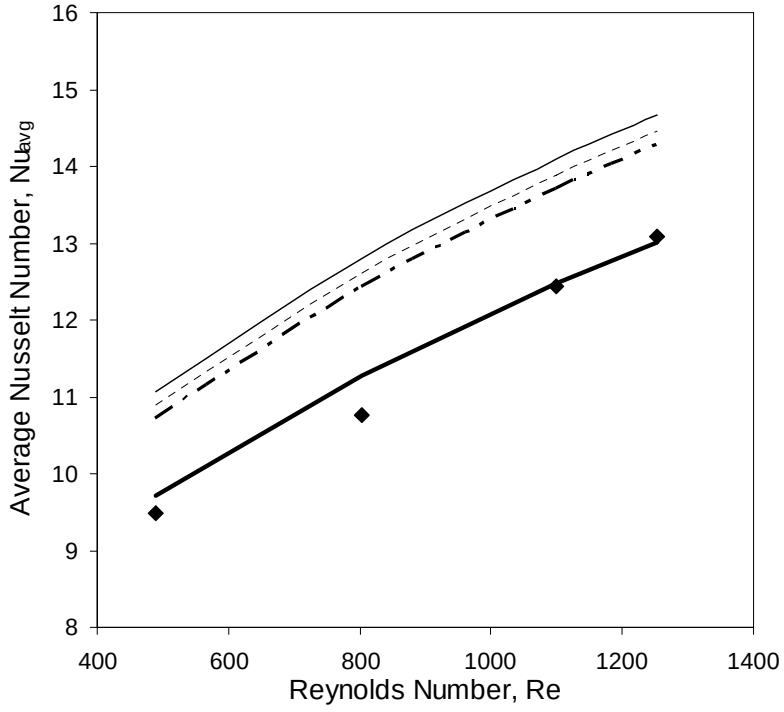

Figure 2.3 (b): Effect of different wall thermal boundary conditions (___) All 4 walls of channel supplying heat to the fluid (case 1), (_____) 3 walls supplying heat with top wall adiabatic (case 2), (_ . _ .) Thin wall model (case 3), (▬) 3d conjugate analysis (case 4), (♦) Experimental data of Lee *et. al.*(2005)

Table 2.1: Simulations parameters used to understand the effect of different wall thermal boundary conditions

Parameter	Case 1	Case 2	Case 3	Case 4
Schematic (CHF:- Constant Heat Flux)	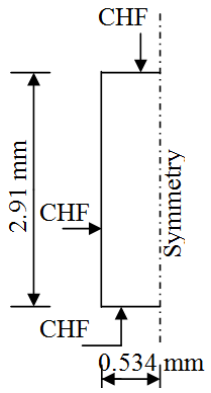	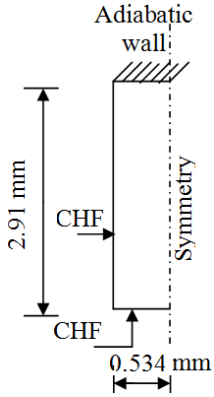	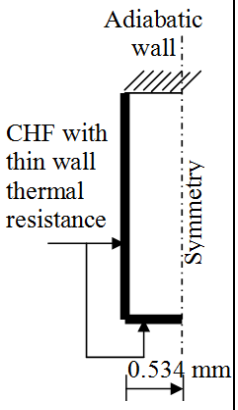	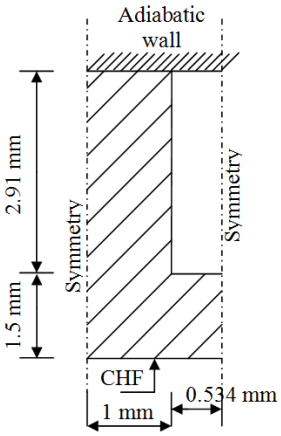
Grid	20x100x100 (Total cells 200000)	20x100x100 (Total cells 200000)	20x100x100 (Total cells 200000)	20x100x100 (Channel) (Total cells 500000)
Boundary conditions for momentum equation	Inlet: Developed velocity profile Outlet: Pressure outlet	Inlet: Developed velocity profile Outlet: Pressure outlet	Inlet: Developed velocity profile Outlet: Pressure outlet	Inlet: Developed velocity profile Outlet: Pressure outlet
Boundary conditions for energy equation	Constant wall heat flux at all 4 walls of channel	Constant wall heat flux at all 3 walls of channel with adiabatic top wall	Constant wall heat flux at all 3 walls of channel with finite wall thickness (1D-conduction) and top wall adiabatic	Constant wall heat flux at bottom, Conjugate heat transfer, Top wall adiabatic
Under relaxation factor	Momentum: 0.2 Energy: 1	Momentum: 0.2 Energy: 1	Momentum: 0.2 Energy: 1	Momentum: 0.2 Energy: 1

2.3.2.2 Flow and heat transfer in a minichannel

In this part a simplified analysis of the multichannel geometry (test piece used in the present experimental setup) was carried out. The geometry of a single channel along with the fin is shown in Figure 2.2. Velocity inlet and pressure outlet boundary condition were used at channel inlet and outlet respectively. The simulations were carried out for thermally developing as well as simultaneously developing flow. For thermally developing flow, at inlet, developed velocity profile was given. For simultaneously developing flow flat velocity profile was given at the inlet. The pressure drop over the middle 20 mm length was calculated as the experimental data was taken over this length. Using this pressure drop the friction factor was calculated using Equation 2.1. For heat transfer studies, a 3d- conjugate heat transfer analysis (based on the understanding of the different boundary conditions studied in the previous section) was carried out. Therefore a constant wall heat flux boundary condition was given at the bottom wall. A zero flux boundary condition was specified at the top of the channel. The material properties of copper were specified for solid regions. The flow and energy equations were discritized using the second order upwind scheme. The entire solution domain was meshed using hexahedral map elements. Grid sensitivity analysis was carried out and a computational grid of 20 x 60 x 200 cells (for half/symmetric channel) was found to be adequate. The channel width was meshed with successive ratio of 1.1 and height was meshed with successive ratio 1.05 while the channel length was meshed with a double successive ratio of 1.02. Total 960000 cells including the channel and the solid domain were used in the simulations. The simulations were carried out for adequate iterations to ensure acceptable convergence. The simulations were carried out over the Re range of 100 to 2000. The calculations of the local and the average Nusselt number was carried out using the similar procedure described in previous section (see Equations 2.9 to 2.14).

2.4. Results and discussion

2.4.1 Flow distribution in channels

The results of manifold flow simulation for total flow rate of 500 ml/min i.e. channel Re of 298 are shown in Figure 2.4. It can be seen from the Figure 2.4 that the variation of

flow rates flowing through different channels is quite small. For higher flow rates (up to Re 1000) the variation was found to be within ± 3 ml/min (not shown in Figure). The experimental pressure drop for central 20 mm length for channel 1, 10 and 15 is shown in Figure 2.4. It can be seen from the Figure 2.4 that all the three channels have same pressure drop (within experimental error). This also supports the conclusion drawn from the manifold simulations and indicates that the design of the manifold used in this work leads to reasonably uniform flow distribution.

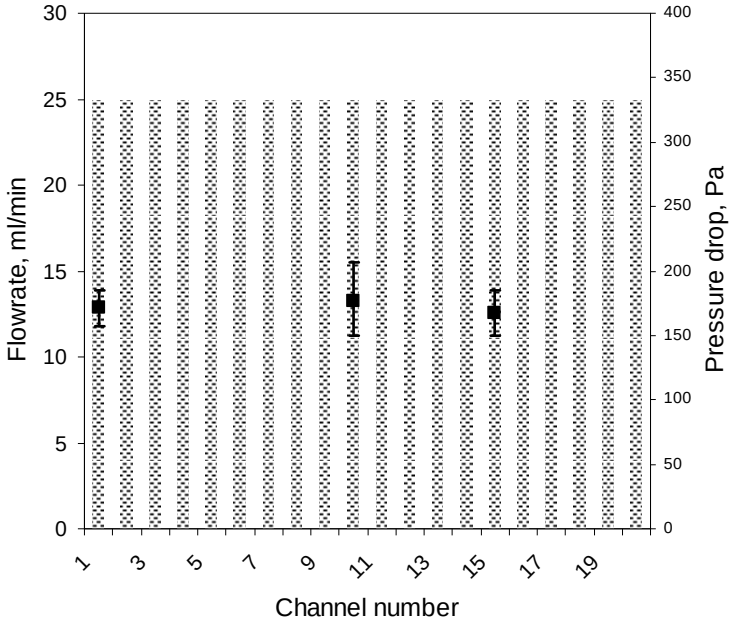

Figure 2.4: Flow distribution between channels (Re- 298), (⁘)CFD simulation of manifold for flow rate between channels, (■) Experimental Pressure drop in three different channels

2.4.2 Pressure drop and friction factor in minichannel

Experiments were carried out up to Re of 2300. The experimentally measured pressure drop data as a function of Re for middle channel (10^{th} channel) is shown in Figure 2.5. It should be noted that the pressure drop was measured across 20 mm length of the channel (Figure 2.1). Fully developed pressure drop for the channel length of 20 mm corresponding to aspect ratio of 1:3 was computed using Equation (2.15) for friction factor given by Shah and London (1978). It can be seen that the experimental pressure

drop is in good agreement with that of computed from Equation (2.15) i.e. pressure drop in fully developed flow. However the pressure drop across the channel deviates from the fully developed pressure drop at Re ~ 1250. The deviation of the pressure drop around Re of 1250 can be explained on the basis of required flow development length for a given Re. In the experiment as the fluid exits through the manifold it contains some velocity profile and this profile further quickly gets developed while traveling certain distance in the channel. Therefore the flow development length is different for the given Re than the corresponding required length if the inlet profile is flat i.e. in the present work even up to Re of 1200 the velocity profile in the channel remained close to developed one that the measured pressure drop over 20 mm is not different from the pressure drop for the developed velocity profile. In other words the deviation of the pressure drop from the developed one can be justified on the basis of the developing velocity profile above Re of 1200 that above/around this Re the length available is not sufficient for the complete development of the velocity profile.

The pressure drop predicted from the CFD model (simulated developing flow with uniform inlet velocity profile for channel length of 30 mm) across the middle 20mm channel length is also shown in Figure 2.5 for comparison. It can be seen that the pressure drop given for the case of the developing flow predicted by CFD model is higher than that of experimental pressure drop up to Re of 2300. This is because for a given Re the pressure drop for the developing flow/velocity profile will be more than that of the developed flow/velocity profile. As discussed earlier, in the experiment as fluid exits from the manifold the inlet profile is not flat/uniform for the range of the Re. Therefore the flow remains in between of the developing flow and developed flow in the entire range of Re studied in the present work.

In general the experimental pressure drop is in good agreement with that of the pressure drop given by the correlation for developed flow up to Re of 1250. In the developed pressure drop region similar results were found by Judy *et. al.* (2002), Mishan *et. al.* (2007) and Hrnjak and Tu (2007).

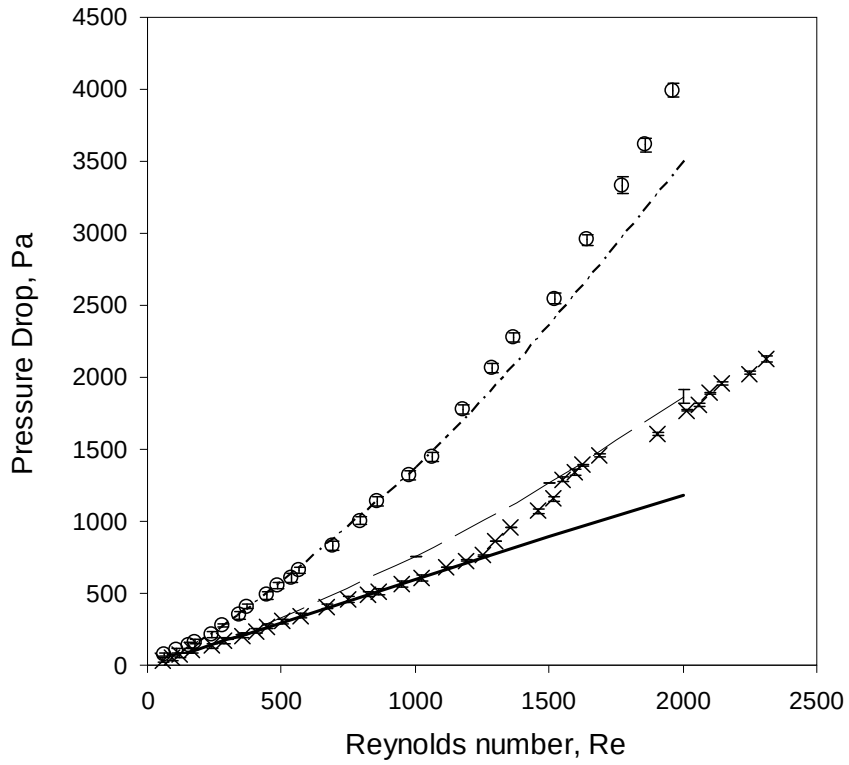

Figure 2.5: Pressure drop in channel and across manifold

(○) Pressure drop across manifold (data is with error bars), (x) Pressure drop in channel for length of 0.02 m (data is with error bars), (_____) Theoretical Pressure drop for channel length of 0.02 m for developed flow, (_ _ _) Pressure drop from CFD simulation for channel length of 0.02 m in case of developing flow, (_ . _ . _) Developing flow pressure drop for channel length of 0.03 m through CFD simulations

The pressure drop across the manifold was also measured as a function of Re (Figure 2.5). For lower Re (up to ~ 1250), the manifold pressure drop was found to be in agreement with the simulated developing flow pressure drop across channel of 30 mm. However, at higher Re, the predicted pressure drop across the manifold was found to deviate from the measured pressure drop. For instance, at Re of 2000, the manifold pressure drop is 1.15 times that of the simulated pressure drop across the channel. In general the design of the manifold was found to be good enough to achieve the equal flow distribution among the channels with only small increase in pressure drop.

The experimental pressure drop value over the length of 20 mm was used to calculate Poiseuille number *f*Re. The data is compared with the Equation (2.15) given by Shah and London (1978) for *f*Re in case of fully developed flow through rectangular channels.

$$f\mathrm{Re} = 24 \times \left(1 - 1.3553\alpha^{+} + 1.9647\alpha^{+2} - 1.7012\alpha^{+3} + 0.9564\alpha^{+4} - 0.2537\alpha^{+5}\right) \ldots\ldots. (2.15)$$

In case of rectangular channel, the *f*Re depends on the aspect ratio (Shah and London 1978). The comparison of the theoretical Poiseuille number (17.1) for developed flow with that of the experimental one is shown in Figure 2.6.

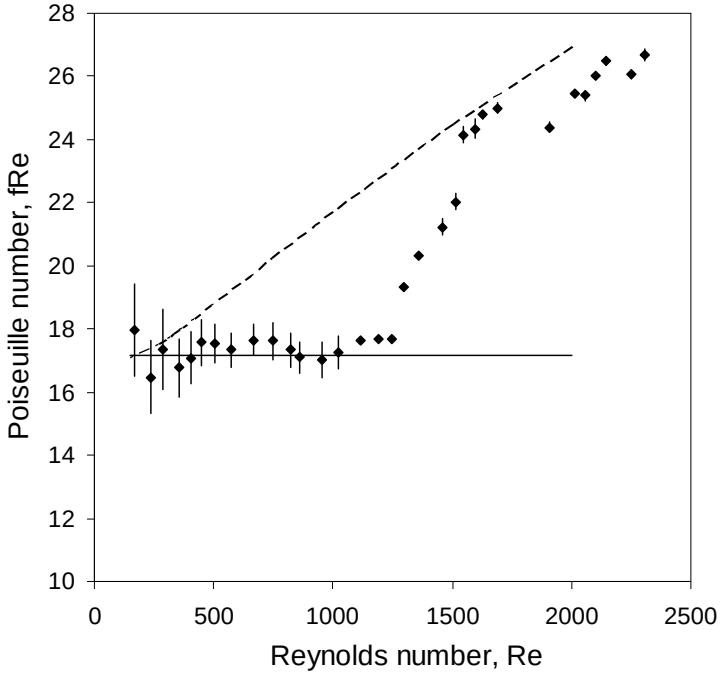

Figure 2.6: Poiseuille Number vs. Re for Middle Channel

(___) Theoretical *f*Re i.e. 17.1 for channel length of 0.02 m, (.....) Theoretical apparent *f*Re for channel length of 0.02 m

The Experimental *f*Re is in good agreement with that of calculated *f*Re for developed velocity profile within the experimental error up to Re equal to 1250. For Re above 1250, the measured values of *f*Re are higher than those of developed flow. This could be because the required length for flow development will be higher for higher Re. The

results shows that the velocity profile was not developed along the flow path that resulted in higher pressure drop for developing flow. Hence the *fRe* for developing flow will be higher than that of the developed flow. This means that in case of laminar flow in a channel there is a bound for *f*Re value i.e. *f*Re lies in between of developed flow and developing flow based on the nature of the velocity profile. The overall result shows that there is good agreement with that of the conventional theory as the present experimental data lies in the limits for developed and developing flow.

2.4.3 Axial heat conduction

Earlier, Tiselj *et. al.* (2004) described the importance of axial conduction in solid wall. In most studies the material used for the microchannel plate is silicon wafer, copper etc that ensured faster rate of heat conduction through the solid than the rate of convective heat transfer to the fluid from the solid wall. The role of axial heat conduction becomes significant for cases with non uniform heat distribution and results in localized supply of heat. In such cases the rate of convective heat transfer from wall to fluid are much higher because of higher local heat transfer coefficient (entrance region) than the heat transfer by conduction in axial direction. Due to non-uniform heat distribution, Tiselj *et. al.*(2004) showed reversal of temperature gradient between the wall and fluid with heat being transferred from fluid to channel. In the case of uniform distribution of heat in the spanwise direction, the fluid temperature rise is linear with axial distance. Almost linear rise was observed in the present work as shown Figure 2.7.

The measured profile deviates from linearity in the later part of the channel. This may be because the heater used in the present work is not fully extended up to the channel length (heater size across the channel length was 20 mm while the channel length was 30 mm). In the present work the heat flux into the test section was quite uniformly distributed in the spanwise direction. No temperature reversal or reversal in direction of heat transfer was observed as compared to the work of Tiselj *et. al.* (2004).

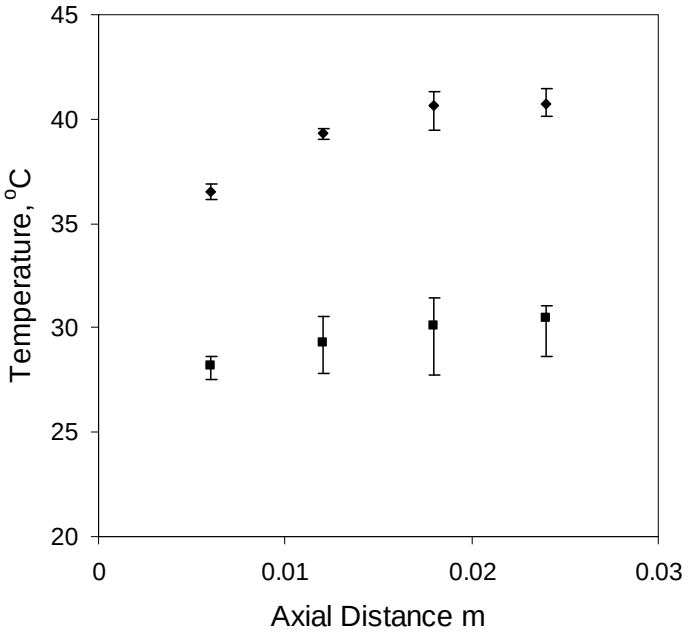

Figure 2.7: Temperature vs. Axial Distance (Re-208, Q: 175W)

(♦) Channel wall temperature, (■) Fluid temperature

2.4.4 Local heat transfer coefficient

The calculation of local heat transfer coefficient requires knowledge of the local mean bulk fluid temperature and wall temperature. The local mean bulk fluid temperature and wall temperature was experimentally measured for three values of Re (148, 208 and 445). For instance, the axial variation of local heat transfer coefficient for Re of 208, 256 with power supply of 175W and 100W respectively is shown in Figure 2.8a and 2.8b. However, for the case of Re of 256 with 100W power supply, local bulk mean fluid temperature was not measured. Instead the same was calculated from Equation (2.4). The local heat transfer coefficient decreases as fluid transverses from the entrance due to thermal boundary layer development. This ultimately results in a constant value for heat transfer coefficient independent of Re and Prandtl number (Pr) i.e. fully developed region. The experimental data is in good agreement with the result of the conjugate heat transfer analysis conducted in the present work. The CFD analysis is able to capture the key effects contributing to heat transfer process.

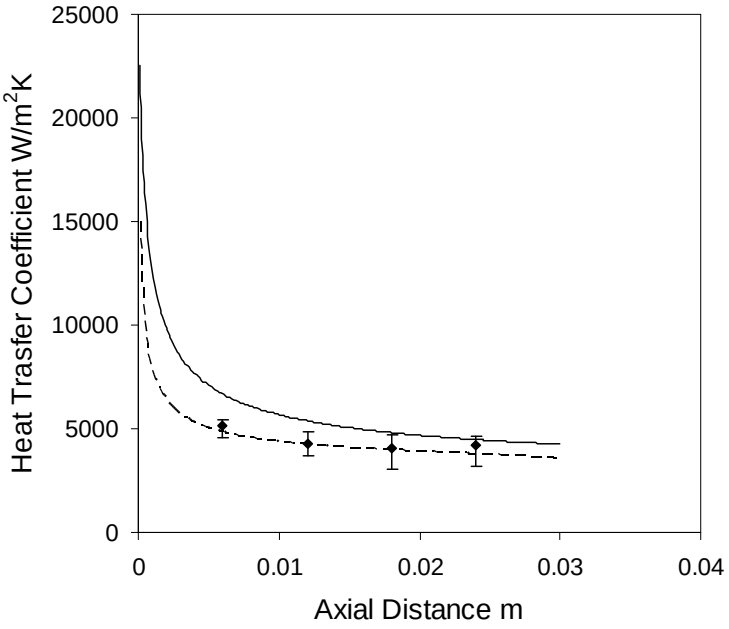

Figure 2.8 (a): Local Heat transfer Coefficient vs. Axial Distance (Q: 175W) (♦) Experimental data present work Re-208, (___) Prediction using Equation 2.16 from Lee *et. al.* (2006), (___) CFD simulation conjugate heat transfer thermally developing flow present work

Lee *et. al.* (2006) proposed a correlation for calculation of local as well as mean Nusselt number based on their CFD work. Equation (2.17) and (2.18) summarize their proposed correlations.

$$Nu_z = \frac{1}{C_1\left(z^*\right)^{C_2} + C_3} + C_4, \text{for} 1 \le \alpha \le 10, z^* < z^*_{th} \quad \text{..... (2.16)}$$

Where,

$C_1 = -3.122\times10^{-3}\,\alpha^3 + 2.435\times10^{-2}\,\alpha^2 - 2.143\times10^{-1}\,\alpha + 7.325$

$C_2 = 6.412\times10^{-1}$

$C_3 = 1.589\times10^{-4}\,\alpha^2 - 2.603\times10^{-3}\,\alpha + 2.444\times10^{-2}$, and

$C_4 = 7.148 - 1.328\times10^{1}/\alpha + 1.515\times10^{1}/\alpha^2 - 5.936/\alpha^3$

$$Nu_{ave} = \frac{1}{C_1 \left(x^*\right)^{C_2} + C_3} + C_4,\ for\ 1 \le \alpha \le 10, z^* < z^*_{th} \quad \text{.....(2.17)}$$

Where,

$C_1 = -2.757 \times 10^{-3}\,\alpha^3 + 3.274 \times 10^{-2}\,\alpha^2 - 7.464 \times 10^{-5}\,\alpha + 4.476$

$C_2 = 6.391 \times 10^{-1}$

$C_3 = 1.604 \times 10^{-4}\,\alpha^2 - 2.622 \times 10^{-3}\,\alpha + 2.568 \times 10^{-2}, and$

$C_4 = 7.301 - 1.311 \times 10^{1}/\alpha + 1.519 \times 10^{1}/\alpha^2 - 6.094/\alpha^3$

The prediction from the above equations is also shown in the Figure 2.8 (a) for comparison. The data in Figure 2.8 (a) is in agreement with the predictions of Lee *et. al.* (2006) in a qualitative manner. However the model for local heat transfer coefficient developed by Lee *et. al.* (2006) does not account for the temperature distribution in solid wall of the channel i.e. effect of conjugate heat transfer. Therefore the effect real thermal boundary conditions at the inside wall resulting due to conjugate heat transfer is not accounted in the model. This could be the reason for the small deviation from the experimental data.

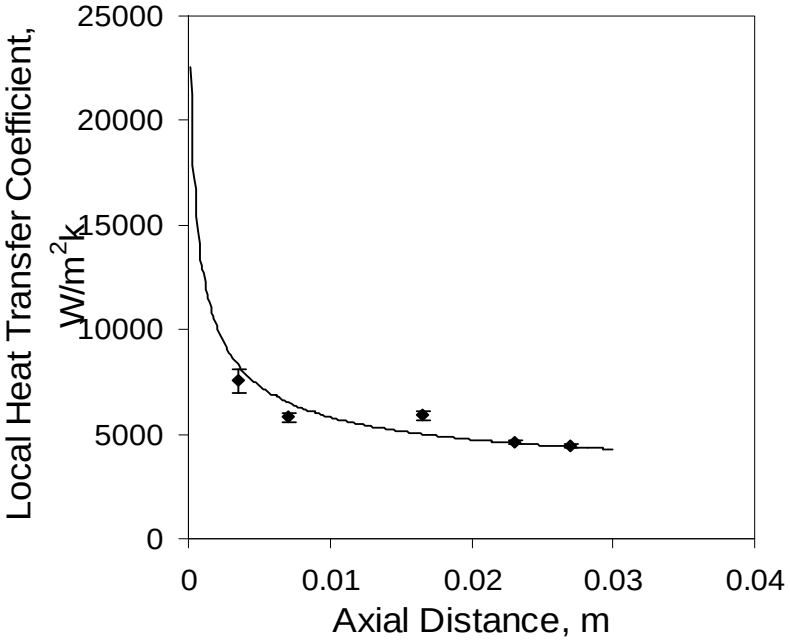

Figure 2.8 (b): Local heat transfer coefficient vs Axial distance, m (Q: 100 W) (♦)Experimental data present work Re-256, (—) Data using Equation 2.16 from Lee. *et. al.*(2006)

Figure 2.8 (b) shows the results of the local heat transfer coefficient vs. the axial distance for the Re 256 with 100W power supply. It can be seen that the data in Figure 2.8 (b) is well predicted by the Lee *et. al.* (2006) model (Equation 2.16). This is because in the experimental analysis the liquid temperature is related to axial length using Equation 2.4 (see section 2.2.4) rather than actually measuring the local bulk fluid temperature. Therefore the liquid bulk temperature used in calculations was not the true local mean liquid bulk temperature (as the liquid temperature is not measured for the data in Figure 2.8 (b)). Equation 2.4 assumes linear variation of the fluid temperature in the axial direction. However even the constant heat flux condition is maintained well to the certain extent the fluid temperature does not really varies linearly with axial distance in certain cases. This can be seen from the Figure 2.7 where the fluid temperature is measured by using thermocouple. Therefore a quantitative agreement between the experimental data and the Lee *et. al.* (2006) correlations (Figure 2.8 (b)) is due to the assumption of the constant heat flux at the inside channel wall or applicability of Equation 2.4 i.e. neglecting the effect of conjugate heat transfer.

2.4.5 Average Nusselt number

The average heat transfer coefficient as function of Re for 100W input power supply is shown in Figure 2.9. Shah and London (1978) summarized the data on heat transfer in laminar flow by numerical analysis for thermally developing flow presented by Wibulswas (1966). It is evident that Nusselt number increases with increase in Reynolds number with large deviations at lower Re. For sake of comparison, the predictions from CFD model with thermally developing and simultaneously developing flow and the correlation of Lee et al. (2006) (Equation 2.17) are also shown in Figure 2.9. As expected the average Nusselt number flow for simultaneously developing flow is more than that for thermally developing flow. The experimental data does not directly overlap with any of the cases but qualitatively is in good agreement with the predictions of the present CFD work. The Lee *et. al.* (2006) correlation and the numerical results of Wibulswas (1966) is also able to predict the average Nusselt number to the certain extent. The numerical predictions of Wibulswas (1966) and Lee et al (2006) does not account for

effect of conduction in solid i.e. conjugate heat transfer. No deviation from the conventional correlation/numerical data is observed in the present work.

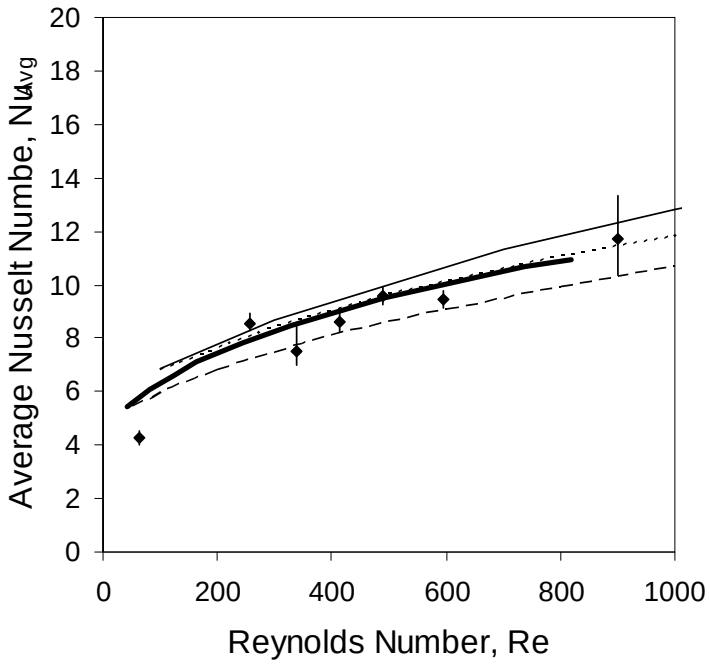

Figure 2.9: Average Nusselt Number vs. Re (Q: 100W)

(♦) Experimental data present work, (___) CFD analysis simultaneously developing flow present work, (_____) CFD analysis thermally developing flow present work, (_ _) Predictions using Equation 2.18 from Lee *et. al.*(2006) (▬) Wibulwas (1966) predictions from Shah and London (1978)

2.5. Conclusions

Fluid flow and heat transfer was investigated experimentally in rectangular minichannels of D_h 1.05 mm with water as a working fluid. The experimental results were compared with the published results and the present CFD simulations. Following are the conclusions:

1. Experimental as well as CFD results obtained here indicate that the design of the manifold used in the present work generates uniform distribution of flow (within

±3%) without adding significant penalty to pressure drop (<15% of that of channel pressure drop).

2. The Poiseuille number calculated from the measured pressure drop is in good agreement with the published value of 17.1 for developed flow up to Reynolds number of 1250. For higher Re values (Re > 1250), the value of Poiseuille number is higher than 17.1 due developing flow nature in the channel over a given length. The observed higher Poiseuille number is however less than that calculated from CFD with flat velocity profile at the inlet.
3. Heat conduction plays crucial role in determining effective heat transfer in minichannels. Simulations carried out with conjugate heat transfer led to good agreement with the experimental data.
4. Experimental data on the local heat transfer coefficient show that it decreases with increase in channel length. As expected, the average Nusselt number increases with increase in Reynolds number. The experimental data obtained in this work is in good agreement with the published results. CFD simulations agree with the experimental data.

The present results highlight significance of the developing velocity profile and conjugate heat transfer in small channels. The present work confirms that the conventional theory/models used for macro-scale systems are also applicable to micro-channels. This work will be useful in improving designs of manifold and parallel microchannel systems.

CHAPTER 3

FLOW AND HEAT TRANSFER IN SERPENTINE CHANNELS

In the present work, flow and heat transfer experiments were carried out with a serpentine channel plate comprising of 10 channels in series. Pressure drop and heat transfer coefficients were experimentally measured. Flow and heat transfer in the experimental set-up were simulated using CFD models to understand the mechanisms responsible for performance enhancement. The CFD methodology thus developed was applied to understand the effect of various geometrical parameters on heat transfer enhancement. For this purpose a new and more appropriate criteria was defined for evaluation of heat transfer performance (heat transfer per unit pumping power) thus ensuring due considerations to required pumping power. The effect of geometrical parameters and the corresponding mechanisms contributing for enhancement are discussed briefly. Based on the results, a design map showing different serpentine channels heat transfer enhancement with pumping power was developed for Reynolds number of 200 which will be useful for further work on flow and heat transfer in serpentine channels.

3.1 Background

In the recent years there is growing interest among the researchers for developing different microreactors systems due to several benefits offered over conventional systems. Many applications of several tubular microreactors can be found in Jensen (2001), Halder *et al*. (2007) etc. The flow rates of the reactants that are used in microreactors are also quite low therefore the flow conditions inside the reactor remains laminar. However in laminar regime, a breaking of fluid compartments cannot occur due to the high viscous forces. This causes the development of the boundary layers (velocity as well as thermal) in a channel resulting in limiting values of transport coefficient as velocity and temperature profile gets developed e.g. in case of pipe flow with constant wall temperature the value of Nusselt number becomes 3.66 which is independent of L, Re and Pr. This is due to the development of thermal boundary layer along the length. One way of overcoming this limitation is breaking this boundary layer along with radial mixing in the pipe. The use of active mixers and the passive mixers were the few choices available for this purpose. Active mixers use external forces or power dissipations to achieve the mixing however the passive devices does not involves either of this except the use of pump for delivering the fluid. Even though the mixing in active mixers is much efficient the use/incorporation of such devices in microreactor devices is a difficult task. In such cases passive devices finds scope in microreactors. Several authors are looking for developing passive micro scale devices that can transport and mix the small fluid volumes efficiently. Serpentine channel configurations are one of the choices that are becoming more popular among the researchers in last few years due to several benefits offered by them. These benefits include compact size, better mixing, higher heat and mass transfer coefficients than straight channels etc.

The serpentine channel consists of a bend section with repeating units. Figure 1 (a) shows simple schematic of the serpentine channel. A typical serpentine configuration can be classified in two broad categories 1) Smooth bend and 2) Sharp bend. Figure 1 (b) shows the serpentine configuration with the smooth bends whereas the configuration with sharp bends is shown in Figure 1(c). A typical serpentine channel as shown in Figure 1(a) is specified using the following parameters a) bend angle (θ) b) straight length before bend

(*L*) or distance between the bends (*2L*) c) radius of curvature at bend section (*Rc*) d) amplitude of the serpentine configuration (*A*). Based on the combinations of these four parameters number of different serpentine configurations can be designed. The performance in terms of pressure drop and heat transfer is much different for different serpentine configurations. Therefore in such cases the selection of the parameter becomes a difficult task. Few limiting cases of the serpentine configurations are sinusoidal channel, saw tooth configuration, etc as shown in Figure 1(b) and (c) respectively.

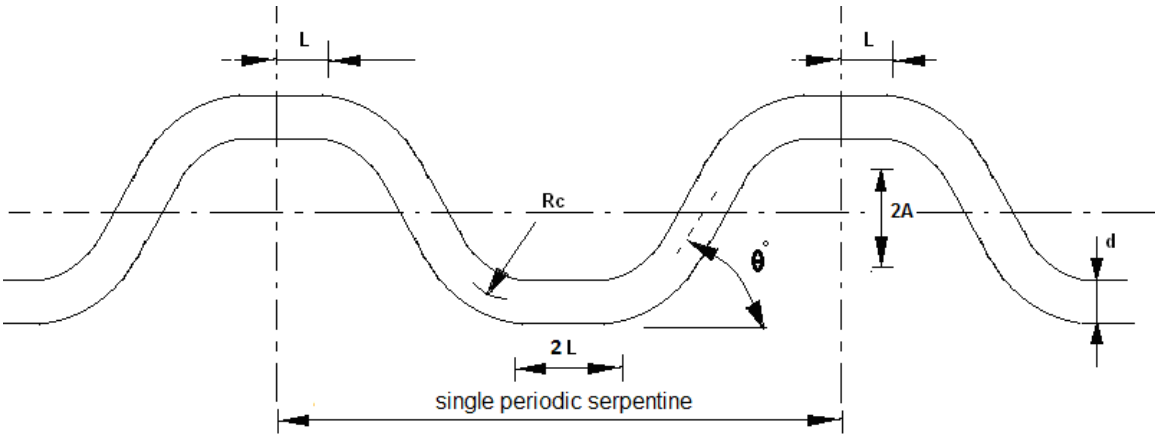

Figure 3.1 (a): Schematic of general serpentine channel

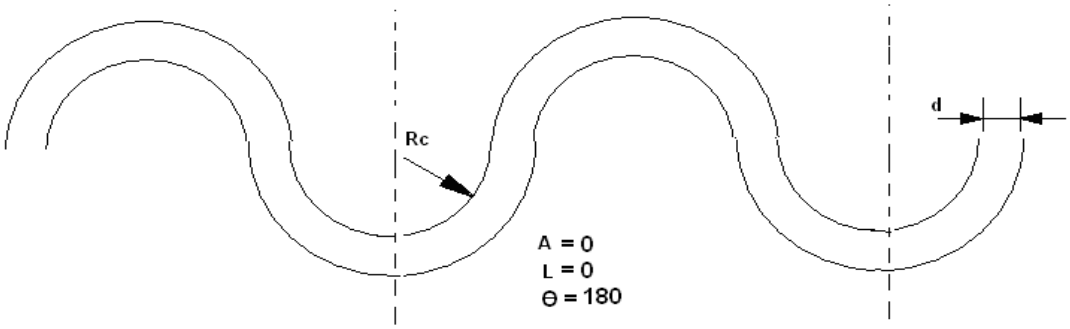

Figure 3.1 (b): Schematic of sinusoidal serpentine channel

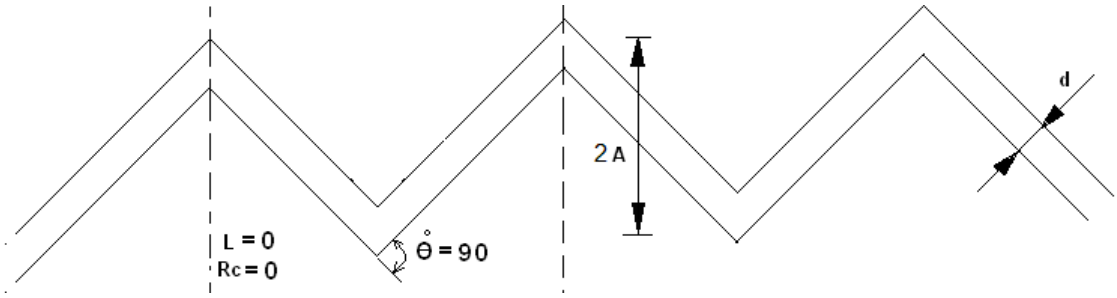

Figure 3.1 (c): Schematic of saw-tooth configuration serpentine channel

One of the key issues concerning is which serpentine configuration gives the maximum heat transfer performance? Based on general knowledge of fluid mechanics and heat transfer one may conclude that the configuration having sharp bend of 90^o will give highest heat transfer enhancement. However at the same time the corresponding pressure drop (power dissipation) to achieve this enhancement will also maximum. Therefore the next question that arises is can there be any geometry that gives better performance (need not be maximum) in heat terms of transfer with less extra pressure drop requirement? For this purpose the effect of various geometrical parameters on heat transfer performance need to be studied thoroughly. In this context some of the published work is briefly reviewed here. In light of this review; attempt is made to quantify this issue computationally in the present work. Computational model and obtained results are discussed in the following sections.

3.2 Literature review

Laminar flow and heat transfer in square serpentine channels with right-angle turns were numerically studied by Chintada *et al.* (1999). The temperature field was solved for the uniform-wall-heat-flux boundary condition. Periodically fully developed flow and heat transfer fields in serpentine channels were solved for different geometry parameters, for different Reynolds numbers, and for two different Prandtl numbers (for air and water, respectively). The enhancement of the heat transfer mechanism was explained by studying the plotted flow-field velocity vectors in different planes. The heat transfer performance of serpentine channels was better than that for straight channels for $Pr > 7.0$ and was worse than that for straight channels for $Pr < 0.7$.

The effect of the geometric parameters and Reynolds number on the flow pattern and the pressure loss characteristics in serpentine channels was investigated by Maharudrayya *et al.* (2004). The authors also developed three regime correlations to predict excess bend coefficient as a function of Reynolds number, curvature ratio, aspect ratio and the space length between the bends. However the definition of the laminar flow in the same study

was not made clear as the contributions from the secondary flow or inertial effects was significant.

Rosaguti *et al.* (2004) studied fully developed flow and heat transfer behaviour in circular serpentine channels for fixed geometry with L/D 4.5 and Rc/d equal to 1 for Reynolds number up to 200. The authors found enhancement in heat transfer and reduction in pressure drop with increase in L/d for Rc/d of 1 and Prandtl number of 6.13. The authors also found absence of flow separation.

Rosaguti *et al.* (2005) investigated fully developed laminar flow and heat transfer behavior in serpentine circular channel using computational fluid dynamics. The authors investigated effect of wavelength, channel diameter and radius of curvature or curvature ratio on the performance of serpentine channel. The authors found that the flow becomes unsteady for Reynolds number above 200. Constant wall heat flux and constant wall temperature boundary condition with Prandtl number 0.7 to 100 was used in their study. According to them Dean vortices produces significant heat transfer enhancements relative to flow in straight pipe with the greater effect at higher Pr with less increase in pressure drop.

Geyer *et al.* (2006) investigated fully developed laminar flow and heat transfer behavior in serpentine channels with a square cross-section using computational fluid dynamics. Studies were performed up to Re 200. The effect of geometric configuration were examined for Re 110, $0.525<Rc/d<2$ and $3.6<L/d<12$ (where d was the side length of the square section, Rc was radius of curvature of the serpentine bends, and L was the half wavelength of the serpentine path). Simulations were carried out at (Pr 0.7, 6.13 and 100) constant wall heat flux (H2 boundary condition) and constant wall temperature (T boundary condition). The results showed that the heat transfer enhances with increases in Re with small pressure drop penalty. Whereas the heat transfer enhancement reduces with the reduction in the curvature ratio.

Rosaguti *et al.* (2006) investigated fully developed laminar flow and heat transfer behavior in semicircular periodic serpentine channel using CFD. The authors studied the effect of wavelength, diameter, and curvature of bends for Reynolds number up to 450 with constant wall heat flux and constant wall temperature boundary condition. The authors also studied effect of Prandtl number from 0.7 to 100. High rates of heat transfer and low pressure loss were found relative to fully-developed flow in a straight pipe, with heat transfer enhancements greater than 10 for a Prandtl number of 100.

Hsieh and Her (2007), investigated flow and heat transfer for developing laminar flow in micro direct methanol fuel cell with serpentine flow fields. The authors reported variation of average Nusselt number and friction factor with the Peclet number. The authors also developed correlation based on their data to predict the average Nusselt number and friction factor as a function of Peclet number and Reynolds number respectively.

Xiong and Chung (2007) investigated flow characteristics of pressure-driven de-ionized water experimentally in straight and serpentine micro-channels with miter bends. The micro-channels had rectangular cross-sections with hydraulic diameters of 0.209 mm, 0.395 mm and 0.549 mm. For serpentine micro-channels, the additional pressure drop can be divided into two regions. The first region was of Re < 100 where no circulation exists. The other region was of Re larger than some value in 100–200 where circulation appears and develops at the inner and outer wall of the bend. The additional pressure drop increases sharply with Re number. The bend loss coefficient was observed to decrease and tend to be a constant with decreasing Re number.

Fully developed flow and heat transfer in semi circular trapezoidal serpentine channel was investigated by Geyer *et al.* (2007) using CFD. The authors studied effect of wavelength, curvature ratio, amplitude and length of the straight portion on the performance of the serpentine channel till Reynolds number up to 400. The authors used constant wall heat flux and constant wall temperature boundary condition with Prandtl number of 6.13. The authors have also given consideration to the stackability of channels

on a plate. They found swept zigzag pathway provides the greatest intensification of heat transfer in a multi-channel plate structure.

Fully developed laminar flow and heat transfer in three-dimensional, streamwise-periodic sinusoidal channels with circular and semi-circular cross-sections was studied by Roasguti *et al.* (2007) using CFD. The authors have investigated the effect of Reynolds number (5<Re<200) and amplitude to half wavelength ratio (0.222<A/L<0.667) on heat transfer enhancement and pressure drop for steady, incompressible, constant property, water (Pr 6.13) flows in geometries with L/d=4.5 for the constant wall heat flux (H2) and constant wall temperature (T) boundary conditions. The authors found that the heat transfer enhancement exceeds the relative pressure-drop penalty by factors as large as 1.5 and 1.8 for the circular and semi-circular cross-sections, respectively.

The fluid circulation taking place at the bends section due to secondary flow helps to increase the rate of heat transfer by increasing the transfer coefficient. The objective of the present work consists of development of CFD methodology to understand the effect of various geometrical parameters on the heat transfer performance of serpentine channel. In the various reported literature the following criteria's were used to analyze the performance of the serpentine channel.

1) $\frac{Nu_{serpentine}}{Nu_{straight}}$ and $\frac{f\,\mathrm{Re}_{serpentine}}{f\,\mathrm{Re}_{straight}}$ …….[Chintada *et al.* (1999), Rosaguti *et al.* (2004), Rosaguti *et al.* (2006), Rosaguti *et al.* (2005), Geyer *et al.* (2006), Geyer *et al.* (2007), Rosaguti *et al.* (2007)]

2) $\frac{Nu_{serpentine}}{Nu_{straight}}$ and $\frac{f_{serpentine}}{f_{straight}}$ and $\frac{\frac{Nu_{serpentine}}{Nu_{straight}}}{\frac{f_{serpentine}}{f_{straight}}}$ …[Chintada et.al. (1999), Geyer *et al.* (2006), Rosaguti *et al.* (2007)]

In all above criteria's the total length of the channel was not kept constant in all the configurations used by above authors. The average Nusselt number and the pressure drop

both depend on the length. Therefore the utility of the above mentioned criteria becomes limited. Along with this, these studies do not directly give information about the total heat transfer rate and pressure drop for the given configuration. For this purpose more general and appropriate criteria need to be developed which will give performance enhancement in terms of heat transfer rate and total pressure drop/pumping power. For this purpose following additional criteria was proposed.

$$Performance\ \ enhancement = \frac{(Q/PP)_{Serpentine}}{(Q/PP)_{Straight\ \ channel}} \quad \text{..... (3.1)}$$

In the above criteria the required pumping power was taken into a consideration that depends on the total length of the channel. In the present study the total length of all serpentine configurations was kept constant therefore the denominator (of Q/PP) remains fixed value. Thus above criteria gives a guideline for selecting the configuration of the serpentine that can be a better choice in terms of heat transfer enhancement per unit required pumping power over a straight channel. The performance investigation of the serpentine channel was carried out by CFD analysis. Experiments were performed for measurement of pressure drop and heat transfer coefficient on the hair-pin like serpentine geometry designed in house to validate the present CFD methodology. The standardized CFD methodology was then applied to understand the effect of various geometrical parameters of the serpentine channel on heat transfer performance.

3.3: Flow and heat transfer in 1 mm x 1.5 mm x 46 mm serpentine channel to evaluate the CFD methodology

3.3.1 CFD methodology

All Numerical analysis was carried out by using commercial code of Fluent 6.3.36 and grids were generated using Gambit 2.4. The geometry used in present CFD analysis consists of rectangular single serpentine channel having dimensions 1 mm x 1.5 mm x 46 mm. The configuration of the present serpentine channel involves smooth bend having

bend angle of 180^{o}, radius of curvature of 1.5 mm, zero straight length portion between bends i.e. case 3. The computational domain is shown in Figure 3.2. The entire domain was meshed using hexahedral map elements. Grid sensitivity analysis was carried out and a computational grid of 30 x 30 x 500 cells (single periodic serpentine) was found to be a better choice. The channel width and height was meshed with double successive ratio of 1.1 while the channel length was meshed with a double successive ratio of 1.02. Total 450000 cells were used in simulation.

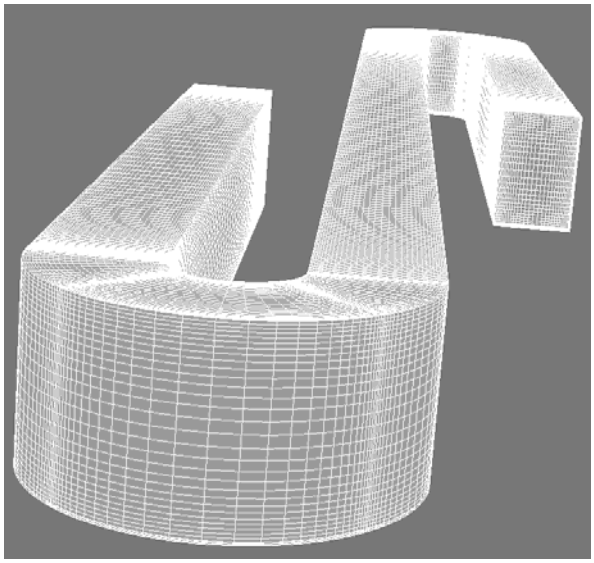

Figure 3.2: Computational domain in section 3.3

Steady state flow and heat transfer solutions have been found for fully-developed laminar flow in the Re range of 133 to 666. The physical properties of the working fluid were constant with Prandtl number (Pr) of 6.97 (i.e. Water). The solutions were obtained for the periodic case which represents periodically developed conditions in velocity as well as in temperature. This approach benefits in design procedure e.g. the pressure drop of lets say for 10 serpentine channels in series can be directly calculated by multiplying single periodic channel pressure drop to the number of channels in series. Therefore numbering up strategy for design can thus be utilized easily. The inlet temperature of the fluid was kept at 300K. The flow and energy equations were discretized using second order upwind scheme. The under-relaxation factor of 0.2 and 0.9 was used for flow and energy equations respectively. The standard scheme was used for pressure discretization.

The SIMPLE algorithm was employed for velocity–pressure coupling. At first only flow field was solved completely. In the next step the converged flow field was freezed and only energy equation for the fluid was solved. The convergence for the flow equation was continuity $<1x10^{-9}$ and energy $<1x10^{-10}$ was used.

As mentioned earlier the simulations were carried using constant wall temperature boundary condition of 373 K. In this case the heat transferred from the wall to fluid becomes the calculated parameter which depends on the hydrodynamics of the fluid inside the channel. The total heat transfer from the wall to fluid (Q) over a heat transfer area (A_h) was obtained from the enthalpy change in working fluid. With these quantities, the overall convective heat transfer coefficient, h_{avg}, and Nusselt number, Nu was evaluated using the following Equation 3.2 and 3.3 respectively as given below.

$$h_{avg} = \frac{Q}{A_h \times \left[\frac{(T_w - T_{in}) - (T_w - T_{out})}{\ln \frac{(T_w - T_{in})}{(T_w - T_{out})}} \right]} \quad \text{..... (3.2)}$$

$$Nu = h_{avg} \times \frac{d}{k} \quad \text{..... (3.3)}$$

The total pumping power per serpentine can be calculated from the pressure drop as

$$Pumping\ Power\ (PP) = \text{Pr}essure\ Drop\ (\Delta P) \times Volumetric\ Flowrate\ (Q_f) \quad \text{..... (3.4)}$$

For comparison the numerical simulations were also carried out for the case of straight channel having similar dimensions as that of serpentine channel under the conditions of thermally developing flow. In this case the inlet boundary condition for the momentum equation consists of a developed velocity profile for the channel aspect ratio of 1.5. The rest of the simulation methodology was similar as discussed above.

3.3.2. Experimental setup and procedure

3.3.2.1 Test piece

The experimental test piece consisted of a copper block having dimensions of 34 mm x 30 mm x 5 mm. On this block, 10 serpentine channels in series were machined on one side using milling technique. The dimensions of single serpentine channel were 1 mm wide and 1.5 mm deep and 46 mm in length with accuracy of ±10 µm. Figure 3.3 shows the image of the serpentine plate. The top portion of the geometry was closed by 8 mm thick acrylic plate which was provided with 1 mm holes for arrangement of stainless steel needles to measure pressure as well temperature. For inlet and outlet 1 mm stainless steel needles were fitted at the ends. . For heat transfer studies, the test piece was heated using A.C. strip heater with power/heat input controlled by the dimmerstat. The power supplied to cartridge heater was measured by Digital Wattmeter (Conzerve make). The thermocouples of size 0.12 mm were placed inside channel and at copper surface to measure the temperature of the channel fluid as well as channel wall as shown in Figure 3.

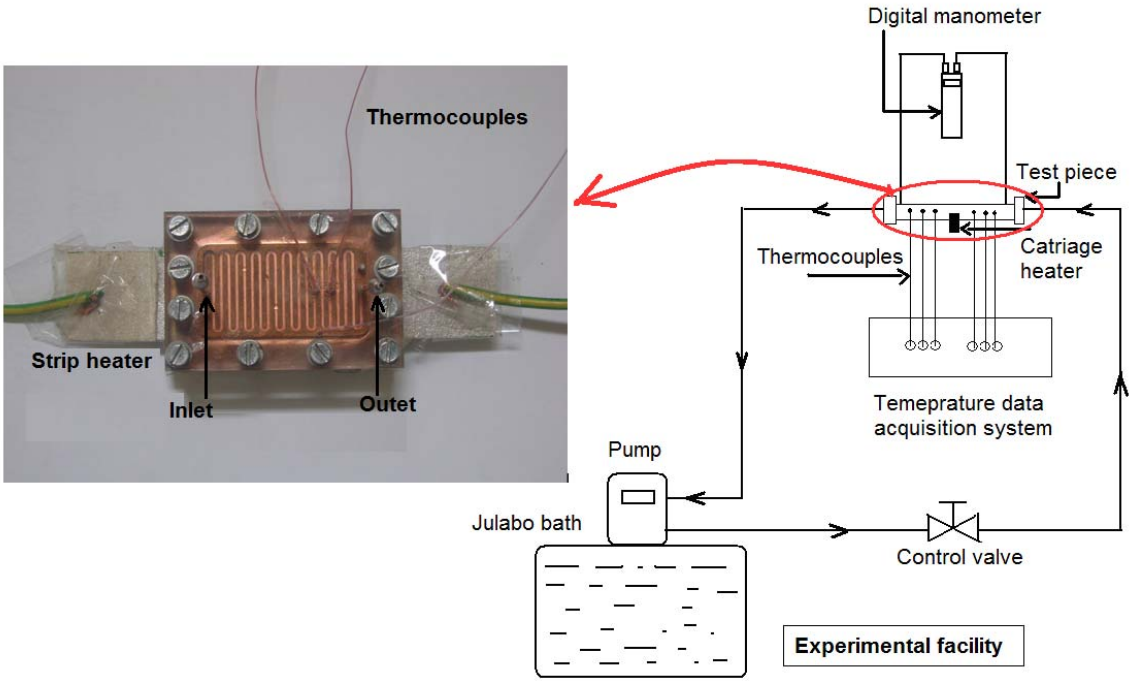

Figure 3.3: Experimental facility and test piece

3.3.2.2 Measurement apparatus and procedures

The fluid was pumped using the pump facility provided on the standard Julabo bath. The flow through the geometry was controlled by using the control valve. The flow rates used in this study were in the range of 10 ml/min to 50 ml/min that was measured by collecting the volume of liquid in specific time. Figure 3 also shows the schematic of the experimental setup. For pressure drop measurements two holes of diameter 1 mm were drilled on the top polycarbonate cover exactly on the top of the channel with 46 mm axial distance (single serpentine) between them. By this way the pressure drop over only single serpentine channel was measured. Through these holes two SS tubes/needles having internal diameter of 0.8 mm were inserted so that the tube will be inline with the top surface of the channel. These two tubes were connected to the digital manometer having sensitivity of 7 Pa and accuracy of $\pm$ 0.3% of full scale. When fluid moves through the channel the frictional pressure drop over the 46 mm length was directly measured by the digital manometer. For heat transfer studies the temperatures were recorded using the data acquisition at scanning rate of 1 s within accuracy of ± 0.5 ^{o}C. Two thermocouples (Omega, J Type, Accuracy: ±0.5 ^{o}C) of size 0.076 mm were placed on the serpentine channel wall/fin to measure the wall temperature along the length of the channel. The water temperature in the single serpentine channel was measured by using two thermocouples placed in channel so that it gives information about the heat transferred to the water in a single serpentine channel. The magnified region of the mini-channel plate shown in Figure 3.3 illustrates the thermocouple locations to measure the temperature of channel wall and fluid. For testing procedure, the Julabo pump was turned on at flow rates from 10 ml/min to 50 ml/min. The electrical power to the heater was adjusted to a desired level by a variable voltage of the dimmerstat. After allowing the system to establish steady state, flow rate, temperatures were measured.

3.3.2.3 Data reduction

The collected pressure drop data was used to calculate effective friction factor using the following equation:

$$\Delta P = \frac{2 f L \rho V^2}{D_h} \quad \text{.....} \quad (3.5)$$

The total energy given by steam condensation was getting distributed in two parts. A) heat supplied to water (Q1) B) heat loss to the environment (Q2). The heat taken by the water was calculated as:

$$Q1 = \dot{m} Cp (T_{f,out} - T_{f,in}) \quad \text{..... (3.6)}$$

The heat loss to the environment (part B) was calculated using the difference between the heat supplied which was measured by wattmeter and heat taken by water. The overall heat loss to the environment was found to be less than 5-10%. More than 100 temperature data points were used in calculations for every flow rate.

At the bottom of the test piece the strip heater provides uniform heat flux over the length of the channel. Since the thermal conductivity of copper is very high, at certain finite thickness of the test piece, the channel internal wall temperature becomes uniform along the length of the channel due to conduction inside the copper. Detailed information on this phenomenon can be found in Shah and London (1978). Measurement of channel inside wall temperature was difficult task therefore in the present the work the channel wall temperatures were measured at the top surface of channel wall. Since the thermal conductivity of copper is very high, we assumed that at a given cross-section the side-wall temperature of the micro-channel did not differ significantly from the channel bottom temperature. Therefore the thermal boundary condition for the wall becomes as constant wall temperature.

The overall heat transfer coefficient was calculated from Equation 3.7 given below:

$$q1 = \frac{Q1}{(W \times L + 2 \times H \times L)_{\text{sin}\,gle\ serpentine}} = h \times \left(\frac{(T_{w,in} - T_{f,in}) - (T_{w,out} - T_{f,out})}{\ln \frac{(T_{w,in} - T_{f,in})}{(T_{w,out} - T_{f,out})}} \right) \quad \text{.....} \quad \text{(3.7)}$$

The mean Nusselt number was calculated as:

$$Nu = \frac{h D_h}{k} \quad \text{..... (3.8)}$$

3.4 CFD analysis in 2mm x 2mm x 100 mm serpentine channel to understand the effect of various geometrical parameters

3.4.1 Computational methodology

In the present work the periodic serpentine geometry consists of a square channel of 2 mm x 2 mm in cross section with periodic length of 100 mm. The effect of bend angle (θ), straight length before bend (L) (i.e distance between the bends/2) and radius of curvature (Rc) on overall heat transfer enhancement over a straight channel was studied. The range of the parameters under the study was given in the Table 3.1:

The individual total length of all of the above serpentine geometries listed in Table 3.1 is 100 mm that kept constant in all serpentine configurations. Once the angle was defined the amplitude of the serpentine gets specified because of the constraint of the total length of 100 mm. The sample calculation is shown in Appendix I.

The sample computational domain for one of the serpentine configuration of case 3 is shown in Figure 3.4.

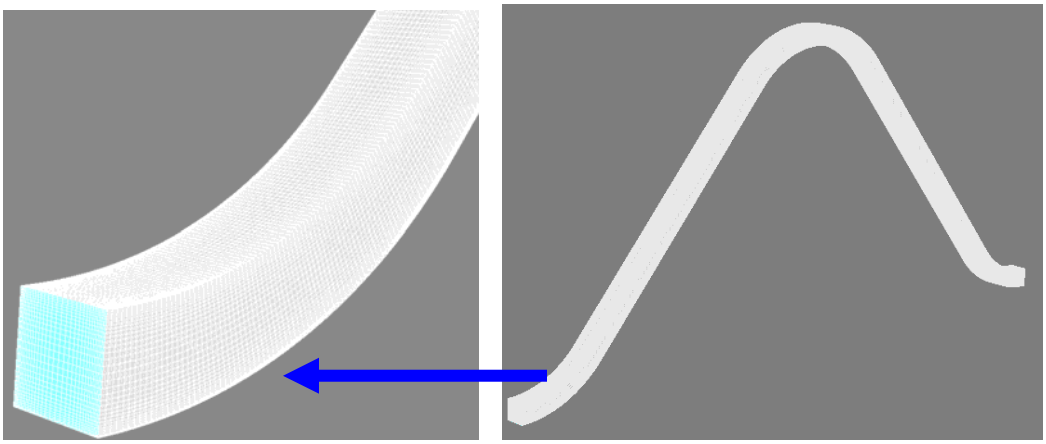

Figure 3.4: Example of computational domain in section 3.4

The entire domain was meshed using hexahedral map elements. Grid sensitivity analysis was carried out and a computational grid of 30 x 30 x 720 cells (single periodic serpentine) was found to be a better choice. The channel width and height was meshed with double successive ratio of 1.1 while the channel length was meshed with a double successive ratio of 1.02. Total 648000 cells were used in simulation. The rest of the simulation procedure was same as mentioned in section 3.3.1. Following four criteria were used to compare or analyze the effect of various geometrical parameters of serpentine channel.

Criteria 1	Criteria 2	Criteria 3	Criteria 4
$\frac{(PP)_{Serpentine}}{(PP)_{Straight\ channel}}$	$\frac{(Q)_{Serpentine}}{(Q)_{Straight\ channel}}$	$\frac{(Q/PP)_{Serpentine}}{(Q/PP)_{Straight\ channel}}$	$\frac{(Nu/f\,\mathrm{Re})_{Serpentine}}{(Nu/f\,\mathrm{Re})_{Straight\ channel}}$

Where,

Q: Heat transferred, PP: Pumping power

3.5 Results and discussion

3.5.1 Evaluation of CFD methodology with experimental data

Figure 3.5 (a) shows the results of pressure drop predicated using CFD simulation for the present serpentine channel configuration used in the experiments. The theoretical pressure drop for fully developed flow in case of straight channel is also plotted in the Figure 3.5 (a) for comparison. The theoretical pressure drop in case of incompressible laminar flow for square channel was calculated by using fRe = 14.1 (Shah and London 1978). It can be seen from the Figure 3.5 (a) that the pressure drop for serpentine channel is more than that of straight channel. The difference of pressure drop between serpentine channel and the straight channel is more at higher Re compared to that at lower Re. Serpentine channel pressure drop is almost 1.28 times than that of straight channel for Re of 130. The same increases to 1.98 times for Re of 660. For comparison the experimental data of pressure is also plotted in the same Figure 3.5 (a). The predicted pressure drop from the CFD simulations agrees well with the experimental value.

Figure 3.5 (b) shows the results of heat transfer coefficient predicated using CFD simulation vs. Re for serpentine channel used in the experiments. The theoretical heat transfer coefficient for fully developed flow in case of straight channel is also plotted in the Figure 3.5 (b) for comparison. The theoretical heat transfer coefficient in case of incompressible laminar flow for square channel can be calculated by using Nu = 2.7 (Shah and London 1978).

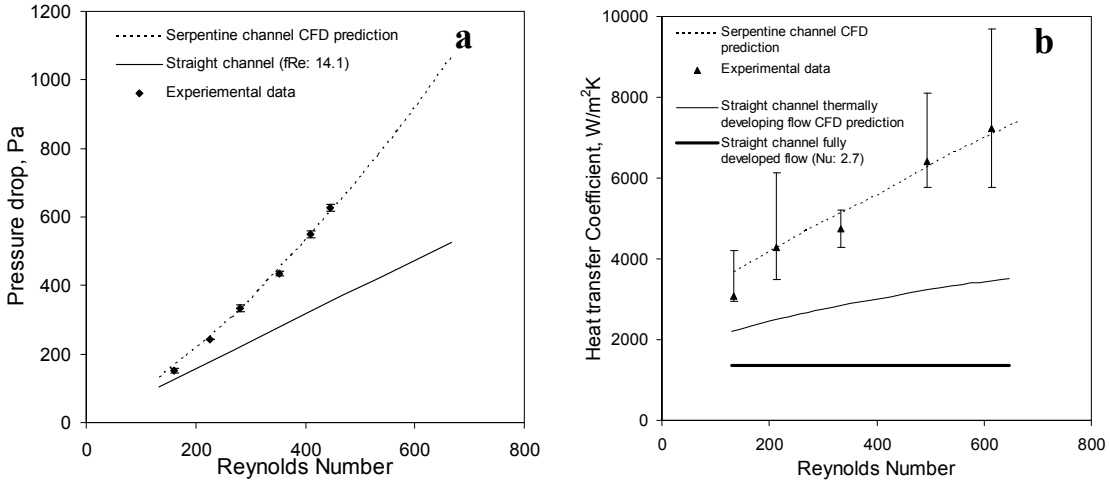

Figure 3.5: Comparison between experimental data and CFD simulation
(a) pressure drop in serpentine channel (b): heat transfer in serpentine channel

It can be seen from the Figure 3.5 (b) that the heat transfer coefficient for serpentine channel is much more than that of straight channel. The difference of heat transfer coefficient between serpentine channel and the straight channel is more at higher Re than at lower Re. As discussed earlier due to the mixing taking place at the bends section, the secondary forces don't allow the thermal boundary layer to develop. Thus this results in better performance in terms of heat transfer. Serpentine channel heat transfer coefficient is almost 2.7 times than that of straight channel for Re of 130 when compared to the fully developed flow. The same increases to 5.1 times that of straight channel for Re of 660. Figure 3.5 (b) also shows the heat transfer coefficient for the straight channel having same dimensions as that of serpentine channel for the case of thermally developing flow. Serpentine channel heat transfer coefficient is almost 1.6 times than that of straight

channel for Re of 130 when compared to the fully developed flow. The same increases to 2.1 times for Re of 660. For comparison the experimental data of heat transfer coefficient is also plotted in the Figure 3.5 (b.) The predicted heat transfer coefficient from the CFD simulations agrees well with the experimental value.

The careful observation of the results shows that the serpentine channel gives much better performance in terms of heat transfer than the straight one with requiring marginal increase in pressure drop. Comparison of the serpentine channel performance with the straight channel in the thermally developing region shows that the serpentine channel performs better at lower Re than that at higher Re. However the serpentine channel appears to be always good choice over a straight channel for all Re when compared to a fully developed region of straight channel.

From these results it can be seen that the CFD methodology developed to study flow and heat transfer in serpentine channel is well validated with the experiments and thus the same can be applied to understand the effect of various geometrical parameters on heat transfer in serpentine channel.

3.5.2 Effect of inclination/bend angle (θ) on performance

In the first case the effect of different bend angles was studied. Here the serpentine configuration was zigzag (saw tooth like) in nature (see Appendix I or Table 3.1) and the crossing of fluid streamlines was achieved by using sharp bends. Because of the bend effect, the velocity profile gets distorted and depending on the bend angle the intensity of the fluid mixing varies. This distortion of the velocity profile also affects the required flow development length after the bend. Figure 3.6 (a, b, c and d) summarizes the effect of pumping power, heat transferred, heat transferred per unit pumping power and *Nu/fRe* respectively for the serpentine configurations of case 1 for Re of 200 . All values were normalized with the results of the straight channel with same Re, length, aspect ratio and cross sectional area.

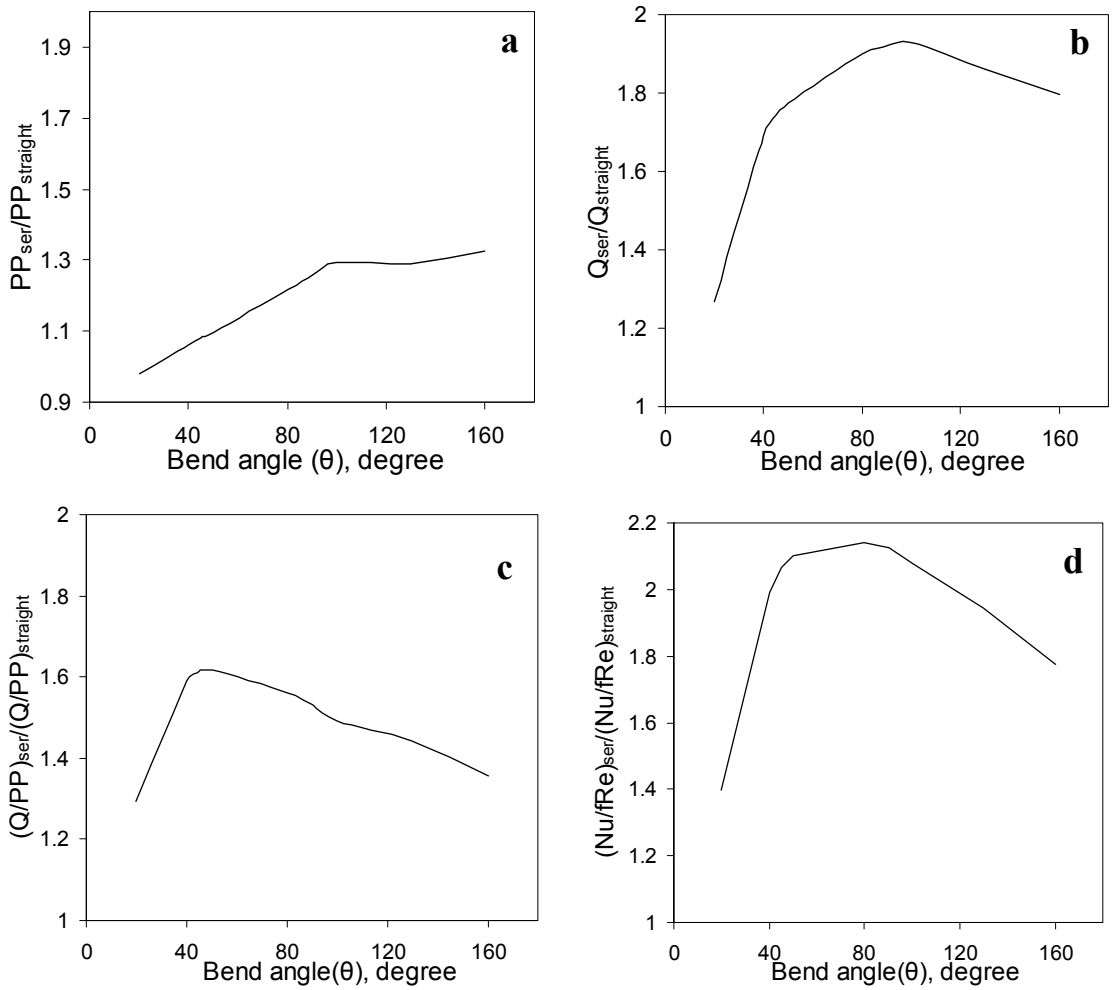

Figure 3.6: Case 1- effect bend angle on (a) pumping power (b) heat transfer enhancement (c) heat transfer per unit pumping power (d) *Nu/fRe*

It can be seen from the results that the pumping power increases with increase in the bend angle (Figure 3.6 (a)). This is due to the higher energy dissipation required to turn the fluid streamlines by higher angles. This rise in pumping power with the bend angle reduces above the 90^o bend demanding lesser power for further turning the fluid by certain angle. However observations in heat transfer are quite different. The enhancement in heat transfer increases with the bend angle till 90^o (Figure 3.6 (b)). With further increase in angle the performance of the serpentine decreases. This may be because of the dead zones developed at the bend corner for higher inclination angle geometries. This can be seen in velocity contour plot for different angle geometries shown in Figure 3.7.

Therefore the heat transfer coefficient decreases above the 90^{o} (for the same heat transfer area).

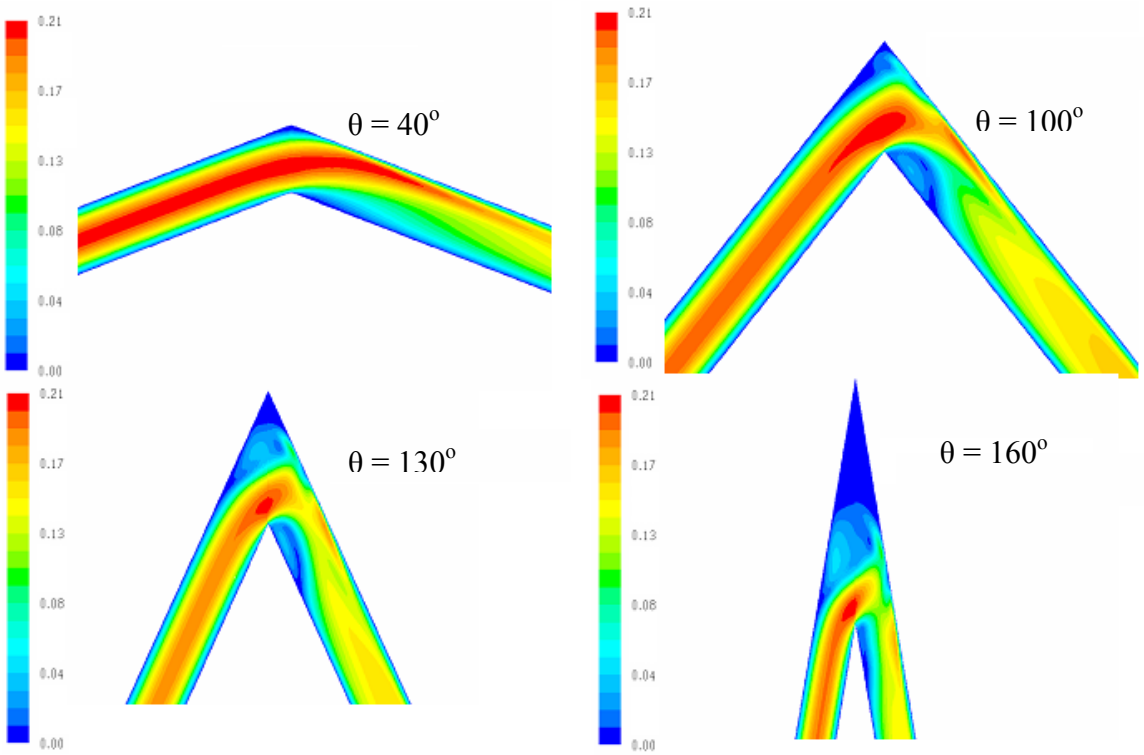

Figure 3.7: Velocity contour plot for different bend angles (Re: 200)

In this case the maximum heat transfer enhancement is obtained for the serpentine configurations having bend angle of 90^{o}. The ratio of heat transfer rate divided by pumping power of serpentine channel to that of straight channel is found to be highest for 50^{o} bend angle (Figure 3.6 (c)). From the overall result it can be seen that the ~ 50^{o} bend angle gives the better result in terms of heat transferred per unit pumping power compared to the other inclinations. However as per the ratio of *Nu/fRe* (Figure 3.6 (d)) for serpentine channel to that of straight channel all serpentine configurations within 40 to 90 inclination/bend angles found to be a better choice.

3.5.3 Effect of straight length (*L*) before bend on performance

In the second case the effect of straight length before bend was studied. The difference between the case 1 and the present case is that the sharp bend in the case 1 is separated by

the straight portion/length between them. Figure 3.8 (a, b, c and d) summarizes the results of the same. The Figure 3.8 also shows the comparison with the results of case 1 i.e. L=0. It can be seen from the results that for all angles the pressure drop in the present case is more than that of case 1.

In case 3 for serpentine configurations having small bend angles i.e. 20^o increasing the straight length before bend from 5 mm to 15 mm increases the pumping power significantly (Figure 3.8 (a)). In this case (i.e. case 2) the pressure loss in bend is same in all cases (for a range of L studied for a particular angle) because of the same bend angle (i.e. same pressure drop due to turning the fluid streamlines by particular angle) for various straight lengths. The rest of the pressure loss is governed by the developing flow pressure drop for the restoration of the distorted velocity profile. However the scenario is quite different in case of heat transfer enhancement for lower angle geometries (Figure 3.8 (b)) or serpentine configurations having lower bend angle. Here the heat transfer enhancement is highest when length before bend is 5 mm and decreases with further increase in the length. In case of small length (i.e. 5 mm), the distance between the second and the third bend is small (case of 20^o) and together both create good intensity of mixing when placed closed to each other. A single bend of small fluid bending angle (i.e. case 1) does not create a sufficient amount mixing for lower angles.

For serpentine configurations with higher bend angles i.e. 50^o and above, the pumping power increases with increase in the length before the bend. The pumping power in this case is again governed by the flow development length after the bend. Therefore as the length (L) before the bend increases, the overall portion of the continuous straight length reduces (i.e. decrease in amplitude or decrease in distance between the 1^{st} and 2^{nd} bend). Much of the flow remains in developing region whereas for small length case ($L \sim 5$ mm) there is sufficient length to develop the velocity profile immediate after the 1^{st} and 3^{rd} bend. Similar trend is observed in case of heat transfer behavior. The heat transfer enhancement increases with increase in the straight length before the bend (Figure 3.8 (b)). As the intensity of mixing at bend is same in all configurations (for a particular bend angle and various L), the only difference lies in the distance between the bend which is

the region of the developing flow. Therefore as the thermal boundary layer is developing in this region, the higher heat transfer coefficient is obtained with varying the length before the bend.

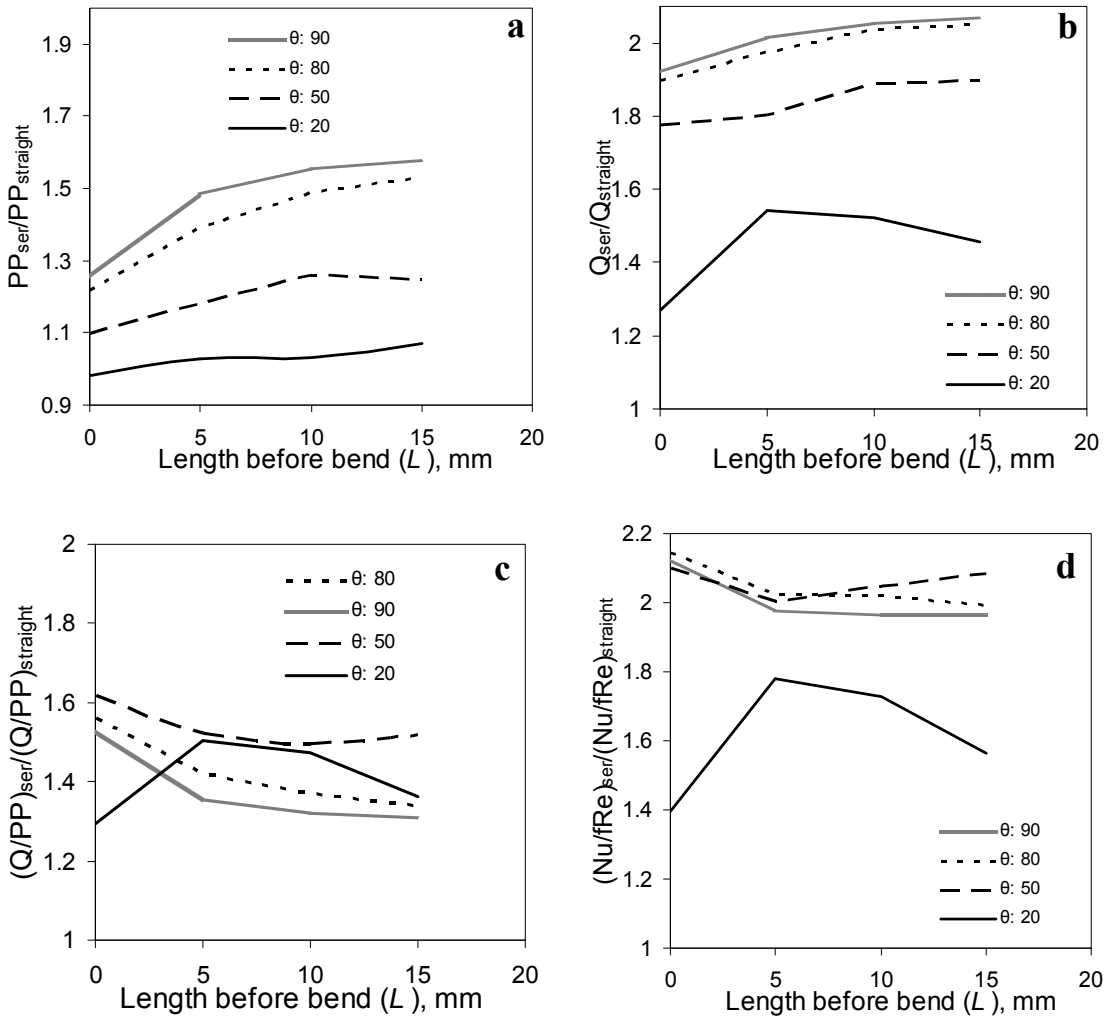

Figure 3.8: Case 2- effect of straight length before bend in sharp bends or in absence of curvature on (a) pumping power (b) heat transfer enhancement (c) heat transfer per unit pumping power (d) *Nu/fRe*

The ratio of heat transfer rate divided by pumping power of serpentine channel to that of straight channel is highest for 50^o bend angle serpentine configuration (Figure 3.8 (c)) even though the highest heat transfer is obtained for 90^o bend angle configuration (Figure 3.8 (c)). From the overall result the 50^o inclination/bend angle gives the better result

compared to the other inclinations. The same is also justified by the ratio of *Nu/fRe* for serpentine channel to that of straight channel (Figure 3.8 (d)).

3.5.4 Effect of curvature (*Rc*) on performance

In third case the effect of radius of curvature i.e. smoothness of the bend is studied. The results are summarized in Figure 3.9 (a, b, c and d). Along with the effect of curvature the Figures 3.9 also shows the results in absence of curvature i.e. for sharp bend (Case 1) or $Rc = L = 0$.

For serpentine configurations having higher bend angle e.g. 180^o with presence of radius of curvature, the concept of bend angle or inclination may not be applicable. This is because for very high radius of curvature the effect of secondary forces will be less (as dean number (*Dn*) varies inversely with *Rc*) and the performance of the channel will be close to the straight one e.g. 180^o bend with very high radius of curvature the serpentine configuration will be no more curved channel from performance point of view. For the sake of simplicity and the lower values of the radius of curvatures used, the terminology of bend angle (θ) is still retained in this section.

For serpentine configurations having bend angle around 40^o, replacement of sharp bend with curvature (i.e. replacement of sharp bend with smooth bend) decreases the pumping power slightly (Figure 3.9 (a)). However this slight decrease is due to the region of secondary flow structure at the bend section requiring less pumping power to turn the fluid streamlines by certain angles compared to case 1. For serpentine configurations where fluid streamlines were turned by higher angle i.e. 100^o-160^o, replacing sharp bend with curvature/smooth bend immediately decreases the total pumping power. This is expected as more power is dissipated at sharp bend for turning fluid streamline by a certain angle than carrying out the same by use the smooth bend/curvature. In case of 100^o bend angle serpentine configuration, the effect of further increase in radius of curvature/smoothness of a bend (above 5 mm) on pumping power is somewhat significant, whereas for 160^o bend angle serpentine the effect of increase in radius of curvature above 5 mm on pumping power is much significant. As the total length of all

serpentine configurations used in the present work is same, the higher curvature results in higher curved length potion i.e. more physical region of a secondary flow (160^o configuration, see Table 3.1) whereas in case of smaller curvature the bend is followed by a straight portion where the flow gets reestablished. Therefore in case of higher curvature (160^o configuration) the increase in pressure drop is due to the higher curved length portion/section.

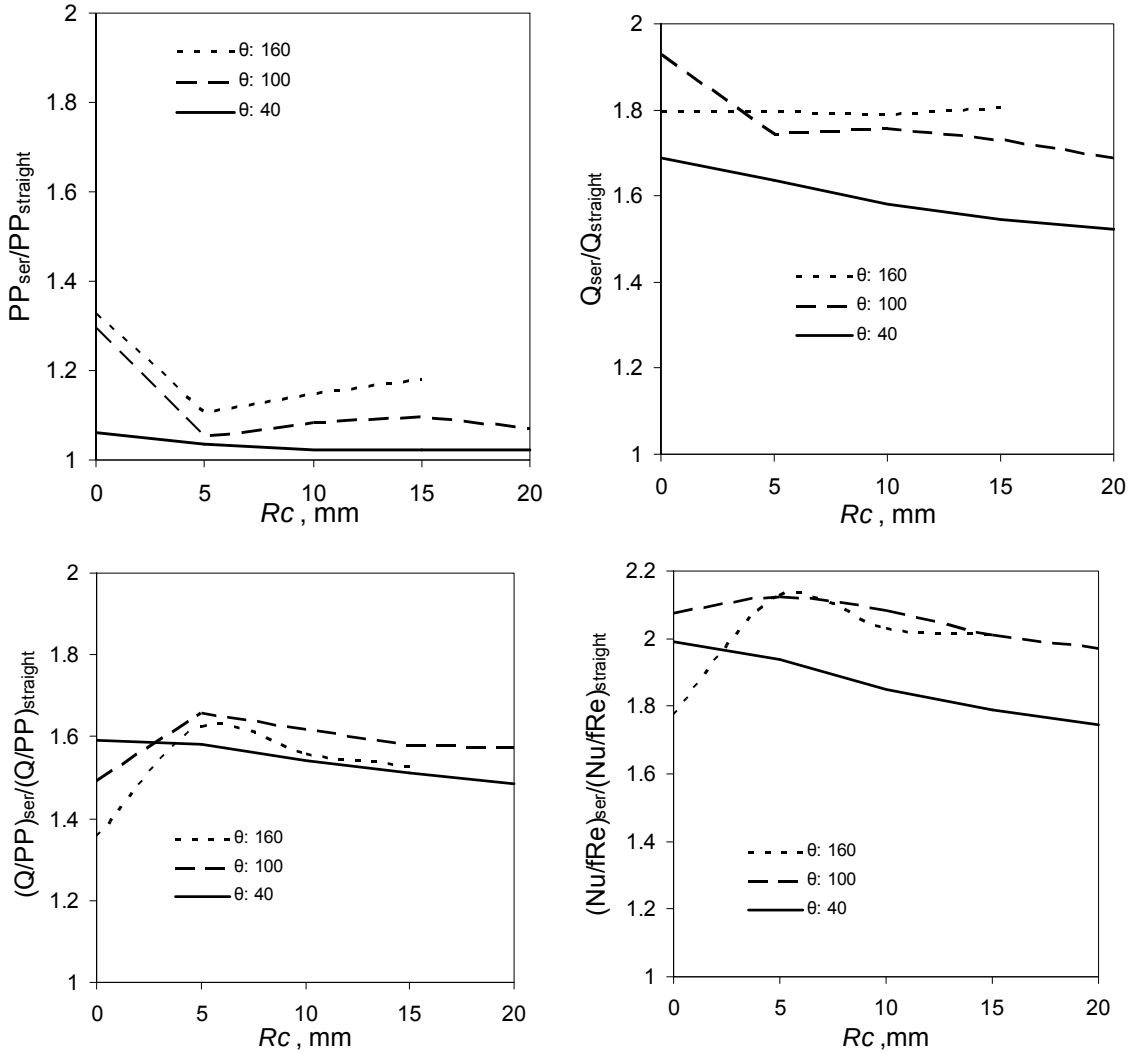

Figure 3.9: Case 3- effect of radius curvature in absence of straight length between bend on (a) pumping power (b) heat transfer enhancement (c) heat transfer per unit pumping power (d) *Nu/fRe*

The variations of radius of curvature or degree of smoothness for a given bend angle results in nearly same mixing behaviour therefore have insignificant effect on heat

transfer enhancement (Figure 3.9 (b)) i.e. all curvature gives almost similar extent of enhancement apart from the smaller bend angle (40^o) where the heat transfer enhancement decreases with increase in curvature. This is due to the decrease in the mixing intensity at the curved potion with increase in the curvature i.e. decreasing *Dn* with increase in *Rc*.

The highest enhancement is obtained for a serpentine configuration (with presence of curvature) having bend angle of 160^o (i.e. when the fluid streamlines were turned by 160^o). It can be seen that high angle serpentine configuration gives highest enhancement with lesser increase in pumping power in presence of curvature than that of in the absence of curvature. The ratio of heat transfer rate divided by pumping power of serpentine channel to that of straight channel is highest for the serpentine configuration having bending angle of 100^o for all the curvatures (Figure 3.9 (c)). From the overall result, higher angle geometries i.e. 100^o and above gives the better result compared to the other inclinations. The same is also justified by the ratio of *Nu/fRe* for serpentine channel to that of straight channel (Figure 3.9 (d)).

3.3.5 Effect of curvature (*Rc*) with constant straight length before bend (*L*) on performance

The case 4 involved the study of effect of radius of curvature (smoothness of a bend) when the straight length before bend (*L*) is fixed at 5 mm. The results are summarized in Figure 3.10 (a, b, c and d). In this case the sharp bend after the straight length of case 2 is replaced by the curvature (i.e. sharp bend of case 2 is replaced by smooth bend). Along with the effect of curvature (i.e. studies of case 4) these Figures also shows the results case 2 for comparison i.e. absence of curvature or presence of sharp bend with $L = 5$ and $Rc = 0$.

For serpentine configurations having low bend angle e.g. 20^o replacing the sharp bend with the curvature have insignificant effect on pumping power (Figure 3.10 (a)). However increasing the curvature increases the pressure drop to certain extent due to reduction in the total straight length portion available after the bend with replacement of

the curved portion. For serpentine configurations having bend angle of 50^o, replacing sharp bend with the curvature or smooth bend results in slightly lesser pressure drop however the decrease is not remarkable. For serpentine configurations having higher bend angle (i.e. 80^o in this case), the curvature reduces the pressure drop significantly than that of absence of curvature (i.e. 80^o in case 2). As the sharp bend after the straight length is absent in this case the velocity profile is not suddenly distorted significantly and therefore less pumping energy is required to turn the fluid by certain angle.

Similar observations as case 3 were found here for heat transfer enhancement with variation of curvature. No significant change was observed with curvature for serpentine configurations having bend angle up to 50^o (Figure 3.10 (b)). However higher is the curvature for a given Re, lower is the *Dn* and therefore lower is the intensity of the secondary flow. Therefore the heat transfer enhancement decreases to certain extent with increase in curvature as can be seen in case of 80^o bend angle serpentine configuration.

The plots of, ratio of heat transfer rate divided by pumping power of serpentine channel to that of straight channel (Figure 3.10 (c)) and the ratio of *Nu/fRe* (Figure 3.10 (d)) for serpentine channel to that of straight channel both justifies the serpentine configurations with bend angle above 50^o are preferred choice.

3.5.6 Effect of different straight length before bend (*L*) with constant curvature (*Rc*) on performance

The case 5 involved the study of different straight length (*L*) before bend for the fixed radius of curvature (i.e. constant bend smoothness, *Rc)* of 5 mm. The results are summarized in Figure 3.11 (a, b, c and d). In this case the smooth bend of case 3 is separated by the straight length portion (i.e. smooth bend of case 3 is separated by straight length portion). Along with the effect of straight length before bend (i.e. studies of case 5) these Figures also shows the results of case 3 for comparison i.e. absence of straight length and presence of curvature (smooth bend) with $L = 0$ and $Rc = 5$ mm.

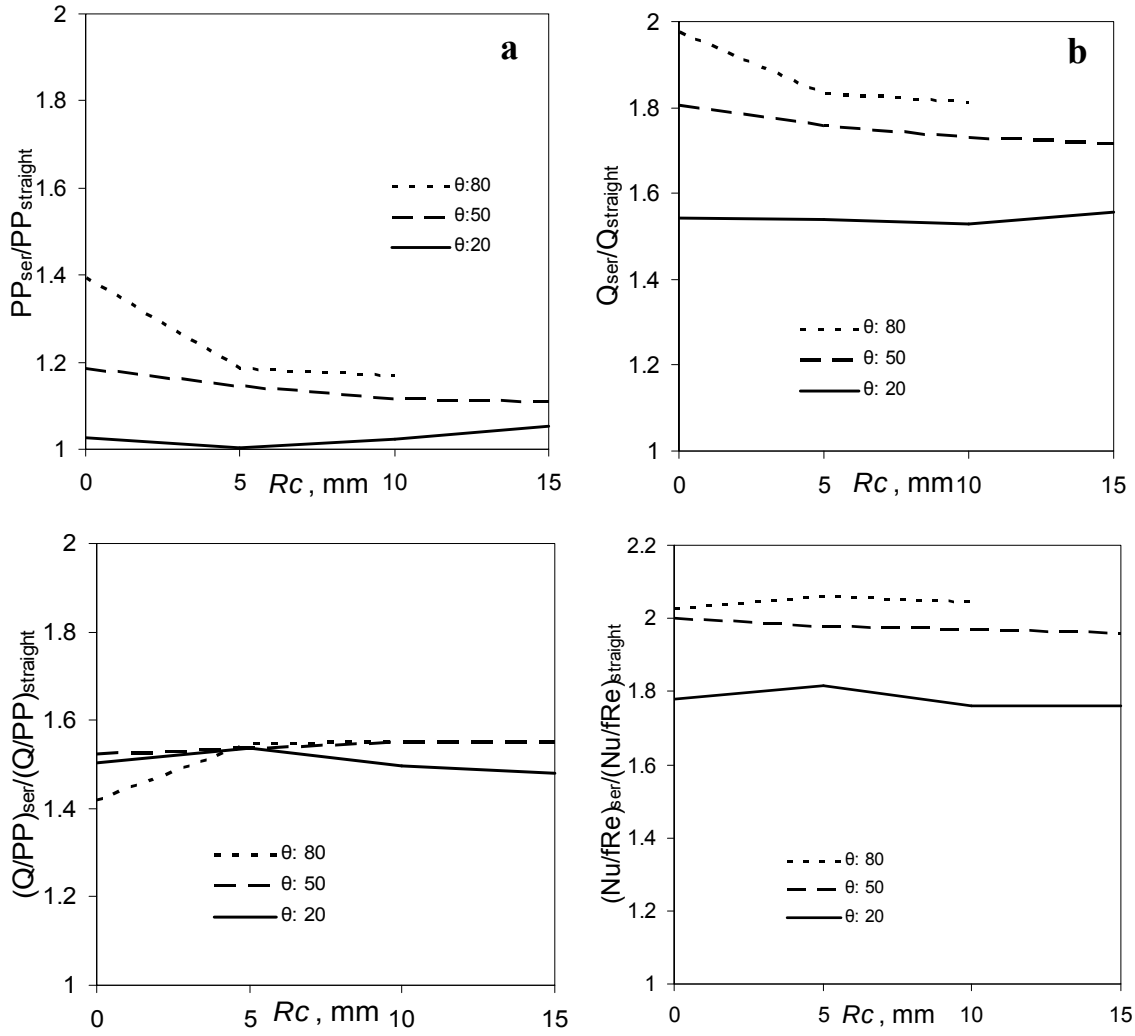

Figure 3.10: Case 4- effect of radius curvature for a fixed straight length before bend of 5 mm on (a) pumping power (b) heat transfer enhancement (c) heat transfer per unit pumping power (d) *Nu/fRe*

For serpentine configurations having low bend angle e.g. 20^{o} increasing the straight length before the curvature have insignificant effect on pumping power (Figure 3.11 (a)). The presence of straight length before the curved portion however increases the heat transfer to certain extent. As discussed in case 2, for lower angle serpentine configurations, the closer bend (i.e. smaller length before bend) creates good mixing intensity and hence results in good heat transfer enhancement (Figure 3.11 (b)). Increasing this length above certain value (L = 10 mm) however resulted in decrease in heat transfer enhancement.

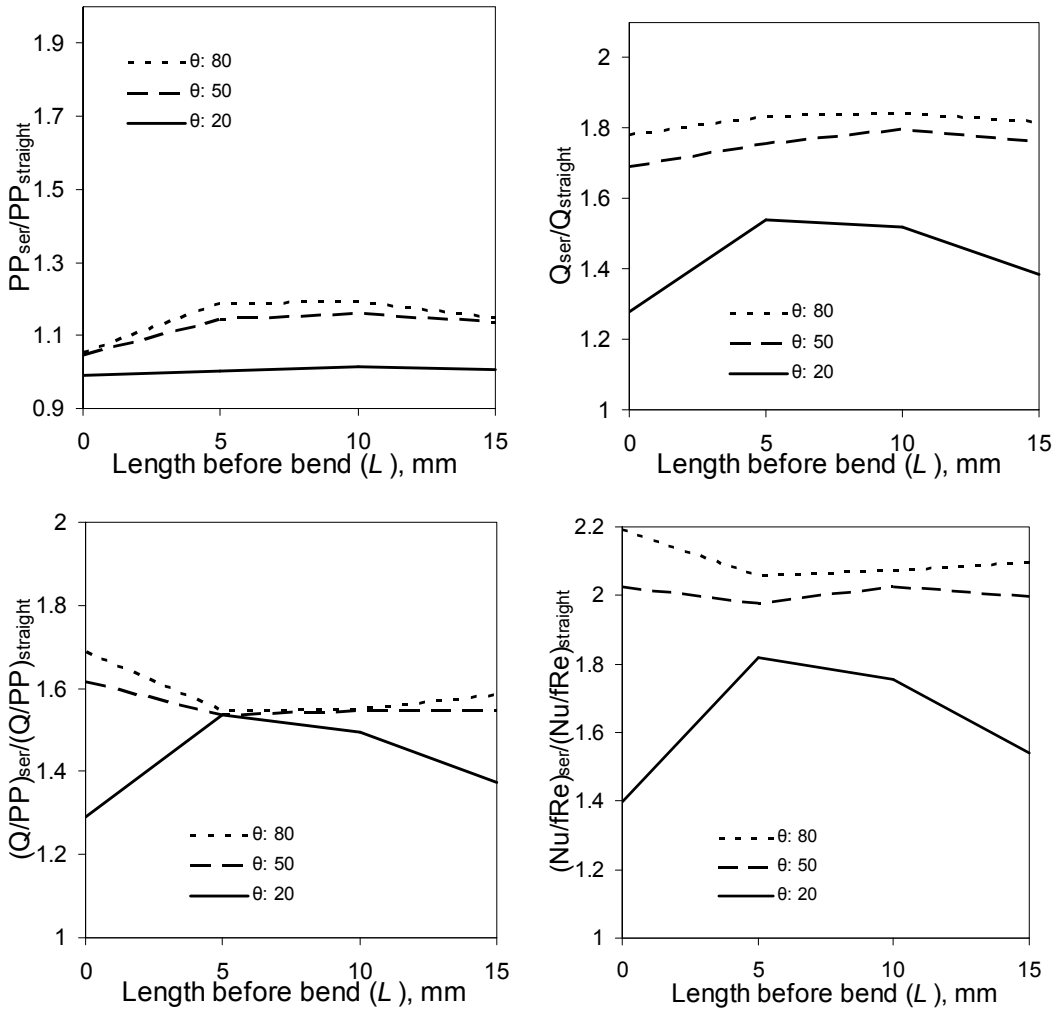

Figure 3.11: Case 5- effect of straight length before bend for a fixed curvature of 5 mm between the bend on (a) pumping power (b) heat transfer enhancement (c) heat transfer per unit pumping power (d) *Nu/fRe*

For serpentine configurations having higher bend angle e.g. 50^{o} and above putting straight length (L of about 5 mm) before curvature increases the pumping power to certain extent but above certain value of straight length before bend i.e. L= 5 mm it remains constant. In case of heat transfer too very small enhancement is observed for L = 5 mm and no significant change above L = 5 mm is seen (Figure 3.11 (b)). In this case a decrease in the amplitude (A or the distance between the first and the second) of the bend is expected with the increase in the straight length before bend. Therefore in this case much of the flow after the bend should remain in developing region. The available region

of the developing flow should increase with the increase in the straight length before bend (*L,* see case 2 in section 3.5.3). However it should be noticed that the variation in straight length before bend and the amplitude are always opposite to each other i.e. for a constant total length (100 mm in this case) as straight length before the bend increases (i.e. increase in the distance between the second and the third bend) the corresponding amplitude decreases (i.e. vertical distance between the first and the second bend decreases). Therefore in the case of much higher straight length before bend (L =15 mm), though the flow in the section between the first and the second bend remains in developing region (i.e. higher heat transfer due to developing region) at the same time the increased distance between the second and the third bend results in much developed velocity profile (i.e. lower heat transfer due to developed region). Therefore the two complementary effects results in only somewhat increase in heat transfer enhancement for serpentine configuration with 50^o and above bend angle (for increase in straight length before bend from 5 mm to 15 mm, see Figure 3.11(b)).

For serpentine configurations having higher bend angle e.g. 50^o and above the performance in terms of ratio of heat transfer rate divided by pumping power of serpentine channel to that of straight channel (in case 5) is less compared to the serpentine configurations having curvatures with zero straight length before the bend (i.e. case 2 see Figure 3.11 (c)). The serpentine configurations above 50^o fluid bending angle gives quite favorable performances in terms of *Q/PP*. However for these angles the effect of variation of straight length before the bend is found to have no remarkable effect on the performance in terms of *Nu/fRe* (see Figure 3.11 (d)). In this case, the serpentine configuration of 80^o fluid bend angle gives quite favorable performances in terms of *Nu/fRe*..

3.5.7 Effect of bend angle (θ) for different Reynolds number

Dean number gives the significance of the secondary forces or dean forces therefore the intensity of the secondary forces also depends on Reynolds number. The serpentine configurations that are performing better at certain Reynolds number need not have to perform better or give similar performance at other Reynolds number. Therefore the

performance of the serpentine channel depends on the operational Reynolds number. As mentioned earlier the simulations were carried out for Re of 200 and 50. Only the effect of different bend angle i.e case 1 is shown here to compare the performance for two different Re.

Figure 3.12 (a, b, c and d) summarizes the results. It is obvious that pressure drop for Re 200 is more than that of Re 50. The pressure drop increases with increase in bend angle for Re of 200 till angle of 100^o. The effect of bend angle on the pumping power is insignificant beyond 100^o. However for the case where value of Re is 50 there is only slight increase in pressure drop till angle of 100^o. Above this angle there is reduction in pumping power (Figure 3.12 (a)). The reason for this behavior is not well understood. The highest heat transfer enhancement is achieved by 90^o bend angle serpentine configuration for the value of Re equal to 200 but for Re equal to 50 the highest heat transfer enhancement is achieved by 130^o bend angle serpentine configuration (Figure 3.12 (b)). The heat transfer enhancement demands better fluid mixing and therefore certain amount of power dissipation. This cannot be well achieved by lower angles in case of Re equal to 50. The 130^o bend angle serpentine configuration is capable of achieving better mixing thus giving highest heat transfer enhancement where the value of Re is equal to 50. Above this angle the performance reduces as the pumping power also gets reduced i.e. lesser power dissipation.

The plots of, ratio of heat transfer enhancement divided by pumping power of serpentine channel to that of straight channel (*Q/PP*) and the ratio of *Nu/fRe* for serpentine channel to that of straight channel both gives serpentine configuration with 130^o bend angle to be better choice for Re equal to 50. It can be observed from the results that for this Re, the serpentine configuration giving highest heat transfer enhancement also performs well when compared with unit pumping power. However in case of Re 200, the scenario is much different.

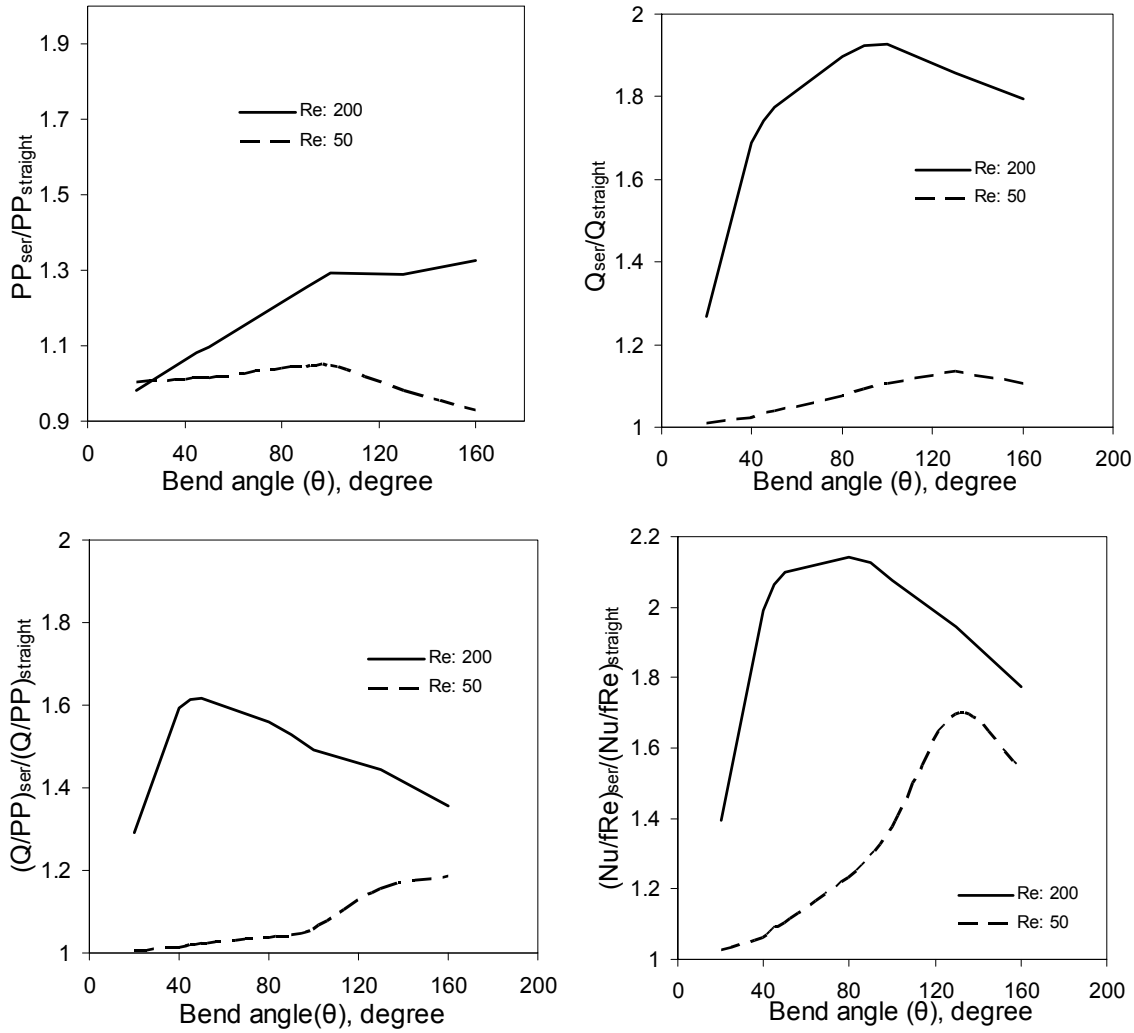

Figure 3.12: Effect of bend angle for different Re (a) pumping power (b) heat transfer enhancement (c) heat transfer per unit pumping power (d) *Nu/fRe*

It can be seen from the results that the serpentine configurations which gives higher heat transfer enhancement are not a better choice in terms of heat transfer enhancement per unit pumping power. For the complete analysis all four criteria's (see section 3.4.1) are necessary. One of the key issues concerning is whether the mechanism of fluid mixing in smooth bends/curvature and the sharp bend is same?

In case of sharp bend (Case-1), the streamlines gets turned depending upon the angle of bend. The highest heat transfer enhancement is obtained when the fluid streamlines are turning by 90^{o} in case 1. However the serpentine configurations where the fluid

streamlines turns by angle more than 90^o, dead zones occurs and the performance in terms of heat transfer enhancement reduces. Therefore in case-1, the 90^o bend angle serpentine configuration gives the highest performance in terms of heat transfer enhancement. However the pressure drop at this bend angle is also very high. Therefore in case 1, 45^o bend angle serpentine configuration is found to be beneficial as per the criteria-3 and 4.

In the serpentine configurations having straight length before sharp bend i.e. case 2, serpentine configuration with bend angle of 90^o is giving highest mixing or heat transfer enhancement very similar to the case 1. However to achieve this intensity of mixing, considerable amount of pumping power is needed. As per the criteria 3 and 4, serpentine configuration with 50^o bend angle is found to be better choice.

The concept of the turning of fluid streamlines depending on the bend angle loses its meaning in case of curvatures i.e. case 3 or smooth bends. The reason is, in case of very high curvature the fluid elements gradually moves along the curvature and terminology of turning of fluid streamlines by certain angle will not exists if the curvature is very high. However in the present work the serpentine configurations of case 3 are still compared based on bend angle due to the serpentine configurations with small curvatures used. Curvature produces good heat transfer enhancement with comparatively lower pumping power than that of sharp bends. The reason should be associated to the development of secondary flow structure at curved section. However in case 3 i.e. smooth bends, serpentine configurations with higher bend angle gives highest performance in terms of heat transfer enhancement. This enhancement is not associated entirely to curvature alone but also to the turning the fluid streamlines by certain angle. Therefore though the curvature and sharp bends creates good degree of heat transfer enhancement but the mechanism is quite different. A brief discussion on this is presented in the subsequent following text. As per the criteria 3 and 4, in case of curvature 100^o bend angle serpentine configuration is found to be beneficial.

In the second case, the sharp bend from the case 1 was separated by the straight length which we defined as straight length before bend (L). In this case also the fluid streamlines turns by certain angles similar to the case 1. The only difference lies here is that the length after the bend is changed/lowered so that the flow remains in a developing state. Therefore in second case for lower bend angle serpentine configurations (i.e. 20^o) with the sharp bends, the nature of the bend itself is not capable of folding/crossing the fluid streamlines to the required level. Therefore the closer sharp bends i.e. lower straight length before bend creates better crossing of streamlines than that of the higher straight length before bend. In case of higher straight length before bend (i.e. L = 15 mm), the third bend (see Appendix I: 3^{rd} bend) experiences much developed velocity profile. The same might be responsible for decrease in the heat transfer enhancement (Figure 3.8 (b)). However in case of serpentine configurations with higher bend (i.e. 50^o and above), the bending angle (or sharp bend) itself creates sufficient amount of mixing in streamlines which enhances heat transfer considerably. Therefore further enhancement in heat transfer is governed by the heat transfer coefficient in the straight portion after the bend. Increasing the straight length before bend reduces the length between the 1^{st} and 2^{nd} (or reduces amplitude) so flow remains in developing region. This ultimately results in higher heat transfer coefficient. In this case also serpentine configuration with 90^o bend angle creates highest intensity of mixing or heat transfer coefficient however 50^o bend angle configuration is found to a better choice as per the criteria 3 and 4.

The third case under the study was the effect of curvature in smooth bends on the heat transfer enhancement. Here the sharp bends from the case 1 was replaced by the curvature. However it is important to understand that the bend angle (or streamlines turning angle) may loose its significance if the radius of curvature is very high. As mentioned earlier for the sake of simplicity the terminology is still retained in this section. This also works because of the small curvatures used in the present study (approximately $0.66 < r/Rc < 2$). In case three, the curvature results in good heat transfer enhancement at lower pressure drop than that of case 2 i.e. straight length before bend and case 1 i.e. sharp bends. In case of curvature, serpentine configuration with 160^o bend angle creates highest enhancement in heat transfer. However as per the criteria 3 (Q/PP),

100^o bend angle is found to be more beneficial. Therefore it is important to understand the mechanism by which the radial mixing took place.

As we saw in case 1 and case 2 that the radial mixing took place because of the sharp bends i.e. crossing of fluid streamlines. However in case 3 due to absence of the sharp bend and the presence of the curvature the radial mixing taking place due to the secondary flow structure created at the bend section. Both cases are carrying out the similar operations i.e. mixing however the pressure drop required to achieve this operation is much different. The pressure drop in case of smooth bends i.e. case 3 is much lower than that of the sharp bends i.e. case 1 as can be seen in Figure 3.9 (a). Particularly for serpentine configurations with higher bend angle of 160^o the presence of curvature reduces the pressure drop significantly. As discussed in the section 3.5.2, the dead zones present in higher bend angle serpentine configurations were responsible for the degradation in heat transfer enhancement. However the presence of curvature overcomes these dead zones resulting in good heat transfer enhancement with a much decrease in pressure drop than that of sharp bend of similar angle.

The dean numbers (*Dn*) at the bend regions are 126 to 73 for radius of curvature of 5 mm to 15 mm for case 3. Thus dean number at the bend section reduces with increasing the curvature (as dean number (*Dn*) varies inversely with *Rc*)). Therefore all enhancements are result of a development of secondary flow at the curved bend. However the effect of variation in the radius of curvature (*Rc*) is not significant in the range studied. This is due to the smaller physical total length of the curved portions resulting in lesser effect of the secondary forces (comparing to the typical curved lengths available in helical coils with significant effect of secondary forces). The significance of the criteria 3 ((*Q/PP*) can be clearly visible in this case. Criteria 4 (*Nu/fRe*) gives both 100^o and 160^o bend angles serpentine configurations to be better. However this is not entirely true. Serpentine configurations with 100^o bend angle perform better in terms of overall performance than 160^o degree.

In case four i.e. specifying straight length at 5 mm with variation in radius of curvature, gives different trends for higher bend angle and lower bend angle serpentine configurations e.g. for lower bend angles (20^o), increasing radius of curvature increases the total curved portion length so as to increase the pressure drop (Figure 3.10 (a)). Whereas for higher bend angle (80^o) serpentine configurations pressure drop reduces because of the sharp bend replacement using the radius of curvature or smooth bend. However as noted previously the variation in radius of curvature does not result in any more heat transfer enhancement. 80^o bend angle serpentine configuration gives highest heat transfer enhancement (Figure 3.10 (b)) but 50^o fluid bending geometry was found to be economically (Q/PP) most favorable (Figure 3.10 (c)). The combination of straight length before bend and curvature (combinations of case 1, 2, and 3) in single serpentine configuration makes approximately all bend angles to be better choice.

In the case five, fixing radius of curvature at bend equal to 5 mm, the effect of straight length before bend is different for lower and higher bend angle serpentine configurations. For serpentine configurations having low bend angle e.g. 20^o increasing the straight length before the curvature have insignificant effect on pumping power (Figure 3.11 (a)). The presence of straight length before the curved portion however increases the heat transfer to certain extent and above certain straight length (L = 10 mm) the heat transfer enhancement decreases. As there is absence of sharp bend; the curvature is not able to fold or mix the fluid to the required level. Therefore the heat transfer enhancement is because of development of secondary flow. Two closer bends (distance between the second and the third bend) creates reasonable development of secondary flow structure than the bends far from each other. Therefore the pumping power and the heat transfer are higher at straight length before bend of 5 mm in case of 20^o bend angle of case 5 (i.e., fixed radius of curvature). For serpentine configurations having higher bend angle (above 50^o in this case) the variation of straight length before bend results in little enhancement in heat transfer. Now as discussed in section 3.5.3, increasing the straight length before the bend (i.e. decrease in amplitude of serpentine A) increases the distance between the second and the third bend. However decrease in amplitude (A) also means that decrease in the distance between first and the second bend. Therefore there is certain

optimum dimension of the straight length before bend when used in combinations with the radius of curvature. In other words no more benefit of the higher straight length before bend can be obtained (as obtained in case 2, see Figure 3.8 and section 3.5.3) in case 5 due to the almost developed flow (and therefore lower heat transfer) in the region between second and the third bend. It should also be noticed that the mixing intensity at the bend region in case 2 (sharp bend) is much more compared to the bend section in case 5 (smooth bend). This also means that the velocity profile in case 2 is more damaged at the bend than that in case 5 and therefore only smaller straight length portion is sufficient for the flow development in case 5. The flow in the total straight length region available does not remains entirely in developing state and therefore no benefit of developing flow is obtained here compared to case 2. In this case, criteria 3 (*Q/PP*) shows that both 50 and 80^o bend angle serpentine configuration are favorable one. However criteria 4 (*Nu/fRe*) makes higher bend angle serpentine configurations as a better choice.

Case 4 and 5 both consists of combination of cases 1, 2 and 3. It can be seen from these two cases (i.e. case 4 and 5) that the serpentine configurations which gives highest heat transfer enhancement also becomes a better choice in terms of heat transfer per unit pumping power (*Q/PP*). This is only possible in case 4 and 5. This makes a choice simple or the serpentine configurations giving highest heat transfer performance also performs better in terms of power dissipation. This is the benefit behind using the combination of curvature (*Rc*), straight length before bend (*L*) and bend angle (θ).

One more observation that can be made from first three cases is that the better serpentine bend angle found by criteria 2 is one half of the one given by criteria 3 e.g. In case 1, the highest heat transfer enhancement is given by the serpentine configurations having bend angle around 100^o. However the optimum bend angle in terms of heat transfer per unit pumping power is found to be around 50^o. Similar results are found in case 2 and 3. In case 2 the criteria 2 gives 90^o to be highest heat transfer serpentine configuration however criteria 3 gives 50^o serpentine configuration to be better. In case 3, criteria 2 gives 160^o serpentine configuration giving highest heat transfer however criteria 3 gives 100^o serpentine configuration to be a better choice.

Ottino and Wiggins (2004) have reviewed the main elements of mixing and how it interfaces with mixing in microfluidic devices i.e. chaotic mixing based on stretching and folding. The author says "The objective of mixing is to produce the maximum amount of interfacial area between two initially segregated fluids in the minimum amount of time or using the least amount of energy. Creation of interfacial area is connected to stretching of lines in two dimensions and the surface in three dimensions. A fluid element of length $\delta(0)$ at time zero has length $\delta(t)$ at time t; the length stretch is defined as $\lambda = \delta(t)/\delta(0)$; if mixing is effective, λ increases nearly everywhere, though there can be regions of compression where $\lambda < 1$. In simple shear flow, the fastest rate of stretching, $d\lambda/dt$, corresponds to the instant when the element passes through the 45◦ orientation corresponding to the maximum direction of stretching in shear flow; for long times the stretching is linear ($\lambda \sim t$) in time as the element becomes aligned with the streamlines. In an elongational flow the rate of stretching is exponential, $\lambda \sim e^t$. The distance between striations is inversely proportional to the surface area: the thinner the striations, the faster the diffusion. Note that the effects of stretching on accelerating interdiffusion enter in two different ways: a greater interfacial area means a greater area for transfer; at the same time, diminishing striation thicknesses increase the concentration gradients and increase the mass flux." The concept of stretching may not be applicable in any of the cases studied here in the present work as apart from the stretching there is also radial mixing due to crossing of streamlines taking place. Therefore the phenomenon of stretching may be applicable to very low flow rates. As per the present results the highest performance in transport coefficients are obtained at higher bend angle serpentine configurations (90^o or above) rather than at 45^o.

The mechanism of heat transfer enhancement in case of serpentine channel involves intense mixing at bends resulting in breaking of thermal boundary layer which ultimately depends on bend angle or curvature. As discussed earlier the sharp bend and the curvature creates the intense mixing with different modes/mechanisms. The second governing parameter is the distance between the bends. If the distance between the bends is higher, the flow remains developed one in terms of velocity profile and thermal

boundary layer or temperature profile which is the region of the lower heat transfer coefficients. Based on these results a map of heat transfer enhancement vs. pumping power is generated to understand the effect of various geometrical parameters for Re 200. Figure 3.13 shows the same. It can be seen from the map that highest pumping requirement is 1.55 times that of the straight channel whereas the heat transfer enhancement is up to 2.1 times that of the straight channel for the range of the serpentine configurations studied in the present work. The serpentine channel is always a better choice to achieve mixing (and hence better transport coefficients) than that of the straight channel. Comparison between the performance of serpentine configuration with radius of curvature, sharp bend and straight length before bend shows that the lower radius of curvature with higher bend angle to be a good choice. For this case the pumping power is only 1.10 times that of the straight channel compared to the heat transfer enhancement of 1.8 times that of the straight channel.

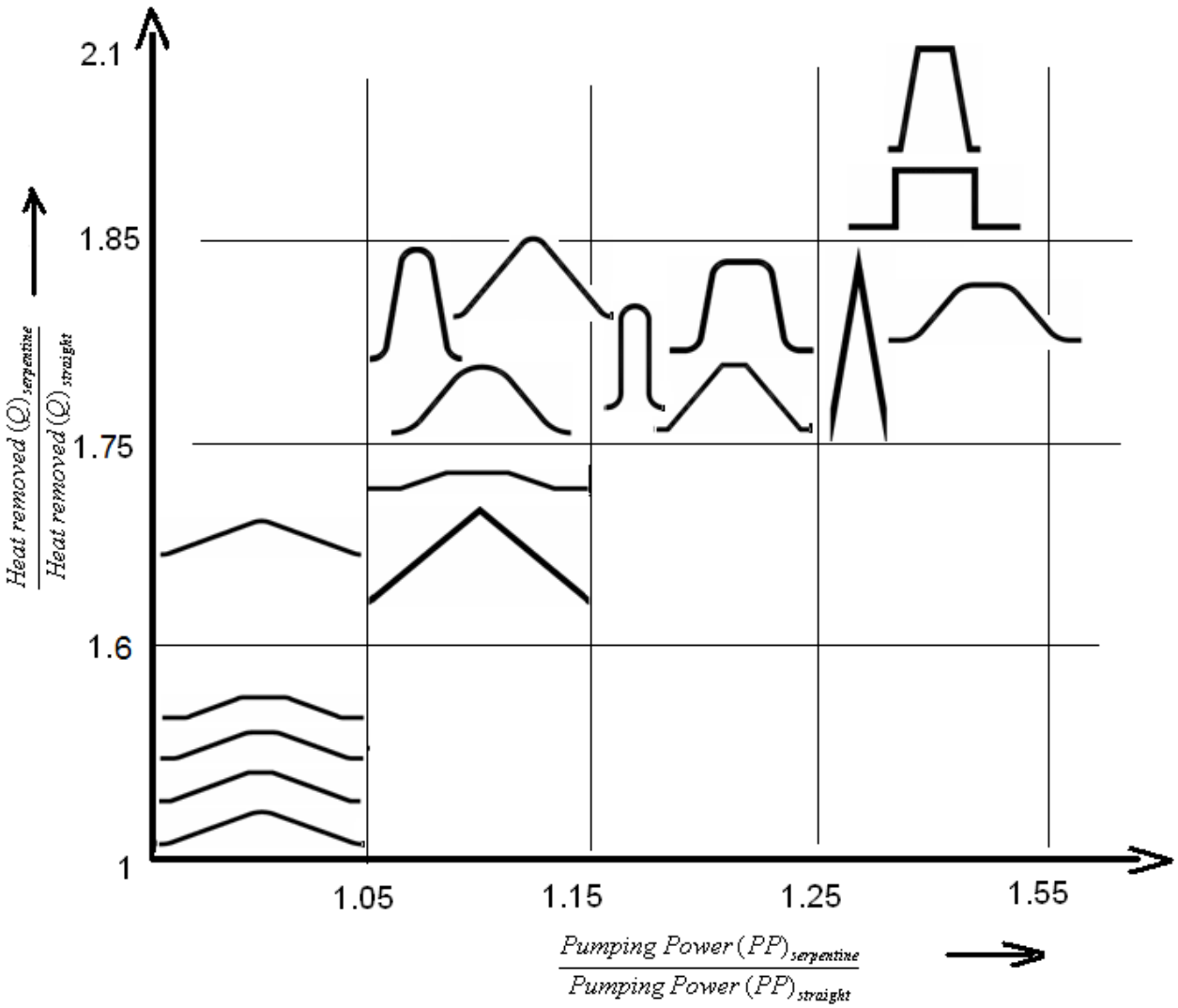

Figure 3.12: Design map of different serpentine configurations (Note: Axis not to scale)

3.5 Conclusions

CFD methodology developed to study flow and heat transfer in serpentine channel was first verified by comparing predictions with the experimental data. The model was then applied to understand the effect of various geometrical parameters serpentine channel on heat transfer enhancement.

CFD simulations of periodically developed laminar flow heat transfer in serpentine channel of square cross section were performed for a wide range of parameters like bend

angle, straight length before bend and curvature. Simulations were carried out for Reynolds number of 200 and Prandtl number 6.13 with constant wall temperature thermal boundary condition. Following conclusions are drawn from the study:

- For sharp bends (case 1), straight length before bends (case 2) and curvatures (case3) the highest heat transfer enhancement is obtained for 90^o bend angle. However 50^o bend angle serpentine configuration is found to be better when compared with unit pumping power basis
- Effect of variation of radius of curvature in case of smooth bend is found to be insignificant (in the range studied)
- Serpentine configurations with smooth bends offers lower pressure drop compared to sharp bends
- Developing flow, crossing of streamlines and secondary flows due to bends are some of the reasons for enhancing heat transfer in serpentine channels
- The optimal bend angle (based on heat transfer per unit pumping power) is sensitive to the value of Reynolds number. For example, 100^o bend angle is optimum for Re 200 whereas 130^o bend angle is optimum for Re 50
- Based on this work a design map for selecting suitable configuration of serpentine channels is presented.

CHAPTER 4

RESIDENCE TIME DISTRIBUTION IN SERPENTINE CHANNELS

In the present work the effect of various geometrical parameters of the serpentine channel on the residence time distribution was investigated using CFD. The CFD methodology was divided in two parts. In the first part the methodology was validated for the simple system of laminar pipe flow. The second part involved application of this standardized methodology to study the residence time distribution in various serpentine channel configurations. The performance of different serpentine configurations was compared using variance as a parameter calculated from the E-t curve obtained from simulations. Using variance of E-t curve, an optimization of the geometrical configurations was done for narrowing the residence time distribution thus achieving lesser axial dispersion. 60-80 % reduction in variance (and therefore dispersion) was obtained with use of serpentine channel compared to the straight channel. The mechanisms responsible for reduced axial dispersion were discussed briefly.

4.1. Background

In any continuous flow process where chemical reactions occur, the performance of the reactor depends on nature of the flow taking place inside the reactor. In such cases the knowledge of the residence time distribution (RTD) is of significant importance and therefore reveals useful information. In general plug flow and the mixed flow are the two basic classifications of the nature of the flow can be found in the literature (see, for example, Levenspiel, 1999). In ideal plug flow, the flow of fluid through the reactor is orderly with no element of fluid overtaking or mixing with any other element ahead or behind. However there may be lateral mixing of fluid in a plug flow reactor but no mixing or diffusion along the flow path. In this case the residence time for all the fluid elements is same in the reactor. Many practical tubular reactors are designed on the basis of assumption of ideal plug flow however the same is rarely achieved. In case of mixed flow the contents in a given volume are well stirred such that the concentration of species everywhere is same. However similar to plug flow the mixed flow is also difficult to achieve in a practical applications.

In the recent years there is growing interest among the researchers for developing different microreactors systems due to several benefits offered over conventional systems. Many applications of several tubular microreactors can be found in De Bellefon *et al.* (2000), Jensen (2001), Halder *et al.*(2007), Engl *et al.*(2007) etc. The flow rates of the reactants that are used in microreactors are also quite low therefore the flow conditions inside the reactor remains laminar. However in laminar regime, a breaking of fluid compartments cannot occur due to the high viscous forces. This results in a considerable amount of axial/longitudinal dispersion due to the radial gradient in the velocity profile. In case of slowly flowing systems with small channel diameters, molecular diffusion effects occur. Therefore the contribution of the velocity profile and the diffusion to the dispersion depends on Schmidt number (*Sc*) and the dimensionless time of interest (τ). A brief summary of the same can be found in Nunge and Gill (1963).

As mentioned the laminar flow profile results in considerable amount of dispersion due to the radial gradient in the velocity. One way of overcoming this limitation is breaking the

boundary layer for achieving the radial mixing in the pipe. The use of active mixers and the passive mixers are the few choices available for this purpose. Active mixers use external forces or power dissipations to achieve the mixing however the passive devices does not involves either of this except the use of pump for delivering the fluid. Even though the mixing in active mixers is much efficient the use/incorporation of such devices in microreactor devices is a difficult task. In such cases passive devices finds scope in microreactors.

Several authors are looking for developing passive microscale devices that can transport and mix the small fluid volumes efficiently. Serpentine channel configurations are one of the choices that are becoming more popular among the researchers in last few years due to several benefits offered by them. These include compact size, better mixing, higher mass transfer coefficients than straight channels etc. Therefore the reactions with higher residence time can be easily handled in a smaller space or reactor size. The secondary flow generated at bends results in a better mixing. A precise characterization of microreactors can be achieved by determining the residence time distribution as one of the most important flow characteristics. This system also offers narrow RTD thus reducing the dispersion.

The serpentine channel consists of a bend section with repeating units. Figure 4.1(a) shows simple schematic of the serpentine channel. A typical serpentine configuration can be classified in two broad categories 1) Smooth bend and 2) Sharp bend. Figure 4.1 (b) shows the serpentine configuration with the smooth bends whereas the configuration with sharp bends is shown in Figure 4.1(c). A typical serpentine channel as shown in Figure 4.1(a) is specified using the following parameters a) bend angle (θ) b) straight length before bend (L) or distance between the bends ($2L$) c) radius of curvature at bend section (Rc) d) amplitude of the serpentine configuration (A). Based on the variations and combinations of these parameters various configurations of serpentine are possible. Few limiting cases of the serpentine configurations are sinusoidal channel, saw tooth configuration, etc as shown in Figure 4.1(b) and (c) respectively. As the combinations of these four parameters can give number of possible configurations therefore in such cases

the selection of the parameter becomes a difficult task as the performance of the serpentine channel varies with designed geometrical parameters.

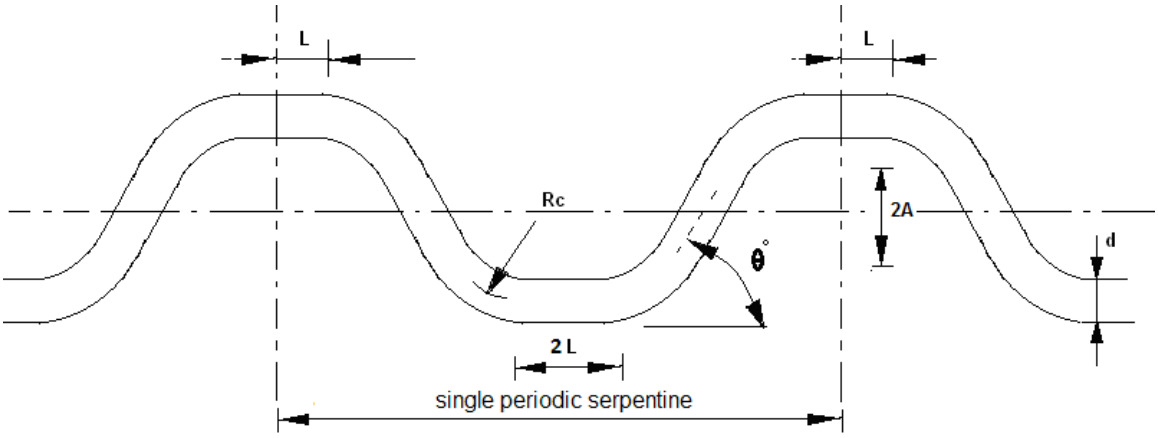

Figure 4.1 (a): Schematic of general serpentine channel

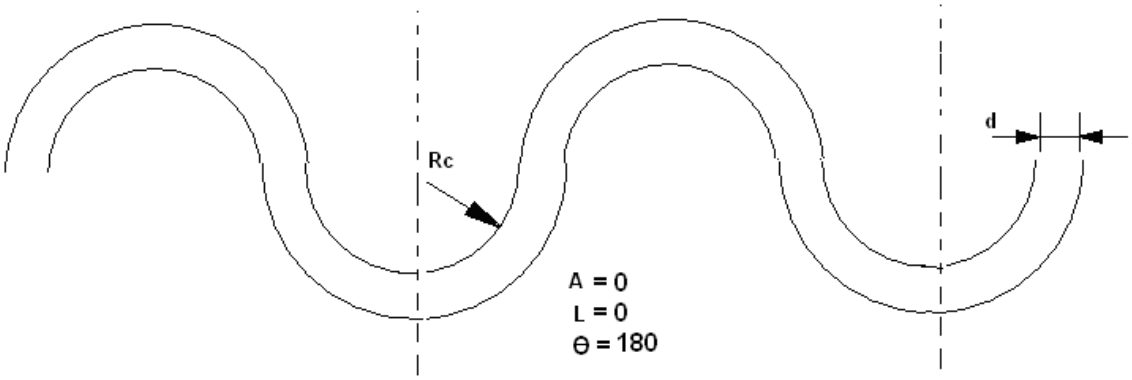

Figure 4.1 (b): Schematic of sinusoidal serpentine channel

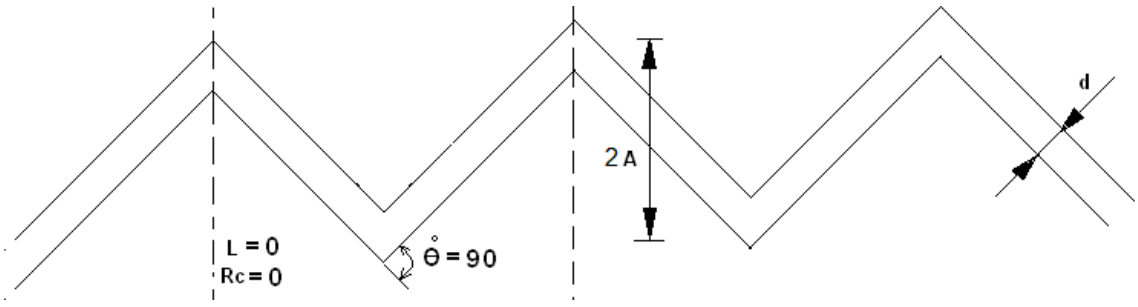

Figure 4.1 (c): Schematic of saw-tooth configuration serpentine channel

For this purpose the effect of various geometrical parameters on residence time distribution (or intensity of dispersion) needs to be studied thoroughly. In this context

some of the published work is briefly reviewed here. In light of this review, attempt is made to quantify this issue computationally in the present work. Computational fluid dynamics (CFD) model and obtained results are discussed in the following sections.

4.2. Literature review

Only few attempts can be found in the literature for the RTD analysis in serpentine channel systems. Majority of these consist of experimental investigations rather than the computational ones.

Trachsel *et al.*(2005) presented method for measuring the RTD in microfluidic systems. A piezoelectrically actuated sample injector releases approximately 100 nl of tracer liquid into a microchannel of rectangular cross section. The spreading of the tracer pulse in pressure-driven microflows was monitored with fluorescence microscopy measurements. RTDs were determined for single-phase liquid and segmented gas–liquid microflows, with the RTD being significantly narrower for the latter case. The selected flow conditions were relevant to synthesis in microreactors with residence times up to several minutes.

The effect of microchannel aspect ratio (ratio of channel depth to channel width) on residence time distributions and the axial dispersion coefficient have been investigated for Newtonian and shear-thinning non-Newtonian flow using computational fluid dynamics by Aubin *et al.*(2009). The results reveal that for a fixed cross-sectional area and throughput, there was a narrowing of the residence time distribution as the aspect ratio decreases. This was quantified by an axial dispersion coefficient that increases rapidly for aspect ratios less than 0.3 and then tends towards an asymptote as the aspect ratio goes to 1. The results also show that the axial dispersion coefficient was related linearly to the Reynolds number (Re) when either the aspect ratio or the mean fluid velocity was varied. However, the fluid Peclet number was a linear function of the Reynolds number only when the aspect ratio (and therefore hydraulic diameter) was

varied. Globally, the results indicated that microchannels should be designed with low aspect ratios (≤0.3) for reduced axial dispersion.

Lohse *et al.* (2007) developed an approach specially designed for microreactor applications which employs a tracer 'injection' using the optical activation of a caged fluorescent dye. Furthermore, the effect of the laminar flow on the determination of the residence time distribution in microreactors has been taken into account during the measurements and their interpretation to fulfill the requirements of the so-called 'mixing-cup-problem' on the microscale. Residence time distributions for an intricately structured thin microreactor were determined for different velocities. The ideality of the stimulus signal generated by the newly introduced technique was demonstrated for an analytically well-defined straight channel and compared with a signal derived from deconvolution of non-ideal input signals.

From the above review it is clear that the no information is available in literature about the effect of various geometrical parameters of the serpentine channel on the residence time distribution. The knowledge of the residence time distribution is necessary as serpentine microreactors are finding new opportunities among the researchers for achieving better chemistries. Therefore the knowledge of the effect of the various geometrical parameters on the mass transfer is essential for carrying out reactions in serpentine channel. Developing this knowledge with experiments is a difficult task. This can be easily handled with the help of CFD with lesser efforts. The study of heat transfer in serpentine channel from the previous chapter is thus extended here for getting the knowledge of residence time distribution and the dispersion present in serpentine channel.

The present CFD methodology was divided in two parts. In the first part the CFD model was validated for the simple system of tubular pipe flow. The developed methodology was further extended to understand the effect of various geometrical parameters of the serpentine channel on RTD. All Numerical analysis were carried out by using Commercial code of Fluent 6.3.36 and geometries are generated using Gambit 2.4

4.3: RTD in 1.5 mm circular tube to evaluate the CFD methodology

4.3.1 CFD methodology

The computational domain consists of an axisymmetric circular tube of 1.5 mm in diameter and 200 mm in length. The entire domain was meshed using hexahedral map elements. For grid sensitivity analysis simulations were carried out by using two different grid sizes. In the first case the channel radius was meshed with 25 elements having successive ratio of 1.1 and length was meshed with 500 elements having double successive ratio of 1.1. In second case the channel radius was meshed with 30 elements having successive ratio of 1.1 and length was meshed with 2000 elements having double successive ratio of 1.1.

Velocity inlet and pressure outlet boundary condition was used at inlet and outlet respectively for momentum equation with laminar flow model. At wall no slip boundary condition was used. At inlet laminar fully developed velocity profile corresponding to Re of 100 was given with water as a working fluid (i.e. Sc = 455) having constant physical properties. The entire fluid domain is nothing but a fully developed flow in velocity. The momentum equation was discritized using second order upwind scheme. The under-relaxation factor of 0.2 was used for momentum equations. The standard scheme was used for pressure discretization. The SIMPLE algorithm was employed for velocity–pressure coupling in the multi-grid solution procedure. At first only flow field (steady state) was solved completely. In the next step the converged flow field was freezed and the transport equation for the species was solved. The tracer having similar physical properties as water was injected. The under-relaxation factor of 1 was used while solving species transport model equations.

The effect of different tracer injection times and different time step was studied while solving transport equation for species. For this purpose time step between 0.0001s to 0.001s were used and the tracer injection time was changed from 0.015 to 0.1s. It is important that the time of tracer injection should be close to the true pulse input. Under-relaxation factor of 1 was used while solving concentration equations. The theoretical residence time corresponding to Re of 200 was 1.5s. Therefore the simulations were

carried out for minimum 15s thus ensuring complete exit of the tracer. The simulations were carried out for adequate iterations per time step to ensure acceptable convergence.

It is essential to use appropriate boundary condition at inlet and outlet while solving the equation of species transport. Two types boundary conditions for inlet and outlet makes total four possibilities (Levenspiel, 1999). These are 1) open at inlet and open at outlet 2) open at inlet and closed at outlet 3) closed at inlet and closed at outlet 4) closed at outlet and open at outlet. The effect of these boundary conditions was also studied.

The concentration of the species was monitored at the outlet at each time step. The concentration was reported as mass weighted average or mixing cup average. The data of concentration time (C vs. t) was processed to get the exit age distribution using Equation 4.1 as:

$$E(t)=\frac{C(t)}{\int_0^\infty C(t)dt} \text{ with } \int_0^\infty E(t)dt=1 \quad \text{.....} \quad (4.1)$$

This is nothing but E-t curve. This method is similar to that given in Levenspiel (1999). The mean residence time was calculated using Equation 4.2 as:

$$t_m=\frac{\int_0^\infty t\,E(t)dt}{\int_0^\infty E(t)dt} \quad \text{.....} \quad (4.2)$$

The variance was further calculated further as:

$$\sigma^2=\int_0^\infty (t-t_m)^2\,E(t)dt \quad \text{.....} \quad (4.3)$$

The knowledge of dispersion coefficient is essential to model process for representing flow in real vessels, for scale up etc. For estimating dispersion coefficient various model are available in literature e.g. axial dispersion model, tank in series model, Aries dispersion model, pure convection model etc. Which model to be used to fit the data of E(t) curve to get the information about the dispersion coefficient is always a question or a

difficult task. However for systems like pipe flow the things are quite simpler. A regime map for use of different model depending on the Reynolds number can be found in Levenspiel (1999). Figure 4.2 shows the same applicable for sufficient long residence times. Based on the operating condition used in the present simulation the regime appears as convention dominated regime. The convection model (Levenspiel (1999) for pipe flow is given by Equation 4.4 as:

$$E(t)=\frac{\bar{t}^2}{2t^3}\ for\ t\geq\frac{\bar{t}}{2}\ and\ E(\theta)=\frac{1}{2\theta^3}\ for\ \theta\geq\frac{1}{2} \quad \text{..... (4.4)}$$

The results from the present simulation were compared with the above theoretical convection model.

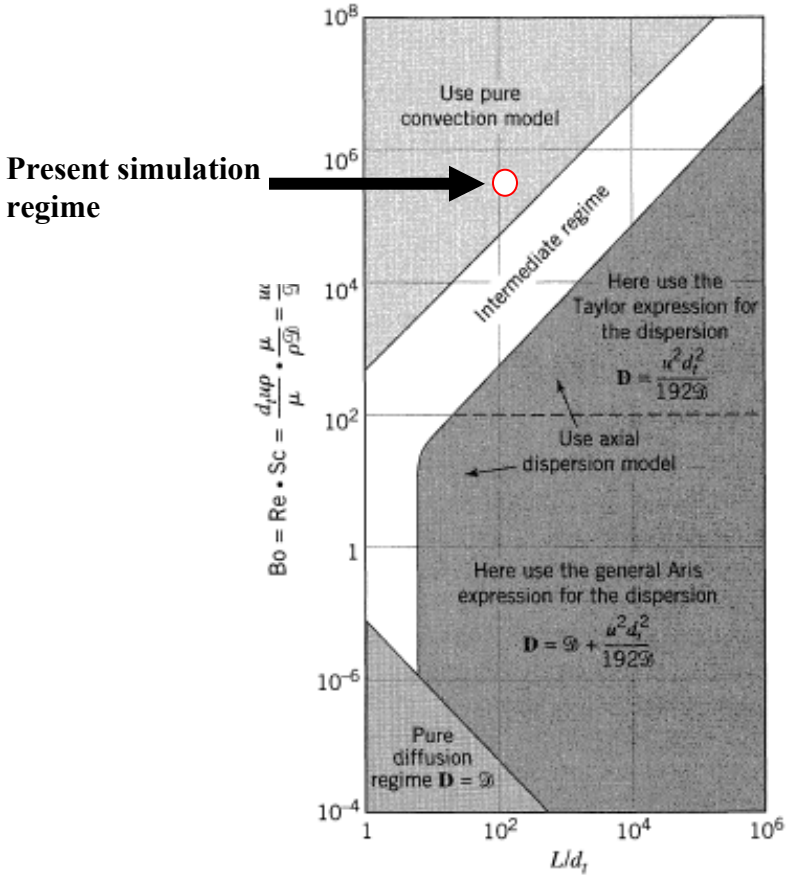

Figure 4.2: Map showing which flow models should be used in any situations (Levenspiel 1999)

4.4 CFD analysis in 2mm x 2mm x 100 mm serpentine channel to understand the effect of various geometrical parameters on RTD

4.4.1 Computational methodology

In previous section the CFD methodology was developed for pipe flow. The results from the same were validated with that of theoretical E-t curve of pure convection model. The objective or need of doing the same lies on the fact that there is no RTD data available in literature either experimentally or theoretically for serpentine case to be studied in this section. Therefore one must ensure or adapt correct methodology while applying it to study RTD in serpentine channel.

In the present work the periodic serpentine geometry consists of a square channel with 2 mm x 2 mm in cross section with periodic length of 100 mm. The effect of bend angle (θ), straight length before bend (*L* i.e. distance between the bends/2) and radius of curvature (*Rc*) on the intensity of dispersion present in the various serpentine configurations as compared to that of straight channel was studied. The ranges of the serpentine geometrical parameters were given in the Table 4.1.

The individual total length of all of the above serpentine configurations listed in the Table 1 is 100 mm that kept constant in all serpentine configurations. Once the angle was defined the amplitude of the serpentine gets specified because of the constraint of the total length of 100 mm. The sample calculation is shown in Appendix I.

The sample computational domain for one of the serpentine configuration of case 3 is shown in Figure 4.3. The entire domain was meshed using hexahedral map elements. Grid sensitivity analysis was carried out and a computational grid of 30 x 30 x 720 cells (for a single periodic serpentine) was found to be a better choice. The channel width and height was meshed with double successive ratio of 1.1 while the channel length was meshed with a double successive ratio of 1.02. Total 648000 cells were used in simulation.

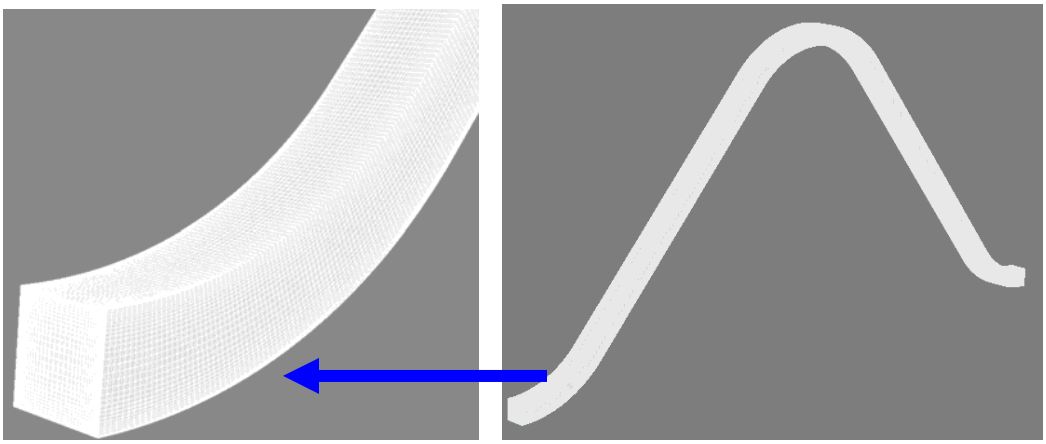

Figure 4.3: Example of computational domain in section 4.4.1

Steady state solution of momentum equations have been found for channel Re of 200 with laminar flow model. Water was used as working fluid with constant physical properties (*Sc* = 455). The solutions were obtained for the periodic case which represents periodically developed conditions in velocity. The other simulation parameters for the flow equations were same as used in section 4.3.1. At first only flow field (steady state) was solved completely. In the next step the converged flow field was freezed and the transport equation for the species was solved. The tracer having similar physical properties as water was injected. The under-relaxation factor of 1 was used while solving species transport model equations. Open-open boundary condition was used at inlet and outlet respectively for the species transport model. The theoretical residence time corresponding to Re of 200 was 1s. Therefore the simulations were carried out for minimum 25 s thus ensuring complete exit of the tracer. The time step of 0.001 s was used in the present simulations with adequate iterations per time step to ensure acceptable convergence.

The rest of the data monitoring and analysis procedure was same as mentioned in section 4.3.1.The results from the present simulations were compared using variance (Equation 4.3) as criteria to compare or analyze the effect of various geometrical parameters of serpentine channel on intensity of dispersion.

4.5 Results and discussion

4.5.1 Evaluation of CFD methodology with literature data: RTD in 1.5 mm circular tube

At first the effect of boundary conditions at inlet and outlet on RTD is studied. Figure 4.4 shows the E-t curve for all four different boundary conditions (see section 4.3.1) for time step of 0.001s with tracer injection time of 0.015s. The present tracer injection time is 1% of theoretical mean residence time of tracer. It can be seen that for the convection dominated system the boundary condition does not play a significant role as the RTD curves for all boundary conditions are overlapping each other. It must be noted that the present simulations operating conditions falls in convection dominated regime.

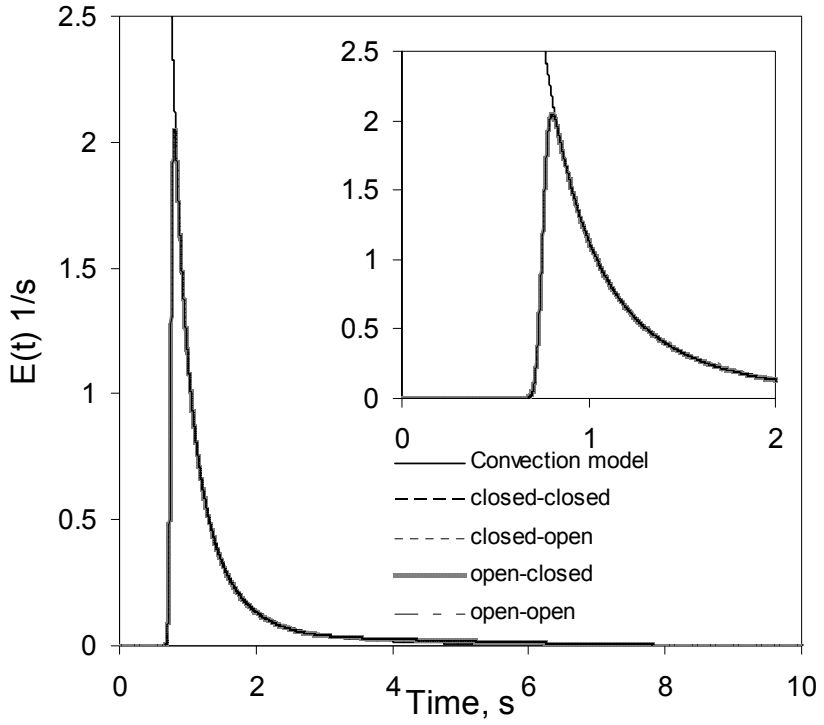

Figure 4.4: Effect of different boundary conditions on residence time distribution (time step 0.001s, tracer injection time 0.015s, grid 32 x 2000)

Figure 4.5 shows the comparison of residence time distribution for two different grid sizes. Both the distribution curve overlaps with almost similar variance as can be seen from Table 4.2. For further simulations the computations domain having grid size of 32 x 2000 was used.

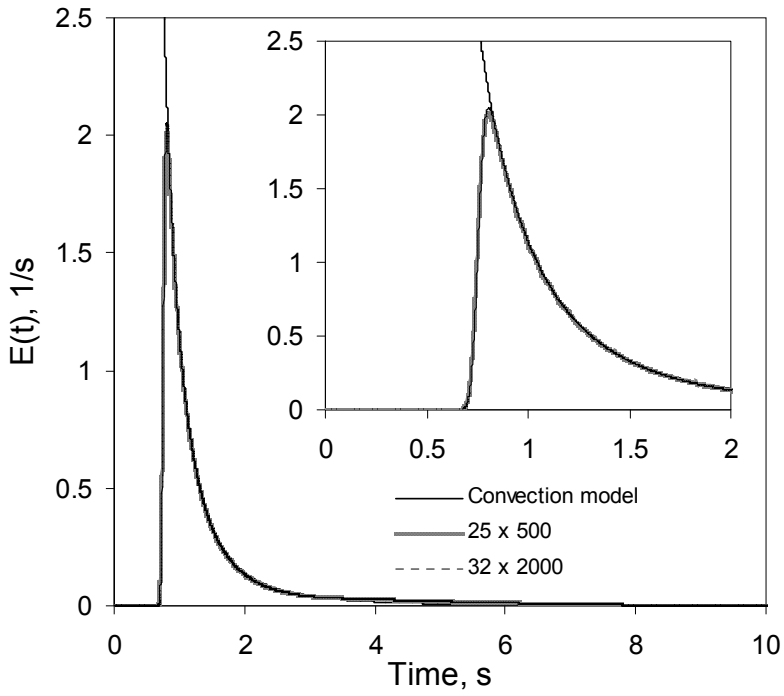

Figure 4.5: Effect of different grid size on residence time distribution (time step 0.001s, tracer injection time 0.015s, open-open boundary condition)

Table 4.2: Effect of time step and tracer injection time on variance

Grid	Time of Tracer Injection (s)	Time step (s)	Area (Et)	Mean residence time (s)	σ^2 (s^2)
25 x 500	0.015	0.001	1	1.512853	1.406861
32 x 2000	0.015	0.001	1	1.511618	1.401306
32 x 2000	0.1	0.0001	1	1.553368	1.400078
32 x 2000	0.1	0.001	1	1.553816	1.401327
32 x 2000	0.015	0.0001	1	1.511292	1.399951
32 x 2000	0.015	0.001	1	1.511618	1.401306

The effect of time step as well as time of tracer injection is shown in Figure 4.6. It is worth noting here that the true pulse input is difficult to achieve in numerical simulation. For comparison the theoretical convection model was also plotted in Figure 4.6. It can be seen that there is little difference in amplitude of the curve between simulated and theoretical curve. This is because of deviation from the true pulse input for tracer injection. The amplitude increases as the tracer injection time reduces. This also reduces the amount of tracer injected in to the system. It is also necessary that sufficient amount

(concentration) of tracer to be injected in to the system. It can be seen from the graph that lesser the tracer injection time much close is the amplitude value with the theoretical one but it does not affect the variance in any case. Table 4.2 shows the variance and mean residence time for different time step as well as for different tracer injection times. The simulated E-curve using 0.001s time step and 0.015s tracer injection time gives almost similar residence time distribution curve as theoretical one.

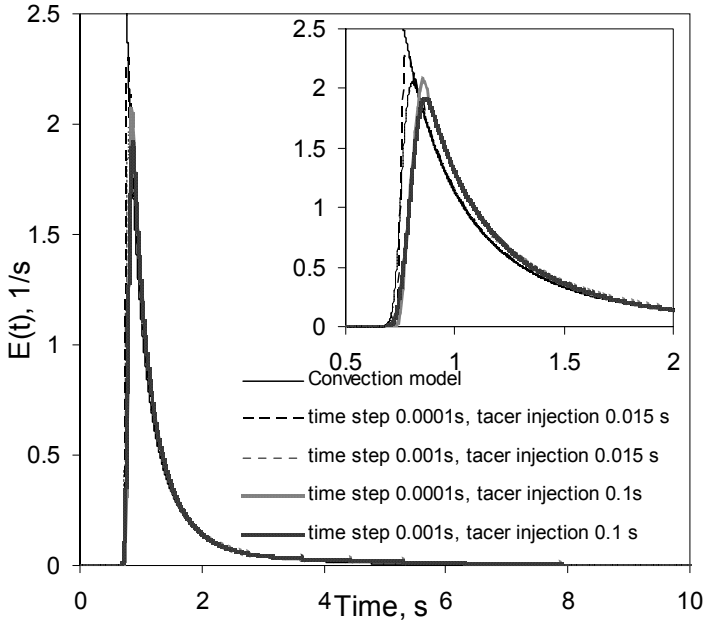

Figure 4.6: Effect of time step and tracer injection time on residence time distribution (open-open boundary condition)

The species transport equation considers the transport of tracer by diffusive as well as convective mechanisms. The relative contribution of the individual mechanism gives different performance in residence time distribution. In the present case the operating condition is fully developed laminar flow (in terms of velocity). The properties of tracer are as same as that of parent fluid (water). Therefore due to convection dominated nature, the tracer element of fluid slides past its neighbor with no interaction by molecular diffusion. Thus the spread in residence times is caused only by velocity variations. It can be seen from above results theoretical residence time distribution can be well obtained using present CFD methodology.

As the present simulation conditions falls in a convention dominated region the axial dispersion model cannot be used to calculate the dispersion coefficient. This can be clear from the regime map shown in Figure 4.2. In many cases the dispersion coefficient *D* is not constant along the flow length i.e. it changes from position to position. Therefore estimation of dispersion coefficient is not done in the present work. However variance is one of the important parameter that is used in all models (e.g. axial dispersion model, tank in series model etc.) involving dispersion coefficient and therefore one can judge the performance of the reactor using residence time distribution as well as variance.

Based on the result it can be seen that the present CFD methodology can be used to study the effect of different geometrical parameters on the residence time distribution/intensity of dispersion in serpentine channel. The variance of a residence time distribution curve was found to be the better and appropriate choice to understand the intensity of dispersion present in different serpentine configurations.

4.5.2 Effect of inclination/bend angle (θ) on performance

In the first case the effect of different bend angles was studied. Here the serpentine configuration was zigzag (saw tooth like) in nature (see Appendix I or Table 4.1). The crossing of fluid streamlines was achieved by using sharp bends. Because of the bend effect, the velocity profile gets distorted and depending on the bend angle the intensity of the fluid mixing varies. This distortion of the velocity profile also affects the required flow development length after the bend. Figure 4.7 shows the effect of different bend angles on variance obtained. All values were normalized with the results of the straight channel with same Re, length, aspect ratio and in cross section area.

The first observation that can be made from the Figure 4.7 is that the variance in case of serpentine with sharp bend is much less than that of straight channel. The straight channel always gives long tail of the tracer and therefore results in longer residence time distribution (see Equation 4.4). Further it can be seen that the serpentine variance decreases with increase in the bend angle up to 90^o degree however above 90^o bend angle the variance increases. The reason for higher variance is longer tail length. Longer the

tail, higher is the variance. In case of serpentine configurations having higher bend angles the dead zones gets developed at the bend corner. This can be seen in velocity contour plot shown in Figure 4.8. Dues to this, the tracer stays in these regions for quite longer time and therefore results in higher variance. Typically smaller is the variance, lesser is the dispersion and therefore performance is towards the plug flow behavior. However this is not entirely true. In the case where dead zones are present, variance will be higher due to the long tail of the tracer. This does not mean that the dispersion is higher in the case where dead zones are present just because of higher variance. However the drawback of the dead zones is that the amount of effective volume gets lowered that affects the performance of the reactor in terms of lower conversion. In the present case 90^o bend angle serpentine configuration gives narrower RTD compared to other bend angles studied in the present work.

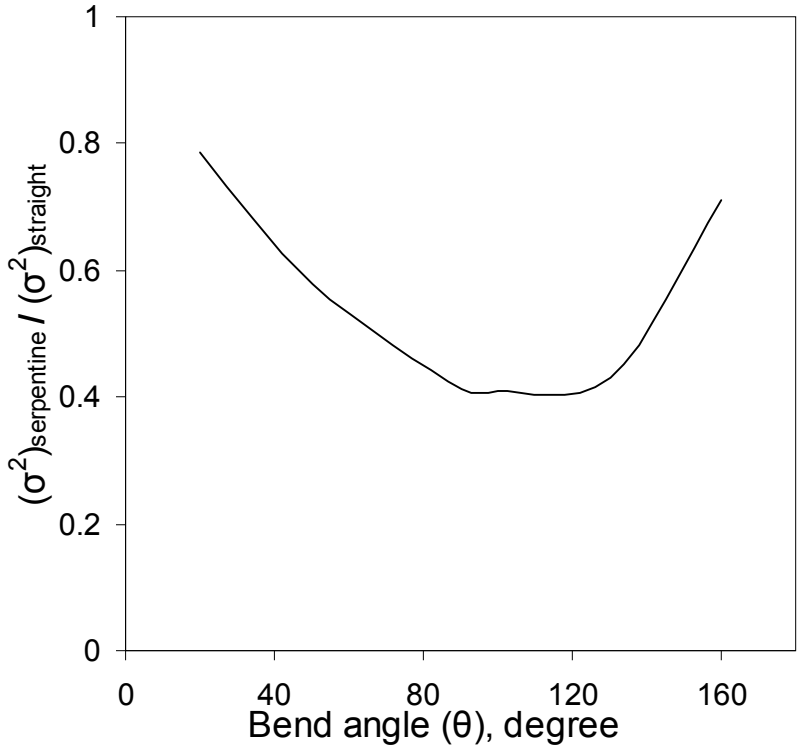

Figure 4.7: Case 1- effect of bend angle on σ^2

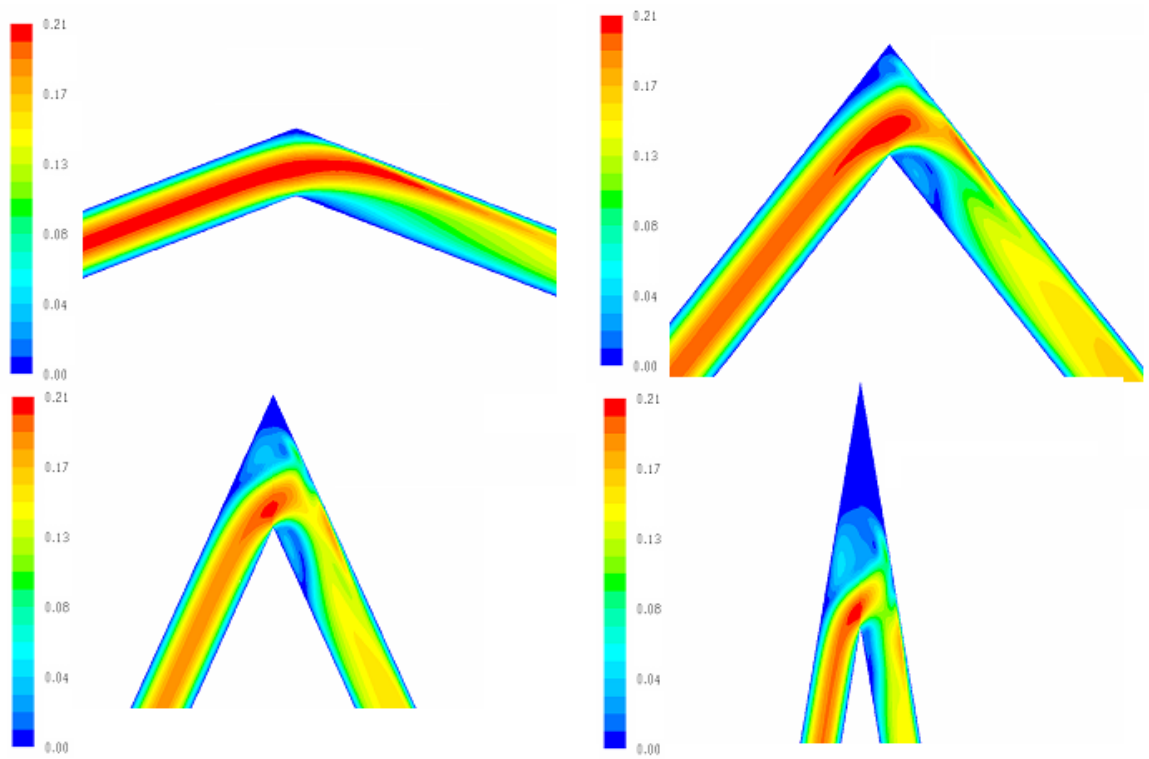

Figure 4.8: Velocity contour plot for different bend angle (Re: 200)

4.5.3 Effect of straight length before bend on performance

In the second case the effect of straight length before bend was studied. The difference between the case 1 and the present case is that the sharp bend in the case 1 is separated by the straight portion or length between them. Figure 4.9 summarizes the results in terms of effect on variance. Along with the effect of straight length, the Figure 4.9 also shows the variance in absence of straight length i.e. comparison with the results of case 1 i.e. $L = Rc = 0$.

The presence of straight length before bend decreases the variance than that of absence of straight length i.e. case 1. This means that the presence of straight length before bend helps in narrowing the RTD rather than having only bend without straight length before bend (see Figure 1 for terminology of straight length before bend). It should be noted that the number of bends in case 2 are double than that of case 1. Meaning in absence of straight length before bend i.e. having only sharp bend, in 100 mm total length, the fluid gets turned by a given bend angle two times whereas in the case of presence of straight

length before bend the total number of bend becomes 4 i.e. fluid gets turned by a given inclination/bend angle by four times in case 2. Due to this the case 2 becomes more efficient in decreasing the variance for a given bend angle. Therefore it can be seen that to get the performance towards the plug flow from the straight channel, the channel have to be broken in different part or bend sections resulting in good radial mixing at those locations. This also means higher the number bends higher is the radial mixing at those locations. As we know higher is the number of mixed reactors in series the performance of the systems goes near to the plug flow. The present result shows the similar phenomena.

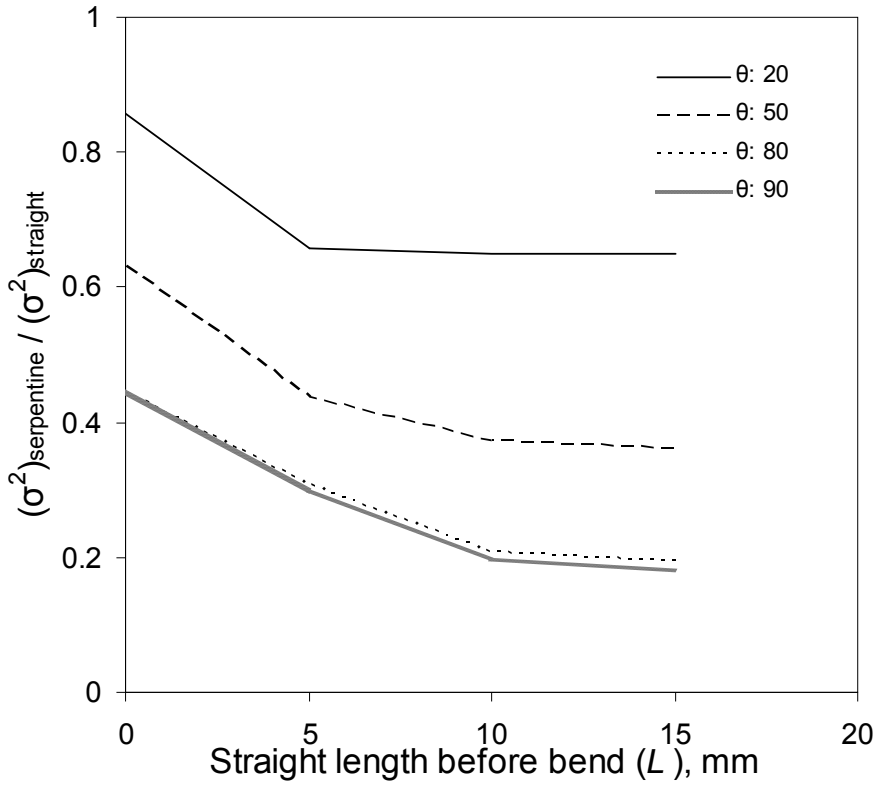

Figure 4.9: Case 2- effect of straight length before bend in sharp bends or in absence of curvature on σ^2

In case 2 for serpentine configurations having small bend angles i.e. 20^o the pressure loss in bend is same in all cases (range of straight length (L) studied for a particular angle) because of the same bend angle (i.e. same pressure drop due to turning the fluid streamlines by particular angle) for various straight lengths (L) studied. The rest of the

pressure loss is governed by the developing flow pressure drop for the restoration of the distorted velocity profile. This also means that the RTD depends on velocity profile in the channel e.g. developed velocity profile or developing velocity profile. In case of smaller bend angle serpentine configuration there is not much distortion of the velocity profile at the bend. Therefore the length required to develop the velocity profile again is less i.e. the flow quickly develops as it passes the bend and therefore no reduction in dispersion is obtained due to presence of velocity gradient in radial direction. In case of 20^o bend angle serpentine configuration changing the length from 5 mm to 15 mm does not show any remarkable change in RTD curve and therefore no change in variance also. In case of small length (i.e. L = 5 mm), the distance between the second and the third bend is small and together both create good intensity of mixing when placed closed to each other. A single sharp bend (for the case of L = 15 mm) of small bending angle (i.e. 20^o) does not create a sufficient amount mixing.

In case 2 for serpentine configurations having higher bend angle i.e. 50^o and above, the changes in straight length before the bend make significant effect on RTD curve. For higher angles the RTD is also governed by the flow development length after the bend. Therefore as the straight length before bend (L) increases, the length between the second and the third bend ($2L$) also increases. Much of the flow remains in developing region whereas for small length case (L = 5 mm) there is sufficient length to develop the velocity profile immediate after the first and the third bend. Therefore higher the straight length before bend (i.e. L = 10 mm and above) much of the flow remains in developing region and therefore the narrowed RTD is observed due to lesser radial gradient in the velocity.

4.5.4 Effect of curvature (*Rc*) on performance

In the third case the effect of radius of curvature i.e. smoothness of the bend is studied. Figure 4.10 (a) summarizes the results in terms of effect on variance. Along with the effect of curvature the Figure 4.10 (a) also shows the variance in absence of curvature i.e. for sharp bend or $L = Rc = 0$.

It can be seen from the Figure 4.10 (a) that in all cases the variance is much smaller as compared to that of straight channel. For serpentine configurations having bend angle around 40^o, replacement of sharp bend with curvature (i.e. replacement of sharp bend with smooth bend) does not improve the performance in terms of variance. Along with this it can be seen that the increase in radius of curvature somewhat increases the variance. In general, the dispersion decreases with increase in a dean number (*Dn*) or increasing the effect of secondary flow. Increasing the radius of curvature for a constant channel size and Re, decreases *Dn* and hence decreases the intensity of the secondary flow structure. This affects the radial mixing in a channel to the certain extent. Therefore decrease in radial mixing due to decrease in *Dn* results in somewhat increase in variance.

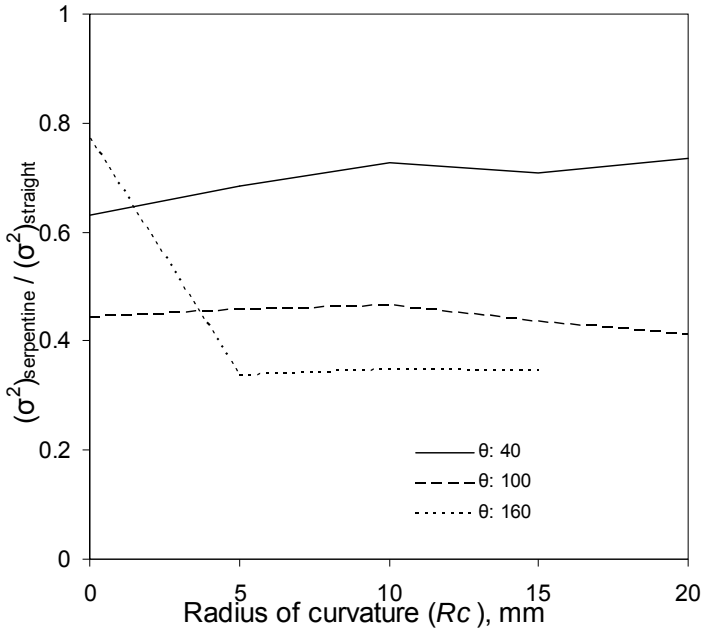

Figure 4.10 (a): Case 3- effect of radius curvature in absence of straight length between bend on σ^2

For serpentine configurations having higher bend angle e.g. 180^o with presence of radius of curvature, the concept of bend angle or inclination may not be applicable. This is because for very high radius of curvature the effect of secondary forces will be less (due to lesser *Dn*) and the channel will behave as a straight one. e.g. 180^o bend with very high curvature the serpentine configuration will be no more curved channel from performance

point of view. For the sake of simplicity and the lower values of the radius of curvatures used, the terminology of bend angle is still retained in this section.

Similar results were found for the serpentine configuration with 100^o bend angle with presence of curvature as obtained for lower bend angle serpentine configurations. No improvement in terms of reduction in variance is observed with increases in radius of curvature. The result also shows that even though there is presence of curvature; the variance reduction is only due to the turning of fluid by certain angle. This means the curvature doesn't affect the performance in the range of the *Dn* at curvature section used in the present study.

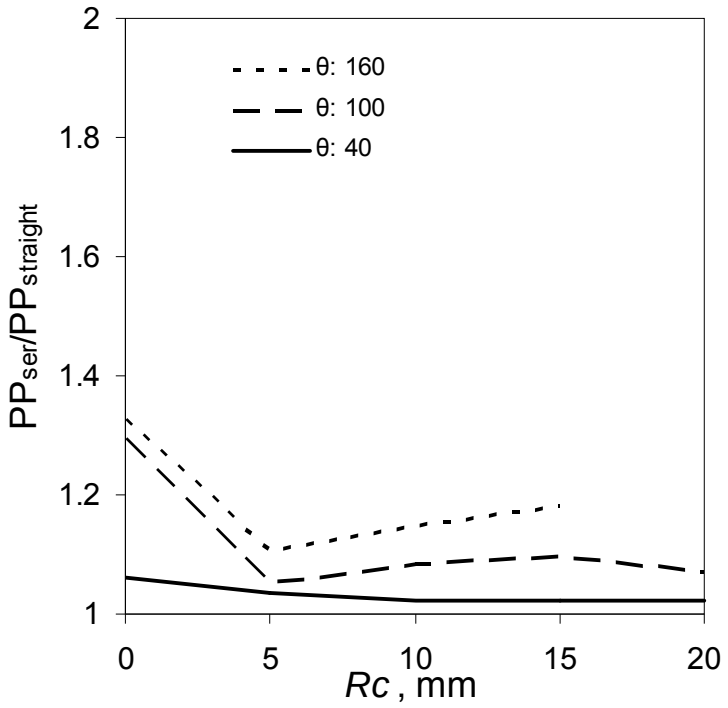

Figure 4.10 (b): Case 3- effect of radius curvature in absence of straight length between bend on pumping power

One important observation that can be seen from the present results (i.e. case 3) is that the serpentine configurations with bend angle around 160^o there is significant reduction in variance compared to case 1 i.e. sharp bend/absence of curvature. As discussed in the Case 1, there were dead zones (see Figure 4.8) present in the corners when the mixing is

taking place at the corners. The presence of curvature at the bend helps in removing these dead zones thus eliminating the possibility of the dead zones resulting in improvement in reduction in variance. For the lower bend angle serpentine configurations the variation of curvature does change the variance to the considerable extent. However it must be noticed that the pressure drop in case of smooth bends i.e. case 3 is much lower than that of the sharp bends (i.e. case 1) as can be seen in Figure 4.10 (b). A detailed discussion is followed in the later section.

4.5.5 Effect of curvature with constant straight length before bend on performance

The case 4 involved the study of effect of radius of curvature (*Rc* or smoothness of a bend) when the straight length before bend (*L*) is fixed at 5 mm. The results are summarized in Figure 4.11. In this case the sharp bend after the straight length of case 2 is replaced by the curvature (i.e. sharp bend of case 2 is replaced by smooth bend). Along with the effect of curvature (i.e. studies of case 4) the Figure 4.11 also shows the results case 2 for comparison i.e. absence of curvature or presence of sharp bend with L= 5 and Rc = 0.

For serpentine configurations having low bend angle e.g. 20^o replacing the sharp bend with the curvature slightly increases the variance. As discussed in section the dispersion decreases with increase in a dean number or increasing the effect of secondary flow. Increasing the radius of curvature (*Rc*) for a constant channel size and Re, decreases the *Dn* and hence the intensity of the secondary flow pattern. Therefore in the present case the intensity of the secondary flow reduces with higher curvature. The result shows that the reduction in variance is solely due to the turning fluid by angle achieved by use of curvature/smooth bend. There is also a benefit of using curvature for turning the fluid streamline. This benefit lies in pressure drop required to achieve the operation. Definitely for higher bend angle i.e. 80^0 the performance as in absence of curvature (or performance as that of sharp bend) can be achieved by using the curvature at much lesser power.

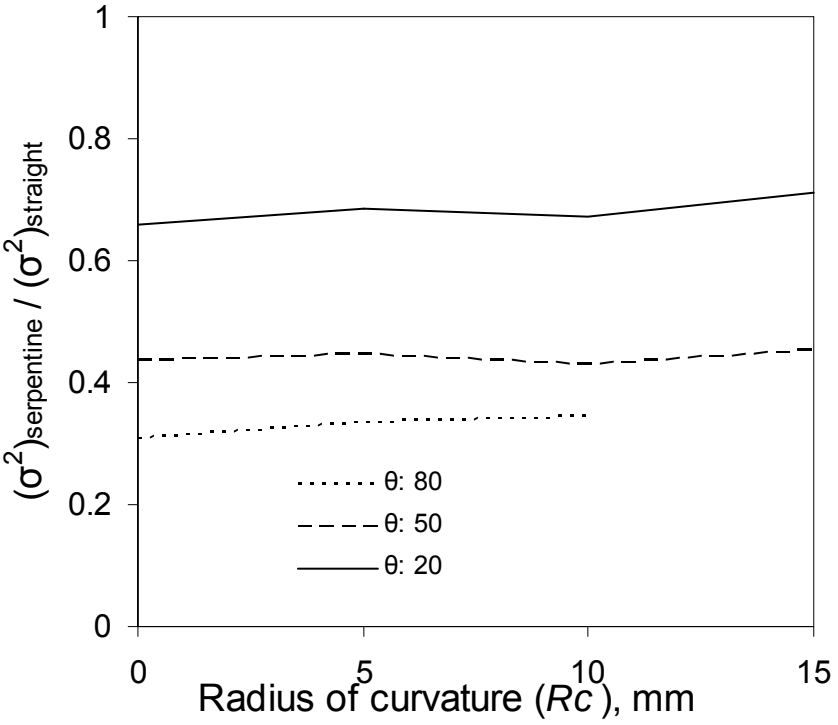

Figure 4.11: Case 4- effect of radius curvature for a fixed straight length before bend of 5 mm on σ^2

4.5.6 Effect of different straight length before bend with constant curvature on performance

The case 5 involved the study of different straight length (*L*) before bend for the fixed radius of curvature (i.e. constant bend smoothness) *Rc* at 5 mm. The results are summarized in Figure 4.12. In this case the smooth bend of case 3 is separated by the straight length portion (i.e. smooth bend of case 3 is separated by straight length portion). Along with the effect of straight length before bend (i.e. studies of case 5) the Figure 4.12 also shows the results of case 3 for comparison i.e. absence of straight length and presence of curvature (smooth bend) with $L = 0$ and $Rc = 5$ mm.

As discussed in case 2, for lower bend angle serpentine configurations, the closer bend (i.e. smaller length before bend e.g. $L = 5$ mm) creates good mixing intensity and hence results in decreased variance. However for serpentine configurations having low bend

angle i.e. 20^o increasing the straight length before bend (from L = 5 mm to 10 mm) have insignificant effect on variance.

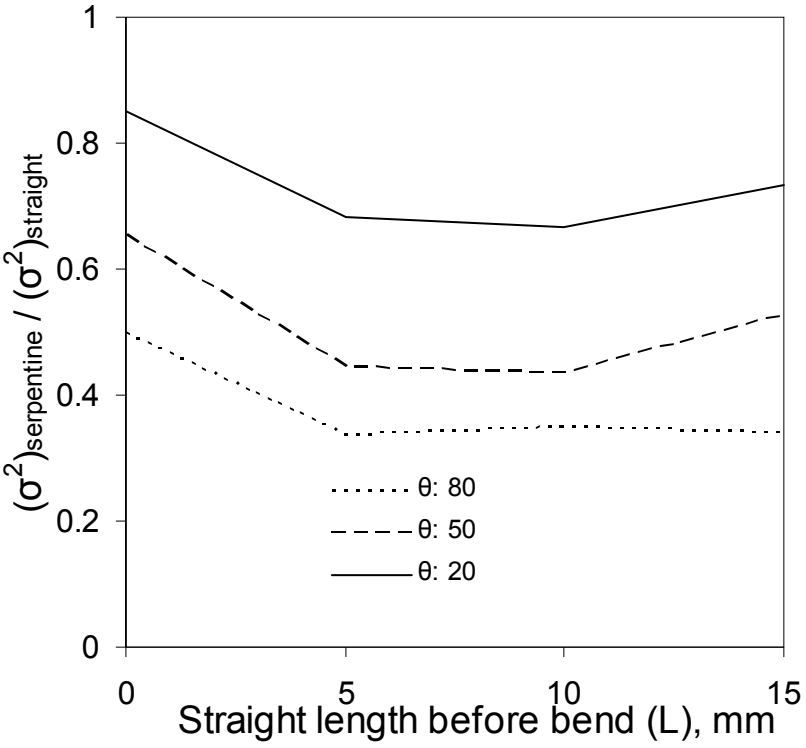

Figure 4.12: Case 5- effect of straight length before bend for a fixed curvature of 5 mm between the bend on σ^2

For serpentine configurations having bend angle 50^o, increasing the straight length before the bend from 5 mm to 15 mm somewhat increases the variance. In this case a decrease in the amplitude (A or the distance between the first and the second) of the bend is expected with the increase in the straight length before bend. Therefore in this case much of the flow after the bend should remain in developing region. The available region of the developing flow should increase with the increase in the straight length before bend (L). However it should be noticed that the variation in straight length before bend and the amplitude are always opposite to each other i.e. for a constant total length (100 mm in this case) as straight length before the bend increases (i.e. increase in the distance between the second and the third bend) the corresponding amplitude decreases (i.e. vertical distance between the first and the second bend decreases). Therefore in the case of much higher straight length before bend (L =15 mm), though the flow in the section

between the first and the second bend remains in developing region (i.e. lesser dispersion) at the same time the increased distance between the second and the third bend results in much developed velocity profile (i.e. increased dispersion). Therefore the two complementary effects results in only somewhat increase in variance for serpentine configuration with 50^o bend angle (for increase in straight length before bend from 5 mm to 15 mm) and almost makes no significant changes in case of serpentine configuration with 80^o bend angle (see Figure 4.12).

4.5.7 Effect of bend angle for different Reynolds number

Dean number gives the significance of the secondary forces or dean forces therefore the intensity of the secondary forces also depends on Reynolds number. The serpentine configurations that are performing better at certain Reynolds number need not have to perform better or give similar performance at other Reynolds number. Therefore the performance of the serpentine channel depends on the operational Reynolds number. As mentioned earlier the simulations were carried out for Re of 200 and 50. Only the effect of different bend angle i.e. case 1 is shown here to compare the performance for two different Re.

Figure 4.13 summarizes the results obtained. It can be seen from the Figure 4.13 that higher is the mean residence time higher is the variance or dispersion. Therefore the variance is more for Re equal to 50 as compared to Re equal to 200. The lowest variance is obtained by the serpentine configuration having bend angle of 90^o for Re of 200. However for the value of Re equal to 50, the variance decreases with increase in the bend angle up to 120^o and the same increase again with further increase in bend angle. Lowest variance is obtained by the serpentine configuration having bend angle around 120^o. Reduction in dispersion demands better fluid mixing that may not be well achieved by lower angles in case of Re 50. Approximately 120^o bend angle serpentine configuration is capable of achieving better mixing thus giving lowest variance (or dispersion) for Re equal to 50.

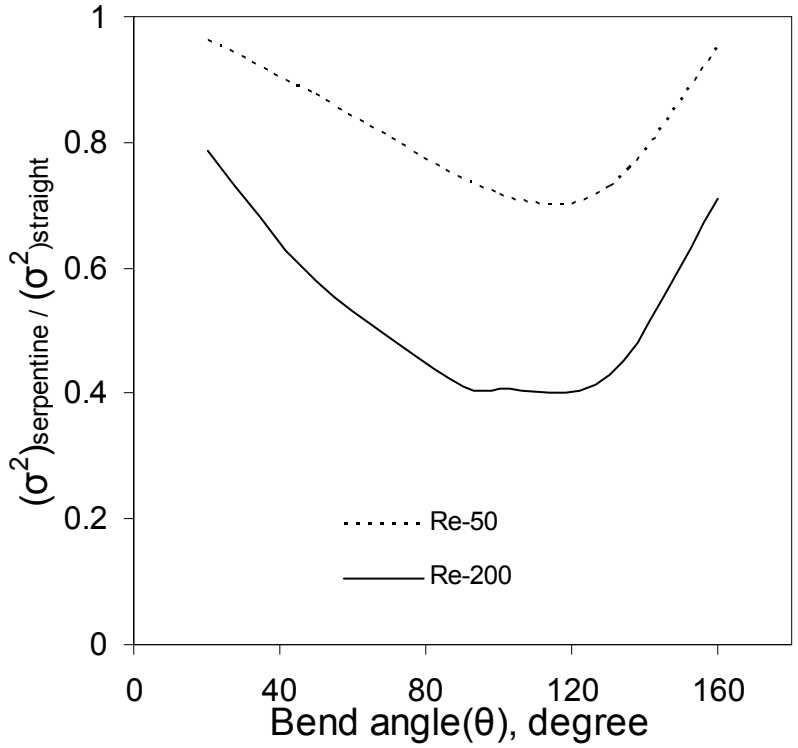

Figure 4.13: Effect of bend angle for different Re

For through understating of the dispersion in serpentine channel it is necessary to understand the available knowledge about the dispersion in circular/square straight channels and helical channels. For circular straight channel the summary of the literature can be found in Ekambara and Joshi (2004). The authors have used a numerical method to get the concentration profiles of the tracer and compared their results with the available literature models for concentration profiles. The authors have covered a wide range of Peclet number and dimensionless time (τ). However the area of dispersion in circular helical coils is still in developing state compared to that of straight channels. Trivedi and Vaudeva (1975) reported the experimental study of dispersion of solute in helical coils in the range of $10 < \lambda < 280$, $10 < Re < 1600$ and $1500 < Sc < 8700$. The authors also gave the criteria for the validity of dispersion model over the range of the studies in their work as $\tau > 6Re^{-1}$. According to the authors over the Reynolds number range investigated the τ_{min} (minimum required residence time for Taylor's dispersion to occur) for helical coils was much less than that for straight tubes. Janessen (1975) correlated the ratio of dispersion coefficient in coiled tubes to that of straight tubes as a function of Dn^2Sc,

provided $\lambda > 20$. Shetty and Vasudeva (1976) later correlated ratio of to $DnSc^{1/2}$ based on the available literature data. The range of the applicability of the correlation was $7 < DnSc^{1/2} < 75$. Dimensionless time (τ) is an important parameter that decides the contribution of the diffusion to the axial dispersion. The primary reason behind much higher residence time distribution in straight tube lies in the parabolic velocity profile (see Equation 4.3). This profile makes the fluid elements near the wall to travel slowly. In case of helical coils the secondary flow structures greatly reduces the difference between the mean axial velocities for the various streamlines, which results in the decrease in the axial dispersion i.e. decrease in the intensity of dispersion with increase in the *Dn*.

The present simulation cases of serpentine channel configurations are not exactly reassembling with the helical coils but the principal phenomenon is same i.e. radial mixing using secondary flow to reduce the axial dispersion. Both the sharp bend and the curvature fulfill this task except at different intensity and different pumping power. The primary classification of the different cases is discussed in the section 4.1.

Considering the first case where the classification of the serpentine configurations was based on the bend angle (i.e. the angle by which the fluid streamlines gets turned). In case 1 this is achieved by using sharp bends. In case of sharp bend complete or partial mixing of streamlines takes place depending on the bend angle. There are two benefits in this process. The first is achieving radial mixing thereby reducing the difference in the mean velocity among the streamlines thus resulting in lesser dispersion. The second benefit is, due to the bend the velocity profile gets distorted and the flow next to the bend region remains in developing state for certain length. The system behaves as the entrance region and therefore lower dispersion can be obtained as the dispersion for the developing flow is smaller than fully developed flow (Nunge and Gill 1969). In the present case the serpentine configuration having bend angle of 90^o (or nearby configurations) is found to be giving least variance i.e. narrower residence time distribution. More the destruction of the velocity boundary layer better is the performance in terms of smaller dispersion. One would expect the better performance from the higher bend angle serpentine configurations (e.g. 160^o than that of 90^o) assuming that the higher bend angle would

cause greater amount of radial mixing or complete breaking of velocity boundary layer. However the operating parameters used in the present study (i.e. Re-200) creates the dead zone at the bend region (see Figure 4.8) making it difficult for the tracer to come out easily thus giving wider residence time distribution. In this case it is practically difficult to analyze of the concentration time data due to difficulty in ensuring the complete tracer collection at the outlet. However the theoretical residence time used in the present simulation was 1s and the tracer from the outlet was collected for more than 40s. The performance of the higher bend angle serpentine configurations can be better if one can overcome the dead zones. This is discussed in more details in subsequent sections.

In the second case, the sharp bend from the case 1 was separated by the straight length which we defined as straight length before bend (L). In this case also the fluid streamlines turns by certain angles similar to the case 1. The only difference lies here is that the length after the bend is changed/lowered so that the flow remains in a developing state. Similar to the comments made in the previous paragraph that the serpentine configurations with the bend higher angle creates more transverse mixing giving the narrower residence time distribution. Thus 90^{o} bend angle serpentine configuration can be seen to be giving least variance than any other bend angle. However in this case apart from turning the fluid by certain angle using sharp bend (i.e. intermixing of the streamlines) there is another mechanism that contributes for lowering the variance. The mechanism for this is developing nature of the flow after the bend. Due to destruction in the velocity boundary layer at the bend region, the velocity profile immediate after the bend region remains in the developing region up to next bend. This can be seen clearly in the serpentine configuration having straight length portion before bend more than 10 mm (see Figure 4.9). Lesser radial velocity gradient immediate after the bend section i.e. developing flow region (due to mixing at bend) also results in uniform radial distribution of the tracer. However the pressure drop for the developing flow region is always more than that of developed flow region. The serpentine configurations with higher straight length before bend (e.g. L = 15 mm) also offers somewhat higher pressure drop. However the significant contribution of the developing nature of the flow towards the lesser residence time distribution can be noticed in this study of case 2.

The third case under the study was the effect of curvature in smooth bends on the residence time distribution. Here the sharp bends from the case 1 were replaced by the curvature. However it is important to understand that the bend angle (or streamlines turning angle) may loose its significance if the radius of curvature is very high. As mentioned earlier for the sake of simplicity the terminology is still retained in this section. This also works because of the small curvatures used in the present study (approximately $0.66 < r/Rc < 2$). Here it becomes necessary to understand the mechanism by which the radial mixing takes place. As we saw in case 1 and case 2 that the radial mixing took place because of the sharp bends i.e. crossing of fluid streamlines. However in case 3 due to absence of the sharp bend and the presence of the curvature the radial mixing taking place due to the secondary flow structure created at the bend section. It can be seen from the Figure 4.10 (a) that for serpentine configurations having bend angle of 100^o there is hardly any difference in the variance between presence of curvature (i.e. case 3 or smooth bend) and absence of curvature (i.e. case 1 or sharp bend). Both cases are carrying out the similar operations i.e. mixing however the pressure drop required to achieve this operation is much different. The pressure drop in case of smooth bends i.e. case 3 is much lower than that of the sharp bends (i.e. case 1) as can be seen in Figure 4.10 (b). Particularly for serpentine configurations with higher bend angle of 160^o the presence of curvature reduces the variance significantly. As discussed in the section 4.5.2, the dead zones present in 160^o bend angle serpentine configuration were responsible for the wider residence time distribution. However the presence of curvature (i.e. switching from sharp bend to smooth bend) overcome these dead zones resulting in narrower residence time distribution with much lesser pressure drop than that of sharp bend of similar angle (Figure 4.10 (a, b)). The dean numbers (*Dn*) at the bends sections changes from 126 to 73 for the radius of curvature (*Rc*) 5 mm to 15 mm. Thus dean number at the bend section reduces with increasing the curvature (*Rc*). An increase in the dispersion is expected with the decrease in *Dn*. However due to insufficient region available for the secondary flow structure (very small curved potion available), the effect of variation of curvature cannot be seen from the present study.

The fourth case is nothing but the combination of all first three cases. In this case, the effect of variation in radius of curvature with specifying a constant straight length before bend (L) at 5 mm on the residence time distribution was studied. The results shows that the increasing the radius of curvature (i.e. decreasing the dean number at the bend section) does not change variance significantly. This is due to the lesser region of the curved portion comprising of secondary flow structures. Though this smaller region does not affect residence time distribution much but the same can reduce the required pumping power to certain extent as the sharp bend of case 2 is replaced by the smooth bend.

In the case five, fixing radius of curvature at bend equal to 5 mm, the effect of straight length before bend was studied for different bend angle serpentine configurations. This case is again the combination of the first three cases. The smooth bend region of case 3 was separated by a straight length portion between the bends. Now as discussed in section 4.5.3, increasing the straight length before the bend (i.e. decrease in amplitude of serpentine, A) increases the distance between the second and the third bend. However decrease in amplitude (A) also means that decrease in the distance between first and the second bend. Therefore there is certain optimum dimension of the straight length before bend when used in combinations with the radius of curvature. In other words no more benefit of the higher straight length before bend can be obtained (as obtained in case 2, see Figure 4.9 and section 4.5.3) in case 5 due to the almost developed flow (and therefore higher dispersion) in the region between second and the third bend. It should also be noticed that the mixing intensity at the bend region in case 2 (sharp bend) is much more compared to the bend section in case 5 (smooth bend). This also means that the velocity profile in case 2 is more damaged at the bend than that in case 5 and therefore only smaller straight length portion (after the bend) is sufficient for the flow development in case 5. The flow in the total straight length region available does not remains entirely in developing state and therefore no benefit of developing flow is obtained here compared to case 2

The primary mechanism for the reduction in intensity of dispersion in case of serpentine channel involves intense mixing at bends resulting in breaking of boundary layer that is

governed by the bend angle or curvature. However the sharp bend and the curvature create the intense mixing with different modes/mechanisms. In case of sharp bends he mixing takes place due to crossing of streamlines whereas in case of curvatures or smooth bends the mixing takes place because of secondary flow. The second governing parameter is the distance between the bends. If the distance between the bends is higher, the flow remains developed one in terms of velocity profile. This means lesser difference between the axial velocities of different streamlines exists and therefore lesser dispersion is obtained. In the present work about 60% reduction in dispersion or variance compared to straight channel is obtained for case 1 with the mechanism of intense mixing (or crossing of streamlines). The same is further lower to 65% in case 3 with the mechanism of secondary flow. However with benefit of the developing flow between the bend the dispersion is further lowered to 80% in case 2. The serpentine channel is always a better choice to achieve mixing (and hence better transport coefficients) than that of the straight channel.

4.6 Conclusions

CFD model was developed to understand the effect of various geometrical parameters of serpentine channel configurations on residence time distribution.

CFD simulations of RTD in periodically developed laminar flow in serpentine channel of square cross section were performed for a wide range of parameters like bend angle, straight length before bend and curvature. Simulations were carried out for Reynolds number of 200. Following conclusions are drawn from the study:

- For sharp bends (case 1) with or without straight length before bends (case 2), the lowest dispersion is obtained for 90^o bend angle serpentine configuration. In case of smooth bends (case 3), 160^o serpentine configurations gives lowest dispersion.
- Replacing sharp bend with a smooth bend reduces or eliminates dead zones present for higher bend angle serpentine configurations (e.g. 160^o) and therefore

- Effect of variation of radius of curvature on RTD (and therefore dispersion) in case of smooth bend is found to be insignificant (in the range studied).
- Developing flow, crossing of streamlines and secondary flows due to bends are some of the reasons for reducing dispersion in serpentine channels
- The optimal bend angle (based on variance) is sensitive to the value of Reynolds number. For example, ~100^{o} bend angle was optimum for Re 200 whereas ~130^{o} bend angle was optimum for Re 50
- 60-85 % reduction in variance (and therefore dispersion) is possible by using serpentine channel compared to the straight channel (for Re 200)

CHAPTER 5

PRESSURE DROP AND HEAT TRANSFER IN LAMINAR PULSATING FLOW

This chapter summarizes the attempt made to investigate pressure drop and heat transfer in a circular isothermal duct with imposed flow pulsation at the inlet using computational fluid dynamics (CFD). At inlet the velocity profile consisted of a fixed part and a pulsating component that varies sinusoidally in time. The flow was both thermally and hydrodynamically developing while the tube wall was kept at a uniform temperature. The study was focused within the frequency range of 1–100 Hz and dimensionless amplitude between 0 and 1 at a mean Reynolds number of 200. The range of the Womersely number was 3 to 37. In the present study a phase lag was observed between pressure and velocity cycles for the range of the Womersely number under investigation that was consistent with the literature. The results showed that there was no effect of pulsation frequency or amplitude on a time averaged pressure drop or heat transfer (Nusselt number).

5.1 Background

Micro-reactors comprising small channels (ranging from few microns to millimeter) have been shown to offer unprecedented opportunities for process intensification [see for example reviews by Ehrfeld *et al.* (2000), Gavriilidis *et al*. (2002) and Hessel *et al.* (2006)]. However the practical feasibility of the operations depends on many other factors also e.g. pump facility for the delivery of the reactant. Due to smaller channel size the resulting pressure drop for the delivery of the fluid will be quite high. Therefore the reciprocating or the peristaltic pumps are the first choice among the researchers (see for example Dummann *et al.* (2003), Halder *et al.* (2007)). Almost in all studies where authors have used the microreactor system for process intensification one can find the use of peristaltic pump. One of the limitations of the peristaltic or reciprocating action is discontinuity in the instantaneous flow. However the overall time averaged flow rate remains same as that of steady state value. Due to this discontinuous instantaneous flow in the channel the flow or fluid elements keeps pulsating in the channel at its mean position. In such cases it becomes necessary to address the effect of these pulsations on transport characteristics. Apart from the key use in microreactors systems discussed earlier these systems (i.e. pulsating action) also find applications in various fields, such as biology (simulation of human breathing, flow through arteries, etc.), the automotive industry (simulation of exhaust from I.C. engines), etc.

Laminar, fully developed, pulsating pipe flows and heat transfer characteristics involved within it forms one of the fundamental classes of flows with periodic time variations in the velocity and pressure properties. The area has attracted substantial attention among the researchers over the years. Numerous analytical, numerical and few experimental studies that deal with flows of this kind are available. Some of the available literature is briefly reviewed here.

Zhao and Cheng (1995) presented a numerical solution for laminar forced convection of an incompressible periodically reversing flow in a pipe of finite length at constant wall temperature. It was found that the parameters that govern the heat transfer characteristics for the problem under consideration were the kinetic Reynolds number Re_ω and the

dimensionless oscillation amplitude. The averaged heat transfer rate was found to increase with both the kinetic Reynolds number and the dimensionless oscillation amplitude. A correlation equation of the space time averaged Nusselt number for air in terms of the three similarity parameters, *Re~*, *Ao* and *L/D* was obtained by the authors.

Pressure drop in a fully developed laminar incompressible reciprocating pipe flow have been investigated analytically and experimentally by Zhao and Cheng (1996). An exact analytical solution for the instantaneous and cycle-averaged friction coefficients of a fully developed laminar reciprocating flow has been obtained. It was found that, although the dimensionless axial velocity profiles of a fully developed flow depend only on the kinetic Reynolds number, the friction coefficients depend not only on the kinetic Reynolds number but also the dimensionless oscillation amplitude of fluid.

Moschandreou and Zamir (1997) considered the problem of pulsatile flow in a tube with constant heat flux at the wall analytically to determine how pulsation affects the rate of heat transfer and how the phenomenon depends on the Prandtl number and on pulsation frequency. The results indicated that in a range of moderate values of the frequency ($\omega \sim 15$) there was a positive peak in the effect of pulsation whereby the bulk temperature of the fluid and the Nusselt number were increased, but the effect was reversed when the frequency was outside that range.

Guo and Sung (1997) tested many versions of the Nusselt number to clarify the conflicting results in the heat transfer characteristics for pulsating flow in a pipe. An improved version of the Nusselt number was proposed by the authors, which was shown to be in close agreement with available measurements. The main emphasis was placed on the large amplitude of the pulsation flow rate ($A_0 > 1$). For a small amplitude ($0 < A_0 < 1$), both heat transfer enhancement and reduction were detected depending on the pulsation frequency. However the authors found that for large amplitude ($A0 > 1$) the heat transfer due to pulsation was always augmented.

Heat transfer characteristics to a laminar pulsating flow under different conditions of Reynolds number and pulsating frequency were experimentally investigated by Habib *et al.* (2002). The authors considered tube wall of uniform heat condition and Reynolds number was varied from 780 to 1987 while the frequency of pulsations ranged from 1 Hz to 29 Hz. The results showed that the relative mean Nusselt number was strongly affected by pulsating frequency and slightly affected by Reynolds number. Empirical correlations have been developed for the relative mean Nusselt number that related to Reynolds number ($750 < Re < 2000$) and the dimensionless frequency ($3 < \Omega < 18$).

Hamida *et al.* (2002) theoretically investigated the pulsation effect on heat transfer in laminar incompressible flow. The analytical solution of the fully developed thermal and hydraulic profiles under constant wall heat flux was obtained by the authors. New time average heat transfer coefficient for pulsating flow was defined. Results were numerically obtained for the thermally developing region with a fully developed velocity profile. Different types of thermal boundary conditions were considered, including the effect of wall thermal inertia. The effects of Reynolds and Prandtl numbers, as well as pulsation amplitude and frequency on heat transfer were investigated. The mechanism, by which pulsation affects the developing region, by creating damped oscillations along the tube length of the time average Nusselt number, was explained.

Yu *et al.* (2004) presented an analytical study of pulsating laminar convection heat transfer in a circular tube with constant wall heat flux. The results showed that both the temperature profile and the Nusselt number fluctuate periodically about steady laminar convection, with the fluctuation amplitude depending on the dimensionless pulsation amplitude and the Prandtl number. It was also shown that pulsation has no effect on the time- average Nusselt number for pulsating convection heat transfer in a circular tube with constant wall heat flux.

Combined analytical and experimental investigation of sinusoidal mass flow-controlled, pulsating, laminar and fully developed pipe flow was carried out by Unsal *et. al.* (2005). The experimental investigation employed a mass flow control unit while for the

analytical investigation; the equations describing such flows were normalized to allow for a general solution, depending only on the normalized amplitude $m*A$ of the mass flow pulsation and the normalized frequency F. The analytical and experimental results were presented in normalized way. A diagram was presented for the condition of flow reversal in terms of the dimensionless frequency F and the mass flow rate amplitude $m*A$.

Chattopadhyay *et al.* (2006) presented numerical studies of flow and heat transfer in a circular tube under pulsating flow condition in the laminar regime. The flow at the inlet consists of a fixed part and a pulsating component, which varies sinusoidally in time. The flow was both thermally and hydrodynamically developing while the tube wall was kept at a uniform temperature. The solution of two dimensional Navier–Stokes equation was performed. The authors observed that in the range of frequency 0–20 Hz; dimensionless amplitude 0-1 pulsation has no effect on time-averaged heat transfer but reduces the friction factor than that of a steady flow.

One of the key issues concerning pulsating flow and convection heat transfer in tubes was whether a superposed flow pulsation alters the pressure drop and/or heat transfer present in the original steady flow? In case of steady flow there exists a definite relationship between the momentum and the heat transfer phenomenon i.e. to achieve higher heat transfer one must dissipate higher pumping power. However the scenario in case of pulsating convection is not so straight forward and is not well understood. The answer to the above question based on the several previous studies can be classified into different opinions as given below:

(a) No change in fluid friction (pressure drop) or heat transfer
(b) Enhances fluid friction (pressure drop) and/or heat transfer
(c) Decreases fluid friction (pressure drop) and/or heat transfer
(d) Enhances or deteriorates fluid friction (pressure drop) and heat transfer, depending on flow parameters

There is no satisfactory answer to this question in the literature. Unfortunately only few studies reporting the effect of pulsations on pressure drop/fluid friction as well as heat transfer are available. In other studies only either one of these is reported. Table 5.1 summarizes the work of various authors with parameters used and the key outcome of the studies.

Table 5.1: Summary of literature studies

Author	**Case**	**Parameters**	**Fluid Friction**	**Heat transfer**
Zhao and Cheng 1995	Numerical CWT	Reω: 64-250 - A_0: 10-35		**-Increase**
Zhao and Cheng 1996	Analytical & Experimental	A_0: 10-22.5 Reω: 64-256	**-Cf Decreases with amplitude and frequency**	------
Moschandreou *et al.*1997	Analytical CHF	ω= 0-40	------	**-Depends on f, A and Pr**
Guo *et al.*1997	Numerical	A_0: 0-2 - f_p: 1- 6	------	**-Depends on frequency**
Habib *et al.*2002	Experimental	f_p: 1-29.5 Hz -3< Ω<18	------	**-Degradation but Effect is small**
Hemida *et al.*2002	Analytical CHF	Wo: 1.732- 2.236 -β: A_1/ A_0= 0.5-1.5	------	**-No Change**
Yu *et al.*2004	Analytical	-γ: 0.5 -Wo:1- 7.07	------	**-No Change**
Ray *et al.*2005	Analytical and Experimental	f_p: 0.027 to 1.866 Wo: 0.1 to 7	**-Depends on frequency**	------
Chattopadhyay *et al.*2006	Numerical CWT	0.1<St<20, 0.1< A_0<1,	**-Decreases**	**-No Change**

From a review of current literature (refer Table 5.1), it was found that there was a need for systematic analysis of the contribution of flow pulsation in friction factor or pressure drop and heat transfer from circular ducts at constant wall temperature. In light of this review, attempt is made to quantify these issues computationally in the present work. Computational model and obtained results are discussed in the following sections.

The present study is an attempt to investigate the heat transfer in a circular isothermal duct with imposed flow pulsation at the inlet. At inlet the velocity profile consisted of a fixed part and a pulsating component that varies sinusoidally in time. It should be noted that the sinusoidal variation on velocity was simplest approximation to the real life systems involving the pulsations. The flow was both thermally as well as hydrodynamically developing while the tube wall was kept at a uniform temperature. The solution of two dimensional Navier–Stokes equations was performed.

The present study focuses within the frequency range of 1–100 Hz and dimensionless amplitude between 0 and 1 at a mean Reynolds number of 200. In case of pulsating flow the dimensionless numbers which are of much relevance are Strouhal number and Womersley number. The Strouhal number is defined as $St = \frac{f_p R}{U}$ i.e. non-dimensional frequency. For large Strouhal numbers (order of 1), viscosity dominates fluid flow, resulting in a collective oscillating movement of the fluid "plug". For low Strouhal numbers (order of 10^{-4} and below), the high-speed, quasi steady state portion of the movement dominates the oscillation.

In many cases Womersley number (*Wo*) is also the standard non-dimensional parameter defined as $\alpha \text{ or } Wo = R\left(\frac{\omega \rho}{\mu}\right)^{\frac{1}{2}}$. When *Wo* is small (1 or less), it means the frequency of pulsations is sufficiently low that a parabolic velocity profile has time to develop during each cycle, and the flow will be very nearly in phase with the pressure gradient, and will be given to a good approximation by Poiseuille law, using the instantaneous pressure gradient. When *Wo* is large (10 or more), it means the frequency of pulsations is

sufficiently large that the velocity profile is relatively flat or plug-like, and the mean flow lags the pressure gradient by about 90 degrees (Womersley, 1954). The relationship between *Wo* and *St* can be given as $\alpha \; or \; Wo = \left(2\pi \,\mathrm{Re}\, St\right)^{\frac{1}{2}}$. For the present values of interest the range of *St* is 0.1 to 1.125 and *Wo* is 3 to 38.

5.2 CFD methodology:

All Numerical analysis was carried out by using commercial CFD code Fluent 6.3.36 and grids were generated using Gambit 2.4.

In the present work the emphasis was given on investigating the effect of pulsations on laminar simultaneously developing flow. The geometry consists of an axisymmetric circular tube of 1.5 mm in diameter and 200 mm in length. The entire domain was meshed using hexahedral map elements.

Pulsating flow in a tube can be modeled either by using pulsating (a) velocity profile at inlet or (b) pressure profile at inlet. In case of velocity inlet boundary condition the instantaneous velocity profile was found by adding the uniform velocity profile with a sinusoidal pulsation. Thus, the inlet velocity profile was given by:

$$U = U_{avg}\left(1 + A_0 \, Sin\left(2\pi \, f_p \, t\right)\right) \quad \text{(5.1 a)}$$

where A_0 was the non-dimensional amplitude and f_p was the oscillation frequency. The U_{avg} was the one corresponding to the Reynolds number of 200.

In case of pressure inlet boundary condition the instantaneous pressure profile was found by adding the average pressure drop with a sinusoidal pulsation. Thus, the inlet pressure profile was given by:

$$P = P_{avg}\left(1 + A_0 \, Sin\left(2\pi \, f \, t\right)\right) \quad \text{(5.1 b)}$$

Where, P_{avg} was the average pressure drop corresponding to Re 200. In the present work both the inlet boundary conditions was studied.

At wall no slip boundary condition was used.

The momentum and energy equations were discretized using second order upwind scheme. The under-relaxation factor of 0.5 was used for momentum equations while 1 was used for energy equation. The standard scheme was used for pressure discretization. SIMPLE algorithm was employed for velocity–pressure. The energy equation was simultaneously solved with the momentum equations. The range of frequency studied here was from 1 Hz to 100 Hz. This gives the range of Strouhal number of 0.01 to 1.125. The corresponding Womersely number for this range becomes 3.76 to 37.6. The range of the nondimensional amplitude was 0 to 1.

It is essential to use appropriate boundary condition at the outlet which is not very obvious for pulsating flows. Two types boundary conditions commonly used at the outlet boundary are 1) pressure outlet i.e. 1 atmosphere pressure at outlet 2) outflow i.e. gradients in the cross-stream direction may exist at an outflow boundary and the diffusion fluxes in the direction normal to the exit plane are assumed to be zero. The effect of these boundary conditions on predicted results was also investigated. The simulations were carried out till the periodic steady state was observed.

The static pressure at the inlet and outlet was monitored with each time step. Figure 5.1 (a) shows one of the simulation result of pressure drop and velocity with time for Reynolds number of 200, time step 0.05 ms, frequency 100 Hz (*Wo*: 37.6) and pulsating amplitude of 0.5. The outlet boundary condition for momentum equation was pressure outlet. The Reynolds number varies in between 100 to 300 in a single cycle. As mentioned earlier for higher *Wo* i.e. 10 or more the mean flow lags the pressure gradient by about 90^{o}. In the present work the phase lag was found to be of 80^{o}. The calculation of the instantaneous friction factor from the pressure drop ($\Delta P = \frac{2 f L_T \rho U^2}{D_h}$) becomes complicated due to the existence of lag between the pressure drop and mean flow rate. For example in Figure 5.1 (a) the flow time corresponding to the maximum pressure drop was different from the flow time at which the maximum velocity magnitude was present. Therefore to calculate instantaneous friction factor at flow time equal to maximum

pressure drop one would use the average inlet velocity at the same flow time. However this may introduce an error in calculation due to term of velocity square for calculations of friction factor from the pressure drop. Therefore due to complexity in the definition of the friction factor to be used the task was kept limited with comparison of time averaged pressure drop with that of steady state value. For this purpose the instantaneous pressure drop over the length was averaged over three consecutive cycles.

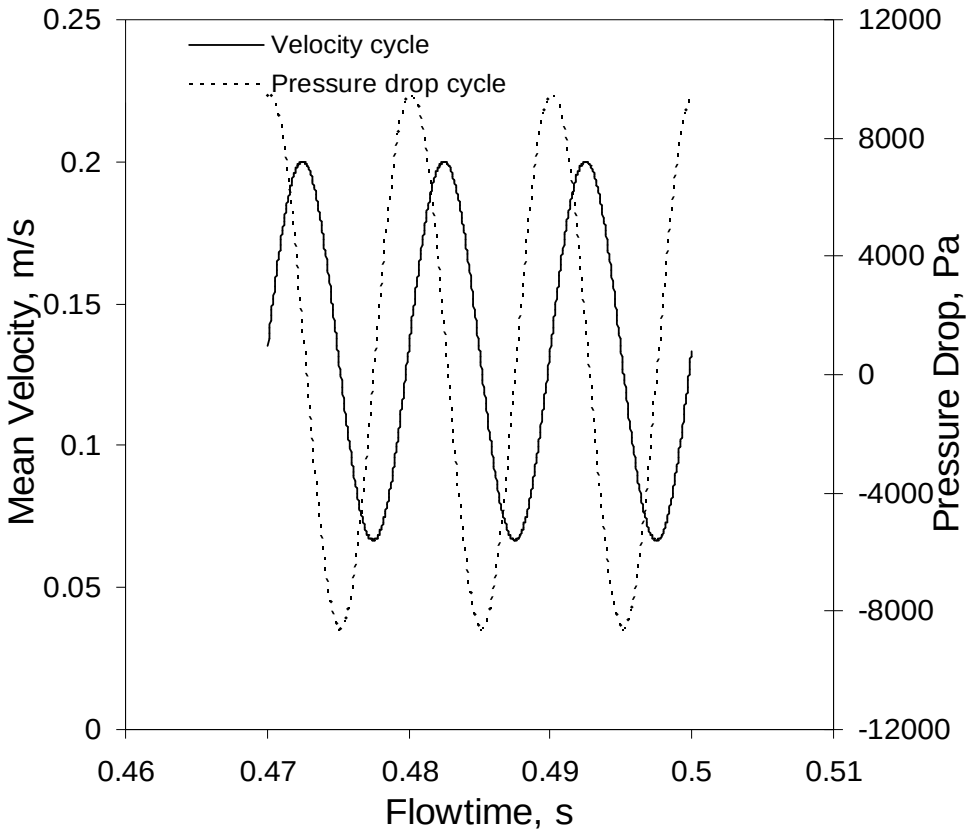

Figure 5.1 (a): A typical velocity and pressure drop cycle (f_p: 100 Hz, A_0: 0.5, Re_m: 200, time step: 0.05ms)

For studying the use of pressure cycle as inlet, the pressure cycle from Figure 5.1 was given as inlet and after solving the momentum equations (for Reynolds number of 200, time step 0.05 ms, frequency 100 Hz (*Wo*: 37.6), pressure outlet at exit) the velocity was monitored at inlet. The same (as used in velocity inlet in Figure 5.1) velocity cycle was reproduced when pressure inlet boundary condition was used and therefore rest of the

studies were continued with using velocity cycle as inlet to investigate the effect of pulsating amplitude and frequency.

The definition of instantaneous local Nusselt number is an important aspect while analyzing the data. Many authors defined various different definitions for the simplicity in analysis (see Hamida *et al.* 2009 for summary of definitions of instantaneous Nusselt number). The appropriate definition must include the instantaneous local mean bulk temperature of the fluid and not the inlet temperature (see Chattopadhyay *et al.* 2006). Equation 5.2 gives the definition of instantaneous local Nusselt number used in the present work.

$$N_{u(t,z)} = \frac{D_h}{k} \times \frac{1}{\sum_{r=R} dA_{(r,z)}} \times \sum_{r=R} \frac{q''_{(t,z)}}{\left[T_{w(z)} - T_{m(t,z)}\right]} dA_{(r,z)} \quad \text{..... (5.2)}$$

$$\text{Where, } q''_{(t,z)} = \frac{-k\left(\frac{dT}{dr_{(r=R)}}\right)_{(t,z)}}{\left(A_{(r=R)}\right)_{(z)}} \quad \text{..... (5.3)}$$

and

$$T_{m(t,z)} = \frac{\sum_{r} \rho \dot{u}_{(t,r,z)} A_{(,r,z)} Cp T_{f(t,r,z)}}{\sum_{r} \rho \dot{u}_{(t,r,z)} A_{(r,z)} Cp} \quad \text{..... (5.4)}$$

The above definition has an importance of involving instantaneous mixing cup temperature in it making it more logical and appropriate one.

The instantaneous Nusselt number was averaged over three consecutive cycles.

$$Nu_{(z)} = \frac{1}{T} \int Nu_{(t,z)} dt \quad \text{..... (5.5)}$$

The time averaged local Nusselt number was further averaged over the heat transfer area to get the average Nusselt number.

$$Nu_{(avg)} = \frac{1}{L_T} \int Nu_{(z)} dL \quad \text{..... (5.6)}$$

The result of average Nusselt number for different frequency and amplitude was then compared with that of steady state Nusselt number for the cases under study.

Figures 5.2 (a) and 5.2 (b) show influence of outlet boundary condition for momentum equation on the simulated time averaged pressure drop and local Nusselt number respectively. It can be seen that both the boundary conditions give similar results. The pressure outlet boundary condition was therefore used in further investigations. Table 5.2 summarizes the simulation parameters along with the simulated time averaged mean Nusselt number for the two boundary conditions.

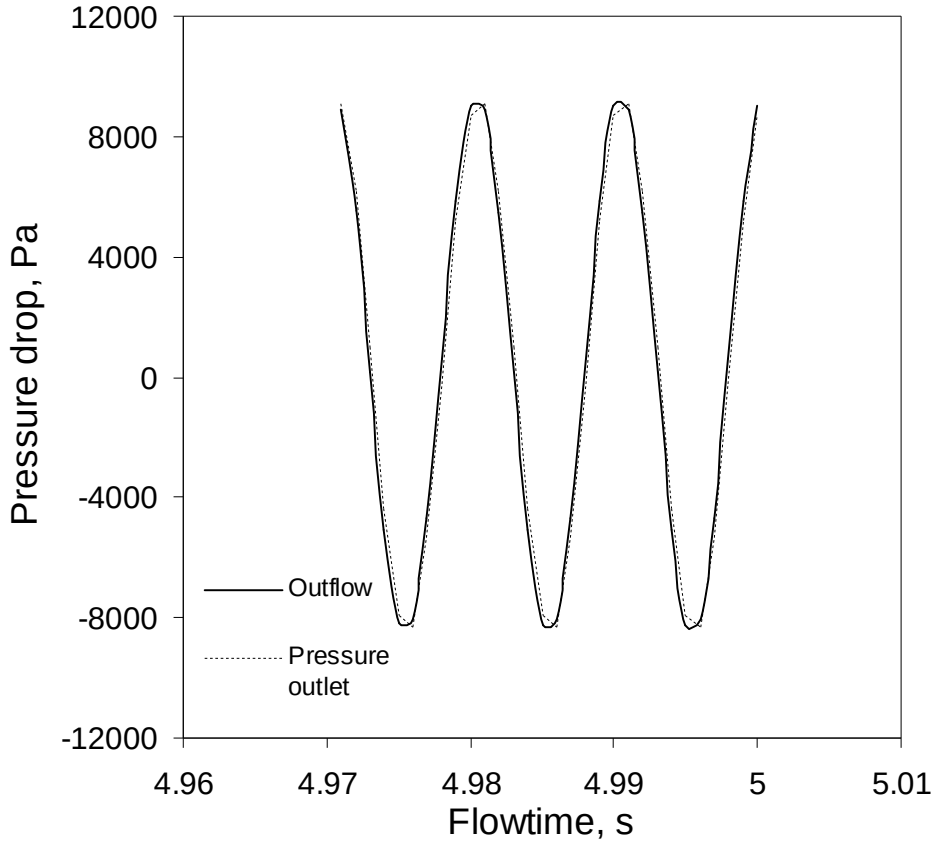

Figure 5.2 (a): Effect of outlet boundary conditions on instantaneous pressure drop (f_p: 100 Hz, A_0: 0.5, Re_m: 200, time step: 1ms)

Table 5.2: Effect of outlet boundary condition (Grid: 12x500)

Outlet BC	Mean Re	Amplitude A_0	frequency, f_p Hz	Strouhal Number	Womersely Number	Time Step (ms)	Time averaged ΔP (Pa)	Time Averaged Nu
Pressure Outlet	200	0.5	100	1.125	37.6	1	392.21	4.06
Outflow	200	0.5	100	1.125	37.6	1	393.05	4.06

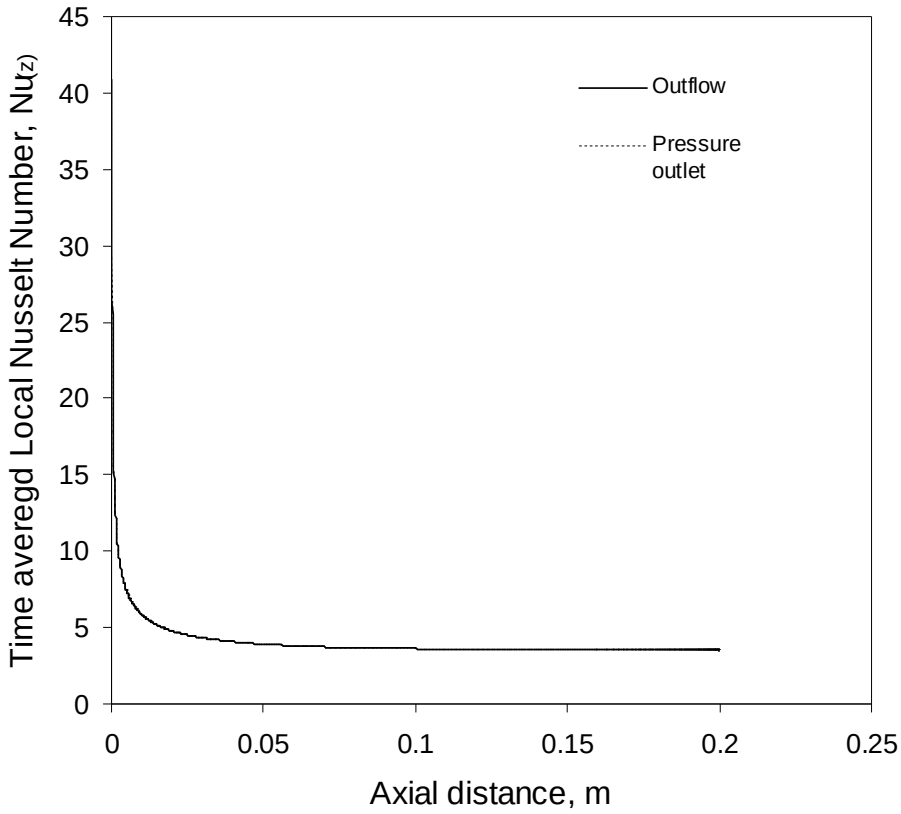

Figure 5.2 (b): Effect of inlet outlet boundary conditions on time averaged Local Nusselt number (f_p: 100, A_0:0.5, Re_m: 200, time step: 1ms)

Table 5.3: Effect of different grid size

Grid	Mean Re	Amplitude A_0	frequency, f_p Hz	Strouhal Number	Womersley Number	Time Step (ms)	Time averaged ΔP (Pa)	Time Averaged Nu
12 x 500	200	0.5	100	1.125	37.6	0.1	393.37	4.06
30 x 2000	200	0.5	100	1.125	37.6	0.1	394.11	4.07

For grid sensitivity analysis simulations were carried out by using two different grid sizes. In the first case, the channel radius was meshed with 25 elements having successive ratio of 1.1 and length was meshed with 500 elements having double successive ratio of 1.1. In the second case the channel radius was meshed with 30 elements having successive ratio of 1.1 and length was meshed with 2000 elements having double successive ratio of 1.1. Table 5.3 shows the comparison of time averaged pressure drop and Nusselt number for above two mesh sizes. No significant effect of grid size was observed and therefore 25x500 cells were used for further analysis.

The effect of various time steps on the solution was investigated. For this purpose the timestep was changed from 0.05 ms to 1 ms. The effect of iteration per time step was studied and 100 iterations per timestep were found to be adequate to ensure acceptable convergence. Table 5.4 shows the comparison of the time averaged pressure drop and Nusselt number for different time steps. It was found that the time step below 0.1 ms was sufficient and was resulting in same results for time averaged pressure drop and average Nusselt number. Therefore the time step of 0.05 ms was set to study the effect of frequency and the pulsating amplitude.

Table 5.4: Effect of different time steps

Amplitude A_0	frequency, f_p Hz	Strouhal Number	Womersley Number	Time Step (ms)	Time averaged ΔP (Pa)	Time Averaged Nu
0	0	-	-	Steady	391.69	4.14
0.5	100	1.125	37.6	1	392.21	4.07
0.5	100	1.125	37.6	0.5	392.18	4.06
0.5	100	1.125	37.6	0.1	392.21	4.06
0.5	100	1.125	37.6	0.05	392.18	4.06

With these simulations parameters the effect of pulsations was studied for frequency range of 1 Hz to 100 Hz with the non dimensional amplitude between 0 and 1. In all the studies the mean Reynolds number was 200.

At the end the work was further extended to understand the effect of pulsations in case of thermally developing flow. For this purpose a single simulation was carried out for pulsation frequency of 100 and dimensionless amplitude of 0.5. At the inlet, the velocity profile was found by adding the parabolic velocity profile with a sinusoidal pulsation. Thus, the inlet velocity profile in this case was given by

$$U = 2U_{avg}\left(1 + A_0\, Sin\left(2\pi\, f_p\, t\right)\right)\left(1 - \left(\frac{r}{R}\right)^2\right) \quad \text{..... (5.7)}$$

The rest of the methodology for calculations of pressure drop and Nusselt number was same as discussed earlier.

5.3. Results and discussion

Figure 5.3 (a) shows the instantaneous local Nusselt number at different phase angles (60^o apart) in a single pulsation cycle. It can be seen that the Nusselt number profiles for different phase angles are quite close to each other. Figure 3 (b) shows normalized instantaneous local Nusselt number at different phase angles in a single pulsation cycle.

For this purpose the enhancement ratio is defined as $\eta_x = Nu_{(t,z)} / Nu_{(steady,z)}$ i.e. ratio of instantaneous local Nusselt number in case of pulsation to that of steady state. Therefore $\eta_x < 1$ shows the degradation in heat transfer performance and $\eta_x > 1$ shows enhancement in heat transfer.

From the Figure 5.3 (b) it can be seen that the instantaneous local Nusselt number is quite different compared to that at steady state as $\eta_x \neq 1$ in almost profiles. At the entrance section (axial distance < 0.005 m) significant effect of pulsation is observed. In this region an enhancement up to 20 % (e.g. 120^o phase) and degradation up to 23 % (e.g. 300^o phase angle) in heat transfer can be seen depending on the phase angle. In the later part of the channel an enhancement up to 7 % (e.g. 60^o phase) and degradation up to 12 % (e.g. 240^o phase angle) in heat transfer is observed depending on the phase angle. The magnitude of increase and decrease is therefore can be complementary to each other and therefore it may be possible that when instantaneous local Nusselt number is averaged out in time (or in cycle) and area of heat transfer, no remarkable effect of pulsation may be observed.

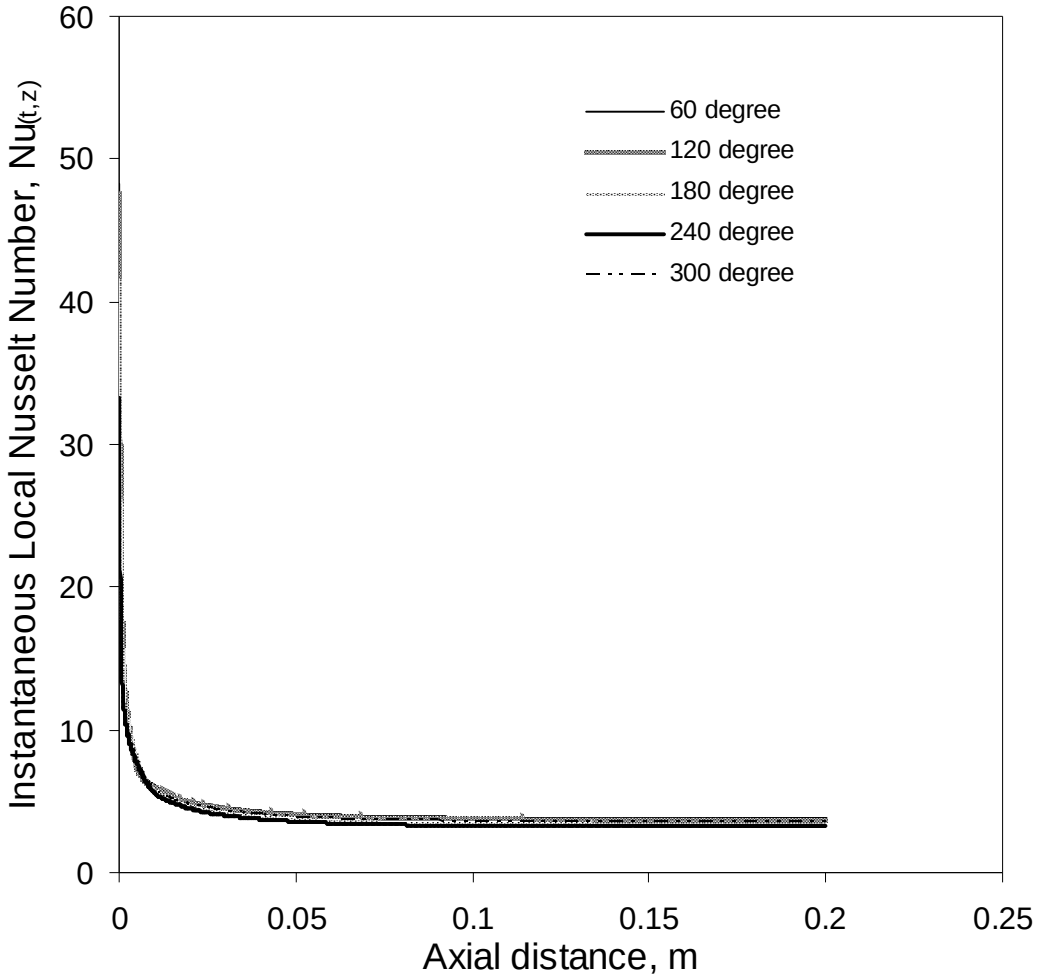

Figure 5.3 (a): Instantaneous local Nusselt number at different phase angle (f_p: 10 Hz, A_0: 0.5, Re_m; 200, time step: 0.05ms)

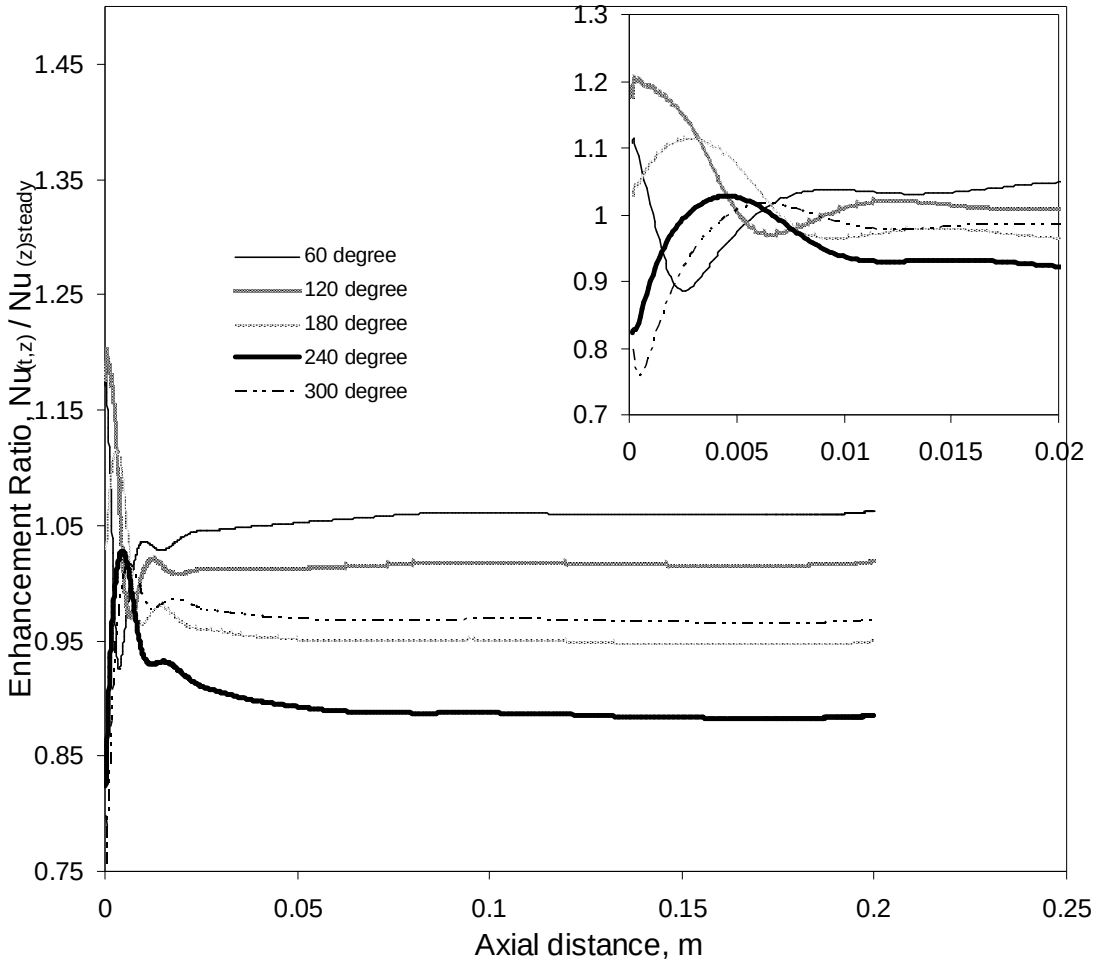

Figure 5.3 (b): Enhancement ratio at different phase angle (f_p: 10 Hz, A_0: 0.5, Re_m; 200, time step: 0.05ms)

Figure 5.3 (c) and 5.3 (d) show the plots of instantaneous area averaged Nusselt number and mean velocity with different phase angles in a single cycle for two different pulsating frequencies of 10 Hz and 100 Hz respectively. The similar results for frequency of 10 Hz is listed in Table 5.5 It can be seen that the Nusselt number cycle and the mean velocity cycle are not in a same phase. Similar to the pressure cycle (see Section 5.2 and Figure 5.1 (a)) here also the phase lag is observed between the average Nusselt number cycle and the mean velocity cycle. One more observation that can be made is the velocity cycle is sinusoidal in space however the Nusselt number cycle is not. The reason for such behavior is not clear.

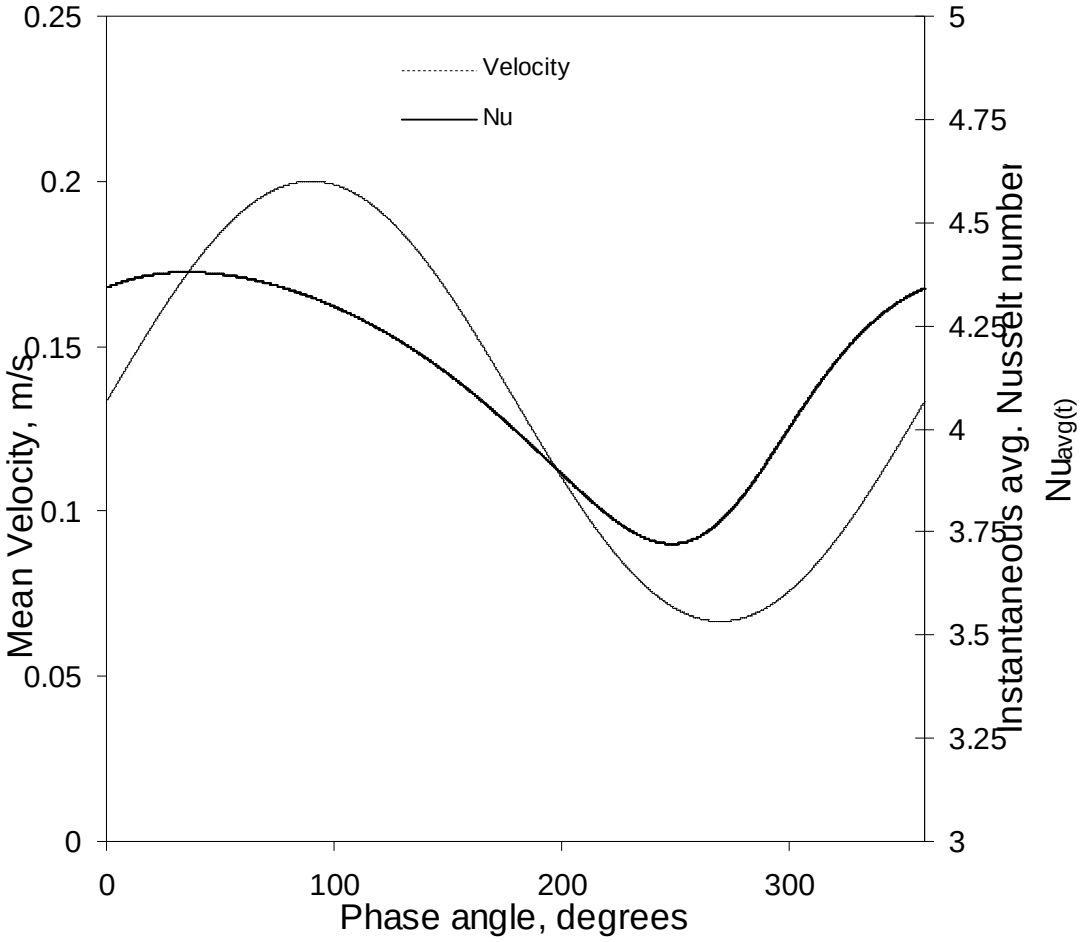

Figure 5.3 (c): A typical velocity and instantaneous area averaged Nusselt number (f_p: 10 Hz, A_0: 0.5, Re_m: 200, time step: 0.05ms)

Table 5.5: Effect of phase angle

Phase Angle φ	Amplitude A_0	frequency, f_p Hz	Strouhal Number	Womersley Number	Time Step (ms)	Instantaneous $\Delta P_{(t)}$ (Pa)	Instantaneous avg. Nusselt Number $Nu_{avg(t)}$
	0	0	-	-	Steady	391.69	4.14
0	0	0	0.112	11.8	0.05	1411.325	4.47
60	0.5	10	0.112	11.8	0.05	1153.11	4.36
120	0.5	10	0.112	11.8	0.05	133.18	4.24
180	0.5	10	0.112	11.8	0.05	-626.40	3.99
240	0.5	10	0.112	11.8	0.05	-367.78	3.73
300	0.5	10	0.112	11.8	0.05	653.62	4.00
360	0	0	0.112	11.8	0.05	1411.325	4.34

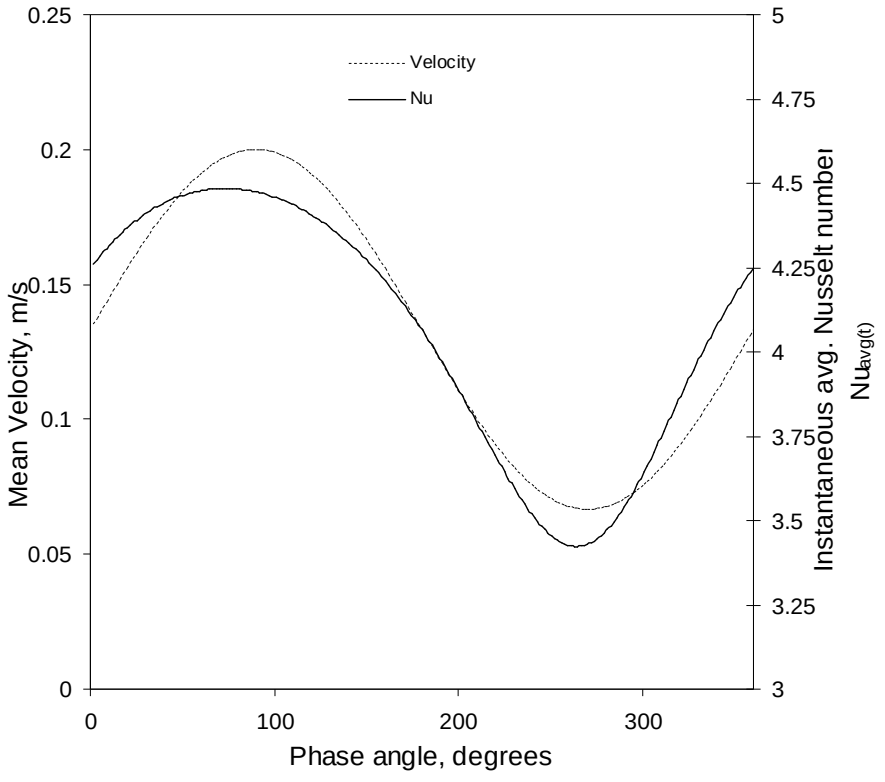

Figure 5.3 (d): A typical velocity and instantaneous area averaged Nusselt number (f_p: 100 Hz, A_0:0.5, Re_m: 200, time step: 0.05ms)

Figure 5.4 (a) shows the effect of frequency on instantaneous pressure drop for the pulsation amplitude of 0.5. Table 5.6 summarizes the result of the time averaged pressure drop for different pulsation frequencies. It can be seen from the Figure 5.4 (a) that all the three pressure cycles have a common mean pressure drop. However all the three pressure cycles have different amplitude of the pressure drop even though the amplitude of the velocity is same in all cases i.e. 0.5. The reason for such behavior is not well understood. The pressure drop for the steady state developing flow for the case of Re of 200 is 391 Pa. It can be seen from the simulation data that for different pulsating frequencies the time averaged pressure drop is same. In the present study as discussed earlier (see section 5.2) the comparison is not based on the friction factor due to difficulties in the calculations involved. In case of pulsations the friction factor can also be function of axial location due to different local velocity field at the wall. Therefore for the simplicity the studies are limited for investigating the effect on time average pressure drop. The results show that the pulsation frequency does not change the time averaged pressure drop.

Table 5.6: Effect of pulsation frequency

Amplitude A_0	frequency, f_p Hz	Strouhal Number	Womersley Number	Time Step (ms)	Time averaged ΔP (Pa)	Time averaged Nu
0	0	0		Steady	391.69	4.14
0.5	100	1.125	37.6	0.05	392.18	4.06
0.5	10	0.112	11.8	0.05	392.83	4.11
0.5	1	0.011	3.76	0.05	393.37	4.16

Figure 5.4 (b) shows the effect of frequency on time and area averaged local Nusselt number (or mean Nu) for the pulsation amplitude of 0.5. It can be seen from the Figure 5.4 (b) that the profiles of time averaged local Nusselt number for different frequencies overlap with the profile of steady state local Nusselt number. Thus, no effect of pulsation is visible over the time averaged values of local Nusselt number. Table 5.6 also summarizes the result of the time and area averaged Nusselt number for different

pulsation frequencies. The steady state average Nusselt number for simultaneously developing flow obtained from the present simulations is 4.14. A small decrease in the time averaged Nusselt number is observed with increase in the pulsation frequency. However the decrease is not so significant and all the values of the time averaged Nusselt numbers for different frequencies are very close to the steady state average Nusselt number (± 2% deviation).

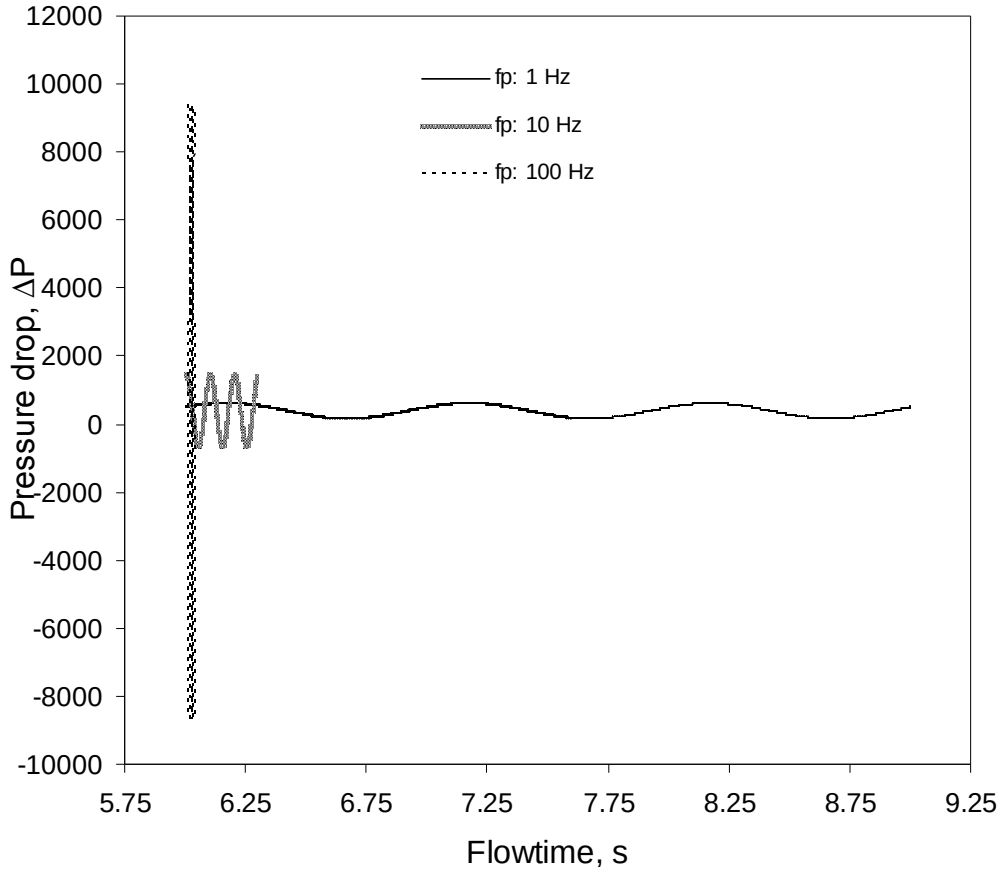

Figure 5.4 (a): Effect frequency on instantaneous pressure drop (A_0: 0.5, Re_m: 200, time step: 0.05ms)

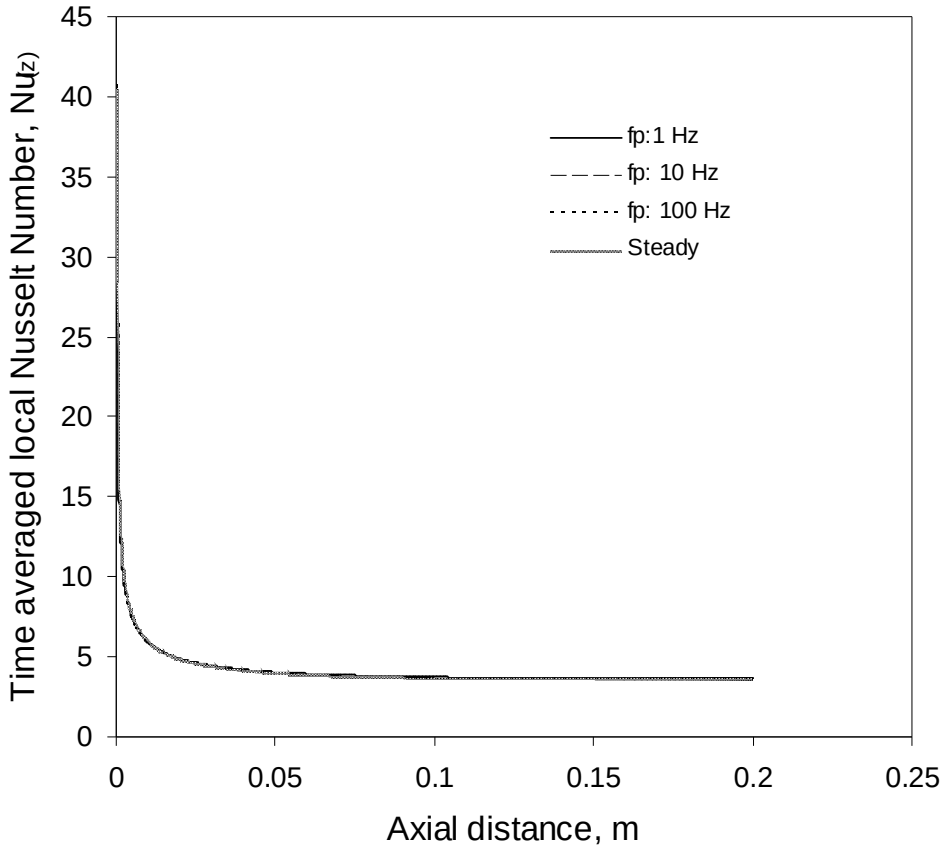

Figure 5.4 (b): Effect frequency on time averaged local Nusselt number (A_0: 0.5, Re_m: 200, time step: 0.05ms)

Figure 5.5 (a) shows the effect of pulsation amplitude on instantaneous pressure drop for the pulsation frequency of 10. Table 5.6 summarizes the result of the time averaged pressure drop for different pulsation amplitudes. It can be seen from the Figure 5.5 (a) that all the three pressure cycles have a common mean pressure drop. The amplitudes of the pressure drop cycles are different for different dimensionless amplitude. This is expected as the pulsation amplitude of the velocity is different in all three cases that results in different instantaneous velocities at the inlet and therefore results in different pressure drop for different velocity amplitudes for the same flow time. In other words the maximum velocity in a given cycle depends on the amplitude and therefore it is expected the pressure drop cycle will also have different amplitude. It can be seen from the data of Table 5.7 that for different pulsating amplitudes the time averaged pressure drop is same

as that of steady state pressure drop. The results show that the pulsation amplitude does not change the time averaged pressure drop.

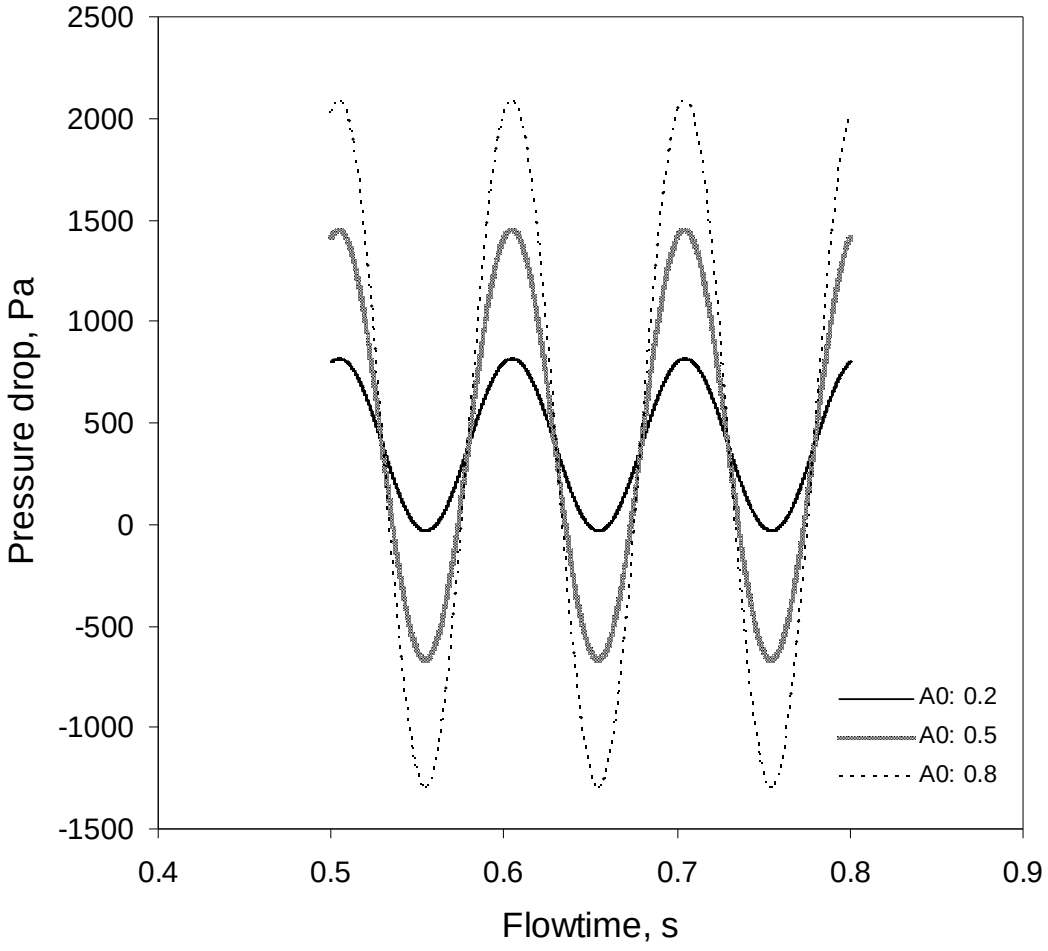

Figure 5.5 (a): Effect amplitude on instantaneous pressure drop (f_p: 10 Hz, Re_m: 200, time step: 0.05ms)

Figure 5.5 (b) shows the effect of frequency on time averaged local Nusselt number for the pulsation frequency of 10. It can be seen from the Figure 5.5 (b) that the profiles of time averaged local Nusselt number for different amplitudes overlap with the profile of steady state local Nusselt number. Thus, no effect of pulsation is visible over the time averaged values of local Nusselt number. Table 5.7 also summarizes the result of the time and area averaged local Nusselt number for different pulsation amplitudes. The steady state average Nusselt number for simultaneously developing flow obtained from the

present simulations is 4.14. A small decrease in the time averaged Nusselt number is observed with increase in the pulsation amplitude. However the decrease is not so significant and all the values of the time averaged Nusselt numbers for different pulsation amplitudes are very close to the steady state average Nusselt number (± 2% deviation).

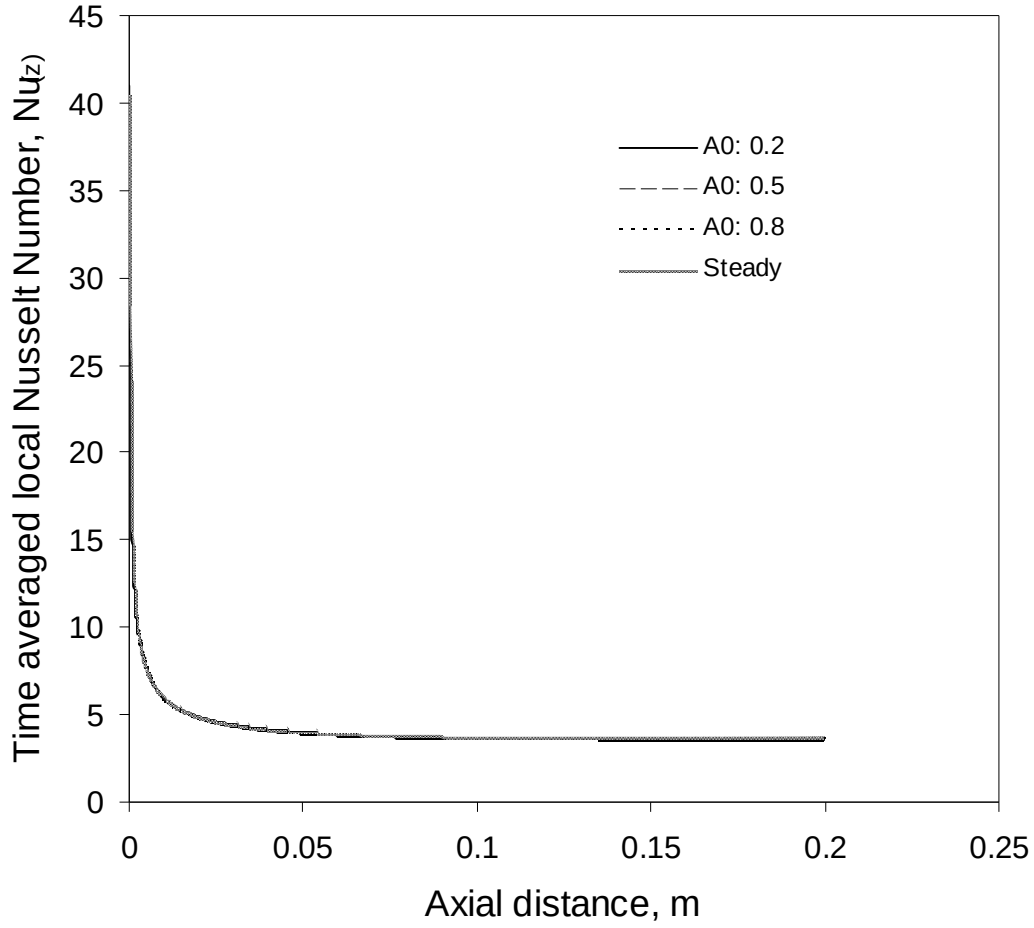

Figure 5.5 (b): Effect amplitude on time averaged local Nusselt number (f_p: 10 Hz, Re_m: 200, time step: 0.05ms)

Table 5.7: Effect of pulsation amplitude

Amplitude A_0	frequency, f_p Hz	Strouhal Number	Womersley Number	Time Step (ms)	Time averaged ΔP (Pa)	Time averaged Nu
0	0	0		Steady	391.69	4.14
0.2	10	0.112	11.8	0.05	392.08	4.14
0.5	10	0.112	11.8	0.05	392.83	4.11
0.8	10	0.112	11.8	0.05	394.21	4.00

Figure 5.6 (a) shows the instantaneous pressure drop comparison between thermally developing flow and the simultaneously developing flow i.e. the effect of pulsation frequency of 100 and dimensionless amplitude of 0.5 on instantaneous pressure drop for the case of different inlet velocity profile. It can be seen from the Figure 5.6 (a) that both pressure cycles have a same mean pressure drop corresponding to the respective steady state pressure drop. Table 5.8 summarizes the result of the time averaged pressure drop for both the cases with the corresponding steady state pressure drop. The pressure drop for the steady state thermally developing flow for the case of Re of 200 is 378 Pa compared to 392 Pa in case of simultaneously developing flow. From the results of the Table 8 it can be seen that the time averaged pressure drop is same as that of steady state pressure drop in both the cases. Therefore similar to simultaneously developing flow, in case of thermally developing flow also no effect of presence of pulsation is observed.

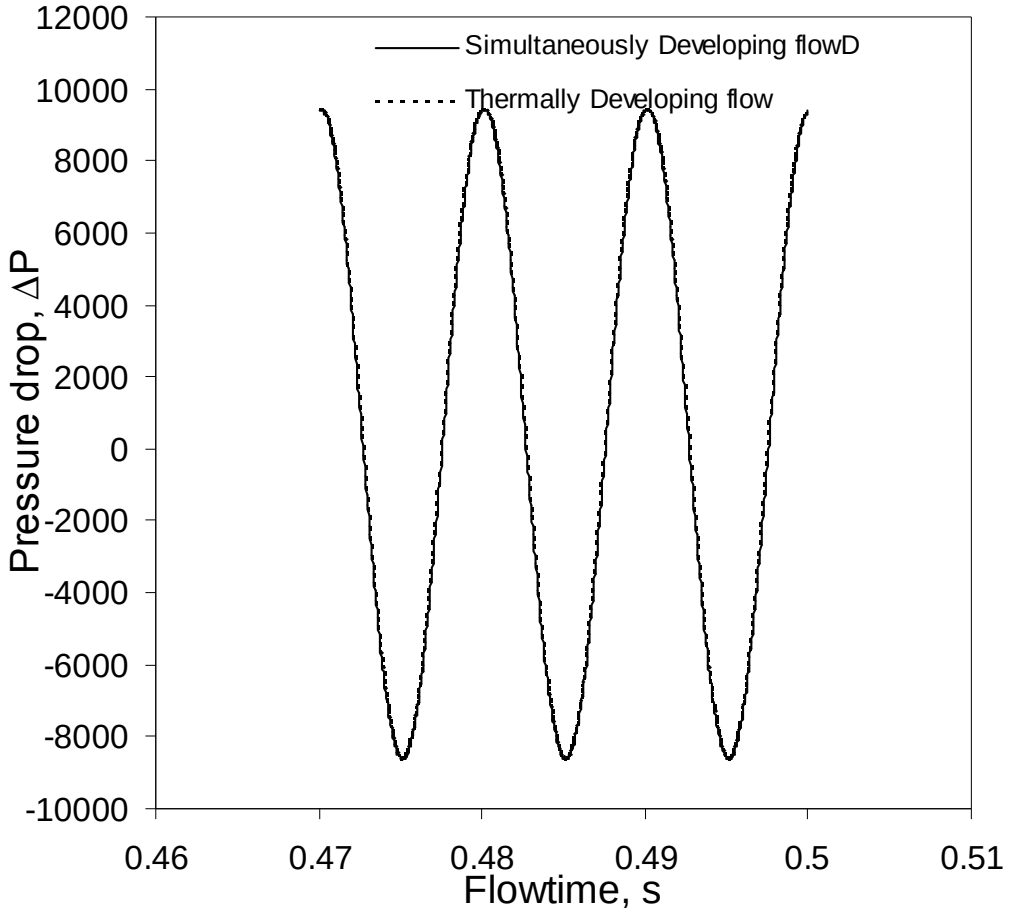

Figure 5.6 (a): Effect of pulsations on instantaneous pressure drop in case of developed velocity profile at inlet (f_p: 100 Hz, A_0: 0.5, Re_m: 200, time step: 0.05ms)

Figure 5.6 (b) shows the comparison between the thermally developing flow and the simultaneously developing flow i.e. the effect of pulsation frequency of 100 and dimensionless amplitude of 0.5 on time averaged local Nusselt number for the case of different velocity profile at inlet. It can be seen from the Figure 5.6 (b) that the profiles of time averaged local Nusselt number overlap with the profile of corresponding steady state local Nusselt number. It should be noticed that due to higher length of the channel and therefore shorter region of the developing velocity and the thermal boundary layer, the profile of steady state local Nusselt number in case of thermally as well as simultaneously developing flow is almost similar to each other. Thus, no effect of inlet velocity profile is visible over the time averaged values of local Nusselt number. Table 5.8 also summarizes

the result of the time and area averaged local Nusselt number for both the cases. The steady state average Nusselt number for thermally developing flow obtained from the present simulations also lies at 4.14. The reason is shorter entrance region (or longer total length of the channel) compared to the total length of the channel so that the velocity and temperature profile remains developed one in almost all part of the channel. Similar to simultaneously developing flow, small decrease in the time averaged Nusselt number in case of thermally developing is also observed. However the decrease is not so significant and the value of the time and the area averaged Nusselt number is very close to the steady state average Nusselt number (± 2% deviation).

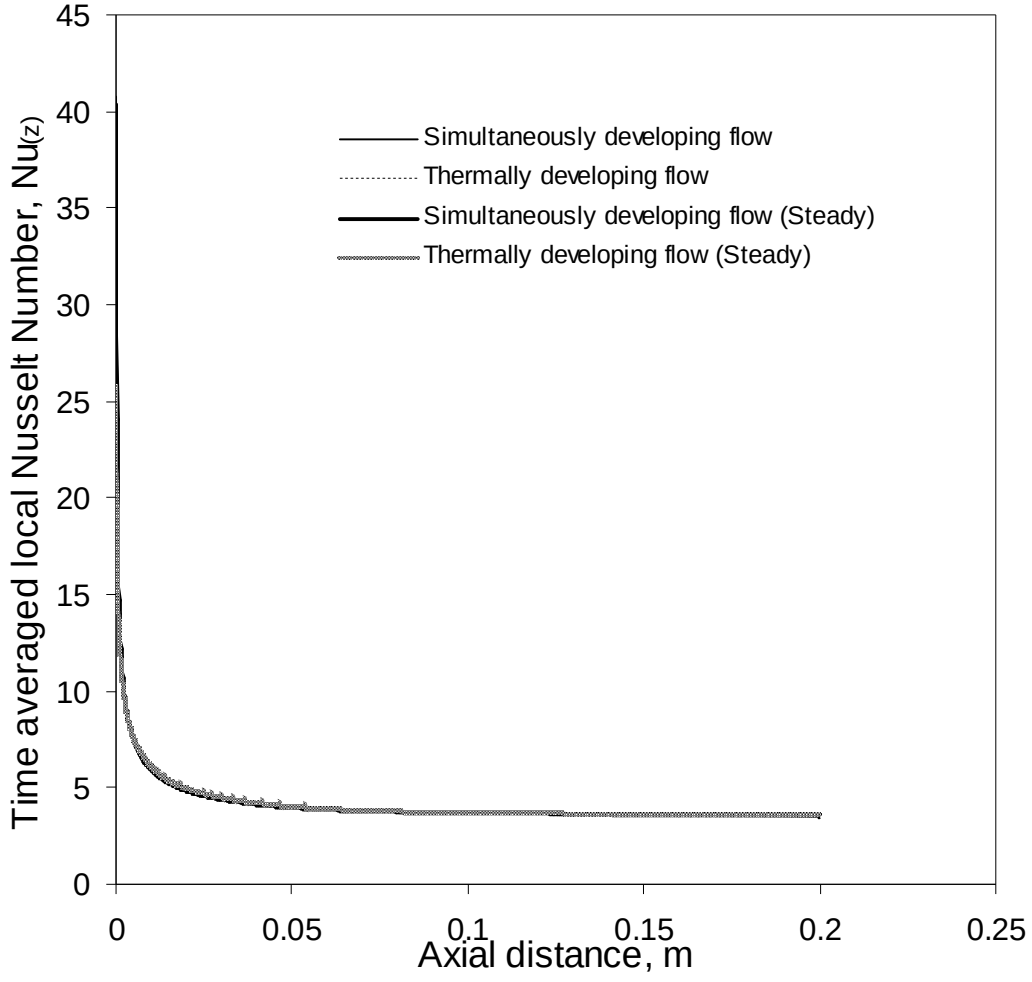

Figure 5.6 (b): Effect of flow pulsations on time averaged local Nusselt in case of developed velocity profile at inlet (f_p: 100 Hz, A_0: 0.5, Re_m: 200, time step: 0.05ms)

Table 5.8: Effect of pulsations in case of developed velocity profile at inlet

Inlet Velocity profile	Amplitude A_0	frequency, f_p Hz	Strouhal Number	Womersley Number	Time Step (ms)	Instantaneous $\Delta P_{(t)}$ (Pa)	Instantaneous avg. Nusselt Number $Nu_{avg(t)}$
Uniform	0	0	-	-	Steady	391.69	4.14
Uniform	0.5	100	0.112	11.8	0.05	392.18	4.06
Parabolic	0	0	-	-	Steady	378.94	4.14
Parabolic	0.5	100	0.112	11.8	0.05	377.57	4.06

As discussed earlier various authors have found different results depending on the frequency and amplitude under the study. In the present study even though amplitudes of the pressure cycles are different in presence of pulsations (for a constant amplitudes and different frequencies, see Figure 5.4 (a)) the mean of the pressure drop cycles remains at steady state value. In case of heat transfer little degradation is observed however the effect is not so significant. Such result of altering the heat transfer depending on the frequency of operation was obtained by Moschandreou *et al.* (1997), Guo *et al.* (1997) and Habib *et al.* (2002). However Chattopadhyay *et al.* (2006) found decrease in the friction factor with increasing frequency and no effect on the Nusselt number/heat transfer. Therefore as per the results of Chattopadhyay *et al.* (2006) it is expected that less pumping power or pressure drop is required to deliver the fluid in presence of pulsation compared to the steady flow. In other words the same amount of momentum transport can be achieved with less energy dissipation (in terms of pumping power because $\Delta P = \frac{2 f L_T \rho U^2}{D_h}$, lower f results in lower ΔP for same momentum transport) in case of pulsating flow. The authors have not given the reason for such behavior. The next question that arises if the pulsation reduces the friction factor (for the literature cases where reduction in f is observed) then why can't the pulsation does not affect heat transfer does at all? In case of steady state laminar developing flow the heat transfer directly depends on the momentum transport. Therefore one may expect significant changes in the momentum transport (in case of pulsations) is getting reflected in terms of

heat transfer also. Our result shows that the time averaged momentum transport itself is not getting affected by the frequency or the amplitude of the pulsations. In case of heat transfer the instantaneous area averaged Nusselt number cycle is also not in the same phase as that of velocity cycle (see Figure 5.3 (c) and (d)). However when averaged in time, no remarkable deviation is seen in Nusselt number compared to the one at steady state.

5.4. Conclusions

The effect of pulsating amplitude and frequency on pressure drop and heat transfer was numerically investigated for laminar flow with constant wall temperature. Following are the key conclusions:

1) The time averaged pressure drop in case of pulsating flow is same as that of steady flow.
2) Appropriate definition of local Nusselt number involving instantaneous mean local mean bulk temperature is used. The time averaged mean Nusselt number in case of pulsating flow is somewhat less than that of steady flow however the difference is not remarkable (within 2%).

Based on the results it can be seen that the pulsation has no effect on time averaged pressure drop or momentum transport and heat transfer in the range of the parameters studied.

CHAPTER 6

TWO PHASE FLOW AND HEAT TRANSFER IN SMALL CHANNELS

This chapter summarizes experimental work carried out to quantify two phase pressure drop and heat transfer in small channels. Flow and heat transfer experiments were carried out in a single minichannel of 1 mm size with air-water as working fluids. Pressure drop and heat transfer coefficients were measured for a range of gas and liquid flow rates. The two phase experimental pressure drop was well correlated by the Lockhart–Martinelli method. In case of heat transfer it was observed that at low gas flow rates, the two phase heat transfer coefficient was more than that of single phase. However for higher gas flow rates the opposite behavior was observed.

6.1 Background

Reactions involving gas liquid systems are quite common in chemical process industries. Mechanically agitated contactors, bubble columns, packed columns are the few contactors used for carrying out gas-liquid reactions. The choice of these contactors depends on several factors such as operating regimes, rate controlling step, production output, heat and mass transfer requirements, interfacial area etc. The characteristic length of these contactors varies from few centimeters to several meters. The interfacial area obtained in these contactors is of the order of 100-300 m^2/m^3 and the volumetric mass transfer coefficient obtained is of the order of 0.2 s^{-1} (Doraiswamy and Sharma 1984). Overall performance of several fast reactions such as sulphonations, fluorinations, chlorination is therefore primarily governed by the heat and mass transfer capacity offered by such contactors.

In recent years, small channel reactors or micro and minireactors are increasing being evaluated for carrying out gas-liquid reactions (see for example Wehle *et al.* 2000, De Mas *et al.* 2003). These small reactors offer significantly larger heat and mass transfer capability because of higher surface area to volume ratio (>10000 m^2/m^3) available with small channels. Several examples of benefits in terms of desired selectivity and yield can be found in Ehrfeld *et al.* (2000) and Hessel *et al.* (2005) among others. It is however essential to critically understand various transport processes occurring in small channels in order to realize true potential of micro-reactors. Specifically, fundamental knowledge of two-phase flow characteristics in small flow passages, such as the flow pattern, void fraction, pressure drop, and heat transfer coefficient, is crucial for engineering design purposes as well as for evaluation of practical performance.

Several studies have been conducted to characterize gas-liquid flows in capillaries (see Liu *et al.* 2005). However heat transfer characteristics are not yet well understood (see Hestroni *et al.* 2009). Our current knowledge on two-phase flow characteristics and heat transfer in micro-channels is still limited and the literature sources are sparse. One of the unanswered questions is whether the two-phase pressure drop and heat transfer characteristics in small channels are different from that encountered in ‘‘conventional”

size channels (see for example Ghajar *et al.* 2004). The objective of the present investigation is to quantify influence of gas flow on two phase pressure drop and heat transfer in a single minichannel. Available information on flow and heat transfer in micro-channels is therefore briefly reviewed here. In light of this review, attempt was made to quantify the two phase pressure drop and heat transfer coefficient in a single mini channel experimentally. Experimental set-up and procedure, and obtained results are discussed in the following sections.

Bao *et al.* (1999) reported an experimental study of non-boiling air water flows in a channel of 1.95 mm. The authors studied the pressure drop and heat transfer coefficients over a range of gas superficial velocity 0.1 – 50 m/s, liquid superficial velocity 0.08 to 0.5 m/s and wall heat flux 3-58 kW/m^2. They found that for a given liquid flow rate, the data exhibit sudden changes in pressure drop and, to a lesser extent, in heat transfer characteristics as the gas flow was increased. These events were believed to correspond to flow transitions, from bubbly, to intermittent slug, to annular flow. Overall, the pressure drops in these non-boiling two-phase flows can be estimated with good accuracy using correlations developed for adiabatic conditions. The heat transfer results were, on average, reasonably well described by the two-phase convective heat transfer components of flow boiling correlations however considerable scatter was also obtained in some cases.

Kaji *et al.* (2009) simultaneously measured heat transfer, pressure drop and void fraction for upward heated air-water non-boiling two-phase flow in 0.51 mm I.D. tube to investigate thermo-hydro dynamic characteristics of two-phase flow in microchannels. At low liquid superficial velocity frictional pressure drop agreed with Mishima-Hibiki's correlation, whereas agreed with Chisholm-Laird's correlation at relatively high liquid superficial velocity. The authors found that the void fraction was lower than the homogeneous model and conventional empirical correlations. To interpret the decrease of void fraction with decrease of tube diameter, a relation among the void fraction, pressure gradient and tube diameter was also derived. The estimated heat transfer coefficient agreed with the data for 1.03 and 2.01 mm I.D. tubes fairly well when superficial liquid

velocity was relatively high. Analogy between heat transfer and frictional pressure drop was proved to hold roughly for the two-phase flow in microchannel.

Hesroni *et al.* (2009) studied the air-water heat transfer in parallel micro-channels of 0.1 mm in size. The authors showed different flow patterns occurring simultaneously in different channels. A regime map showing appearance of different flow patterns as a function of superficial velocity of gas and liquid was presented. The dependence of the Nusselt number, on liquid and gas Reynolds numbers, based on liquid and gas superficial velocity, respectively, was determined in the range of Re_{LS} = 4–56 and Re_{GS} = 4.7–270. It was observed that for a constant gas velocity, increase in superficial liquid velocity leads to increase in heat transfer (Nu_L). However, for a constant liquid superficial velocity, heat transfer (Nu_L) decreases with increasing gas velocity. This trend does not agree with the generally accepted trend of increasing heat transfer with increase in two phase flow rate (see review of Ghajar 2004 and references cited therein).

It can be seen from this brief review that only few studies on non boiling two phase flow and heat transfer in small channels are available. In contrast numerous studies and experimental data are available consisting of flow and heat transfer in a convectional size channels. A good summary of the available experimental data can be found in Ghajar (2004). It can be seen from the data of the two phase flow and heat transfer in conventional channels that rate of heat transfer increases with increase in two phase mass flow (see for example Knott *et al.* 1959, Martin and Sims 1971, Shah *et al.* 1971, Vijay *et al.* 1982). However, experimental results of two phase heat transfer in small channels do not present such a conclusive relationship (see for example, studies of Kaji *et al.* 2009, Bao *et al.* 1999 show trends similar to those observed in larger systems where as recent study of Hestroni *et al.* (2009) show opposite trend). With this background, in the present work two phase flow and heat transfer in a single minichannel were investigated experimentally.

6.2 Experimental setup and procedure

6.2.1 Test piece

The experimental test piece consisted of a copper block having dimensions of 22 mm x 8 mm x 200 mm. On this block, single rectangular channel was machined on one side using wire EDM technique. The minichannel was of 1 mm wide and 1 mm deep with an accuracy of ±10 μm. Figure 6.1 shows the image of the mini-channel plate. The top of the geometry was closed by 8 mm thick acrylic plate which is provided with 1 mm holes for arrangement of needles to measure pressure as well temperature.

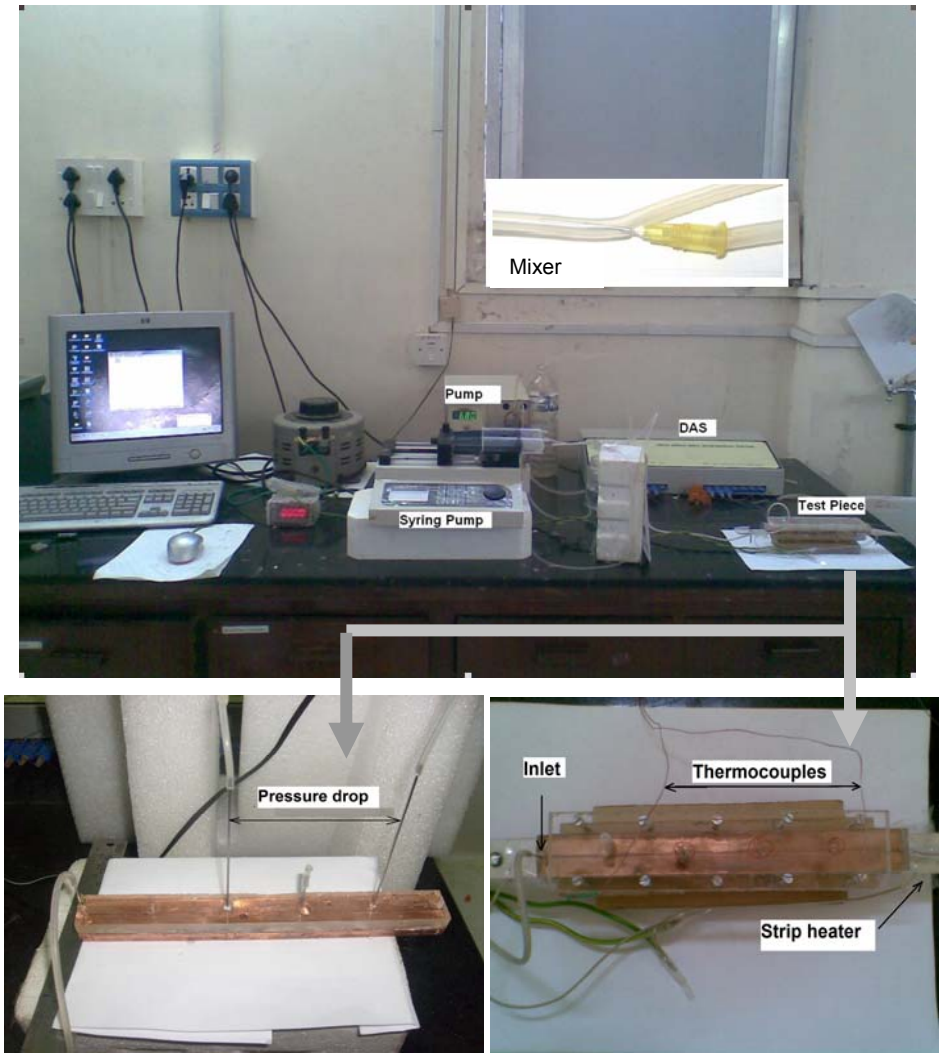

Figure 6.1: Experimental facility and test piece

For mixing the two fluids, an in house mixer was designed to mix the gas and liquid. The mixer is shown in Figure 6.1. The arrangement of the mixer was such that there was least resistance or pressure drop at the junction of the liquid and gas. In this arrangement a single needle consisting of a gas was injected in a silicon tube carrying liquid in such way that the directions of needle and the liquid flow will remain same. For heat transfer studies, the test piece was heated using A.C. strip heater with power or heat input controlled by the dimmerstat. The power supplied to cartridge heater was measured by Digital Wattmeter (Conzerve).

6.2.2 Measurement apparatus and procedures

Water was used as a working fluid for continuous liquid phase that was pumped using the SSI peristaltic HPLC pump provided with flow controller. The flow rates used in the present study were in the range of 0.5 ml/min to 12 ml/min that was also measured by collecting the volume of liquid in a specific time. Figure 6.1 also shows the schematic of the experimental setup. For Pressure drop measurements two holes of diameter 1 mm were drilled on the top polycarbonate cover 80 mm distance between them. Through these holes two SS tubes or needles having internal diameter of 0.6 mm were inserted so that the tube will be inline with the top surface of the channel. These two tubes were connected to the digital manometer having sensitivity of 7 Pa and accuracy of $\pm$ 0.3% of full scale at 25^{o}C. When fluid moves through the channel the frictional pressure drop over the 80 mm length was directly measured by the digital manometer. For two phase pressure drop the other working fluid used was air. Syringe pump supplied by Longer was used for this purpose. The range of the air flow rate used was 0.5 ml/min to 160 ml/min. The water and gas gets mixed in a mixer and the slugs were formed those travels through 2 mm silicon tube which then enters in a test piece through a needle fitted on a an acrylic cover serving as an inlet. Flow pattern visualization was done using high speed camera (Redlake) at 800 fps.

For heat transfer studies, temperatures were measured and recorded using the data acquisition at scanning rate of 1 s within accuracy of $\pm$ 0.5 ^{o}C. Two thermocouples (Omega, J Type, Accuracy: $\pm$0.5 ^{o}C) of size 0.076 mm were placed on the channel wall to

measure the wall temperature at the end of the channel. Two thermocouples were placed at channel inlet and outlet to measure the temperature of the water. The magnified region of the mini-channel plate shown in Figure 6.1 illustrates the thermocouple locations to measure the temperature of channel wall and fluid. For testing procedure, the SSI pump was turned on at flow rates from 1 ml/min to 12 ml/min. The electrical power to the heater was adjusted to a desired level by a variable voltage of the dimmerstat. After allowing the system to establish steady state, flow rate, electrical power and temperatures were measured.

6.2.3 Data reduction

6.2.3.1 Flow visualization

Before carrying out heat transfer experiments, visualization of gas-liquid flow pattern was carried out with high speed camera. The focus of the camera consisted view of length of 30 mm in stream wise direction. A digital camera having frame rate around 30 fps was also used for confirming the periodic steady state of the flow. Actual snapshots of the gas-liquid flows observed in the present minichannel (1 mm) at certain gas and liquid flow rates are shown in Figure 6.2 (a) and (b). The data was further processed to understand different possible flow regimes depending on the gas and liquid velocity. An attempt was made to relate observed heat transfer rates with prevailing flow regimes.

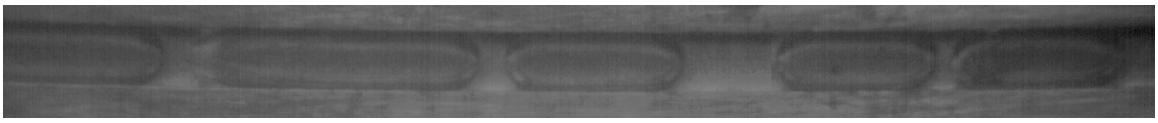

Figure 6.2 (a): snapshot of slug flow in channel (Qw: 8 ml/min, Qa: 12 ml/min)

Figure 6.2 (b): snapshot of slug flow in silicon tubing before the channel (Qw: 8 ml/min, Qa: 12 ml/min)

6.2.3.2 Pressure drop

The determination of a two phase pressure drop in small channels becomes difficult task due to contribution from the acceleration terms because of the small lengths of the channel. The total pressure drop is given by Equation 6.1 as:

$$\left(\frac{\Delta P}{\Delta L}\right)_{TP} = \left(\frac{\Delta P}{\Delta L}\right)_{TPF} + \left(\frac{\Delta P}{\Delta L}\right)_{a} + \left(\frac{\Delta P}{\Delta L}\right)_{H} \quad \text{..... (6.1)}$$

Where $\left(\frac{\Delta P}{\Delta L}\right)_{TPF}$ two phase frictional pressure drop, $\left(\frac{\Delta P}{\Delta L}\right)_{a}$ acceleration pressure drop and $\left(\frac{\Delta P}{\Delta L}\right)_{H}$ hydrostatic pressure drop

A comparison of the two-phase frictional pressure gradient data with the predictions of the Lockhart–Martinelli correlation (using appropriate C-value) and the Friedel's correlation was done. The Lockhart–Martinelli correlation is given by Equation 6.2 as:

$$\left(\frac{\Delta P}{\Delta L}\right)_{TP} = \phi_L^2 \left(\frac{\Delta P}{\Delta L}\right)_{L} \quad \text{..... (6.2)}$$

Where ϕ_L^2 : friction multiplier and $\left(\frac{\Delta P}{\Delta L}\right) = \frac{2 f \rho V^2}{D_h}$

The friction multiplier is correlated in terms of the Lockhart–Martinelli parameter, *X*, as:

$$\phi_L^2 = 1 + \frac{C}{X} + \frac{1}{X^2} \quad \text{..... (6.3)}$$

Where $X^2 = \frac{\left(\frac{\Delta P}{\Delta L}\right)_L}{\left(\frac{\Delta P}{\Delta L}\right)_G}$ and *C*: constant depends on flow conditions

C= 5 for laminar flow and *C* = 20 for turbulent flow.

In the Friedel's correlation it is assumed that the two phase flow resistance is proportional to the pressure drop which would occur if the whole flowing mass (total mass flow m_ of the two-phase system) was treated as one phase, i.e. as a liquid (water), or as gas (air).

The dependence which determines the frictional pressure drop during a two-phase flow can then be expressed as given by Equation 6.4 as:

$$\left(\frac{\Delta P}{\Delta L}\right)_{TP} = \phi_{LO}^2 \left(\frac{\Delta P}{\Delta L}\right)_{LO} \quad \text{..... (6.4)}$$

Where, $\left(\frac{\Delta P}{\Delta L}\right)_{LO} = \frac{2 f_{LO} \rho_L V_{LO}^2}{D_h}$, $\mathrm{Re}_{LO} = \frac{D_h V_{LO} \rho_L}{\mu_L}$ and $V_{LO} = \frac{\dot{m}_L + \dot{m}_G}{\rho_L A}$

Friedel proposed following correlation for the calculation of the correction factor of the two-phase flow resistance ϕ_{LO}^2 as:

$$\phi_{LO}^2 = \left[(1-x)^2 + x^2 \frac{\rho_L f_G}{\rho_G f_L}\right] + \frac{3.24 x^{0.78}(1-x)^{0.224} + \left(\frac{\rho_L}{\rho_G}\right)^{-0.91} \left(\frac{\mu_G}{\mu_L}\right)^{0.19} \left(1-\frac{\mu_G}{\mu_L}\right)^{0.7}}{Fr_{HOM}^{0.045} \, Wer_{HOM}^{0.035}} \quad \text{(6.5)}$$

Where Fr_{HOM} is the Froud number calculated as for a homogeneous flow:

$$Fr_{HOM} = \frac{(G)^2}{d_h \, g \, \rho_{HOM}^2} \quad \text{..... (6.6)}$$

while We_{HOM} is the Weber number in this correlation defined as:

$$We_{HOM} = \frac{d_h (G)^2}{\sigma \, \rho_{HOM}} \quad \text{..... (6.7)}$$

The density of the homogeneous mixture is calculated as:

$$\frac{1}{\rho_{HOM}} = \frac{x}{\rho_G} + \frac{1-x}{\rho_L} \quad \text{..... (6.8)}$$

Where, x is mass fraction of gas in mixture and G is total mass flux

6.2.3.3 Heat transfer:

The total power given to the strip heater was getting distributed in two parts. A) Heat supplied to water (Q1) B) Heat loss to the environment (Q2). The heat taken by the water was calculated as:

$$Q1 = \dot{m} Cp (T_{f,out} - T_{f,in}) \quad \text{..... (6.9)}$$

The heat loss to the environment (part B) was calculated using the difference between the heat supplied to the cartridge heater and heat taken by water. The overall heat loss to the environment was found to be less than 10%. In the present study all heat transfer calculations were based on liquid temperature since heat capacity flow rates of gas phase were less than 3 % of the liquid phase. More than 100 temperature data points were used in calculations for every flow rate.

At the bottom of the test piece, the strip heater provides uniform heat flux over the length of the channel. Since the thermal conductivity of copper was very high and with certain finite thickness of the test piece, the channel internal temperature becomes uniform along the length of the channel. This is due to the conduction inside the copper. Detailed information on this phenomenon can be found in Shah and London (1978). In the present work this was also confirmed by the measurement of wall temperature just below the channel bottom wall. We assumed that at a given cross-section the side-wall temperature of the micro-channel did not differ significantly from the channel bottom temperature. Therefore thermal boundary condition for the wall becomes as a constant wall temperature.

The log mean temperature difference (LMTD) based on the wall temperature and the liquid inlet and outlet temperature was calculated as:

$$LMTD = \frac{(T_W - T_{f,in}) - (T_W - T_{f,out})}{\dfrac{(T_W - T_{f,in})}{(T_W - T_{f,out})}} \quad \text{..... (6.10)}$$

Based on LMTD the Overall internal heat transfer coefficient can be calculated as:

$$q1 = \frac{Q1}{(W \times L + 2 \times H \times L) \times 20} = h_{L1} \times \frac{(T_W - T_{f,in}) - (T_W - T_{f,out})}{\dfrac{(T_W - T_{f,in})}{(T_W - T_{f,out})}} \quad \text{..... (6.11)}$$

The average two phase Nusselt number based on the liquid properties was calculated as:

$$Nu_{avg(TP)} = \frac{h_{L1}\, d_h}{k_L} \quad \text{..... (6.12)}$$

The results were further compared with the available experimental correlations for two phase heat transfer coefficient in conventional size channels

6.3 Results and discussion

6.3.1 Flow regime map

For the range of operating conditions studied slug flow pattern was expected to prevail, however different sub-flow patterns of slug flow were also observed depending upon the flow conditions. Depending on their interfacial configuration these flow patterns were classified as a) bubbly-slug flow b) slug flow c) slug-annular flow d) bubbly-slug-annular flow and e) annular flow. It must be noticed that in all the five cases the length of the gas bubbles and liquid slugs do not remain constant throughout the experimental run. However the situation is very close to the periodic steady state i.e. the similar pattern is observed over a unit time, in this case say 2-5 s. Figure 6.3 shows the regime map showing different flow pattern observed in the present work.

a) Bubbly-slug flow

This pattern consists of periodic occurrence of small bubbles that are equal to or little longer than the tube diameter followed by liquid slugs. Such a flow pattern occurs for all liquid velocities and relatively low superficial gas velocities. These flows are completely dominated by surface tension forces.

b) Slug flow

This flow pattern consists of regularly distributed gas bubbles that are ellipsoidal in shape also described as Taylor flow. In this case a liquid film is formed surrounding the gas bubbles thus wetting the wall of the channel by liquid. This flow pattern is also surface tension dominated; however, inertial forces tend to break the bigger size bubble into two

or three bubbles of smaller size. Such a flow pattern occurs for all liquid velocities and relatively higher superficial gas velocities as compared to the one of earlier of case. Therefore the gas holdup is also high in this case compared to earlier one.

c) Slug-annular flow

This flow pattern consists of regularly distributed gas bubbles that are much longer in size compared to the diameter of the channel. Along with this due to somewhat higher gas velocities the gas bubble coalesce with each other to create the pattern that covers the complete central core of the channel with the water flowing in the thing film along the wall also referred as annular flow. The range of the gas velocities for this flow pattern is 0.5 to 2 m/s and for liquid 0.05 to 0.15 m/s.

d) Bubbly-slug-annular

This pattern is a combination of slug-bubble and slug-annular flow i.e. presence of bubbles, slug and the annular regions at regular intervals. This flow pattern is observed in a specific range of gas and liquid velocity. Due to somewhat higher liquid velocity than the earlier case the longer gas bubbles are breaking down into smaller gas bubbles. The range of the gas velocities for this flow pattern is 0.5 to 2 m/s and for liquid 0.15 to 0.2 m/s.

e) Annular flow

When the inertial forces of the gas phase become high enough to rupture the interface between the bubbles, the flow becomes annular and is characterized by a thin wavy liquid film flowing along the wall with a mist of gas and entrained liquid in the core. The range of the gas velocities for this flow pattern is 1.5 to 3 m/s and for liquid 0.1 to 0.15 m/s.

No stratified flow is observed in the entire range of experiments.

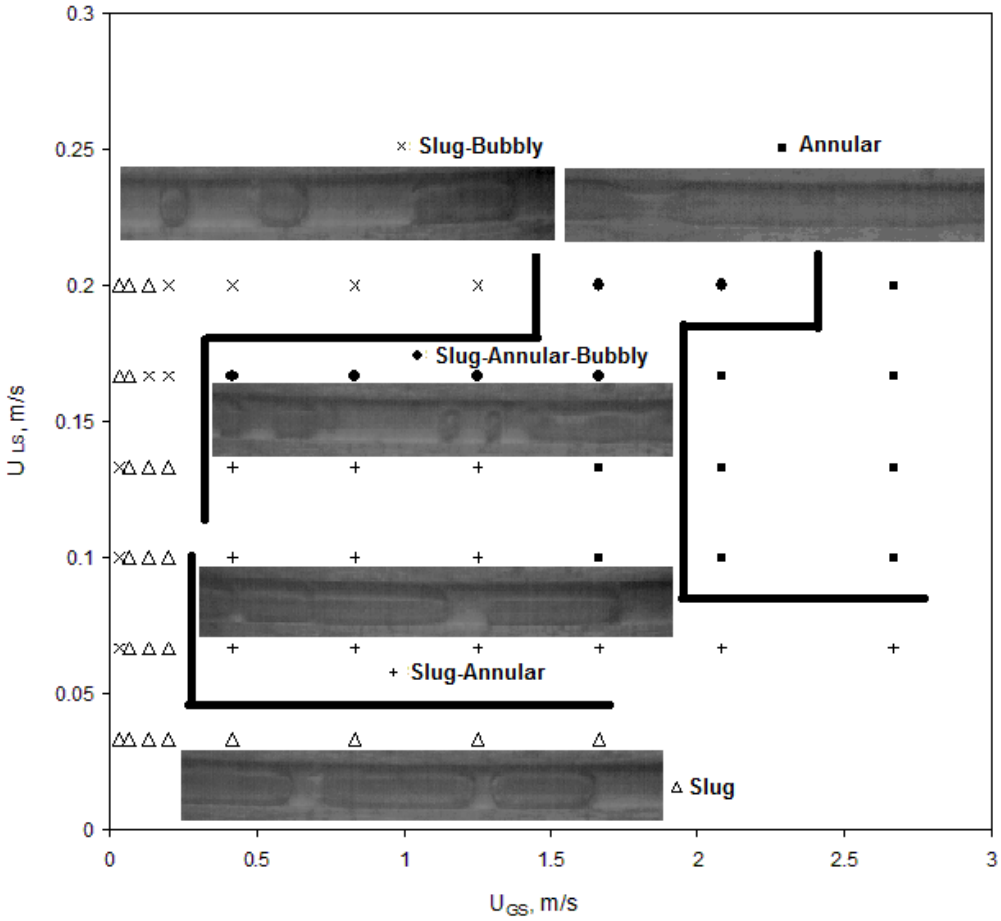

Figure 6.3: Flow regime map

6.3.2 Two phase pressure drop

In the present work, the range of the Reynolds number for gas phase was 2 to 180 and 33 to 200 for the liquid phase. Figure 6.4 shows the two phase pressure drop vs. superficial gas velocity for a given superficial liquid velocity. For a constant liquid velocity, addition of a gas in to the system increases the two phase pressure drop. The relationship is very much similar to that generally observed in conventional size channels i.e. the two phase pressure drop increases with increases in total mass flow rate. The experimental pressure drop was modeled using Lockhart Martinelli method and Friedel method.

Figure 6.6 shows the two phase pressure drop results in terms of φ_L^2 vs. 1/X for a given liquid velocity along with the predictions from the Lockhart Martinelli (LM) model and Friedels model (assuming laminar-laminar flow regime for Friedels model and

considering two limiting values of $Fr_{HOM}^{0.045}\ Wer_{HOM}^{0.035}$ as 1 and 1.4). Good agreement is observed between the Lockhart Martinelli (LM) model with C = 8 and the present experimental data. The present results are consistent with data of Dutkowski (2009) for 1.3 mm circular channel. The predictions of Friedels correlation are however much higher (>100 %) compared to the experimental values.

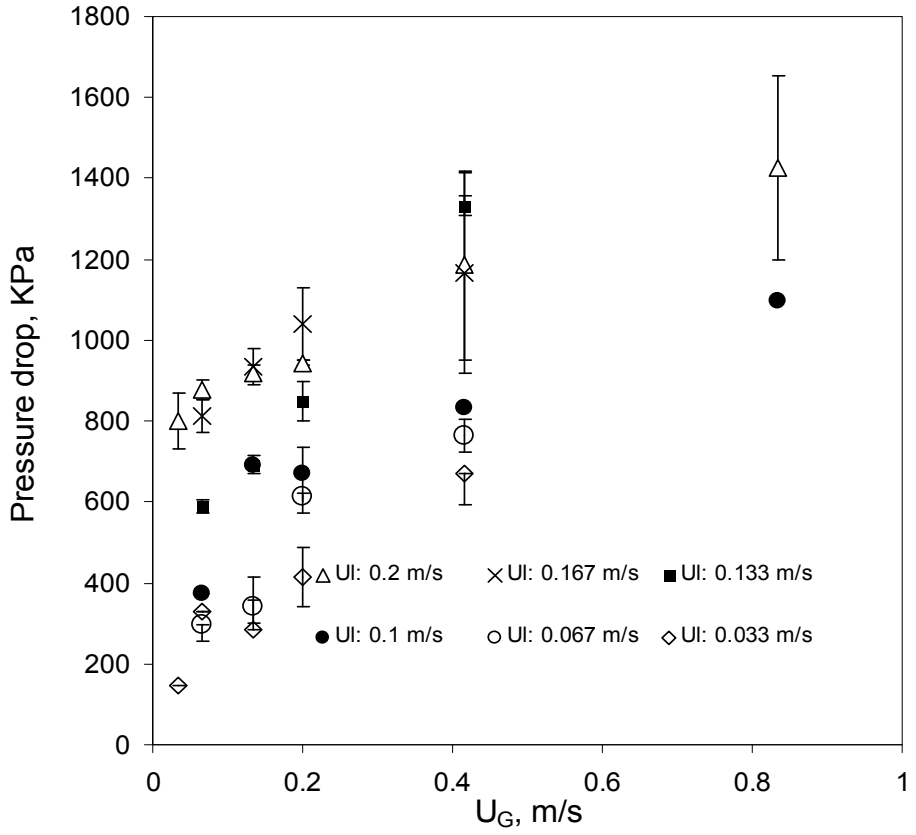

Figure 6.4: Experimental data of two phase pressure drop

6.3.3 Two phase heat transfer

Figure 6.6 (a) shows the result of two phase average Nusselt number (calculated from the overall liquid heat transfer coefficient) vs. the liquid phase Re for a given gas phase Re. As expected the two phase Nusselt increases with the increase in the liquid superficial velocity. The present data of two phase Nusselt number approximately varies with $Re^{0.65}$. Figure 6.6 (b) shows the result of two phase average Nusselt number vs. the gas phase Re for a given liquid phase Re. It must be noticed that the definition of the two phase Nusselt

number was based on liquid properties (see Equation 6.12). The single phase Nusselt number for the case of simultaneously developing flow with constant wall temperature for a square channel is approximately 3 (Shah and London 1978).

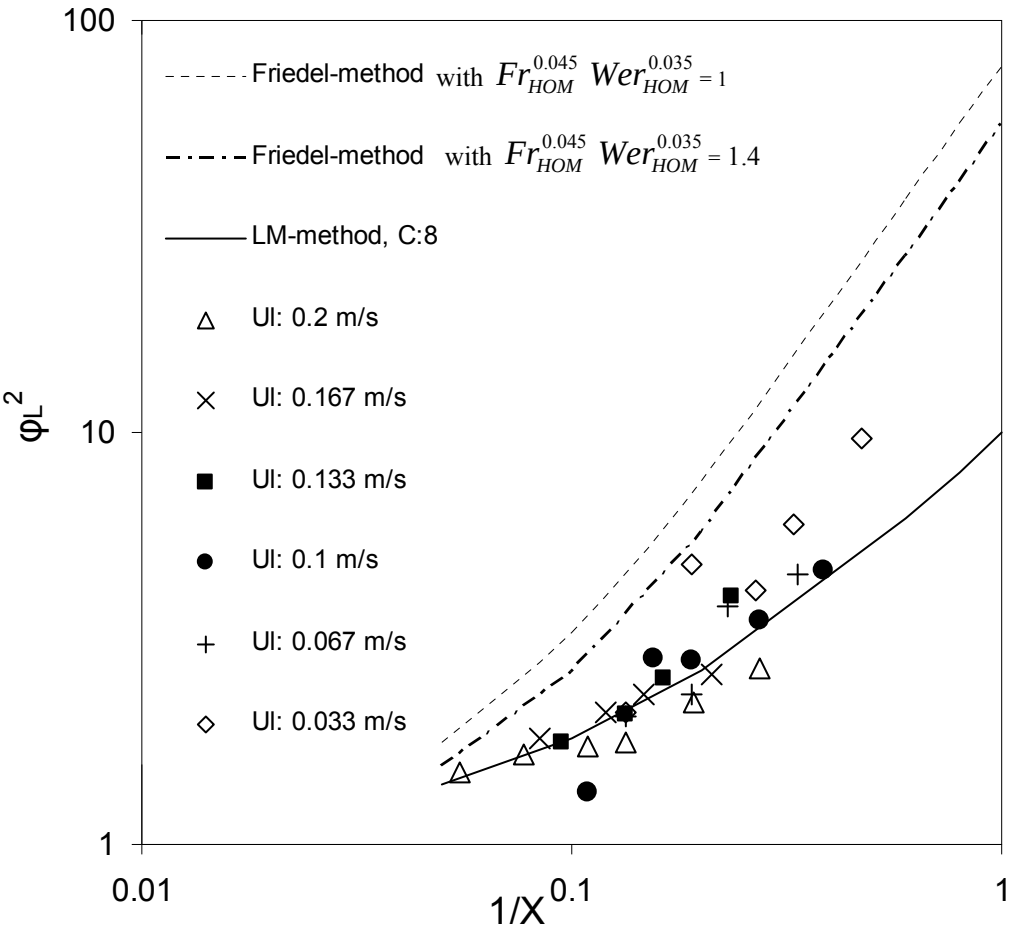

Figure 6.5: Comparison of experimental φ_L^2 with LM model and Friedel model (error bars not shown)

In the present case, for the range of the liquid flow rates used, it is found that the overall/average single phase Nusselt number is 3 for all liquid flow rates. This is due to the smaller thermal developing length (due to quite small flow rates 2 ml/min to 12 ml/min) and therefore much of the flow remained in thermally developed region i.e. very little or negligible contribution from the thermally developing region.

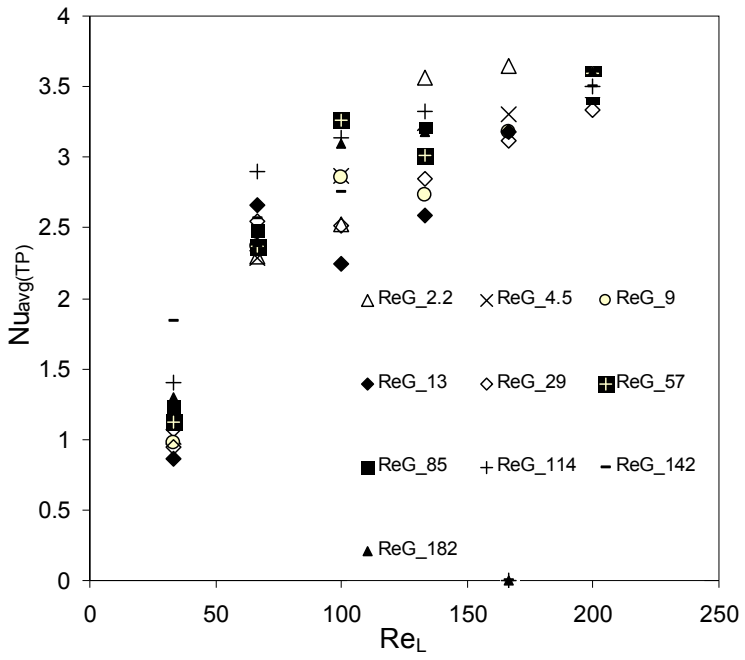

Figure 6.6 (a): Effect of superficial liquid velocity on two phase average Nusselt number (error bars not shown)

Figure 6.6 (c) shows that for higher liquid flow rates (i.e. Re_L 100-200) the presence of gas increases the two phase average Nusselt number. This can be expected because for higher liquid flow rates as the presence of gas with lower flow rates results in a bubbly or slug flow (see Figure 6.4). As discussed earlier the single phase Nusselt number was 3 due to fully developed flow nature of the flow in the channel i.e. developed thermal boundary layer. Presence of small gas bubbles wash out the developed thermal boundary layer in the liquid phase therefore generating higher temperature gradient at wall thus enhancing heat transfer between wall and fluid. In addition to this in case of slug flow there was intense mixing in the liquid slug due to circulation of fluid elements. This also helps to enhance the heat transfer from the solid wall to the fluid.

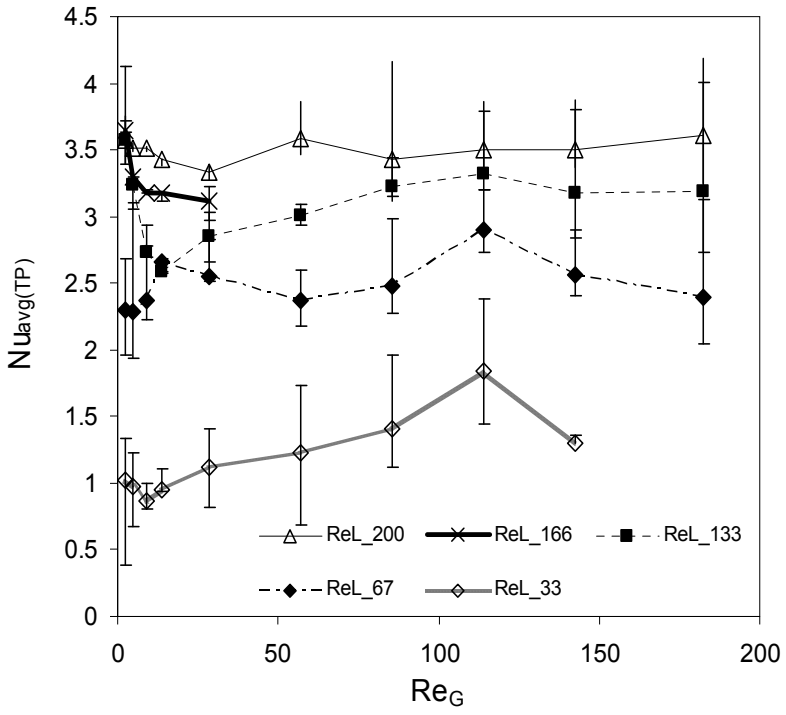

Figure 6.6 (b): Effect of superficial gas velocity on two phase average Nusselt number (Re_L: 33- 200, Q: 10W)

This scenario is only applicable for the higher liquid flow rate ($Re_L > 100$) and lower gas flow rates ($Re_G < 20$). For the same higher liquid flow rates ($Re_L > 100$) the effect of increasing the gas flow rates above certain value (i.e. $Re_G > 20$) is not remarkable. The reason for such behavior cannot be the entirely justified by the present results due to large error bar associated with the experimental data in the region of higher gas flow rates.

In case of lower liquid flow rates ($Re_L < 100$), the average two phase Nusselt number is found to be much lower than that of the single phase (see Figure 6.6 (a)). In this range also the effect of increasing the gas flow rate (i.e. $Re_G > 20$) is not remarkable. Due to lower liquid flow rate and higher gas flow rate, the resulting gas hold up is much more and the flow regime therefore is semi annular (See Figure 6.4). One can expect higher heat transfer coefficient due to very small thickness of the liquid film near the wall. However the present data does not reflect the same. Unfortunately measured liquid

temperature was found to fluctuate significantly for higher gas flow rates making the reliability of the data in this range questionable.

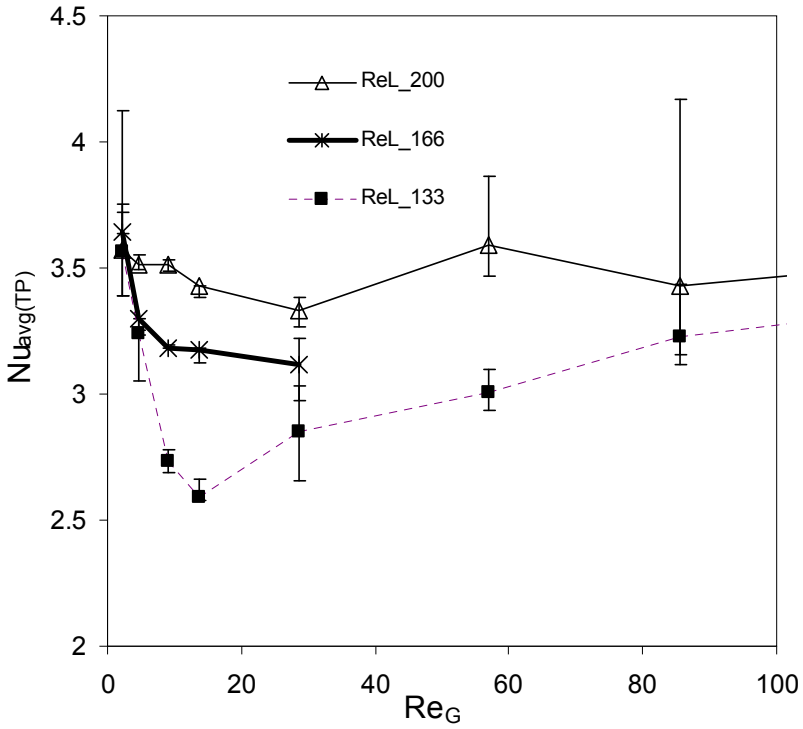

Figure 6.6 (c): Effect of superficial gas velocity on two phase average Nusselt number (Re_L > 100, Q: 10W)

It is necessary to understand the relationship or the analogy between heat transfer and the frictional pressure drop in minichannels. As mentioned in section 6.1 in case of conventional size channels, the rate of heat transfer increases with increase in two phase mass flow (Knott *et al*. 1959, Martin and Sims 1971, Shah et al. 1981, Vijay et. al. 1982 summarized in Ghajar 2004). A recent study of Kaji *et al.* (2009) found increase in the overall heat transfer due to presence of gas than that of single phase alone. Results of Hestroni *et al.* (2009) however have complete opposite findings. In their work the presence of gas decreases the two phase heat transfer (while insignificant effect of gas flow rate on two phase pressure drop for a constant liquid flow rate) compared to single phase alone. The authors have not given any reason for the same. Figure 6.7 shows the relation between heat the transfer ratio h_{TP}/h_L (i.e. two phase heat transfer coefficient to single phase heat transfer coefficient) and Martinelli parameter *1/X*. It can be seen that for

Re_L > 100 the ratio is above 1 and for Re_L < 100 the ratio is less than 1. Figure 6.7 also shows the predictions of h_{TP}/h_L obtained from various correlations available in the literature for macro channels (Knott *et al.* 1959, Martin and Sims 1971, Shah *et al.* 1971, Vijay *et al.* 1982) as well as minichannels (Kaji *et al* 2009, Hestroni *et al.* 2009). Table 6.1 shows the various correlations used for comparison of present experimental data. It can be seen from the Figure 6.7 that increasing gas flow rates does not have any remarkable effect on h_{TP}/h_L.

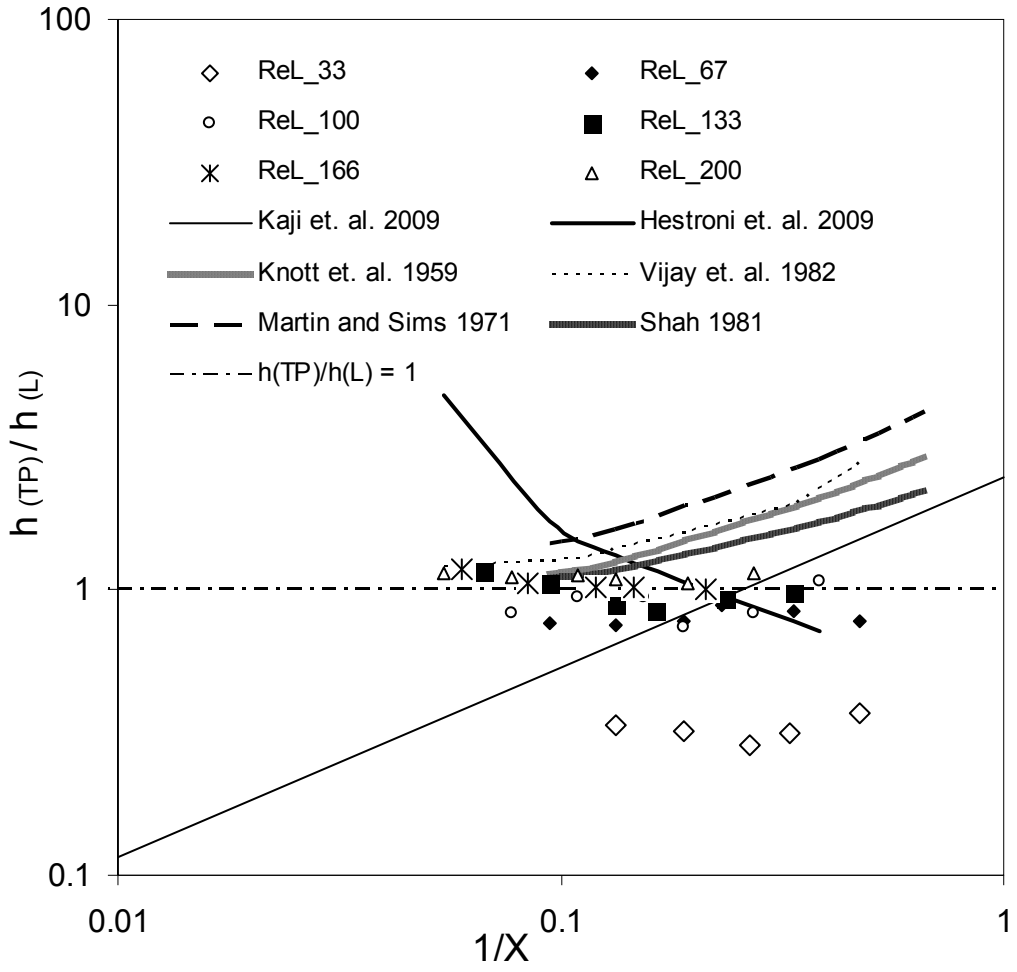

Figure 6.7: Relation between heat the transfer ratio h_{TP}/h_L and Martinelli parameter *1/X* (error bars not shown)

To understand the effect of variation of gas flow rate, the present experimental data is compared with that of Hestroni *et al*. (2009) for a common Re_L. Figure 6.8 shows the

comparison for Re_L of 66. As absolute values of two phase Nusselt numbers obtained in the present work are different than those obtained by Hestroni *et al.* (2009), the data is normalised with arbitrarily selected value of the two phase Nusselt number for Re_G of 33 to highlight differences or similarities in the observed trends. The results of Hestroni *et al.* (2009) show decrease in two phase Nusselt number with increase in gas flow rate while no remarkable effect of increasing gas flow rate on two phase Nusselt number is observed from the present experimental data.

Table 6.1: Correlations for predicting two phase heat transfer coefficient

Author	Correlation
*Knott *et al.* 1959	$\frac{h_{TP}}{h_L} = 1 + \left(\frac{V_G}{V_L}\right)^{\frac{1}{3}}$
*Martin and Sims 1971	$\frac{h_{TP}}{h_L} = 1 + 0.64\left(\frac{V_G}{V_L}\right)^{\frac{1}{2}}$
*Shah *et al.* 1971	$\frac{h_{TP}}{h_L} = 1 + \left(\frac{V_G}{V_L}\right)^{\frac{1}{4}}$
*Vijay *et al.* 1982	$\frac{h_{TP}}{h_L} = 1 + \left(\frac{\Delta P_{TP}}{\Delta P_L}\right)^{0.451}$
Kaji *et al.* 2009	$\frac{h_{TP}}{h_L} = 2.5\left(\frac{1}{X}\right)^{\frac{2}{3}}$
Hestroni *et al.* 2009	$Nu_{L,(TP)} = 0.13\left(\mathrm{Re}_L\right)^{0.96}\left(\mathrm{Re}_G\right)^{-0.4}$

*Data taken from Ghajar (2004)

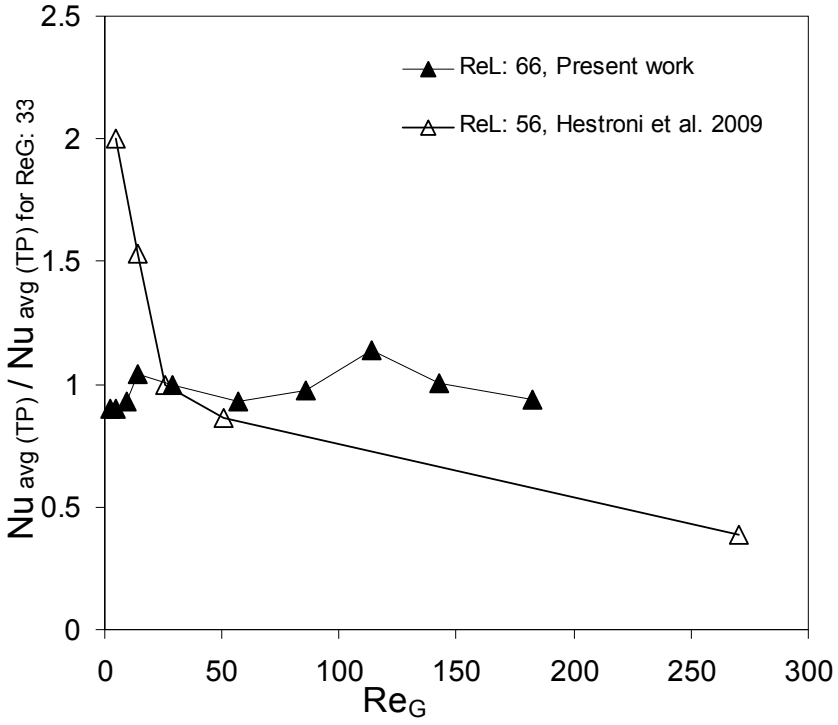

Figure 6.8: Comparison of present experimental data with Hestroni *et al.* (2009), Re_L 56

6.4 Conclusions

Fluid flow and heat transfer for the case of air and water was investigated experimentally in a rectangular minichannel of D_h 1 mm. The experimental results were compared with the available correlations. Following are the conclusions:

1) The two phase pressure drop increases with increase in total mass flow rate. The trend is consistent with those observed in literature for conventional size channels.
2) Good agreement is obtained between the experimental pressure drop and predictions of Lockhart Martinelli model using value of C as 8.
3) No remarkable effect of increasing gas flow rate on two phase Nusselt number is observed in the present work.

Further work is necessary to resolve influence of gas flow rate on two phase heat transfer.

CHAPTER 7

CLOSURE

7.1 Summary

The present research work is focused on developing models, methodology and quantitative understanding of flow, mixing and heat transfer in small channels. The summary and the key contributions from the present research work are discussed in the following.

- Quantitative evaluation of various key issues which are important for understanding and interpreting single flow and heat transfer in parallel micro-channels was carried out. The present results highlight significance of the developing velocity profile and conjugate heat transfer in small channels. The present work confirms that the conventional theory/models used for macroscale systems are also applicable to micro-channels. This work will be useful in improving designs of manifold and parallel microchannel systems.

- CFD simulations of flow and heat transfer in serpentine channel were carried out. The results show good agreement with the experiments. The validated model was used to evolve guidelines on selecting various geometrical parameters of serpentine channels to enhance heat transfer. Based on this work a design map for selecting suitable configuration of serpentine channels was presented.

- The CFD model was extended to investigate residence time distribution in serpentine channel. Influence of various geometrical parameters on RTD was studied. The results will be useful for controlling RTD by selecting configurations.

- Flow and heat transfer in laminar pulsating flow was studied. Appropriate way of calculating the Nusselt number was presented. The methodology used for calculating heat transfer coefficient and the detailed analysis of instantaneous and time averaged data presented in this work will help in finding answers to important questions of influence of flow pulsations on time averaged pressure drop and heat transfer.

- Experimental work conducted on two phase pressure drop and heat transfer in a single minichannel addressed the effect of gas flow rate on two phase heat transfer coefficient. The relationship between the frictional pressure drop and heat transfer is however difficult to understand from the present result. To a certain extent the present experimental results are in agreement with the trends reported in literature (for large size channels).

7.2 Suggestions for future work

Some suggestions for further work on flow and heat transfer in small channels are outlined in the following:

- Further work on distribution of single and two phase flow on parallel channels is needed. Especially influence of small irregularities during the fabrication of parallel channels on flow distribution needs to be studied and quantified.

- Influence of shear and temperature dependent properties on flow and heat transport in microchannels needs to be studied to complement what has been done in this work.

- The present work of heat transfer and RTD in serpentine channel is done only for a specific case of aspect ratio of 1, Re 50 and 200 with Pr 6.97. It will be useful to extend this study to wider range of Re, Pr and geometrical configurations.

- The problem of pressure drop and heat transfer in pulsating flow necessities the sufficient amount of experimental data as the same is limited in literature. Even after so many numerical efforts, the basic question of effect of pulsations on heat transfer is not answered conclusively. Further work is needed to reconcile all the available studies and sort out existing confusion.

- Further work on understanding and quantifying temperature distribution within gas and liquid phases while flowing through microchannel will help to resolve confusion about heat transfer enhancement due to addition of gas.

7.3 Closing remarks

To sum up, the area of flow and heat transfer in small channels still poses challenge to chemical engineering. The knowledge of fluid flow and heat transfer is well established in case of large channels. However the same is still in developing state in case of small channels. The applications of these small channel systems as reactors have shown significant improvement in terms selectivity and yield in various reaction systems. Several issues such as flow distribution, fouling, fabrication accuracy, overall pressure drop and heat transfer coefficient etc. needs to be overcome while implementing these systems on a higher scale (in terms of capacity). Together all these parameters may lower the performance of microreactor systems when used on higher scale as compared to that at laboratory scale. Therefore a critical understanding of various transport processes occurring in small channels is crucial for engineering design purposes as well as for evaluation of practical performance. The present work addressed some of these issues. The present experimental and computational work provided some useful guidelines and will provide a basis for further work.

NOMENCLATURE

Notations

A_{L1}	channel heat transfer area up to location L1, m^2
A	amplitude of serpentine, mm
A_0	nondimensional amplitude
A_h	heat transfer area of serpentine channel, m^2
A(z)	total area of convective heat transfer used in simulation, m^2
$A_{(r,z)}$	flow area of cell, m^2
C	constant depends on flow conditions, dimensionless
Cp	specific heat, J/kg K
C_{pL}	specific heat of liquid, J/kg K
C_{pG}	specific heat of gas, J/kg K
D_h	channel hydraulic diameter, m
D_h	hydraulic diameter of tube, mm
d	hydraulic diameter of serpentine channel, mm
D_n	*Dean number $\left(\frac{d\,u\,\rho}{\mu}\right)\sqrt{\left(\frac{r}{R_c}\right)}$
f	friction factor, dimensionless
f_L:	friction factor for liquid phase, dimensionless
f_G:	friction factor for gas phase, dimensionless
fRe	Poiseuille number, dimensionless
f_p	frequency of pulsation, cycles/s
Fr	Froud number for homogeneous system $\frac{(G)^2}{d_h\, g\, \rho_{HOM}^2}$, dimensionless
H	depth of channel, m
h_{L1}	local heat transfer coefficient allocation 1, W/m^2K
h(z)	local heat transfer coefficient in CFD analysis, W/m^2K
h	overall heat transfer coefficient, W/m^2k
k	thermal conductivity of water, W/mk
k_L	thermal conductivity of liquid, W/mk
L_T	total length of channel, m
L	straight length before bend, mm

$\dot{m}$	mass flowrate, kg/s
Nu	Nusselt number, dimensionless
Nu_{avg}	mean Nusselt number, dimensionless
Nu(z)	local Nusselt number, dimensionless
Nu_{L1}	local Nusselt number at axial location L1, dimensionless
$N_{u(t,z)}$	instantaneous local Nusselt number, dimensionless
$Nu_{(z)}$	time averaged local Nusselt number, dimensionless
$Nu_{(avg)}$	time and area averaged Nusselt number, dimensionless
ΔP	pressure drop, N/m^2
PP	pumping power, W
$\left(\frac{\Delta P}{\Delta L}\right)_{TP}$	two phase pressure drop per unit length, Pa/m
$\left(\frac{\Delta P}{\Delta L}\right)$	single phase pressure drop per unit length, Pa/m
Q1	heat taken by water by convection, W
Q2	heat loss to environment, W
q1	heat flux, W/m^2
$Q_{(x,y,z)}$	local convective heat transfer to fluid in CFD Simulations, W/m^2
q''	heat flux in simulation, W/m^2
Q_{ser}	heat transfer rate in serpentine channel, W
Q_f	volumetric flowrate, m^3/s
Rc	radius of curvature, mm
r	radius of channel, mm
R	radius of channel, mm
Re	Reynolds number, (d u ρ / μ), dimensionless
Re_ω	kinetic Reynolds number, (d_h^2 ω ρ / μ), dimensionless
Sc	Schmidt number $\left(\frac{u}{\rho D}\right)$, dimensionless
St	Strouhal number, $\frac{f_p R}{U}$, dimensionless
$T_{f,out}$	exit temperature of water from channel, K

$T_{f,in}$	inlet temperature of water to channel, K
T_{in}	inlet fluid temperature of serpentine channel, K
T_{out}	outlet fluid temperature of serpentine channel, K
$T_{f,L1}$	temperature of water at location L1, K
T_{w1}	channel wall temperature at axial location L1, K
$T_{m(z)}$	local mean bulk temperature of water, K
$T_{m(t,z)}$	instantaneous local mean bulk temperature of water, K
Tw	channel wall temperature, K
t	flow time, s
U	velocity, m/s
U_{avg}	mean velocity, m/s
u	local or cell velocity, m/s
V	axial velocity, m/s
V_L	superficial liquid velocity, m/s
V_G	superficial gas velocity, m/s
W	width of channel, m
We_{HOM}	Weber number for homogenous system $\frac{d_h (G)^2}{\sigma \ \rho_{HOM}}$, dimensionless
G	mass flux (kg/m^2s)
Wo	Womersely number, $R\left(\frac{\omega \rho}{\mu}\right)^{\frac{1}{2}}$, dimensionless
X	Lockhart–Martinelli parameter
x	mass fraction of gas in two-phase mixture, (quality of gas) dimensionless
x,y,z	coordinate directions

***** Dean number is calculated using channel radius of channel as (d/2)

Greek Letters

α^+	aspect ratio, $\left(\frac{W}{H}\right)$
ρ	density, kg/s
ρ_L	density of liquid, kg/m^3
ρ_G	density of gas, kg/m^3
ρ_{HOM}	Homogeneous density, kg/m^3
μ	viscosity, kg/(m s)
ω	angular velocity, radians/s
θ	angle of bend in serpentine, degree
δ	fluid element length
λ	stretch length of fluid elements
ε	epsilon, gas hold up
ϕ_L^2	two phase friction multiplier, dimensionless
ϕ_{LO}^2	two phase friction multiplier for liquid alone, dimensionless
σ	surface tension, N/m
g	gravitational acceleration, m/s^2

Acronyms

A.C.	Alternate current
CFD	Computational Fluid Dynamics
CHF	Constant Heat Flux
EDM	Electrode Discharge Machining
DAS	Data Acquisition System
SR	Successive Ratio
S.S.	Stainless Steel

Subscripts and Superscripts

a	acceleration
G	gas phase
H	hydrostatic
HOM	homogeneous
L	liquid phase
LO	all mass is assumed liquid only
TP	two phase
TPF	two phase frictional

REFERENCES

References

Adams, T.M., Khalik, S.I.A., Jeter, S.M. and Qureshi, Z., 1998, An experimental investigation of single phase forced convection in microchannel, International Journal of Heat Mass Transfer, 41, 6-7, 851-857.

Aubin, J., Prat, L., Xuereb, C. and Gourdon, C., 2009, Effect of microchannel aspect ratio on residence time distributions and the axial dispersion coefficient, Chemical Engineering and Processing, 48, 554–559.

Bao, Z.Y., Fletcher, D.F. and Haynes, B.S., 2000, An experimental study of gas-liquid flow in a narrow conduit, International Journal of Heat and Mass Transfer, 43, 2313-2324.

Chattopadhyay, H., Durst, F. and Ray, S., 2006, Analysis of heat transfer in simultaneously developing pulsating laminar flow in a pipe with constant wall temperature, International Communications in Heat and Mass Transfer, 33, 475–481.

Chintada, S., Ko, K.H. and Anand, N.K., 1999, Heat Transfer in 3-D Serpentine Channels with Right-Angle Turns, Numerical Heat Transfer, Part A: Applications An International Journal of Computation and Methodology, 36, 781-806.

De Bellefon, C., Tanchoux, N., Caravieilhes, S., Grenouillet, P. and Hessel, V., 2000, Angew. Chem., Int. Ed., 39, 3442.

Dummann, G., Quittmann, U., Gröschel, L., Agar, D.W., Wörz, O. and Morgenschweis, K., 2003, The capillary-microreactor: a new reactor concept for the intensification of heat and mass transfer in liquid–liquid reactions, Catalysis Today, 79–80, 433–439.

Ehrfeld, W., Hessel, V. and Löwe, H., 2000, Microreactors: new technology for modern chemistry, Wiley-Vch Verlag GmbH, Weinheim.

Ekambara, K. and Joshi, J.B., 2004, Axial mixing in laminar pipe flows, Chemical Engineering Science, 59, 3929 – 3944.

Engl, W., Backov, R. and Panizza, P., 2007, Controlled production of emulsions and particles by milli- and microfluidic techniques, Current Opinion in Colloid & Interface Science, 13, 4, 206-216.

Fukagata, K, Kasagi, N., Ua-arayaporn, P. and Himeno, T., 2007, Numerical simulation of gas–liquid two-phase flow and convective heat transfer in a micro tube, International Journal of Heat and Fluid Flow, 28, 72-82.

Gad-el-Hak, M., 2003, Comments on ‘‘critical view on new results in micro-fluid mechanics’’, International Journal in Heat and Mass Transfer, 46, 3941-3945.

Gao, P., Person, S. and Marinet, M.F., 2002, Scale effects on hydrodynamics and heat transfer in two-dimensional mini and microchannels, International Journal of Heat and Mass Transfer, 41, 1017-1047.

Gavriilidis, A., Angeli, P., Cao, E., Yeong, K.K. and Wan, Y.S.S., 2002, Technology and applications of microengineerred reactors, Transactions of Institution of Chemical Engineers, 80, Part A, 3-30.

Geyer, P.E., Rosaguti, N.R., Fletcher, D.F., and Haynes, B.S. 2006, Thermohydraulics of square-section microchannels following a serpentine path, Microfluid Nanofluid , 2, 195-204.

Geyer, P.E., Fletcher, D.F., and Haynes, B.S., 2007, Laminar flow and heat transfer in a periodic trapezoidal channel with semi-circular cross-section, International Journal of Heat and Mass Transfer, 50, 3471-3480.

Ghajar, A., 2004, Two phase heat transfer in gas-liquid non boiling pipe flows, Proceeding of the 3rd International Conference on Heat Transfer, Fluid Mechanics and Thermodynamics, Cape Town, South Africa.

Gokhale, S.V., Tayal, R.K., Jayaraman, V.K., and Kulkarni, B.D., 2005, Microchannel Reactors: Applications and Use in Process Development, International Journal Chemical Reactor Engineering, 3, 1-51.

Guo, Z. and Sung, H., 1997, Analysis of the Nusselt number in pulsating pipe flow, International Journal of Heat and Mass Transfer. 40, 10, 2486-2489.

Habib, M.A., Attya, A.M., Eid, A.I. and Aly, A.Z., 2002, Convective heat transfer characteristics of laminar pulsating air flow, Heat and Mass transfer, 38, 221-232.

Halder, R., Lawal, A., and Damavarapu. A., 2007, Nitration of toluene in microreactor, Catalysis Today, 125, 74-80.

Harms, T.M., Kazmierczak, M.J.K. and Gerner, F.M., 1999, Developing convective heat transfer in deep rectangular microchannels, mechanics'' International Journal of Heat and Mass Transfer, 20, 149-157.

Hemida, H.N., Sabry. M.N., Abdel-Rahim, A. and Mansour, H., 2002, Theoretical analysis of heat transfer in laminar pulsating flow, International Journal of Heat and Mass Transfer, 45, 1767-1780.

Hessel,V., Panagiota A., Gavriilidis, A. and Lo1we, H., 2005, Gas-liquid and gas-liquid-solid microstructured reactors: contacting principles and applications, Industrial Engineering and Chemistry research, 44, 9750-9769.

Hestroni, G., Mosyak, A., Pogrebnyak, E., and Segal, Z., 2009, Heat transfer of gas–liquid mixture in micro-channel heat sink, International Journal of Heat and Mass Transfer, 52, 3963-3971.

Hrnjak, P. and Tu, X., 2007, Single phase pressure drop in microchannels, International Journal of Heat and Fluid Flow, 28, 2-14.

Hsieh, S.S., and Her, B.S., 2007, Heat transfer and pressure drop in serpentine lDMFC flow channels, International Journal of Heat and Mass Transfer, 50, 5323-5327.

Janicke, M. T., Kestenbaum, H., Hagendorf, U., Schu¨th, F., Fichtner, M. and Schubert, K., 2000, The controlled oxidation of hydrogen from an explosive mixture of gases using a microstructured reactor heat exchanger and Pt-Al_2O_3 catalyst, Journal of Catalysis, 191, 282-293.

Jensen, K.F., 2001, 2001, Microreaction engineering is small better?, Chemical Engineering Science, 56, 2001, 293-303.

Judy, J., Maynes, D. and Webb, B.W., 2002, Characterization of frictional pressure drop for liquid flows through microchannels, International Journal of Heat and Mass Transfer, 45, 3477-3489.

Kandlikar, S.G., Garimella, S., Li, D., Colin, S. and King, Heat transfer and Fluid flow in minichannels and microchannels, M.R., 2006

Kawano, K., Sekimura, M., Minakami, H., Iwasaki, H. and Ishizuka, M., 2001, Development of microchannel heat exchanging, JSME: International Journal, B, 44, 4, 592-598.

Kays, W.M., Crawford, M.E., 1980, Convective Heat and Mass Transfer, McGraw-Hill, New York.

Kaji, M., Sawai, T., Kagi, Y. and Ueda, T., 2009, Heat transfer and fluid dynamics of air-water two phase flow in microchannels, Experimental and thermal fluid science, 34, 4, 446-453.

Knott, R. F., Anderson, R. N., Acrivos, A., and Petersen, E. E., 1959, An experimental study of heat transfer to nitrogen-oil mixtures, Industrial and Engineering Chemistry, 51, 11, 1369-1372.

Lakehal, D., Larrignon, G. and Narayanan, C., 2007, Computational heat transfer and two phase flow topology in miniature tube, Microfluid Nanofluid,4, 4, 261-271.

Lee, P. and Garimella, S.V., 2006, Thermally developing flow and heat transfer in rectangular microchannels of different aspect ratios, International Journal of Heat and Mass Transfer, 49, 3060–3067.

Lee, P.S., Garimella, S.V. and Liu, D., 2005, Investigation of heat transfer in rectangular microchannels, International Journal of Heat and Mass Transfer, 48, 1688-1704.

Lelea, D., Nishio, S. and Takano, K., 2004, The experimental research on microtube heat transfer and fluid flow of distilled water, International Journal of Heat and Mass Transfer, 47, 2817-2830.

Levenspiel, O., 1999, Chemical Reaction Engineering, Third Edition, John Wiley & Sons, New York.

Liu, R.H., Stremler, M.A.., Sharp, K.V., Olsen, M.G., Santiago, J.G., Adrian, R.J., Aref, H., and Beebe, D.J., 2000, Passive mixing in a three-dimensional serpentine microchannel, Journal of MicroElectroMechanicalSystems, 9, 2,190-197.

Liu, H., Vandu, C.U. and Krishna, R., 2005, Hydrodynamics of Taylor flow in vertical capillaries: flow regimes, bubble rise velocity, liquid slug length, and pressure drop, Industrial Engineering and Chemistry Research, 44, 4884-4897.

Lohse, S., Kohnen, B.T., Janasek, D., Dittrich, P.S., Franzke, J. and Agar, D.W., 2008, A novel method for determining residence time distribution in intricately structured microreactors, Lab Chip, 8, 431-438 .

Maharudrayya, S., Jayanti, S., and Deshpande, A.P., 2004, Pressure losses in laminar flow through serpentine channels in fuel cell stacks, Journal of Power Sources, 138, 1-13.

Martin, B. W. and Sims, G. E., 1971, Forced convection heat transfer to water with air injection in a rectangular duct Industrial Engineering and Chemistry Research Fundamentals, 14, 1115-1134.

Mishan, Y., Mosyak, A., Pogrebnyak, E. and Hetsroni, G., 2007, Effect of developing flow and thermal regime on momentum and heat transfer in micro-scale heat sink, 50, 3100-3114.

Morini, G.L., 2004, Single-phase convective heat transfer in microchannels: a review of experimental results, International Journal of Thermal Sciences, 43, 631-651.

Moschandreou, H. and Zamir, M., 1997, Heat transfer in a tube with pulsating flow and constant heat flux, International Journal of Heat and Mass Transfer. 40, 10, 2461-2466.

Nunge, R.J. and Gill, W.N., 1969, Mechanisms affecting dispersion and miscible displacement, Flow Through Porous Media Symposium, 61, 33-49.

Ottino, J.M. and Wiggins, S., 2004, Introduction: mixing in microfluidics, Philosophical Transactions of Royal Society London A, 362, 923-935.

Rebrov, E.V., de Croon, M.H.J.M. and Schouten, J.C., 2001, Design of a microstructured reactor with integrated heat-exchanger for optimum performance of a highly exothermic reaction, Catalysis Today, 69, 183-192.

Rosaguti, N.R., Fletcher, D.F., and Haynes, B.S., 2006, Laminar flow and heat transfer in a periodic serpentine channel with semi-circular cross-section, International Journal of Heat and Mass Transfer, 49, 2912-2923.

Rosaguti, N.R., Fletcher, D.F., and Haynes, B.S., 2004, Laminar flow in a periodic serpentine channel, Proceedings of the 5th Australasian Fluid Mechanics Conference.

Rosaguti, N.R., Fletcher, D.F., and Haynes, B.S., 2007, Low-Reynolds number heat transfer enhancement in sinusoidal channels, Chemical Engineering Science, 62, 694-702.

Rosaguti, N.R., Fletcher, D.F., and Haynes, B.S., 2005, Laminar flow and heat transfer in periodic serpentine channel, Chemical Engineering Technology, 28, 3, 353-361.

Shah, M. M., 1981, Generalized prediction of heat transfer during two component gas-liquid flow in tubes and other channels, AIChE Symposium Series, 77, 140-151.

Shah, R.K. and London, A.L., 1978, Academic Press, New York, San Fransisco, London.

Shetty, V.D. and Vasudeva, K., 1977, Effect of Schmidt number on laminar dispersion in helical coils, Chemical Engineering Science, 32, 783-785.

Tiselj, I., Hestroni, G., Mavko, B., Mosyak, A., Pogrebnyak, E., Segal, Z., 2004, Effect of axial conduction on the heat transfer in micro-channels, International Journal of Heat and Mass Transfer ,47, 2551-2565.

Trachsel, F., Günther, A., Khan, S. and Jensen, K.F., 2005, Measurement of residence time distribution in microfluidic systems, Chemical Engineering Science, 60, 729-5737.

Trivedi, R.N., and Vasudeva, K., 1975, Axial dispersion in laminar flow in helical coils, Chemical Engineering Science, 30, 317-325.

Ünsala, B., Ray, S., Durst, F. and Ertunça, O., 2005, Pulsating laminar pipe flows with sinusoidal mass flux variations, Fluid Dynamics Research, 37, 317-333.

Vijay, M. M., Aggour, M. A., and Sims, G. E., 1982, A correlation of mean heat Transfer coefficients for two-phase two-component flow in a vertical tube, Proc.7th International Heat Transfer Coefficient, 5, 367-372.

Wallis, G.B., 1969, One-dimensional two phase flow, McGraw-Hill, Inc., USA.

Wang, B.X. and Peng, X.F., 1993, Experimental investigation on liquid forced convection heat transfer through microchannels, International Journal of Heat and Mass Transfer, 37, I, 73-82.

Warrier, G.R., Dhir, V.K. and Momoda, L.A., 2002, Heat transfer and pressure drop in narrow rectangular channels, Experimental Thermal and Fluid Science, 26, 53-64.

Wehle, D.; Dejmek, M.; Rosenthal, J.; Ernst, H.; Kampmann, D.; Trautschold, S.; Pechatschek, R. Verfahren zur Herstellung von Monochloressigsa¨ure in Mikroreaktoren, 2000.

Wibulswas, P., 1966, Laminar flow heat transfer in non-circular ducts, Ph.D thesis, University College, London.

Womersley, J.R., 1954, Method for the calculation of velocity, rate of flow and viscous drag in arteries when the pressure gradient is known, Journal of Physiology, 127, 553-563.

Xiong, R., and Chung, J.N., 2007, Flow characteristics of water in straight and serpentine micro-channels with miter bends, Experimental Thermal and Fluid Science, 31, 805-812.

Yu, J., Zhi-Xin L. and Zhao, T.S, 2004, An analytical study of pulsating laminar heat convection in a circular tube with constant heat flux, International Journal of Heat and Mass Transfer, 47, 5297-5301.

Zang, H.Y., Pinjala, D., Wong, T.N., Toh, K.C. and Joshi, Y.K., 2005, Single phase liquid cooled microchannel heat sink for electronic packages, Applied Thermal Engg., 25, 1472-1487.

Zhao, T. and Cheng, P., 1995, A numerical solution of laminar forced convection in a heated pipe subjected to a reciprocating flow, International Journal of Heat and Mass Transfer, 38, 16, 3011-3022.

Zhao, T. and Cheng, P., 1996, The friction coefficient of a fully developed laminar reciprocating flow in a circular pipe, International Journal of Heat and Fluid Flow, 17, 167-172.

APPENDIX

Appendix I: Dimensions of serpentine channel configurations: sample calculation

1) Sample calculations of case 1

a) Bend angle of 40^o

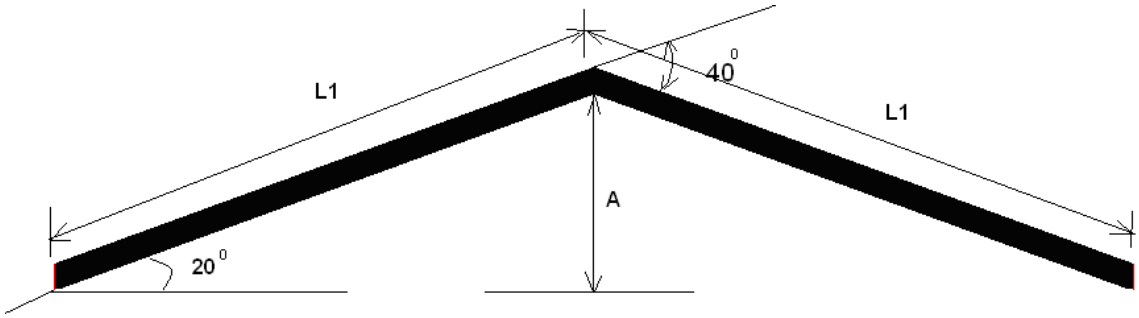

Total Length: 100mm

Straight length before bend (see Figure 2.1 for straight length definition): $L = 0$

Radius of curvature (Rc): 0

This makes 2 x $L1$= 100 mm

i.e. $L1$= 50mm

A= sin (20) x $L1$ = 17.101 mm

2) Sample calculations of case 2

a) Bend angle of 80^o

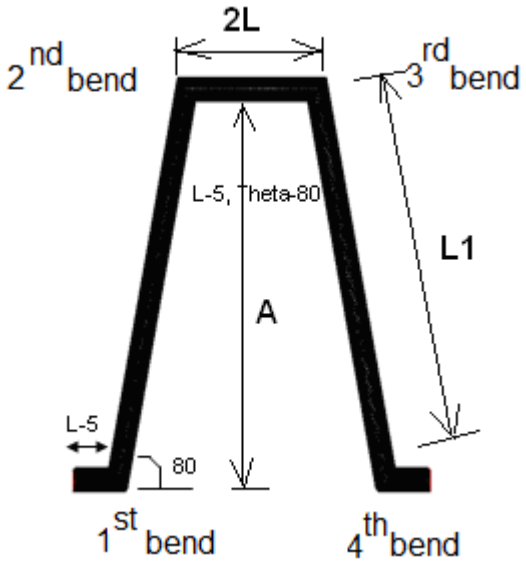

Total Length: 100mm

Straight length before bend (see Figure 2.1 for straight length definition): L = 5mm

Radius of curvature: 0

This makes 2 x $L1$ + 2L + 2 x L = 100 mm

i.e. $L1$= 40mm

A= sin (80) x $L1$ = 39. 39 mm

3) Sample calculations of case 3

a) Bend angle of 80^o

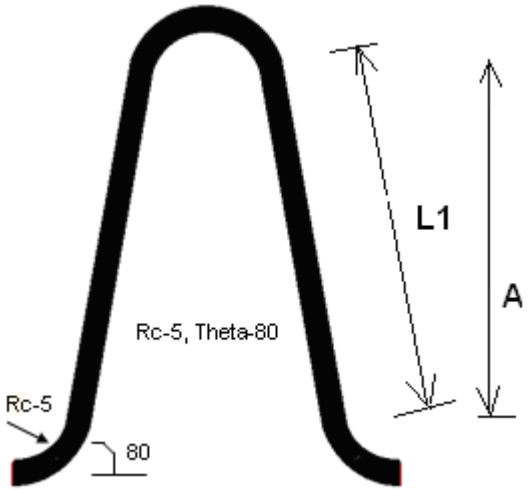

Total Length: 100mm

Straight length before bend (see Figure 2.1 for straight length definition): L = 0 mm

Radius of curvature (Rc): 5 mm

This makes 2 x $L1$ + 4 x Rc = 100 mm

i.e. $L1$= 40 mm

A= sin (80) x $L1$ = 39. 39 mm

Appendix II: Supporting data on flow and heat transfer in serpentine channel (chapter 2)

Case 1: Effect of inclination/bend angle on performance

Ɵ degrees	***L* mm**	***Rc* mm**	$\frac{(PP)_{Serpentine}}{(PP)_{Straight\ channel}}$	$\frac{(Q)_{Serpentine}}{(Q)_{Straight\ channel}}$	$\frac{(Q/PP)_{Serpentine}}{(Q/PP)_{Straight\ channel}}$	$\frac{(Nu/f\,\mathrm{Re})_{Serpentine}}{(Nu/f\,\mathrm{Re})_{Straight\ channel}}$
20	0	0	0.980626	1.26815	1.293204	1.39621
40	0	0	1.061129	1.689538	1.592208	1.992615
45	0	0	1.07989	1.742984	1.614038	2.065013
50	0	0	1.097936	1.776435	1.617977	2.099891
100	0	0	1.292801	1.927937	1.491287	2.076645
130	0	0	1.288306	1.859072	1.443036	1.943785
160	0	0	1.324462	1.796015	1.356034	1.775069

Case 2: Effect of straight length (*L*) before bend on performance

Ɵ degrees	***L* mm**	***Rc* mm**	$\frac{(PP)_{Serpentine}}{(PP)_{Straight\ channel}}$	$\frac{(Q)_{Serpentine}}{(Q)_{Straight\ channel}}$	$\frac{(Q/PP)_{Serpentine}}{(Q/PP)_{Straight\ channel}}$	$\frac{(Nu/f\,\mathrm{Re})_{Serpentine}}{(Nu/f\,\mathrm{Re})_{Straight\ channel}}$
20	5	0	1.026915	1.543805	1.503343	1.779246
20	10	0	1.032894	1.521824	1.473359	1.729986
20	15	0	1.068759	1.456556	1.362847	1.564036
50	5	0	1.183972	1.8044	1.524022	2.002389
50	10	0	1.261582	1.889906	1.498045	2.04757
50	15	0	1.249869	1.89867	1.519096	2.085144
80	5	0	1.392802	1.975992	1.418717	2.024742
80	10	0	1.486975	2.036236	1.369382	2.01921
80	15	0	1.529933	2.051233	1.340734	1.993811
90	5	0	1.484364	2.013778	1.35666	1.975738
90	10	0	1.556174	2.053209	1.319396	1.964294
90	15	0	1.579677	2.06713	1.308578	1.963894

Case 3: Effect of curvature on performance

Ɵ degrees	***L* mm**	***Rc* mm**	$\frac{(PP)_{Serpentine}}{(PP)_{Straight\ channel}}$	$\frac{(Q)_{Serpentine}}{(Q)_{Straight\ channel}}$	$\frac{(Q/PP)_{Serpentine}}{(Q/PP)_{Straight\ channel}}$	$\frac{(Nu/f\,\mathrm{Re})_{Serpentine}}{(Nu/f\,\mathrm{Re})_{Straight\ channel}}$
40	0	5	1.034731	1.636401	1.581476	1.937956
40	0	10	1.023947	1.579621	1.542678	1.850026
40	0	15	1.02251	1.545228	1.511211	1.789484
40	0	20	1.023987	1.521996	1.486344	1.74534
100	0	5	1.051666	1.744237	1.658546	2.12308
100	0	10	1.084341	1.75591	1.619333	2.083178
100	0	15	1.095265	1.730135	1.579649	2.010146
100	0	20	1.072457	1.689717	1.575556	1.971919
160	0	5	1.106523	1.79651	1.623563	2.125734
160	0	10	1.149867	1.789776	1.556508	2.031907
160	0	15	1.182008	1.806141	1.528028	2.009208

Case 4: Effect of curvature with constant straight length before bend on performance

Ɵ degrees	***L* mm**	***Rc* mm**	$\frac{(PP)_{Serpentine}}{(PP)_{Straight\ channel}}$	$\frac{(Q)_{Serpentine}}{(Q)_{Straight\ channel}}$	$\frac{(Q/PP)_{Serpentine}}{(Q/PP)_{Straight\ channel}}$	$\frac{(Nu/f\,\mathrm{Re})_{Serpentine}}{(Nu/f\,\mathrm{Re})_{Straight\ channel}}$
20	5	5	1.5405	1.536808	1.816672	1.5405
20	5	10	1.529155	1.496369	1.761633	1.529155
20	5	15	1.557144	1.480016	1.76019	1.557144
50	5	5	1.758341	1.535419	1.977279	1.758341
50	5	10	1.730817	1.549474	1.972309	1.730817
50	5	15	1.716259	1.549147	1.960005	1.716259
80	5	5	1.834261	1.545764	2.058452	1.834261
80	5	10	1.812155	1.551048	2.044959	1.812155

Case 5: Effect of different straight length before bend with constant curvature on performance

Ɵ degrees	***L* mm**	***Rc* mm**	$\frac{(PP)_{Serpentine}}{(PP)_{Straight\ channel}}$	$\frac{(Q)_{Serpentine}}{(Q)_{Straight\ channel}}$	$\frac{(Q/PP)_{Serpentine}}{(Q/PP)_{Straight\ channel}}$	$\frac{(Nu/f\,\mathrm{Re})_{Serpentine}}{(Nu/f\,\mathrm{Re})_{Straight\ channel}}$
20	5	5	1.002402	1.5405	1.536808	1.816672
20	10	5	1.015725	1.519322	1.4958	1.754764
20	15	5	1.0066	1.384221	1.375146	1.540324
50	5	5	1.145187	1.758341	1.535419	1.977279
50	10	5	1.162137	1.797523	1.546739	2.026054
50	15	5	1.13719	1.760569	1.548175	1.995606
80	5	5	1.186637	1.834261	1.545764	2.058452
80	10	5	1.190279	1.843682	1.54895	2.07162
80	15	5	1.14761	1.818814	1.584871	2.095805

SYNOPSIS

OF THE THESIS TO BE SUBMITTED TO THE

UNIVERSITY OF MUMBAI

IN THE PARTIAL FULFILLMENT OF THE REQUIREMENTS

FOR THE DEGREE OF

DOCTOR OF PHILOSOPHY (TECHNOLOGY)

IN THE FACULTY OF CHEMICAL ENGINEERING

Research Scholar	**:**	**Karale Chaitanya Mallikarjun**
Name and Designation of Research Supervisor	**:**	**Prof. Sunil S. Bhagwat Professor, Chemical Engineering Department**
Title of the Thesis	**:**	**FLOW AND HEAT TRASNER IN SMALL CHANNELS**
Degree	**:**	**Doctor of Philosophy (Technology)**
Institute	**:**	**Institute of Chemical Technology, University of Mumbai, Matunga, Mumbai 400 019.**
Number and Date of Registration	**:**	**934 / 26-02-2008**
Date of submission	**:**	**16/02/2010**
Signature of the Candidate	**:**	
Signature of the Research Guide	**:**	**(Prof. Sunil S. Bhagwat)**

Wide variety of conventional chemical reactors are used in practice. The sizes of these conventional reactors vary from few centimeters (laboratory reactors) to several meters (manufacturing scale). Overall performance of chemical reactors is governed by complex interactions of chemical reactions and transport processes like mixing, heat transfer and mass transfer. In recent years, emphasis is being given to process intensification by eliminating (or at least reducing) limitations imposed by transport processes. Micro-reactors comprising small channels (ranging from few microns to millimeter) have been shown to offer unprecedented opportunities for process intensification [see for example reviews by Ehrfeld *et. al.* (2000), Gavriilidis *et. al*. (2002) and Hessel *et. al.* (2006)].

These small reactors offer an invaluable tool for process development and chemical synthesis. Operations in temperature-concentration-pressure domains difficult to access with conventional equipment e.g. explosive regimes can also be easily carried out in these systems. Due to decrease of the characteristic lengths, the concentration and temperature gradients becomes higher. This results in intensified mass and heat transfer. Larger amounts of energy and mass can be transferred between interfaces because of higher surface area to volume ratio (>10000 m^2/m^3) available with small channels. Isothermal conditions can thus also be easily attained. It is however essential to critically understand various transport processes occurring in small channels in order to realize true potential of micro-reactors. This research work was undertaken with this background.

The present research work is focused on developing models, methodology and quantitative understanding of flow, mixing and heat transfer in small channels. The size of the channels under the study ranges from few micrometers (700 μm) to millimeters (2 mm). Single phase as well as two phase flow and heat transfer in small channels was studied. The study involved experimental as well as numerical investigations. The overall work is divided into two broad categories. A) Single phase studies in small channels and B) Two phase studies in small channels. The single phase studies are further divided into four categories. These include a) Flow and heat transfer in parallel channels b) Flow and heat transfer in serpentine channels c) Residence time distribution in serpentine channels and d) Flow and heat transfer in laminar pulsating convection. In case of two phase studies the work consists of experimental and numerical investigation of heat transfer in gas-liquid flow in a single minichannel. The motivations behind the individual topic, methodology and the results obtained are discussed in a sequential manner as following.

1) Single phase flow and heat transfer in parallel channels

Flow and heat transfer in microchannels is of significant interest to various applications ranging from electronics cooling (see for example, Kandlikar *et. al.* 2006) to micro-reactors (see for example, Ehrfeld *et al.* 2000, Gokhale *et. al.* 2005). However several studies over the last two decades reported the mismatch or disagreement between the conventional correlations and the experimental data (see review by Morini 2004). Various issues such as conjugate heat transfer, entrance effects, wall roughness, viscous heating and axial conduction may become important for understanding and interpreting flow and heat transfer in small channels compared

to conventional size channels. In the present work, attempt was made to quantify these issues experimentally as well as computationally.

Flow and heat transfer experiments were carried out with a micro-channel plate comprising of 20 parallel channels. Pressure drop and heat transfer coefficients were experimentally measured. Flow and heat transfer in the experimental set-up were simulated using CFD models to provide useful and quantitative information on developing flow regions, axial heat conduction, conjugate heat transfer, effect of the design inlet and outlet manifolds.

It was found that including the entrance effects, the experimental Poiseuille number was in agreement with that of conventional theory of laminar flow in macro channels. In case of heat transfer, the Nusselt number calculated from the experimental data was well predicted by the CFD analysis. The conjugate heat transfer methodology was therefore found to be useful for detailed understanding of wall heat conduction. The methodology and the results presented here will be useful for further work on flow and heat transfer in micro-channels.

2) Flow and heat transfer in serpentine channels

Serpentine channel configurations are becoming more popular among the researchers (Liu *et. al.* 2000) in last few years due to several advantages offered over straight channels such as higher Nusselt number compared to straight channels for the same total length/heat transfer area. The secondary flow created at bends creates radial mixing that enhances heat/mass transfer without much increase in pressure drop. In addition due to its serpentine nature the size of the reactor is much smaller than that with straight channels. Thus higher residence time can be achieved in smaller space. However the knowledge of proper design methodology for choice of serpentine channel with due considerations to required pumping power is lacking in literature.

In the present work, an attempt was made to quantify this issue experimentally as well as computationally. Flow and heat transfer experiments were carried out with a serpentine channel plate comprising of 10 channels in series. Pressure drop and heat transfer coefficients were experimentally measured. Flow and heat transfer in the experimental set-up was simulated using CFD models to understand the mechanisms responsible for performance enhancement. The developed CFD methodology was further applied to understand the effect of various geometrical parameters on heat transfer enhancement. For this purpose a new and more appropriate criteria was defined for evaluation of heat transfer performance (heat transfer per unit pumping power) thus ensuring due considerations to required pumping power.

In the present study two mechanisms were found to be responsible for enhancement. These include a) radial mixing (due to crossing of streamlines in case of sharp bends and secondary flow in case of smooth bends) and b) developing nature of flow between the bends. The effect of geometrical parameters and the corresponding mechanisms contributing for enhancement were discussed briefly. Based on the results, a regime map showing different serpentine channels heat transfer enhancement with pumping power was developed for Reynolds number of 200 which will be useful for further work on flow and heat transfer in serpentine channels.

3) Residence time distribution in serpentine channels

In any continuous flow processes, the residence time characteristics of the reactor is of significant importance. This gives information about the intensity of the dispersion present in the reactor. Despite smaller mixing lengths in microreactors, the laminar profile in straight channels results in large axial dispersion. Serpentine channel helps to overcome this issue due to secondary flow created at bends. The secondary flow structure offers radial mixing that helps to overcome the radial concentration gradient present in straight channel. However the proper knowledge of the residence time distribution in different serpentine configurations is limited in literature.

Therefore in the present work the effect of various geometrical parameters of the serpentine channel on the residence time distribution was investigated using CFD. The CFD methodology was divided in two parts. In the first part the methodology was validated for the simple system of laminar pipe flow. The second part involved application of this standardized methodology to study the residence time distribution in various serpentine channel geometries.

The performance of different geometries was compared using variance as a parameter calculated from the E-t curve obtained from simulations. Using variance of E-t curve, an optimization of the geometrical configurations was done for narrowing the residence time distribution thus achieving lesser axial dispersion. The mechanisms responsible for reduced axial dispersion were discussed briefly.

4) Flow and heat transfer in laminar pulsating convection

In case of microreactors, the required pressure drop for the delivery of the reactants is quite high due to smaller size of the channels. Therefore the reciprocating or the peristaltic pumps is the first choice among the researchers. In many studies where the researchers have used the microreactor system for process intensification one can find the use of peristaltic pump. However one of the limitations of the peristaltic or reciprocating action is discontinuity in the instantaneous flow even though the overall time averaged flowrate remains same as that of steady state value. Due to this discontinuous/non uniform instantaneous flow nature in the channel, the flow or fluid elements keeps pulsating/ fluctuating at its mean position. In such cases it becomes necessary to address the effect of these pulsations on transport characteristics.

Review of the current literature showed a need for systematic assessment of the impact of flow pulsation in heat transfer from circular ducts at constant wall temperature. An attempt was made to investigate the heat transfer in a circular isothermal duct with imposed flow pulsation at the inlet using CFD. The flow at the inlet consisted of a fixed part and a pulsating component that was varied sinusoidally in time. The flow was both thermally and hydrodynamically developing while the tube wall was kept at a uniform temperature. The study was focused within the frequency range of 1–100 Hz and amplitude <1 at a Reynolds number of 200. The range of the Womersely number was 3 to 37.

The phase lag was observed between the pressure and the velocity cycles for the range of the Womersely number under investigation that was consistent with the literature knowledge. The results showed that there was no effect of pulsation frequency or amplitude on a time averaged pressure drop or Nusselt number.

5) Heat transfer in gas liquid flow in small channel

In the chemical industry numerous reactions are carried out which are both strongly exothermic and involve two-phase gas–liquid systems. While handling gas-liquid systems at smaller scale a good understanding of the complex multiphase flow behavior must be developed. Several studies have been conducted to characterize gas-liquid flows in capillaries (Liu *et. al.* 2005) however the heat transfer characteristics are not yet well understood (Hestroni *et. al.* 2009).

In the present work an attempt was made to quantify the two phase pressure drop and heat transfer coefficient experimentally. Flow and heat transfer experiments were carried out in a single minichannel of 1 mm size with air-water as working fluids. Pressure drop and heat transfer coefficients were experimentally measured. The effect of different gas and liquid flowrate on two phase heat transfer coefficient was studied.

The two phase experimental pressure drop was well correlated by the Lockhart–Martinelli method. In case of heat transfer it was observed that at low gas flowrates, the two phase heat transfer coefficient was more than that of single phase. However for higher gas flowrates the opposite behaviour was observed. A brief discussion was presented on the probable mechanisms and the limitations of experimental techniques leading to difficulties in understanding the phenomena. A unit cell model was presented to understand the heat transfer interaction between the gas and liquid.

Summary

The summary and the key contributions from the present research work are discussed in the following.

The contribution of the scaling effects was evaluated successfully in the work of single phase flow and heat transfer in parallel channel. The present results highlight significance of the developing velocity profile and conjugate heat transfer in small channels. The agreement of the present results with the conventional theory will be useful for sorting out the disagreement present over the several years. The work will be further useful in better design of microreactors indicating the probable effect of conduction in solid, pressure drop due to developing flow, manifold design for uniform flow distribution etc.

The CFD methodology developed to study flow and heat transfer in serpentine channel was validated with the experiments. The developed methodology was further applied to understand the effect of various geometrical parameters on heat transfer in serpentine channels. The mechanisms responsible for enhancement in heat transfer in serpentine channel were discussed briefly. The regime map for the heat transfer in

serpentine channel developed in this work will provide guidelines for selecting suitable configuration of channels while designing serpentine microreactors.

The extended work on the residence time distribution in serpentine channel will help in understanding the effect of various serpentine configurations on dispersion. With the present work the choice of geometrical configuration giving lesser axial dispersion becomes simple. The brief discussion on the responsible mechanisms for lesser dispersion will increase the understanding of mixing in serpentine channels resulting in better design procedures/guidelines.

In the present work a better way of calculating the Nusselt number was presented compared to that used by various researchers. The methodology used for calculating heat transfer coefficient will help in sorting out the discrepancies present in the literature.

Experimental work conducted on two phase heat transfer in a single minichannel addressed the effect of presence of gas on heat transfer coefficient. The results and the brief discussion presented, gave better understanding of gas liquid heat transfer characteristics in small channels. Simple unit cell model developed in the present work enables the understanding of the heat transfer interactions between gas and liquid and the effect of the physical properties leading to non isothermal conditions. The presented model/methodology will be useful to visualize the real temperature conditions present in the gas liquid microreactors for better design.

References:

Ehrfeld, W., Hessel, V. and Löwe, H., 2000, Microreactors New Technology for Modern Chemistry, WILEY-VCH Verlag GmbH, Weinheim

Gavriilidis, A., Angeli, P., Cao, E., Yeong, K.K. and Wan, Y.S.S., 2002, Technology and Applications of Microengineerred Reactors, Transactions of Institution of Chemical Engineers, 80, Part A, 3-30

Gokhale, S.V., Tayal, R.K., Jayaraman, V.K., and Kulkarni, B.D., 2005, Microchannel Reactors: Applications and Use in Process Development, International Journal of Chemical Reactor Engineering, 3, Review R2

Hessel,V., Panagiota A., Gavriilidis, A. and Lo1we, H., 2005, Gas-Liquid and Gas-Liquid-Solid Microstructured Reactors:Contacting Principles and Applications, Industrial Engineering and Chemistry research, 44, 9750-9769

Hetsroni, G., Mosyak, A., Pogrebnyak, E., and Segal, Z., 2009, Heat Transfer of Gas–Liquid Mixture in Micro-Channel Heat Sink, International Journal of Heat and Mass Transfer, 52, 3963–3971

Kandlikar, S.G., Garimella, S., Li, D., Colin, S. and King, 2006, Heat Transfer and Fluid Flow in Minichannels and Microchannels, Elsevier Ltd.

Liu, R.H., Stremler, M.A.., Sharp, K.V., Olsen, M.G., Santiago, J.G., Adrian, R.J., Aref, H., and Beebe, D.J., 2000, Passive Mixing in a Three-Dimensional Serpentine Microchannel, Journal of MicroElectroMechanicalSystems, 9, 2

Liu, H., Vandu, C.U. and Krishna, R., 2005, Hydrodynamics of Taylor Flow in Vertical Capillaries: Flow Regimes, Bubble Rise Velocity, Liquid Slug Length, and Pressure Drop, Industrial Engineering and Chemistry research, 44, 4884-4897

Morini, G.L., 2004, Single-phase convective heat transfer in microchannels: a review of experimental results, International Journal of Thermal Sciences, 43, 631–651